METHODOLOGY OF FALLOUT-RISK ASSESSMENT

Leo A. Schmidt, Jr.

Institute for Defense Analyses

Prepared for:

Defense Civil Preparedness Agency

January 1975

PAPER P-1065

METHODOLOGY OF FALLOUT-RISK ASSESSMENT

Leo A. Schmidt, Jr.

January 1975

INSTITUTE FOR DEFENSE ANALYSES
PROGRAM ANALYSIS DIVISION

IDA Log No. HQ 75-17165
Copy 72 of 120 copies

The work reported in this document was conducted under Contract DAHC20 70 C 0287 for the Defense Civil Preparedness Agency. The publication of this IDA Paper does not indicate endorsement by the Defense Civil Preparedness Agency, nor should the contents be construed as reflecting the official position of that agency.

PAPER P-1065

METHODOLOGY OF FALLOUT-RISK ASSESSMENT

By

Leo A. Schmidt, Jr.

For

DEFENSE CIVIL PREPAREDNESS AGENCY
WASHINGTON, D.C. 20301

January 1975

DCPA Review Notice

This report has been reviewed in the Defense Civil Preparedness Agency and approved for publication. Approval does not signify that the contents necessarily reflect the views and policies of the Defense Civil Preparedness Agency.

IDA

INSTITUTE FOR DEFENSE ANALYSES
PROGRAM ANALYSIS DIVISION
400 Army-Navy Drive, Arlington, Virginia 22202

CONTRACT DAHC20 70 C 0287
WORK UNIT T 4114F

UNCLASSIFIED

SECURITY CLASSIFICATION OF THIS PAGE (When Data Entered)

REPORT DOCUMENTATION PAGE		READ INSTRUCTIONS BEFORE COMPLETING FORM
1. REPORT NUMBER P-1065	2. GOVT ACCESSION NO.	3. RECIPIENT'S CATALOG NUMBER
4. TITLE (and Subtitle) Methodology of Fallout-Risk Assessment		5. TYPE OF REPORT & PERIOD COVERED Final 6. PERFORMING ORG. REPORT NUMBER P-1065
7. AUTHOR(s) Leo A. Schmidt, Jr.		8. CONTRACT OR GRANT NUMBER(s) DAHC20 70 C 0287
9. PERFORMING ORGANIZATION NAME AND ADDRESS Institute for Defense Analyses Program Analysis Division 400 Army-Navy Drive, Arlington, Virginia 22202		10. PROGRAM ELEMENT, PROJECT, TASK AREA & WORK UNIT NUMBERS Work Unit T 4114F
11. CONTROLLING OFFICE NAME AND ADDRESS DCPA Washington, D.C. 20301		12. REPORT DATE January 1975 13. NUMBER OF PAGES 198
14. MONITORING AGENCY NAME & ADDRESS(if different from Controlling Office)		15. SECURITY CLASS. (of this report) Unclassified 15a. DECLASSIFICATION DOWNGRADING SCHEDULE N/A

16. DISTRIBUTION STATEMENT (of this Report)

Approved for public release; distribution unlimited.

17. DISTRIBUTION STATEMENT (of the abstract entered in Block 20, if different from Report)

18. SUPPLEMENTARY NOTES

19. KEY WORDS (Continue on reverse side if necessary and identify by block number)

Fallout, Damage Assessment, Fallout Winds, Risk Calculations, Fallout Models, Simulation of Nuclear Attack, Fallout Dose Statistics

20. ABSTRACT (Continue on reverse side if necessary and identify by block number)

This paper analyzes the deposition of radioactive fallout in attack environments of varying complexity with both deterministic and probabalistic winds. Based on the WSEG-10 Fallout Model, simplified calculational methods are developed to allow the determination of fallout risk for single weapons and clusters of closely spaced weapons. Monte Carlo methods are used that illustrate the nature of the

(continued)

DD FORM 1 JAN 73 1473 EDITION OF 1 NOV 65 IS OBSOLETE

UNCLASSIFIED

SECURITY CLASSIFICATION OF THIS PAGE (When Data Entered)

20. (continued)

probabality distributions of fallout risk for large attacks with typical seasonal wind distributions for the United States.

SUMMARY

This study presents an analysis of the deposition of radioactive fallout from a nuclear attack in a number of different deterministic and probabilistic attack environments. It addresses the analytic implications that can be drawn through the use of a particular fallout model--rather than the physical basis of such a model. Because of its mathematical structure the WSEG-10 Model is chosen. Calculations are described that begin with very simple situations and progress to the more complex environments that might be expected in a large nuclear attack.

Simplifications of the WSEG-10 Model are developed that provide reasonably good approximations under many wind conditions and that also illustrate the primary factors to which the model is sensitive. When a number of weapons are detonated in proximity, as might be expected in an attack on an urban target, the fallout patterns merge into a single smoothly varying combined-dose pattern. Prediction methods are developed to describe the dose from such a cluster. Methods are developed to analyze fallout-dose distributions for sets of different winds that are consistent with seasonal meteorological conditions. For simple attack environments, the prime sensitivity of dose level is to wind direction, and simple prediction methods based on wind direction are compared with more detailed Monte Carlo simulation results. For large attacks, no relatively simple analytical prediction methods seem universally applicable, though a qualitative understanding of the probability distributions obtained is often possible.

CONTENTS

FIGURES

TABLES

PREFACE

There seems to be general agreement that, to determine the utility of fallout protection, the variability of the wind should be taken into account; because the fallout casualties for one set of wind conditions may not even be close to those for another set. Nevertheless, such analyses have been infrequent. In large part, this may be due to a lack of the basic tools for treating wind variability. The present study attempts to fill this need by developing probabilistic predictive models and describing some simple situations in which an intuitive grasp of the important factors can be obtained. Since the subject is extensive, no exhaustive treatment is presented here; but this report is issued to document some computer programs and analysis methods--and with the hope that it will lead to further efforts along similar lines to estimate fallout hazards realistically.

The analysis of fallout effects from nuclear-weapon attacks is beset with uncertainties. Besides uncertainties that afflict all analyses of nuclear warfare (e.g., uncertainties in enemy targeting), others are peculiar to an analysis of fallout. Principal among the latter are--

- Uncertainties in fallout models, especially for many weapons detonated together in a target area;
- The sensitivity of fallout to weapon-burst heights and details of weapon design, and the uncertainty in enemy intentions or capabilities in these areas; and
- The variability of the wind.

Historically, the analytical treatment of fallout has often tended to one of two extremes: (1) either ignoring the problem and simply concentrating on the analytically better-understood

blast-damage calculations, or (2) assuming away the uncertainties and performing detailed calculations with a particular fallout model and particular wind patterns. Not only are both approaches suspect, but of greater concern from a practical standpoint is the fact that not much insight is gained into the actual fallout hazard.

It is the intent of this paper to develop simplified calculation procedures for fallout effects, in order to gain better insight into the nature of the problem. Hopefully, such insight will lead both to a better qualitative appreciation of why certain effects occur and, ultimately, to improved methods of defense against the fallout hazard. A subsidiary benefit will be to provide a basis for more simplified damage-assessment schemes.

The basic approach used here is to take one particular fallout model as a standard and to assess different situations by using this model. The model chosen was the "WSEG-10 NAS-modified" fallout model--not necessarily because it was the most physically accurate, but for the following dominating factors:

(1) The model format, which is convenient for the types of analysis performed here;

(2) The normalization of the model, which insures that the same total amount of fallout is deposited for any wind condition;

(3) The availability of meteorological wind statistics already processed to the form needed by the model;

(4) The relative simplicity of the model compared to some others;

(5) The previous use of this model in a number of other studies.

It is the author's opinion--and it will necessarily persist until future studies--that many of the qualitative conclusions of this paper would remain substantially the same (though some numerical values might differ somewhat) if other fallout models were studied. It is hoped that this paper will provide a means

of comparing models useful to Civil Defense in developing policies for dealing with the fallout hazard that are, hopefully, not too sensitive to fallout-model details.

Chapter I of this paper is primarily documentary. It describes the WSEG-10 Model and presents two approaches to obtaining a simplified model, one of which is based on obtaining asymptotic expressions and the other of which is based on direct curve fitting. Both methods provide a means for judging the basic sensitivities of the model and give the reader better insight into fallout patterns.

Chapter II addresses the problem of fallout patterns produced by groups of weapons. As has proved fruitful in the analysis of blast effects, the use of the concept of weapon density has allowed some simplified methods to be developed. Fallout patterns obtained when weapons are detonated in regular patterns are studied with the aim of developing simplified prediction schemes for fallout patterns likely with targets receiving many weapons, such as urbanized areas.

Chapter III addresses the probabilistic descriptions of wind data. The statistical wind data needed by the WSEG-10 fallout model are presented for the United States. The nature of the distribution functions of wind speed and wind angle are discussed.

In Chapter IV, wind statistics and the fallout model are combined in a Monte Carlo simulation that calculates fallout-dose distributions based upon input attack geometry and wind statistics. In this chapter the results for simple, idealized weapon geometries are presented; and the nature of the resulting dose distributions is discussed.

Chapter V presents fallout-dose distributions for hypothesized attack patterns in the United States. In these cases, the underlying geometry is complex enough that this chapter

concentrates upon illustrating the nature of the result for several different types of target environments.

This work was conducted under the general guidance of Mr. Neal FitzSimons, of the System Evaluation Division, Defense Civil Preparedness Agency, under Contract DAHC 20-70-C-0287. Appreciation is due to many people for providing the impetus for this study and for many helpful comments; but the author is especially grateful to Mr. James Anderson, Dr. David Benson, Dr. James Buchanan, Mr. Neal FitzSimons, Mr. James Jacobs, and Mr. Donald Hudson (all of the Defense Civil Preparedness Agency); to Mr. Ralph Mason, of the National Military Command System Support Center; and to Mr. Jack Greene.

Chapter I

DESCRIPTION OF THE WSEG-10 NAS-MODIFIED FALLOUT MODEL

In this chapter, the WSEG-10 Model is examined from several viewpoints. Section A documents the basic model by an abstract of the basic document defining it. Section B presents expressions simplified by dropping terms that generally have small influence--which is first done directly, and then in dimensionless form, and illustrates the very simple nature of the basic model before correction terms are added. Section C presents a numerical fitting of the model that yields a somewhat better, if mathematically less neat, approximation. Finally, Section D presents approximate expressions for the inverse function (i.e., to compute distances at which certain dose levels occur).

A. THE BASIC MODEL

The WSEG-10 Model[1] predicts the dose rate at H+1 hours by the following basic equation:

$$D_{H+1} = KAFf_d f_c \ ,$$

[1]The equations describing the WSEG-10 NAS-Modified Model were taken from the following reference: M. Polan, "An Analysis of the Fallout Prediction Models Presented at the USNRDL-DASA Fallout Symposium of September 1962, Volume I: Analysis, Comparison, and Classification of Models, U.S. Naval Radiological Defense Laboratory, USNRDL-TRC-68, September 8, 1966. The original definition of the model is contained in G. E. Pugh and R. J. Galiano, "An Analytic Model of Close-in Deposition of Fallout for use in Operational-Type Studies," Weapons Systems Evaluation Group, Research Memorandum no. 10, 15 October 1959.

where

D_{H+1} = dose rate in roentgens/hour at H+1 hours;[1]

K = a normalization factor, taken as 2×10^6 roentgens/hour/megaton/mile^2;

A = an adjustment factor for Height of Burst (HOB) effects (A = 1 for a surface burst);

F = fission yield of the weapon;

f_d = a downwind-distance shape factor;

f_c = a crosswind-distance shape factor.

The two shape factors are normalized so that their integrals are unity. That is, if x represents downwind distance and y crosswind distance, then

$$\int_{-\infty}^{\infty} f_c(y)dy = 1 \ ,$$

---

[1] In a physical interpretation of the model, D_{H+1} is defined as the gamma dose rate from radioactive fallout in roentgens/hour at one hour after a weapon detonation—assuming that all of the fallout that will be deposited at the point in question has already arrived. The dose rate is that which would apply to a point 3 feet above a smooth infinite plane in the air at standard conditions. (This dose does not include beta radiation, which could cause significant effects on plants and animals but which can be easily protected against by humans.) The physical interpretation of D_{H+1}, when all the fallout is not deposited at one hour, is somewhat more difficult; it is the radiation rate from those particles that will be deposited in fallout that would have occurred if they were in fact all deposited at one hour. Within the confines of this report, such difficulties are avoided by restricting attention to a "radiation rate" which is defined through the mathematical equations in the model and studying the mathematical properties of this "radiation rate." Thus, for example, the "radiation rate" at any time, D(t), is given by $D(t) = D_{H+1}t^{-1.2}$ in the model. From this viewpoint, D_{H+1} is simply stated as the constant of proportionality, which multiplies $t^{-1.2}$ to obtain the model "radiation rate."

The definition of the dose rate is in an idealized situation. Thus, the doses predicted by the model do not include any factors that might modify doses measured or received in a real situation (e.g., instrument response factors, terrain shielding, weathering of radiation, shielding by structures, biological response factors, etc.). Except for one formalized integration of dose rate to obtain a particular type of biological response factor (to be described shortly), all such considerations are extraneous to the model and are not considered here.

$$\int_{-\infty}^{\infty} f_d(x)dx = 1 \ .$$

This normalization and separation of downwind- and crosswind-distance effects renders the model tractable to simplification or modification without gross errors in overall amounts of fallout deposited, as long as the normalization is preserved. The value K is the basic normalization used to determine the total fallout deposited. It has units of roentgen per hour per megaton (MT)/statute mile^2. Discussions of the total amount of fallout deposited by a weapon can be centered upon assigning numerical values to K; a value of 2×10^6 is typical--and the value used here.[1]

The model can most readily be described in terms of parameters to which physical interpretation is given, although in reality the physical interpretation may be quite tenuous. A characteristic time T (hours) over which the rate of deposition has fallen to 1/e of its original value is defined by

$$T = 1.0573203\left[12\frac{H_c}{60} - 2.5\left(\frac{H_c}{60}\right)^2\right]\left[1 - 0.5\exp\left(-\left(\frac{H_c}{25}\right)^2\right)\right],$$

with H_c being the "effective cloud height" in kilofeet, where

$$H_c = 44 + 6.1\log_e Y - 0.205(\log_e Y + 2.42)\,|\log_e Y + 2.42| \ ,$$

where Y is the yeild in megatons.

A distance L is defined, which is basically the distance that fallout is blown downwind in the time T (i.e., $L \approx WT$, where W is "effective fallout wind" velocity). The definition of activity is then given by

---

[1]The fallout considered by this model is only the "local" fallout deposited in a more or less coherent pattern downwind of the weapon. It does not include the radioactivity that goes into the upper atmosphere and travels for long distances and times before reaching the earth's surface (i.e., "worldwide" fallout).

$$f_d \approx \begin{cases} 0, & \text{if } x < 0 ; \\ \frac{1}{L} \exp(-x/L) , & \text{if } x \geq 0 , \end{cases}$$

with corrections added for several effects (e.g., cloud diameter). These corrections, somewhat complicated in form, are as follows:

Call σ_o an "effective cloud radius" in miles, where

$$\sigma_o = \exp\left(0.7 + (\log_e Y)/3 - 3.25\Big/\left(4.0 + (\log_e Y + 5.4)^2\right)\right) .$$

Call

$$L_o = WT ,$$

and define

$$\sigma_d^2 = \sigma_o^2 \frac{L_o^2 + 8\sigma_o^2}{L_o^2 + 2\sigma_o^2} .$$

Define n by

$$n = \frac{L_o^2 + \sigma_d^2}{L_o^2 + 0.5\sigma_d^2} ,$$

and define L by

$$L = \left(L_o^2 + 2\sigma_d^2\right)^{\frac{1}{2}} .$$

Define g(x) by

$$g(x) = \frac{1}{L\Gamma\left(1 + \left(\frac{1}{N}\right)\right)} \exp -\left(\frac{|x|}{L}^n\right) ,$$

where $\Gamma(\cdot)$ is the gamma function. Values of n are close to one, so g(x) is close to the approximate expression for f_d as given above. The actual value of f_d is g(x) multiplied by $\varpi(x)$, where

$$\varpi(x) = \text{cumnor}\left(\frac{L_o x}{L\alpha_1\sigma_d}\right) .$$

The cumulative normal function in effect shapes f_d near ground zero, to give an appropriate rise to a maximum value. The empirical adjustment factor α_1 is given by

$$\alpha_1 = \frac{1}{1 + \frac{0.001\ H_c W}{\sigma_o}} .$$

f_d is then given by $f_d = \varpi(x)g(x)$.

In the model, it is assumed that the crosswind activity is distributed normally[1]--i.e.,

$$f_c = \frac{1}{\sqrt{2\pi}\sigma_c} \exp\left(-\tfrac{1}{2}\left(\frac{y}{\alpha_2 \sigma_c}\right)^2\right) .$$

The spread of the cloud is controlled by the parameter σ_c, which in turn is primarily sensitive to "crosswind shear" S_c, in mph/kilofoot of altitude. σ_c is computed by

$$\sigma_c^2 = \sigma_o^2 + B\sigma_o^2 + 2\left(\frac{\sigma_d T \sigma_H S_c}{L}\right)^2 + \left(\frac{(x + 2\sigma_d) L_o T \sigma_H S_c}{L}\right)^2$$

where

$$B = \min\left(\frac{8|x + 2\sigma_d|}{L}, 3\right) ;$$

$$\sigma_H = 0.18 H_c .$$

The factor α_2 is given by

$$\alpha_2 = \frac{1}{1 + \frac{0.001\ H_c W}{\sigma_o}\left(1 - \text{cumnor}\left(\frac{2x}{W}\right)\right)} .$$

---

[1]To preserve normalization, α_2 should have been in the denominator of the fraction before the exponential expression in the equation for f_c. However, since conventional use of the WSEG-10 Model has been with the equation as shown, this practice is adopted in this report. For most conditions, the reduction in the effective "k-factor" is small, or the error introduced is well within the error in knowledge of this value.

Finally, to complete the description of the model, an equivalent residual dose is computed. This dose is intended, in the model, to represent a measure of radiation effects causing acute injury or fatalities to humans. This computation assumes fallout decays in time as $t^{-1.2}$, when t is the time from the weapon detonation. It is assumed a fraction x (10%) of the dose is "irreparable," while the effect of the "reparable" part delays exponentially with a time constant Y (= 30 days). Thus we have, to define B(t) formally,

$$D(t) = x \int_{t_a}^{t} D_{H+1}\, \tau^{-1.2}\, d\tau + (1-x) \int_{t_a}^{t} D_{H+1}\, \tau^{-1.2}\, \exp\Big(-K(t-\tau)\Big) d\tau \ ,$$

where t_a is the time of fallout arrival. t_a is given by

$$t_a = \left(0.25 + \frac{L_o^2 (x + 2\sigma_d)^2 T^2}{L^2 (L_o^2 + 0.5\sigma_d^2)} + \frac{2\sigma_d^2}{L_o^2 + 0.5\sigma_d^2} \right)^{\frac{1}{2}} .$$

The dose, D, is taken as the maximum value of D(t) and will be expressed in units of ERDs, standing for "Equivalent Residual Dose."[1] If R is defined as the ratio of D/D_{H+1}, then

---

[1]The term "Equivalent Residual Dose" is the preferred term for the expression D(t); and "Maximum Equivalent Residual Dose," for the value D(= max D(t)). (See, for example, "Radiological Factors Affecting Decision Making in a Nuclear Attack," National Council for Radiation Protection and Measurement, NCRP Report no. 42, 15 November 1974.) This value is to be considered as a measure of the radiation effects from the gamma radiation. (Beta radiation might also be present; but it is not included in the dose--even though it may contribute significant damage to crops and animals--since humans can readily protect against the acute injury or fatalities the radiation could cause in fallout.) This measure is clearly not a measure of some type of biological radiation effect (e.g., long-term effects on humans) and has been questioned as the most appropriate measure of radiation effects even for its intended purpose. Independently of these questions, it is used as part of the formal WSEG-10 Model since it is tractable to analytical manipulation. (In the Polan document defining WSEG-10, the value D is called the "Maximum Effective Biological Exposure"; and the expression "Biological Dose" is sometimes used as a shorthand means of expressing D. However, used in a not precisely defined context, this term could lead to confusion.) From the defining equation the units of D are (Roentgens/hr)(hr) or Roentgens (the fraction x is dimensionless). (continued on next page)

we have[1]

$$R = D/D_{H+1} = \exp\left(-0.287 + 0.52 \log_e\left(\frac{t_a}{31.6}\right) + 0.04475 \log_e\left(\frac{t_a}{31.6}\right)^2\right) .$$

This completes the formal definition of the model. In the version implemented by the NMCSSC,[2] the height adjustment factor A for the height of burst (HOB) is taken as the fraction of the fireball intercepting the ground and is given by

$$A = \begin{cases} 1, & \text{if } a = 0 ; \\ 0.5(1 - a)^2(2 + a) + 0.001a, & \text{if } 0 \leq a \leq 1 ; \\ 0, & \text{if } a > 1 , \end{cases}$$

where $a = HOB/180(1.000Y)^{0.4}$.

In a recent report,[3] amongst other issues the value of k-factor and the effects of height of burst were restudied. The following procedure, based upon this recent report, is currently recommended by DCPA. When a weapon is detonated above ground but in contact with urban structures or trees, the recommended value of k-factor including higher-of-burst corrections is

$$K_1 = \exp(7.565 - 1.599 \times 10^{-2}\lambda) ,$$

(cont'd) However, due to the special nature of the calculation, a particular name as the measure of the Maximum Equivalent Radiation Dose is convenient. In NCRP Report 42, the term ERD is used as such a measure. In subsequent parts of this report the name dose will mean Maximum Effective Residual Dose, and its units will be ERDs.

[1]If the doses from many weapons are to be added, it must be assumed that the weapons are detonated simultaneously; or, more precisely, the difference in detonation time is small compared to the time constant K.

[2]Ralph B. Mason, *Single Integrated Damage Analysis Capability (SIDAC) Analytical Manual* (U), National Military Command System Support Center, CSMAM67-68, 18 October 1968.

[3]Response to DCPA Questions on Fallout, DCPA Research Report no. 20, prepared by Subcommittee on Fallout, Advisory Committee on Civil Defense, National Academy of Sciences, with Notes and Comments by J. C. Greene, DCPA, November 1973.

where $\lambda = h/W^{1/3}$, with h = height of burst (feet) and W = total yield (kilotons) for values of λ up to 100, and the value at $\lambda = 100$ (i.e., 0.202) for values of λ greater than 100. If a weapon is detonated above ground and not in contact with extraneous material, the above equation is to be used for values of λ up to 180, and a value of 0 is to be used for higher values of λ.

B. ASYMPTOTIC EXPRESSIONS FOR THE MODEL

If the wind is assumed to be variable, the deposition of fallout as a function of wind velocity will also vary, as illustrated in Figures 1 and 2, where dose along a pattern centerline as a function of downwind distance is presented for a variety of winds.[1] In these figures, the dose is scaled by dividing by the yield, since more yield independent values are obtained. In all the figures of this chapter, a fission fraction (i.e., the ratio of fission yield to total yield of a weapon) of 1 is assumed for simplicity.

Evidently, a simple model might be considered when variations due to wind statistical fluctuations are a part of the overall assessment. An obvious simplification is to replace the expression for f_d by a simple exponential function--i.e., set

$$f_d = \begin{cases} \frac{1}{L} \exp(-x/L), & \text{if } x \geq 0 ; \\ 0, & \text{if } x < 0 , \end{cases}$$

and

$$L = WT ;$$

[1]The dose at zero crosswind distance will be called "centerline dose."

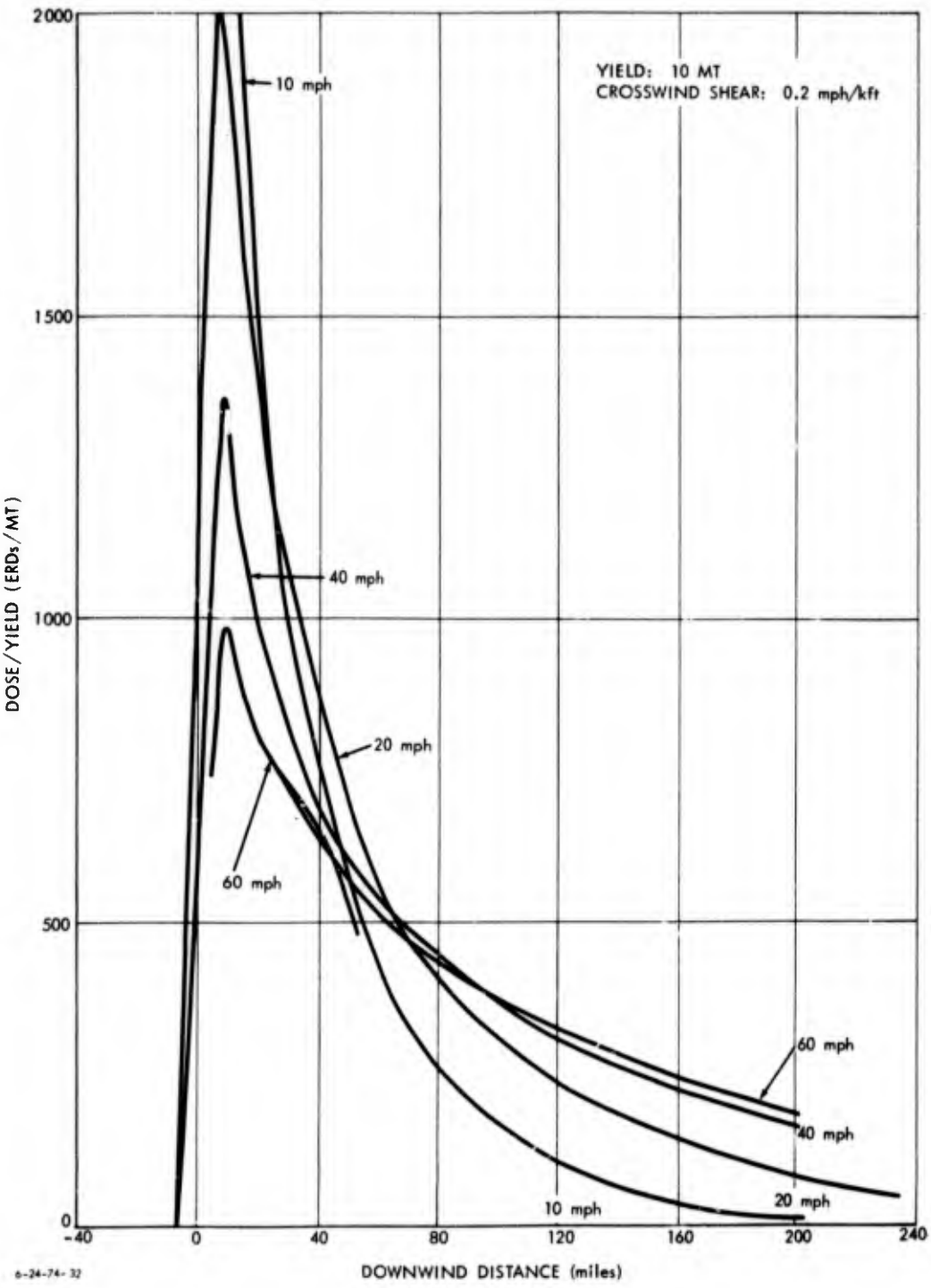

Figure 1. CENTERLINE DOSE/YIELD AS A FUNCTION OF DOWNWIND DISTANCE

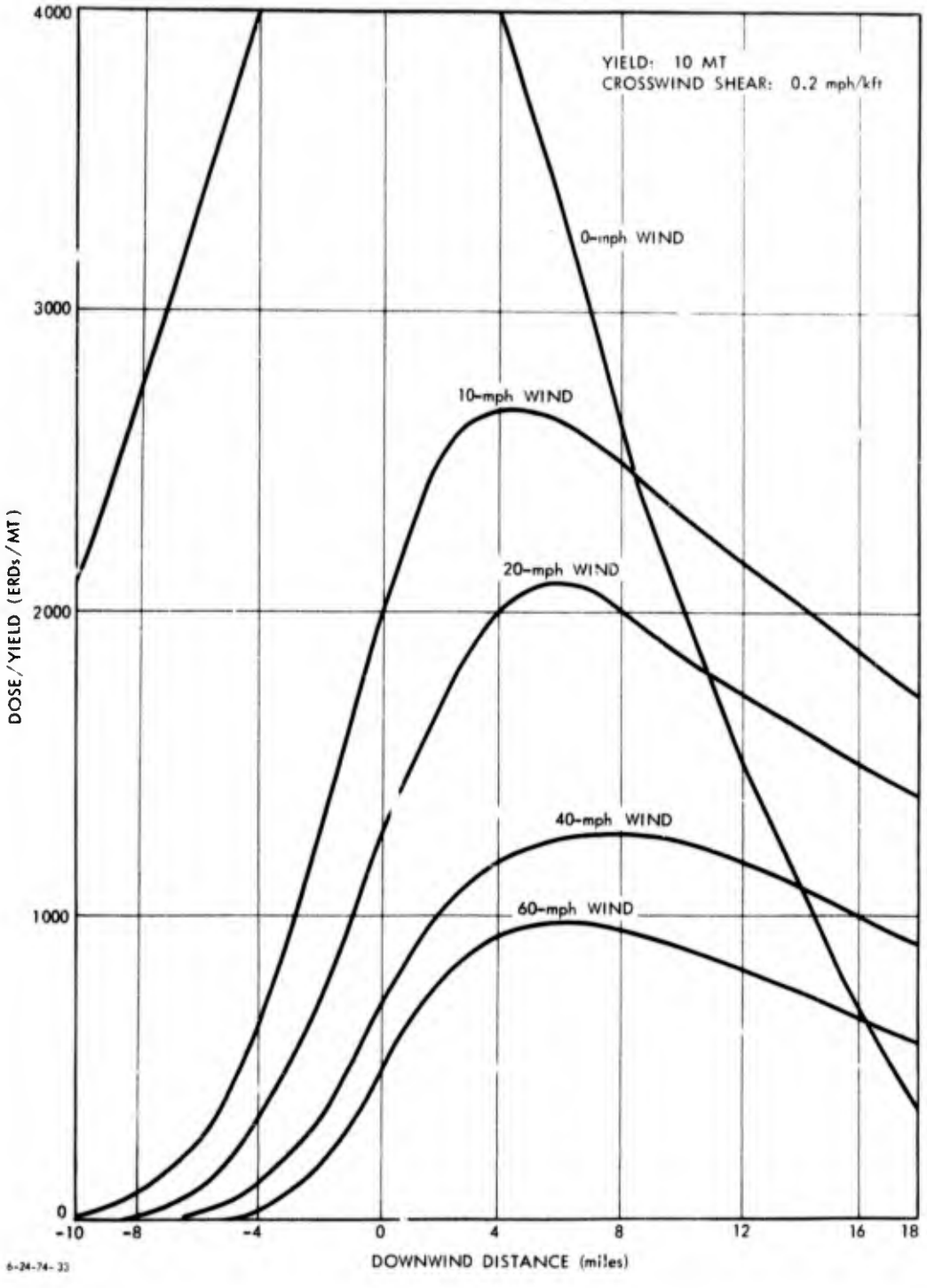

Figure 2. CENTERLINE DOSE/YIELD AS A FUNCTION OF DOWNWIND DISTANCE

then

$$f_d = \begin{cases} \frac{1}{WT} \exp(-x/WT), & \text{if } x \geq 0 ; \\ 0, & \text{if } x < 0 . \end{cases}$$

The characteristic time is a function of yield only. It is plotted in Figure 3 for several values of yield. T will be approximated by the line shown in the figure--i.e.,

$$T = 7.5 + 1.66 \log_{10} Y$$

for yields between 1 and 20 MT.

For studying effects near ground zero, it may be desirable to have a linear rise in f_d that starts at a distance d upwind and terminates at a distance x_c downwind. If d is given, x_c may be chosen to preserve normalization of f_d. To do this normalization, assume the change in slope of the exponential form for f_d is small for $x < x_c$, which can be done if $d << L$. Then, equating area gained under the linear portion of f_d to the area lost under the exponential gives

$$x_c = \frac{d}{1 + d/WT} .$$

Thus, f_d has the form

$$f_d = \begin{cases} 0, & \text{if } x < d ; \\ \frac{x-d}{WT_d\left(2 + \frac{d}{WT}\right)}, & \text{if } d \leq x < x_c ; \\ \frac{1}{WT} \exp(-1/WT), & \text{if } x_c \leq x . \end{cases}$$

A value of d may be chosen by observing that the rise in f_d is controlled mostly by the cumulative normal function, which has standard deviation σ_d, and that a linear fit to the cumulative normal at the origin has slope $1/\sqrt{2\pi}\sigma_d$. Thus, a line starting at $1.25\sigma_d$ would give a reasonable value of d.

From Figure 3, it can be seen that σ_d is given approximately by

$$\sigma_d = 1.75 + 2.35 \log_{10} Y \ .$$

For Y = 10 MT, we have $\sigma_d = 4.12$, to give d = 5.2. As can be seen from Figure 2, a line rising from this distance upwind gives a reasonable fit. An empirical fit for upwind-distance variability due to wind is

$$d = 6 - W/40$$

for 10 MT. For other yields, these distances are multiplied by the rate of change of σ_d with yield so that

$$d = \left(6 - \frac{W}{40}\right) \frac{1.75 + 2.35 \log_{10} Y}{4.10} \ .$$

When values of σ_c are plotted as a function of downwind distance, they are found to be almost linear. Moreover, the slopes are almost proportional to S_c/W. Thus, the variation of σ_c is readily given by a series of straight lines. We have

$$\sigma_c = A + \frac{BS_c x}{W} \ ,$$

with $A = 2 + 3 \log_{10} Y$; $B = 7.5 + 1.5 \log_{10} Y$. For values of x comparable to L and nominal values of S_c (= 0.2) and W (= 20 mph), the constant term becomes relatively small.

In this case, we have

$$f_c = \frac{W}{2\pi S_c x B} \exp\left(-\tfrac{1}{2}\left(\frac{yW}{xBS_c}\right)^2\right) .$$

It is interesting to observe that, at a constant angle from the downwind direction, the fractional decrease in dose due to crosswind distance is constant.

The time of arrival can be approximated by

$$t_a = \left(0.25 + \left(\frac{x}{W}\right)^2\right)^{\frac{1}{2}} .$$

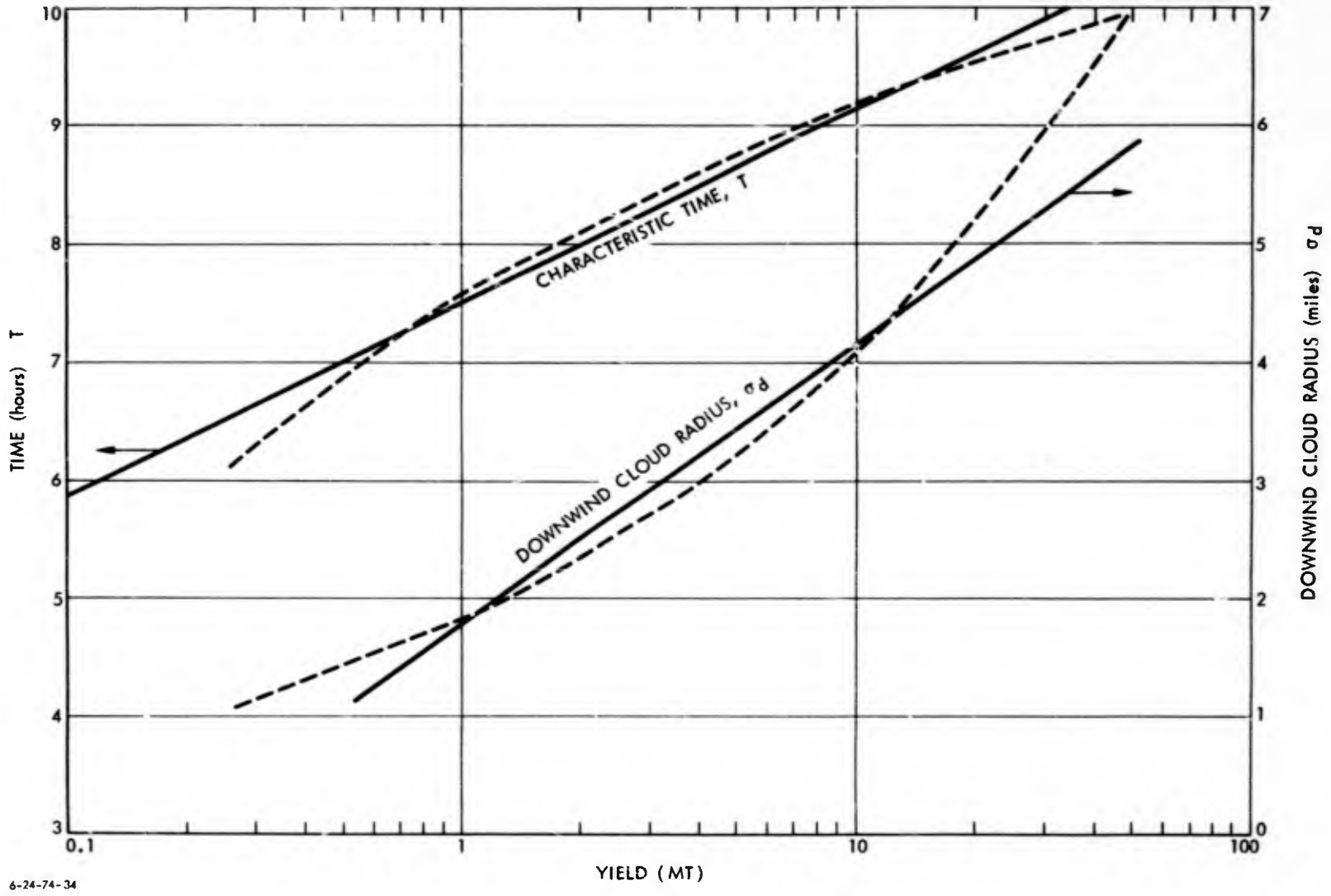

Figure 3. CHARACTERISTIC TIME (T) AND DOWNWIND CLOUD RADIUS (σ_d) AS FUNCTIONS OF LOGARITHM OF YIELD

For appreciable downwind distances, the constant term is small and we have

$$t_a = \frac{x}{W} .$$

As shown in Figure 4, the ratio of dose to H+1 dose rate R can be given by

$$R = 2.71 t_a^{-0.382} .$$

From Figure 4, the time when the equivalent residual dose reaches a maximum is equal to $120t^{0.3}$ hours. It is instructive to combine the various terms for an overall equation applicable for appreciable upwind distances. The dose is

$$D = AKF \frac{2.71}{\sqrt{2\pi}BT} \frac{W^{0.382}}{S_c} \frac{\exp(-x/WT)}{x^{1.382}} \exp\left(-\tfrac{1}{2}\left(\frac{yW}{xBS_c}\right)^2\right) .$$

Dividing by the fission yield F gives a dose normalized per megaton of fission yield. The yield dependence of the normalized dose is in the terms B and T. Increases in these terms cause spreading of the pattern in the crosswind and downwind directions. This spreading is compensated for by the product BT in the denominator of the first term, which decreases the normalized dose in proportion to the spreading.

The term $W^{0.382}$ indicates an increase of normalized dose with wind velocity--which occurs because of the earlier arrival of particles (at a given distance downwind) that increases the ratio of dose to H+1 dose rate, even though the H+1 dose rate is constant.

The dose is inversely proportional to wind shear S_c, since the shear directly affects the overall spread of the pattern.

The variation downwind is reflected by the term $\exp(-x/WT)/x^{1.382}$, which gives a decrease with downwind distance appreciably more rapid than exponential. This more rapid decrease results

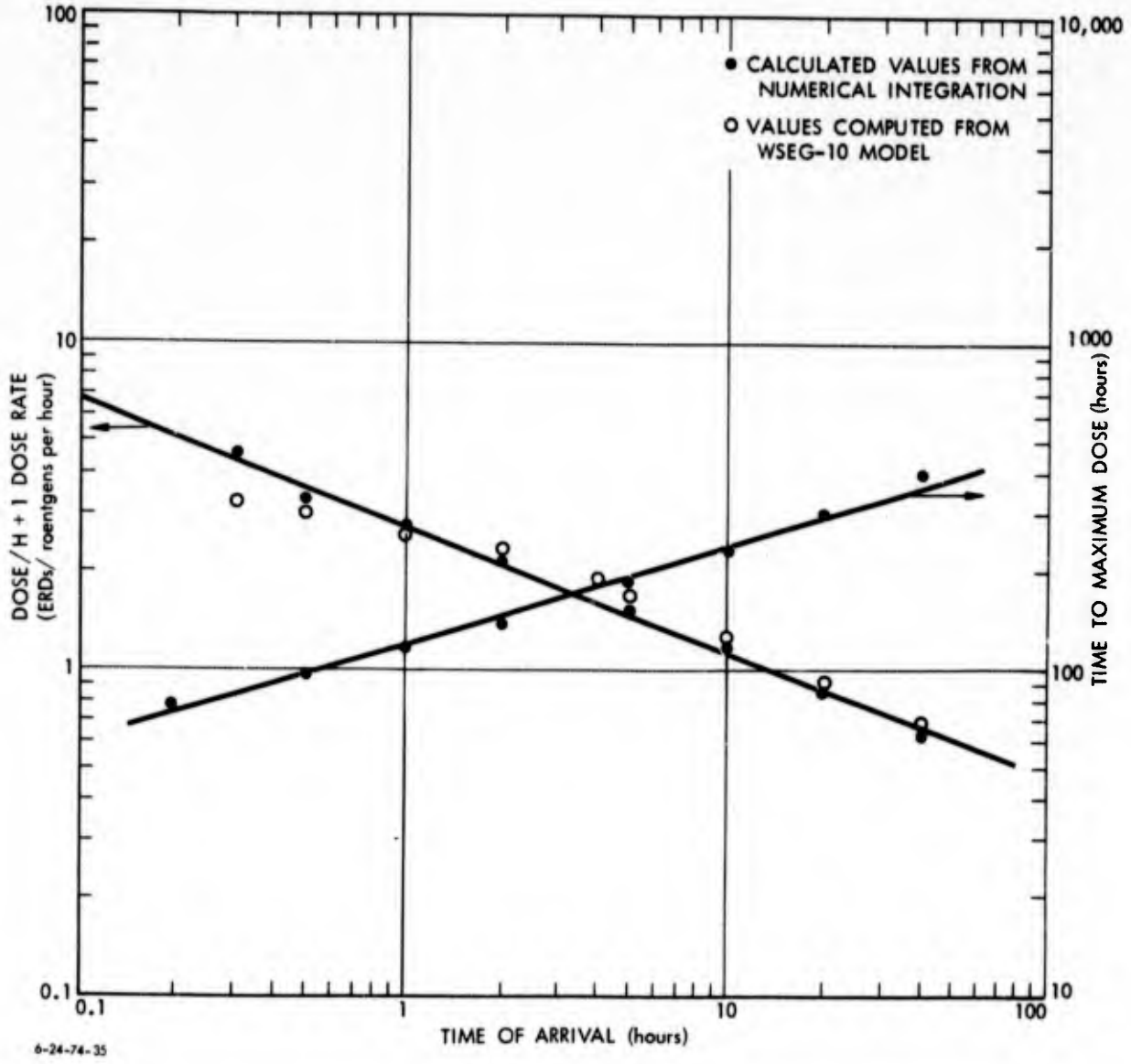

Figure 4. RATIO OF DOSE TO H+1 DOSE RATE, AND TIME TO MAXIMUM DOSE, AS FUNCTIONS OF TIME OF ARRIVAL (t_a)

partly from a spreading of the pattern due to wind shear (which introduces a factor of x^{-1}) and partly from longer arrival time (which reduces the ratio of dose to H+1 dose rate and which introduces a factor of $x^{-0.382}$).

Finally, the crosswind spread is controlled by the factor $(y/x)(w/s_c)$. As mentioned earlier in this section, at a constant angle from the directly downwind direction the attenuation due to crosswind distance is constant. In the last equation (above), the angle is seen to be proportional to wind velocity divided by wind shear--as should be expected.

The effect of wind velocity is difficult to determine directly, since the wind enters in several terms. In Figure 5, the dose is presented as a function of wind velocity. This figure is calculated from the full model, not from the approximate equations given here. Of interest is that at appreciable distances there is very little variation of dose with wind velocity over a considerable range of velocities. At these distances, the prime sensitivity of dose can be expected to be to wind direction (which changes the crosswind distances from the hot line), not to wind speed (which changes values on the hot line). The rapid decrease at ground zero and at 20 miles downwind is due to higher winds blowing the activity farther downwind. At still farther distances, the spreading of the pattern to attenuate the dose is compensated for by the arrival of more fallout. For each wind velocity, Figure 5 presents curves that show the dose that occurs both at a downwind distance equal to the characteristic length WT and at about four times this length.

Further simplifications in appearance can be found by defining some dimensionless variables. One such form is given by defining $L = WT$; $C = BS_c$; $\xi = x/L$; and $\eta = y/c$. Then

$$\frac{DCL}{FK} = \frac{2.71}{\sqrt{2\pi}} \frac{1}{T^{1.382}} \frac{\exp(-\xi)}{\xi^{1.382}} \exp\left(-\tfrac{1}{2}\left(\frac{\eta}{\xi}\right)^2\right)$$

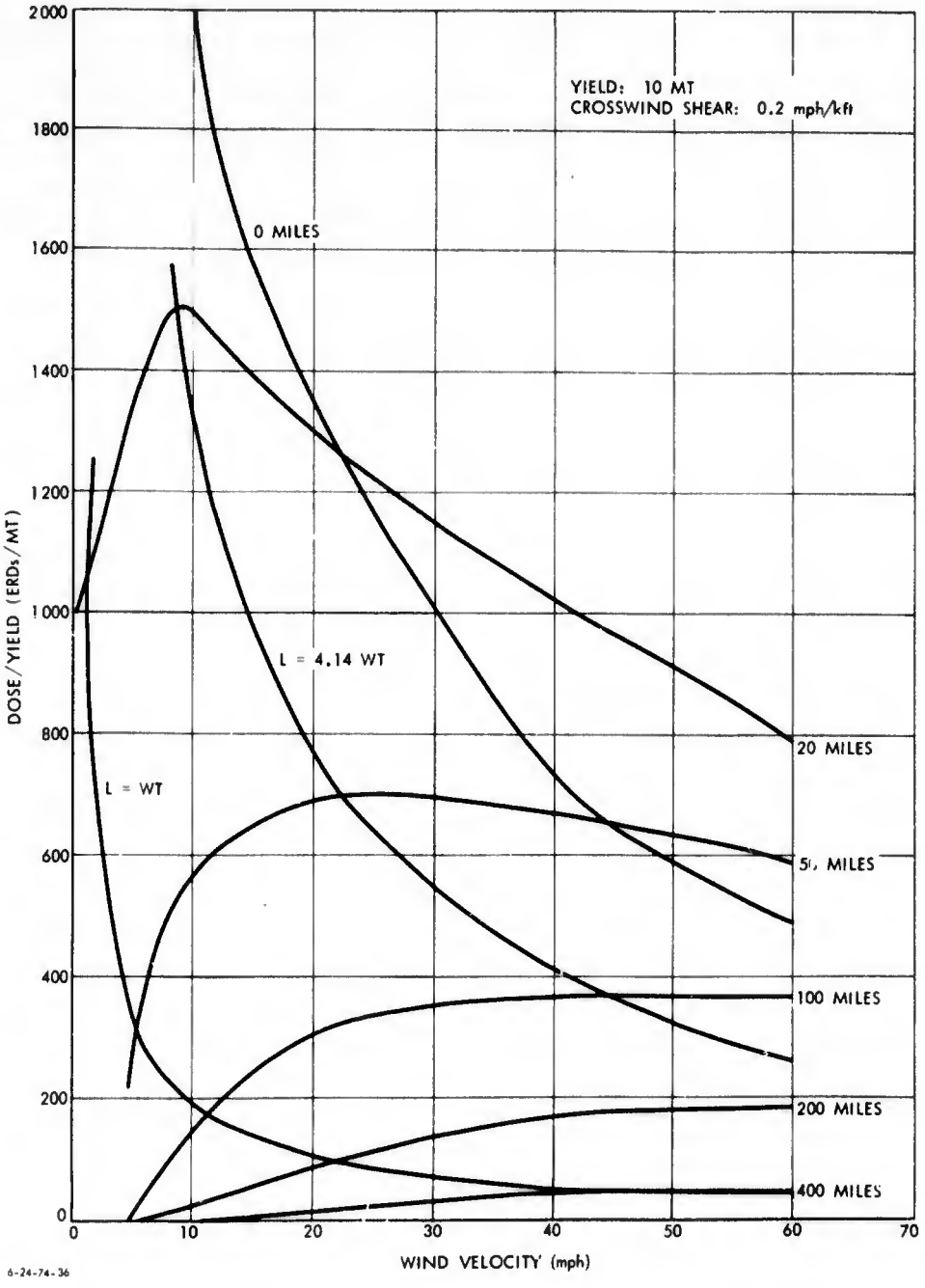

Figure 5. CENTERLINE DOSE DOWNWIND AS A FUNCTION OF WIND VELOCITY, AT SEVERAL DOWNWIND DISTANCES

or

$$\frac{DWS_c}{AF} = 2.16 \times 10^6 \frac{1}{BT^{1.382}} \frac{\exp(-\xi)}{\xi^{1.382}} \exp\left(-\tfrac{1}{2}\left(\frac{\eta}{\xi}\right)^2\right) .$$

Here at constant scaled values of ξ and η the dose is inversely proportional to wind and shear value. The scaled distances, however, are affected by wind and shear. The yield dependence is subsumed in the term $1/BT^{2.382}$. Values of the constant (2.16×10^6) times this term are 2,360 for 1 MT and 1,200 for 10 MT. This form is attractive for rapid calculation. A rational approximation for

$$f(\xi) = \frac{\exp(-\xi)}{\xi^{1.382}}$$

is

$$f(\xi) = \frac{1}{(0.4555+0.80313\xi-0.007562\xi^2+0.89185\xi^3+0.00103345\xi^4)^4} .$$

The percent error between the exact value of this expression and the approximation is shown in Figure 6. For values of ξ between 0.1 and 10, the error is less than 18 percent. This approximation is similar to the exponential approximation given by Hastings,[1] which is

$$\exp(-x) = \frac{1}{(1 + a_1x + a_2x^2 + a_3x^3)^4} ,$$

where $a_1 = 0.2507213$; $a_2 = 0.0292732$; and $a_3 = 0.0038278$. This approximation has a maximum fraction error of seven percent for x between 0 and 10. Because of the constant term in the denominator, this approximation could not be expected to give

[1]Cecil Hastings, "Approximation for Digital Computers" (Princeton, N.J.: Princeton Univ. Press, 1955).

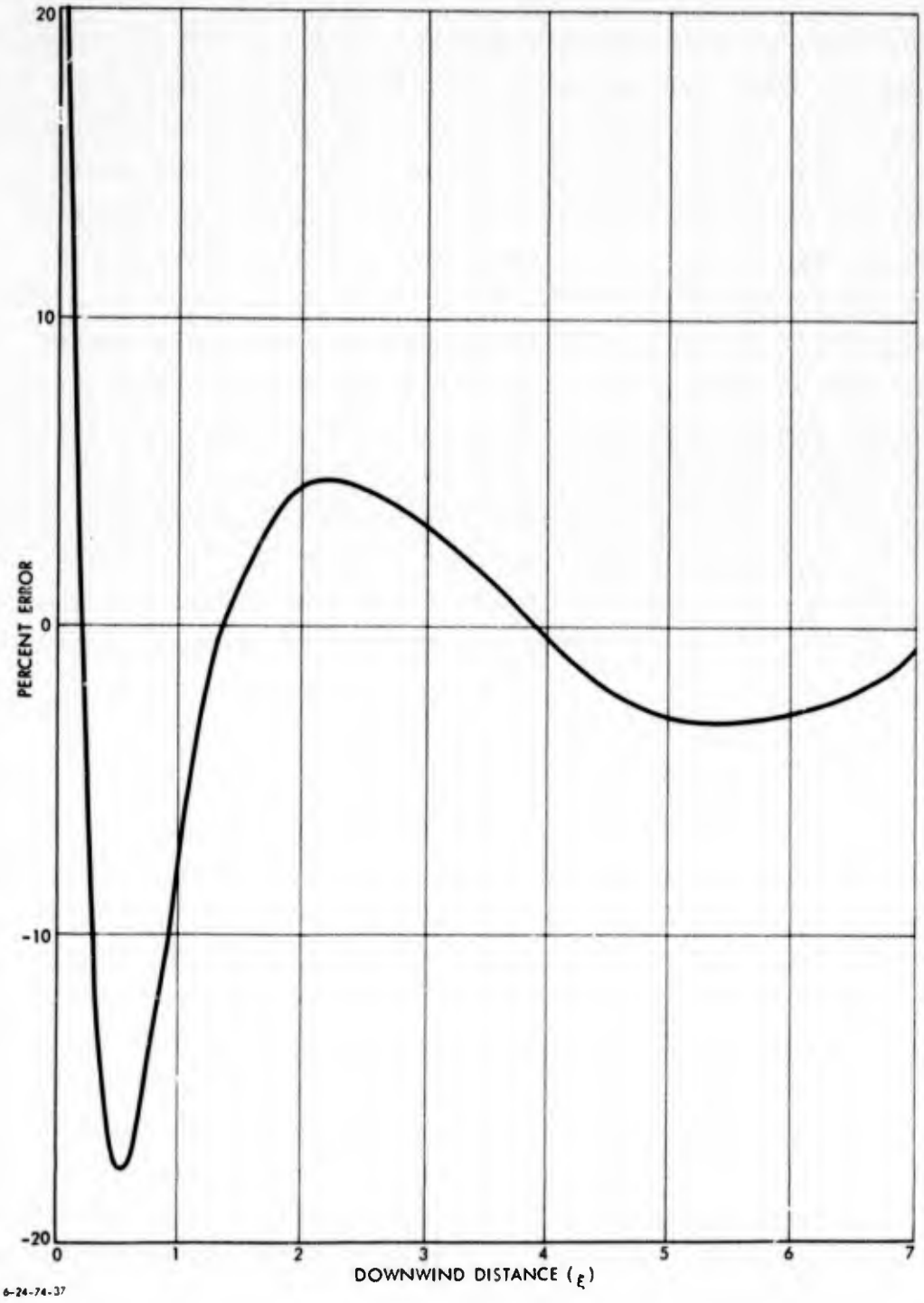

Figure 6. PERCENT ERROR IN FIT TO DOWNWIND-DISTANCE CALCULATION

low percent error for $f(\xi)$ as x approaches zero.[1] However, close enough to $\xi = 0$, the approximate expression is inoperative.

The role of wind becomes clearer from the dimensionless description. As wind is increased, the pattern is spread out in proportion to the wind, with the dose being proportionately reduced. The effect of shear is the same in the crosswind direction. It is necessary, then, to scale the intensities inversely proportional to pattern area as the pattern size changes to conserve the total deposition. The degree to which this compensation is accomplished in the exact calculations is illustrated in Figure 7, where for several wind speeds, dose times wind speed is plotted as a function of distance divided by wind speed. At greater distances the compensation is quite good; however, near ground zero the deviations increase. Moreover, as the wind speed approaches zero, other factors (e.g., cloud size) control the pattern spread--as is illustrated by the more appreciable departure of the 5-mph curve from the others.

C. A DIRECT FITTING OF THE MODEL

An alternative means of approximating the model is through direct numerical approximations to the calculated dose. This approach results in somewhat better accuracy over a larger range of parameters than does the method of the previous section, while still providing for rapid calculations and illustrating some sensitivities of the model better than plots of fallout contours. The significance of the correction factors ignored in Section B (above) is seen more directly here. The range of the fit is for winds from 0 to 80 mph, yields from 0.2 to 30 MT, and wind shear from 0 to 1.6 mph/kft. The approximations were developed by plotting dose from the model under a

[1] In fact, no rational expression could yield a good approximation for both infinitesimal and finite values of x. An expression, for example, yielding less than 15 percent error for $0.005 \leq x \leq 0.2$ is $f(\xi) = 1/(.145 + 3.2\xi^2)$.

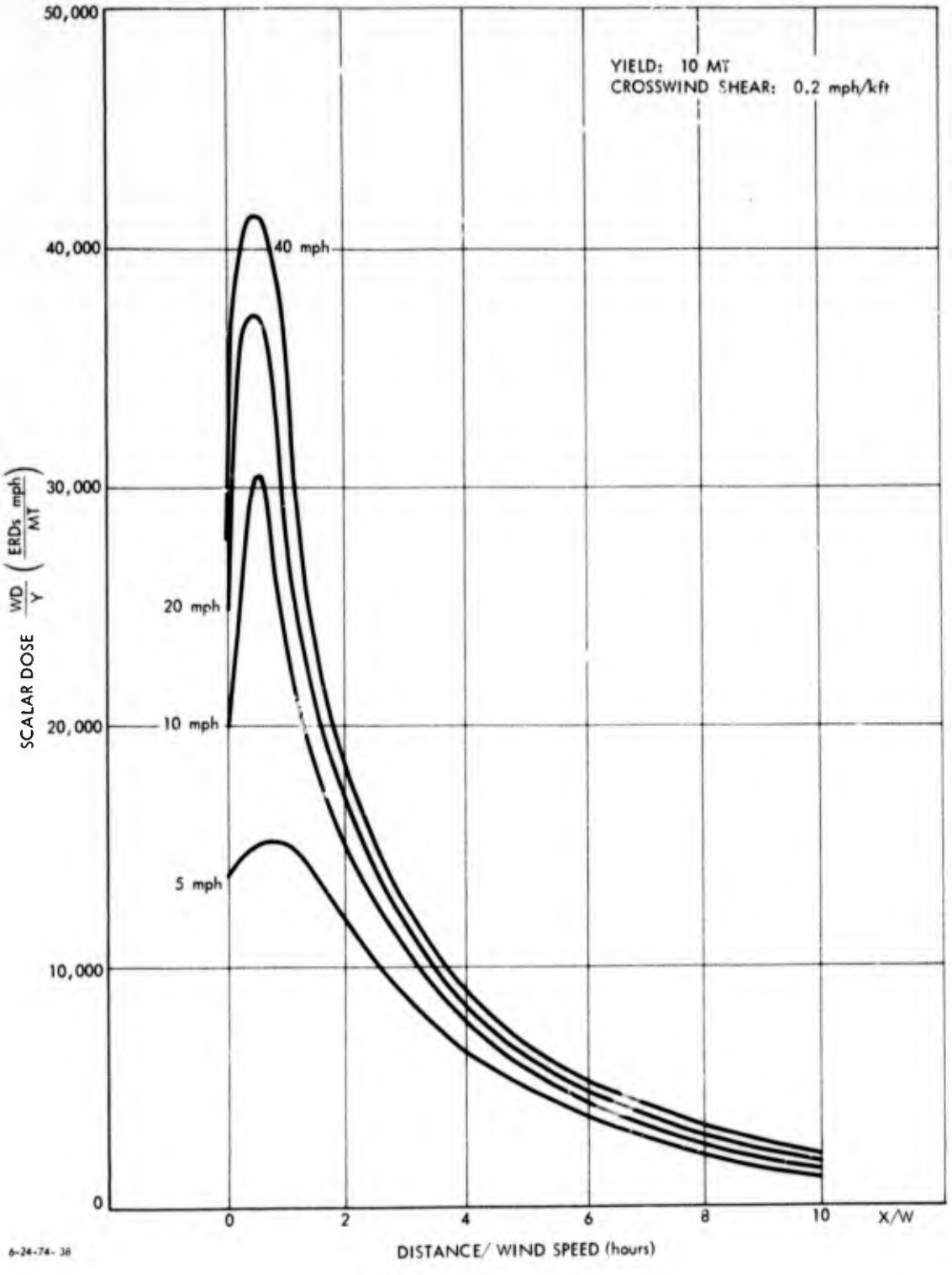

Figure 7. CENTERLINE DOSE TIMES WIND SPEED, AS A FUNCTION OF DISTANCE/WIND SPEED

variety of conditions and attempting to find a means of correlating them. The fits are made separately to $\bar{f}_d \left(= f_d R f_c(0)\right)$ and $\bar{f}_c \left(= f_c(y)/f_c(0)\right)$. (Since crosswind distance does not affect times of deposition in the model, the separability of downwind and crosswind effects is not changed when dose rather than H+1 dose rate is used.) A plot of log f_d as a function of distance is given in Figure 8. For winds greater than 3 mph and distance $\bar{\xi} = x/W$ greater than 3, we have

$$\log_{10} \bar{f}_d = \alpha + \beta \bar{\xi} \ .$$

For $\bar{\xi} < 15.6$, a correction factor of $0.0015(\bar{f}-15.6)^2$ is added to the right-hand side.

α is given by

$$\alpha = \alpha_y + \alpha_w \ ,$$

where $\alpha_y = 5{,}495 - 0.1099 \log_{10} Y + 0.018 \left(\log_{10} Y\right)^2$; $\alpha_w = -0.995$. For β, we have

$$\beta = -0.0641 + 0.0139 \log_{10} Y - 0.0033 \left(\log_{10} Y\right)^2 \ .$$

It is of interest to notice that the yield dependence is almost linear in log Y. Furthermore, if the coefficient for α_w were exactly 1, then the value of $\bar{f}_d$ would be inversely proportional to wind speed--as in Section B (above). Finally, it should be noticed that in mathematical form as the distance becomes large this empirical fit does not asymptotically approach that of the previous section.

The crosswind factor f_c is computed as in the model but with σ_c given by

$$\sigma_c = A + B \frac{S_c x}{W} \ ,$$

with $A = 2 + 1.7309 \log_{10} Y + 1.269 \left(\log_{10} Y\right)^2$; and $B = 7.55 + 1.8714 \log_{10} Y - 0.3314 \left(\log_{10} Y\right)^2$. This fit for σ_c is comparable

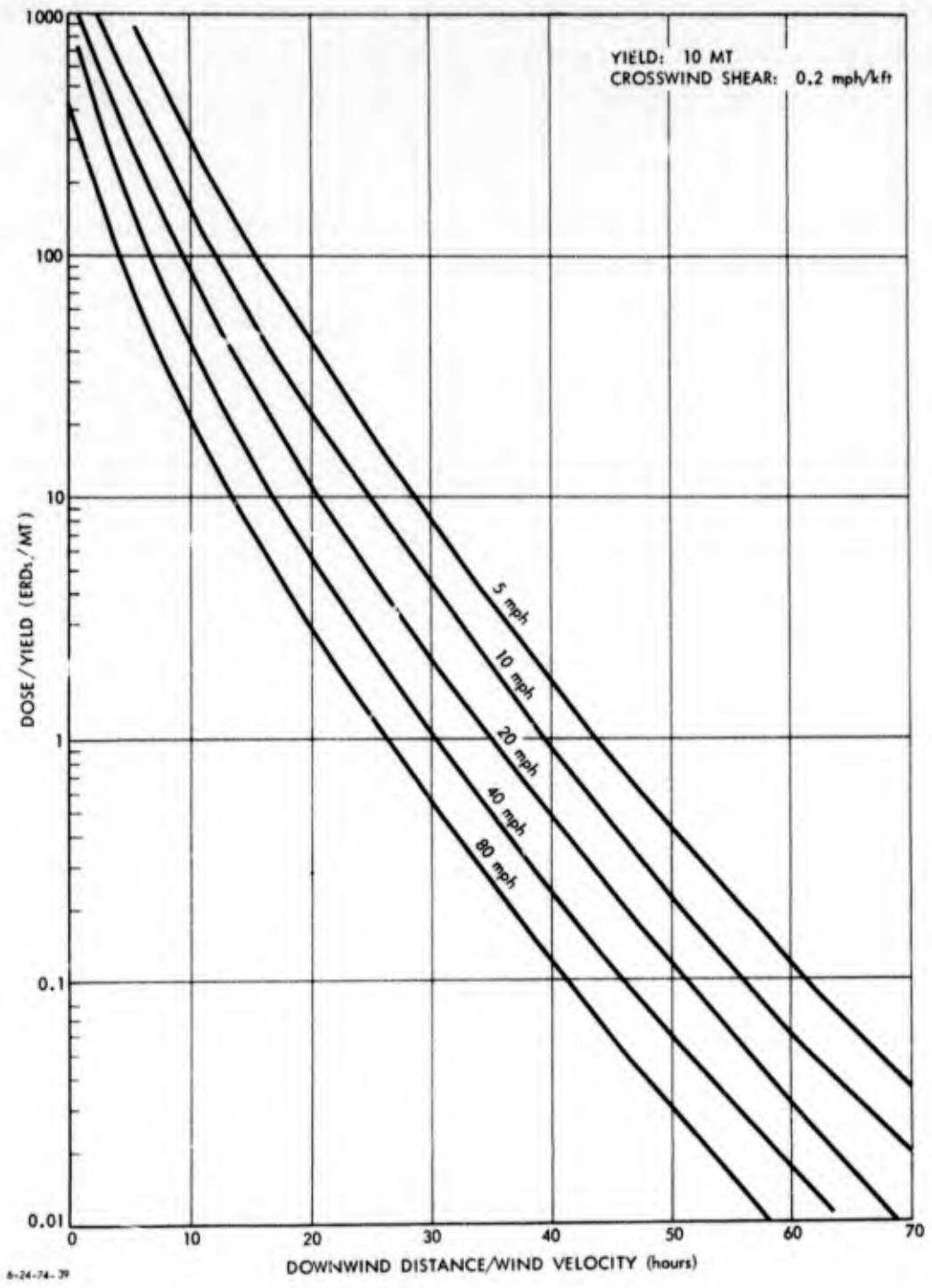

Figure 8. LOGARITHM OF SCALED CENTERLINE DOSE ($\bar{f}_d$) AS A FUNCTION OF SCALED DISTANCE, FOR SEVERAL WIND SPEEDS

to that of the previous section, but here the yield variation is parabolic instead of linear. A plot of σ_c as a function of distance is given in Figure 9. The dose is then calculated as

$$D = AFK\bar{f}_d\bar{f}_c \ .$$

For scaled distances less than 1.0 but winds greater than 3 mph, the following fit is used for $\bar{f}_d$: Let

$$K = 2 - \log_{10} Y \ ;$$

$$\delta = 3 + 5.6 \log_{10}\left(\frac{W}{20}\right) \ ; \text{ and}$$

$$L_{mx} = 3.355 - 0.386 \log_{10}\left(\frac{W}{20}\right) - 0.275S_c + 0.448(K - 1) \ .$$

Then

$$\log \bar{f}_d = \begin{cases} 2\pi\sigma_c L_{mx}, & \text{if } x \geq K\delta \ ; \\ L_{mx} - 1.69(x - \delta K)^2, & \text{if } x < K\delta \ . \end{cases}$$

This fit uses L_{mx} as a maximum dose at a distance $K\delta$ downwind from ground zero. Then the dose downwind is taken as constant for $\xi < 1$. The drop-off in dose upwind is taken to be parabolic with distances, in order to approximate the shape of the cumulative normal-distribution function. The shape of the $\bar{f}_d$ curve is such that no simple shape will approximate it too well in these areas. The forms given should be adequate for many purposes. A plot of $\log \bar{f}_d$ as a function of distance is given in Figure 10.

The coefficient of 0.386 for the log-W term represents a considerable departure from the value of 1, which would apply if the scaling of dose to compensate for wind stretching of the pattern occurred here near ground zero, as it did for larger distances.

For wind speeds under 3 mph, the distribution of the fallout changes considerably. The following equations are used

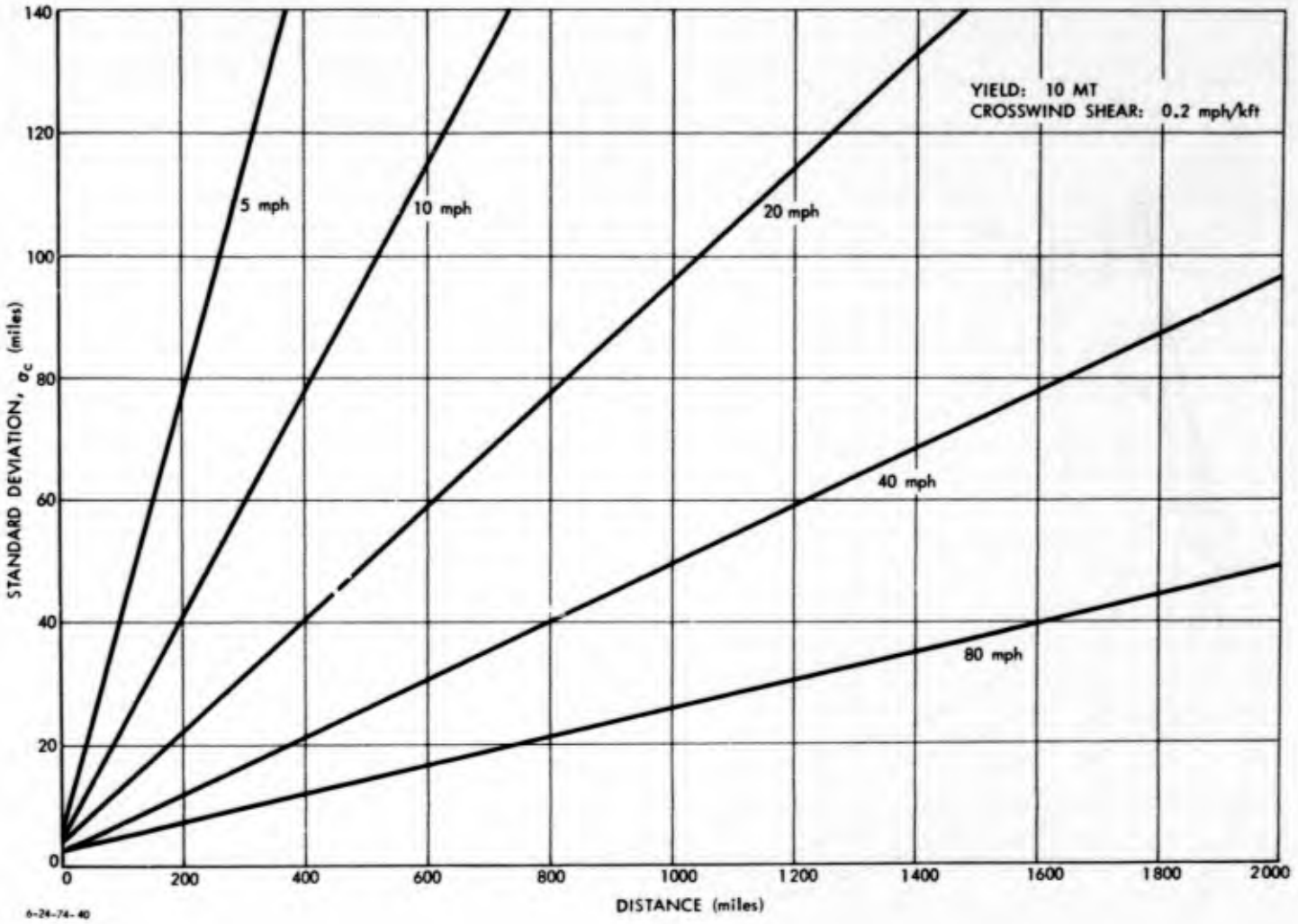

Figure 9. STANDARD DEVIATION OF CROSSWIND DISTRIBUTION AS A FUNCTION OF DISTANCE, FOR SEVERAL WIND VELOCITIES

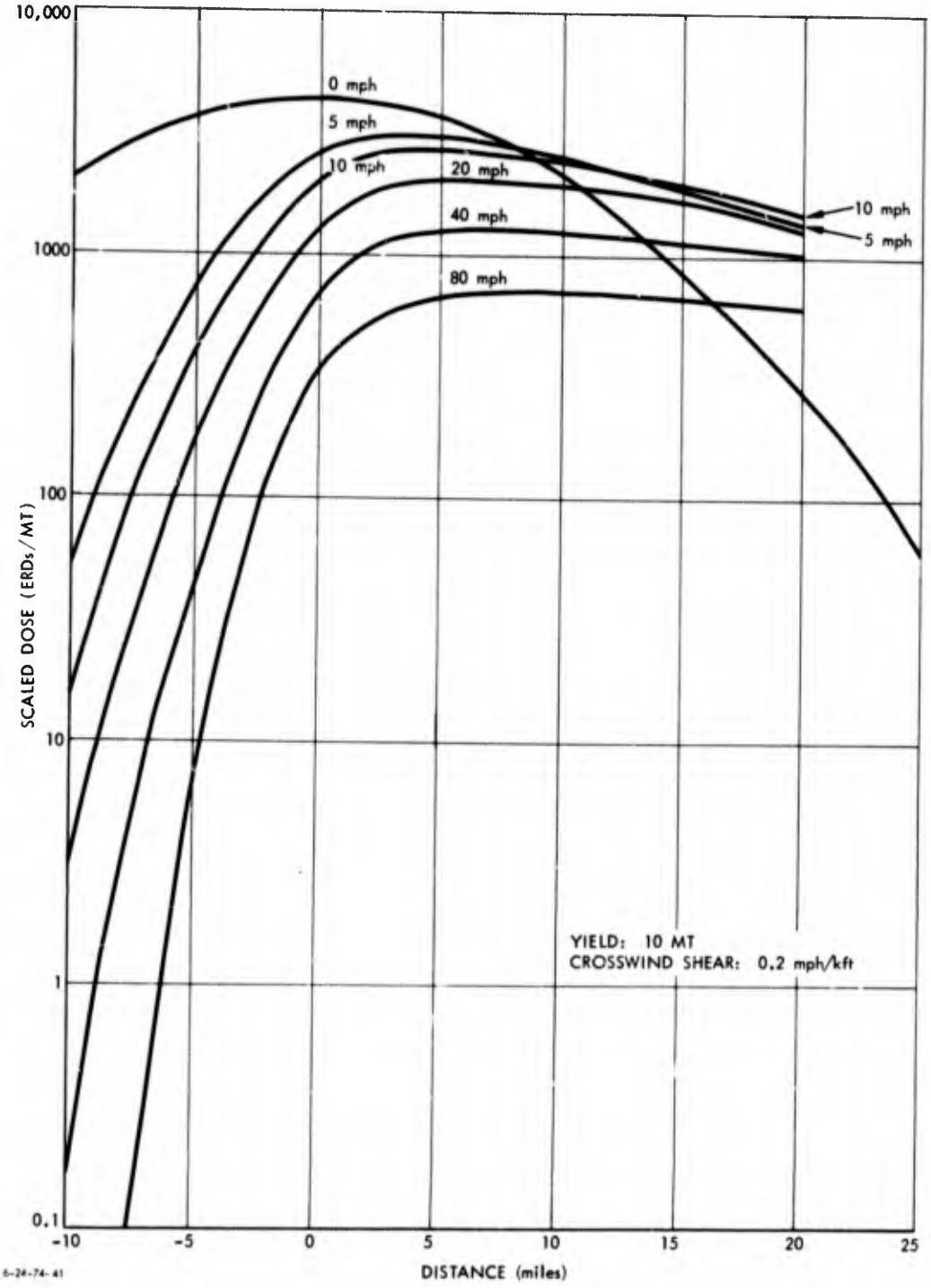

Figure 10. LOGARITHM OF SCALED CENTERLINE DOSE AS A FUNCTION OF DISTANCE, AT SMALL DISTANCES, FOR SEVERAL WIND VELOCITIES

to calculate $\bar{f}_d$ and σ_c. For $x > 0$,

$$\log_{10}\bar{f}_d = A_s + B_s x + C_s x^2 ,$$

where

$$A_s = (4.545 - 0.745Y) + (0.1222 + 0.0078Y)\left(1 - \frac{W}{2}\right) - (1.2223 + 0.0278Y)S_c ;$$

$$B_s = -0.06486 + 0.00316Y ;$$

$$C_s = (0.2444 - 0.0244Y) - (0.8977 + 0.1323Y)\left(1 - \frac{W}{2}\right)10^{-3} .$$

For $x < 0$,

$$L_{mx} = 4.35 - 0.56 - \log_{10}Y - 0.12W - 0.15S_c ;$$

$$\log_{10}\bar{f}_d = L_{mx} - \frac{(W/2 - x)^2}{67 + 257 \log_{10}Y} ;$$

$$\sigma_c = \sigma_a + \sigma_b x ,$$

where

$$\sigma_a = 3.14 + 0.51Y - (0.33 + 0.03Y)W + [42.35 - (19.075 + 0.9225Y)W]S_c + [69 - (27.35 + 1.15Y)W]S_c ;$$

$$\sigma_b = (3.611 + 0.039Y)S_c .$$

For $\log \bar{f}_d$, a single quadratic fit with distance is used. For σ_c, the constant term requires a quadratic variation with wind shear (instead of being independent of wind shear, as was the case with higher wind velocities).

D. SCREENING CALCULATION MODEL

This section addresses an alternative question that may be asked from a fallout model--namely, the distance at which certain doses are calculated. (An alternative set of inverse functions is given by Mason--above, p. 7*n*.) These questions are of particular interest when it is desired to ascertain

over what areas a weapon may contribute significantly to the dose at a prescribed monitor point. A contour of constant dose may be imagined. The distances given below for this contour are the maximum downwind, upwind, and crosswind distances, as well as the downwind distance at which the maximum crosswind distance occurs. With these distances, the entire contour may be approximated by drawing an ellipse through these points. For the following strictly empirical equations, in the unlikely condition that the wind velocity is less than 2 mph, a minimum velocity of 2 mph is assumed. For doses less than 10 ERDs, the maximum downwind distance is determined by

$$x_d = W(x_o) - 15 \log_{10}\left(\frac{D}{Y}\right) + (0.55 + 0.75S_c + 0.0075W)\left(\log_{10}\left(\frac{D}{Y}\right)\right)^2 ,$$

where

$$x_o = \begin{cases} 60.85 - 36.59S_c + 13.14S_c^2 \\ \qquad - 14.8 \log_{10}(W), & \text{if } S_c \leq 1.3929 ; \\ 21.56, & \text{if } S_c > 1.3939 . \end{cases}$$

For doses greater than 10 ERDs, the maximum downwind distance is given by

$$x_d = W(\bar{x}_o) - 10 \log_{10}\left(\frac{D}{Y}\right) + (1 + 0.75\bar{S}_c + 0.0075W)\left(\log_{10}\left(\frac{D}{Y}\right)\right)^2 ,$$

with $\bar{x}_c = 16.1 + 26.2(\bar{S}_c - 0.6)^2 - 8.1 \log_{10}W$; and $S_c = \max(S_c, 0.6)$. The fit is second order in $\log_{10}(D/Y)$ and is separated into two segments, so that this simple parabolic fit may give adequate accuracy.

The maximum crosswind distance is given by

$$y_c = 160S_c \log_{10}(10Y)\left[2.204 - \log_{10}D - 1.18\left(4 - \log_{10}D - \log_{10}\left(\frac{W}{10}\right)\right)\right]$$

for doses under 100 ERDs; and by

$$y_c = 2.5S_c \log_{10}Y\left[50 - \log_{10}\left(\frac{D}{100}\right) - \left(17.5 - 2.5 \log_{10}\left(\frac{D}{100}\right) - \log_{10}\left(\frac{W}{10}\right)\right)\right]$$

for doses above 100 ERDs. The downwind distance at which the maximum crosswind distance occurs is given by

$$x_c = W[(80 + 18.7 - 7.5 \log_{10}D - 7.5S_c)(1 + 0.75 \log_{10}Y)]$$

for doses under 100 ERDs and by

$$x_c = \frac{W}{20}\left[0.5 \log_{10}(10Y)\left(130 - 60 \log_{10}\left(\frac{D}{100}\right)\right) + \left(500 - 250 \log_{10}\left(\frac{D}{100}\right) \log_{10}\left(\frac{W}{10}\right)\right)\right]$$

for doses over 100 ERDs.

Finally, the maximum upwind distance is given by

$$x_u = \log_{10}(10Y)(6.5 - \log_{10}D - 1.25 \log_{10}W)$$

for doses under 100 ERDs; and by

$$x_u = 2 + \log_{10}(10Y)$$

for doses over 100 ERDs.

Chapter II

DOSES FROM SEVERAL WEAPONS DETONATED TOGETHER

A. SEVERAL LIMITING CASES

If a number of weapons are detonated closely spaced in time and distance, then it may be desirable to construct approximate expressions for the fallout losses produced by the combined pattern to find overall pattern characteristics and simple means of computing the resulting fallout effects. This chapter describes several limiting cases in which simple analytical expressions are obtained.

The dose for a single weapon can be written as

$$D(x,y) = FKAf_d(x)f_c(y)R(x) ,$$

using the terminology of the previous chapter. Suppose now that a density of fission production $\omega(x,y)$ is introduced that is the limiting production of fission from a large number of weapons of finite yield with infinitesimal fission fraction determined so that the integral over the entire plane of $\omega(x,y)$ is equal to some specified value of total fission yield, F. Moreover, we assume that doses can be superposed, which is the case if the arrival time for the dose from all weapons is sufficiently close--i.e., so that (at a point ξ,η) the dose divided by the height factor A can be given by

$$D_B(\xi,\eta) = \int_{-\infty}^{\infty}\int_{-\infty}^{\infty} \omega(x,y)D(\xi-x,\eta-y)\, dx\, dy .$$

It would be advantageous to be able to express the total dose from several weapons as a product of two factors--one depending on downwind distance and a second depending on crosswind

distance, as is done in the basic model for a single weapon. In other words, we shall be looking for expressions of the form

$$D_B(\xi,\eta) = F_R K F_d(\xi) F_c(\eta) ,$$

where F_R is the total fission yield in some region of interest (e.g., a strip of constant weapon density in the crosswind direction) and $F_d(\xi)$ and $F_c(\eta)$ are downwind and crosswind shape factors. It will be assumed that F_c is still normalized so that its integral is unity. The normalization of F_d will not be preserved, since in most uses F_d will be assumed to include the ratio of dose to H+1 dose rate.

1. Great Distances from the Explosions

Suppose that the center of the coordinate system is taken as the center of gravity of weapon ground-zeros weighted by the product of fission yield and height-of-burst factor. Suppose that all the explosions are of the same yield (or are simultaneous) and occur within a distance R of the center of gravity. Then as the downwind distance becomes large enough that the ratio of R to pattern spread is much less than one (i.e., $R/\sigma_c << 1$), the crosswind pattern approaches that which would be obtained from a single weapon detonated at the center with a fission yield equal to the sum of fission yields adjusted for height of burst. In fact, at any point, the fraction of crosswind error is less than $1 - \exp(-R^2/2\sigma_c^2)$.

In the downwind direction, the error in H+1 dose rate (using a single weapon at the center of gravity) can also be readily estimated if the downwind distance is again appreciable. In this case, the error becomes small if R divided by the characteristic distance L is small; moreover, the fraction error is bounded by $1 - \exp(-R/L)$. If, as an illustration, a typical value of L = 150 miles is assumed, the fraction error is under 10 percent for R < 16 miles. For most weapon distributions,

this error estimate is probably high; thus, considerably larger patterns would yield a comparable error level.

2. Effect of Crosswind Weapon Distributions

Suppose that all the weapons are detonated along a single line perpendicular to the crosswind axis--which makes the downwind effects the same for each weapon. Suppose, moreover, that the weapon density ω is taken only as a function of crosswind distance y. We assume the density is normalized, to make

$$\int_{-\infty}^{\infty} \omega(y)\, dy = F_R ,$$

where F_R is the total fission yield.

Now at any distance downwind, the crosswind effect from a single weapon is given by a Gaussian function f_c of the form

$$f_c = \frac{1}{\sqrt{2\pi}\sigma_c} \exp\left(-y^2/2\sigma_c^2\right) ,$$

so that

$$\int_{-\infty}^{\infty} f_c(y)\, dy = 1 .$$

If now the weapon density ω is Gaussian of the form

$$\omega(y) = \frac{F_R}{\sqrt{2\pi}\bar{\sigma}} \exp\left(-y^2/2\bar{\sigma}^2\right) ,$$

then the crosswind distribution from this pattern is exactly Gaussian with a standard deviation $\sigma = \left(\sigma_c^2 + \bar{\sigma}^2\right)^{1/2}$. If a number of weapons are clustered over an area target that has greatest density value in the center and drops off in value in Gaussian fashion, and if weapon density is proportional to value, then a Gaussian distribution of crosswind effects is obtained.[1]

[1]The two examples of crosswind distribution presented in this section have been chosen for analytical simplicity and because they are reasonably representative of weapon density distributions (continued on next page)

A second crosswind distribution that yields a simple solution is that of a constant fission density over a length R on each side of the central axis--but zero elsewhere. The distribution of intensity is readily shown to be

$$F_c(y) = \frac{1}{2R/\sigma_c}\left\{\text{cumnor}\left(\frac{y}{\sigma_c} + \frac{R}{\sigma_c}\right) - \text{cumnor}\left(\frac{y}{\sigma_c} - \frac{R}{\sigma_c}\right)\right\},$$

where cumnor (·) is the cumulative normal function. This distribution is plotted in Figure 11 as a function of distance, y/σ_c, for several values of R/σ_c.[1] The value of the dose given in Figure 11 can be interpreted as the average value of the Gaussian distribution function in a band of width 2R, centered at the value y. Then, clearly, as the band width R goes to zero, the function approaches a Gaussian distribution function. For values greater than 2, the cumulative normal curve is close to either 0 or 1. Thus, for large values of R/σ_c, the shape of the distribution is essentially constant as long as $|y/\sigma_c| < R/\sigma_c - 2$. This constant value is readily seen to be $1/(2R/\sigma_c)$. For values of y/σ_c somewhat greater than $R/\sigma_c + 2$, the value is essentially zero. Between the extreme values, the distribution curve decays in a shape approximated by half of the probability density curve with standard deviation $2\sigma_c$. As can be seen from Figure 11, the constant plateau is not evident for values of R/σ_c less than 2. For values of R/σ_c between 0 and 2, the shape of the distribution may be crudely described as a Gaussian probability density curve with standard deviation obtained by linearly interpolating as a function of R/σ_c between a value function equal to σ_c at $R/\sigma_c = 0$ and to $2\sigma_c$ at $R/\sigma_c = 2$. For larger values of R/σ_c, the standard deviation associated with the decay is constant at 2, but a level plateau is inserted at the origin.

(cont'd) obtained from various blast-damage optimization methods. Of course, even for functions not tractable to analytical integration, numerical integration methods could be used.

[1] If a constant amount of radioactivity is spread uniformly over a width 2R (so the weapon density is inversely proportional to R), then for normalization of F_c the first term should be simply 1/2R rather than $1/(2R/\sigma_c)$.

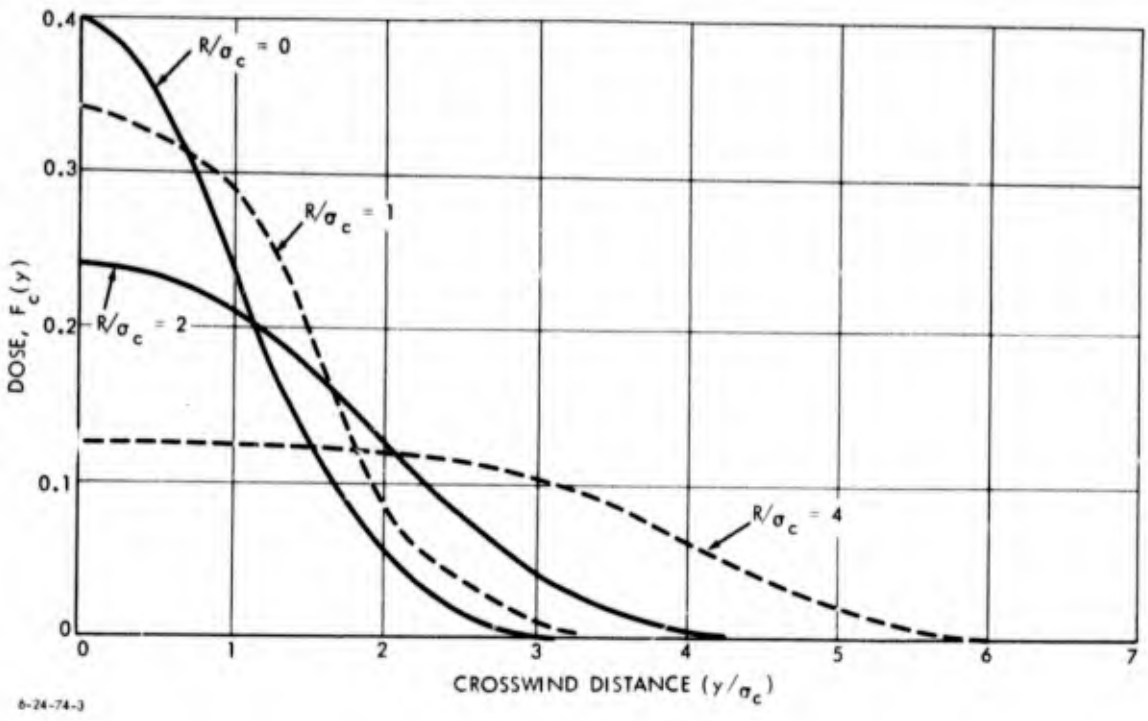

Figure 11. CROSSWIND DISTRIBUTION OF DOSE FOR UNIFORM SOURCE DENSITY, FOR SEVERAL VALUES OF R/σ_c

The assumption of weapon density allows for a simple analytical treatment but raises the question of the seriousness of the approximation of dropping discrete effects. To study this question, N weapons were evenly spaced over a line extending a distance D from each side of the center, and the relative dose from the discrete weapons was plotted as a function of crosswind distance in the same fashion as for Figure 11. To keep the total fission yield constant, the fission yield of each weapon was 1/N.

Figure 12 shows the relative dose for a number of different values of weapons where $D/\sigma_c = 4$. The curve for 1,001 weapons should be almost identical to the curve in Figure 11, which in fact it is. For example, at $y/\sigma_c = 0$ or 4, the error in relative dose is 10^{-4}. For two and three weapons, the lumps

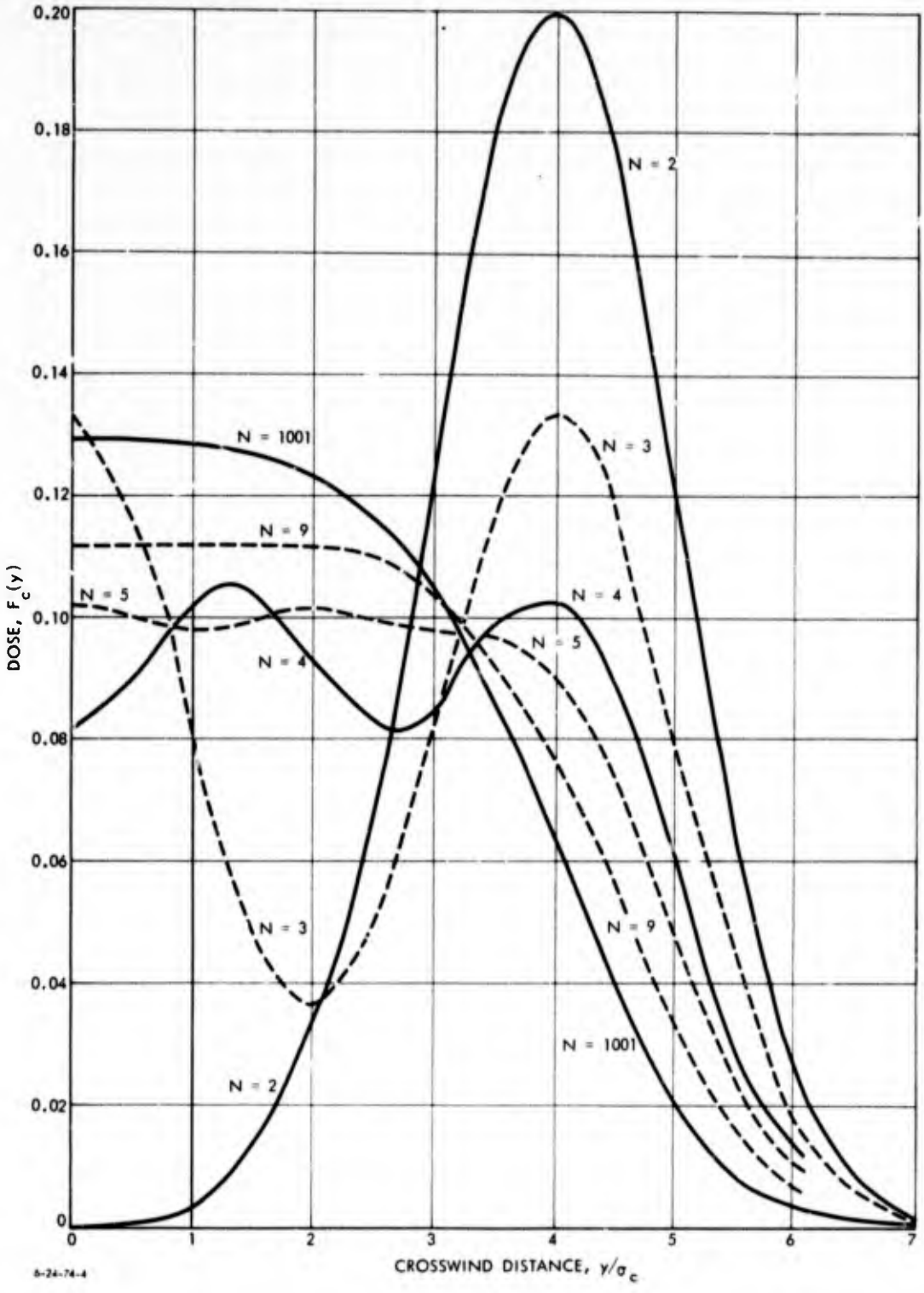

Figure 12. CROSSWIND DISTRIBUTION OF DOSE FOR SEVERAL NUMBERS OF WEAPONS EQUALLY SPACED ALONG A LINE OF LENGTH 2D, WITH $R/\sigma_c = 4$

due to individual weapons dominate the curves. For four weapons, the oscillations due to individual weapons have dampened to about 20 percent; and for five weapons, to less than 5 percent. It thus appears reasonable to assume that, for four or more weapons, the oscillations are small.

A similar situation is shown in Figure 13, where $D/\sigma_c = 2$. Since the weapons are closer, one would expect the oscillations to dampen more rapidly--which is seen to be the case. For $N = 3$, the oscillations have decreased to about the value seen for $N = 5$ in Figure 12.

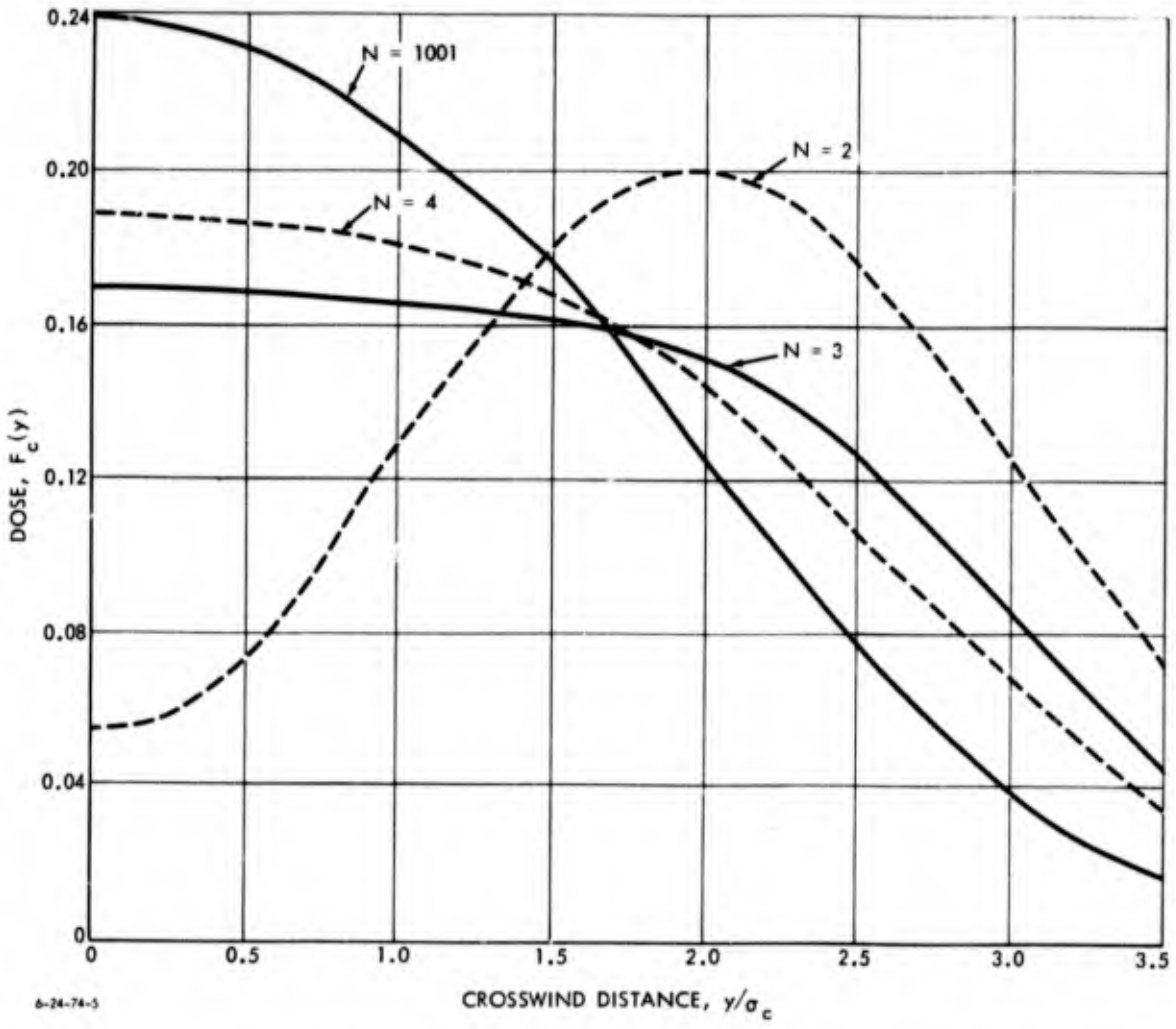

Figure 13. CROSSWIND DISTRIBUTION OF DOSE FOR SEVERAL NUMBERS OF WEAPONS EQUALLY SPACED ALONG A LINE OF LENGTH 2D, WITH $D/\sigma_c = 2$

Although the oscillations due to individual weapons have apparently dampened, nevertheless the curves are somewhat different in overall shape from the weapon density curve. This difference occurs because (for the small number of weapons with weapons extending to the end of the line) there is relatively more fission yield near the extremities of the line. In order to compensate for this effect, it appears reasonable to have the moment of inertia of the fission yield the same for the discrete weapons as for the weapon density--which can be accomplished by spacing weapons equally along a line of length d smaller than the length D of uniform density. For two weapons, $d = D/\sqrt{3}$; for three weapons, $d = D/\sqrt{2}$; and for four weapons, $d = \sqrt{3/5}D$. In Figure 14, with D/σ_c, curves are presented for N = 2 and N = 1,001. For N = 3 and N = 4, the points are plotted at 0.5 intervals; but the curves are too close to the curve for N = 1,001 to be plotted separately. Values of relative dose for several values of y/σ_c are as follows:

y/σ_c	N = 2	N = 3	N = 4	N = 1,001
0	0.2045	0.2309	0.2388	0.2384
1	0.2166	0.2099	0.2095	0.2099
2	0.1411	0.1304	0.1280	0.1251
3	0.0365	0.0393	0.0400	0.0397

As is clear for N = 3 or greater, the assumption of weapon density does not seriously affect dose distribution, while even for N = 2 the error is generally within 10 percent.

3. Effect of Downwind Weapon Distributions

In this subsection, assume that weapons are detonated over a strip that extends over an infinite width in both crosswind directions, so that the weapon density is a function of downwind direction only. The doses will be computed by assuming $F_c = 1$. Using the approximations for f_d of the previous chapter, a linear rise followed by an exponential decay allows rather simple closed-form expressions for H+1 dose rate when the

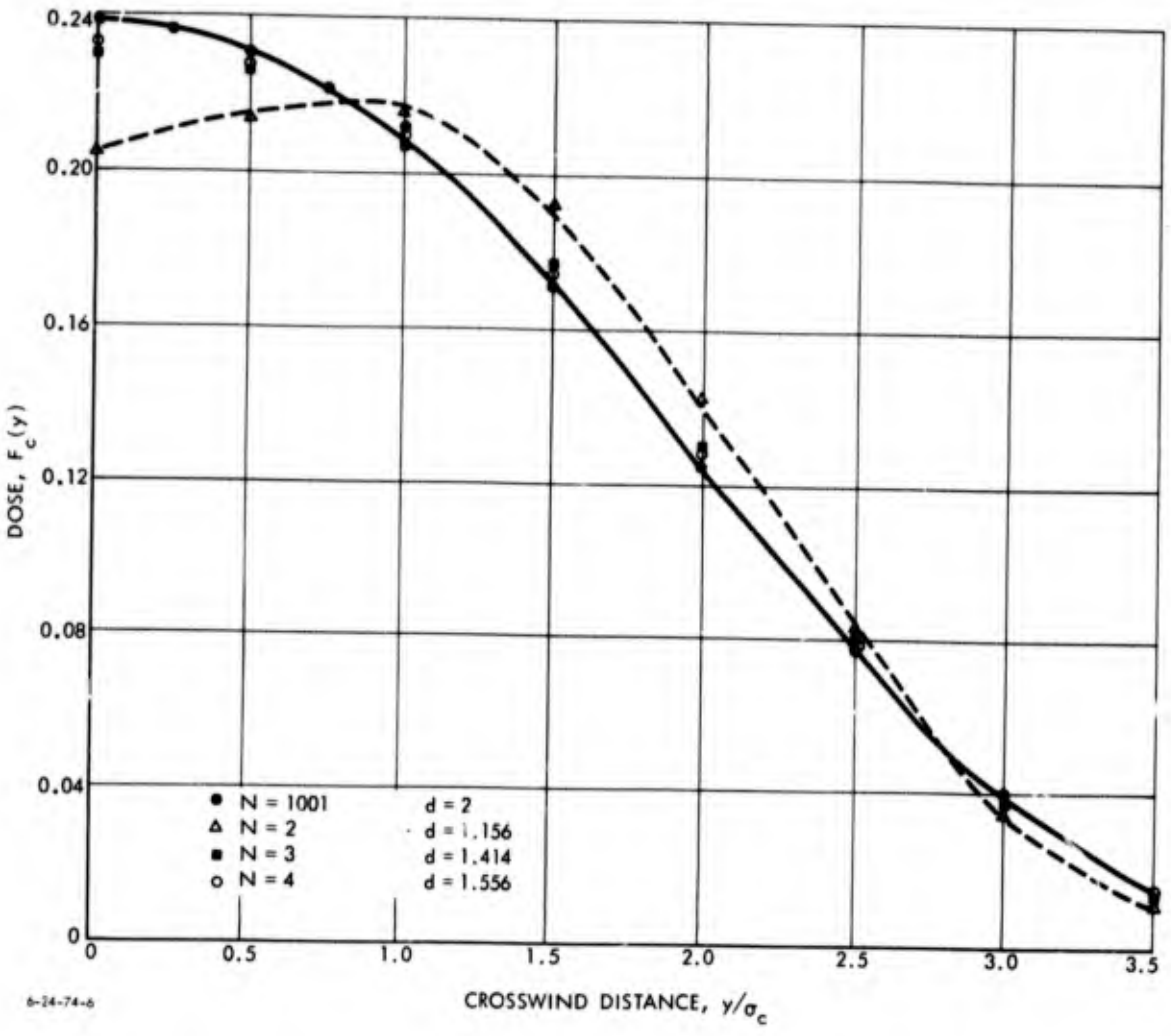

Figure 14. CROSSWIND DISTRIBUTION OF DOSE FOR SEVERAL NUMBERS OF WEAPONS EQUALLY SPACED ALONG A LINE OF LENGTH D, WITH MATCHING MOMENTS OF INERTIA

weapon density is constant. For any weapon density $\omega(x)$, the H+1 dose rate is given by

$$D_{H+1}(x) = \int_{-\infty}^{\infty} \omega(\tau) f_d(x-\tau)\, d\tau \ .$$

In particular, assume that a weapon density $\bar{\omega}$ is constant for $A \leq x \leq B$, so that

$$\bar{\omega}(B - A) = F \ .$$

The H+1 dose rate at any point x is given by

$$D_{H+1}(x) = \bar{\omega}\int_A^B f_d(x-\tau)\, d\tau \ .$$

Since normalization of f_d is not important here, assume for simplicity that f_d is given by the form described in the previous chapter--i.e.,

$$f_d(x) = \begin{cases} 0, & \text{if } x < d \ ; \\ \frac{K}{d}x, & \text{if } 0 \leq x < d \ ; \\ K \exp\Big(-K(x-d)\Big), & \text{if } d \leq x \ . \end{cases}$$

For further simplicity, let d = 0 for a first calculation. Then performing the integration gives

$$D_{H+1}(x) = \begin{cases} 0, & \text{if } x < A \ ; \\ \bar{\omega}\Big(1 - \exp\Big(-K(x-A)\Big)\Big), & \text{if } A \leq x < B \ ; \\ \bar{\omega} \exp(-Kx)\Big(\exp(KB) - \exp(KA)\Big), & \text{if } B \leq x \ . \end{cases}$$

Finally, suppose that $K(B - A) << 1$, as is the case for typical values of wind and of target extent. Then the middle term is of the form

$$\bar{\omega}K(x - A) \ .$$

Now, recalling the definition of $\bar{\omega}$, we obtain

$$D_{H+1}(x) = \begin{cases} 0 & \text{if } x < A \ ; \\ KF\frac{x - A}{B - A}, & \text{if } A \leq x < B \ ; \\ K \exp(-Kx)\Big(\frac{\exp(KB) - \exp(KA)}{B - A}\Big), & \text{if } B \leq x. \end{cases}$$

Thus the H+1 dose rate is seen to have the form of a linear rise across the strip, followed by an exponential decay. As will be seen in Section B (below), this typical type of behavior occurs in less idealized cases as well.

For $d \neq 0$ but when $d < B - A$, this basic behavior is not altered. The linear rise is preceded by a parabolic rise of length d, and the peak is not reached until slightly after $x = B$. With these exceptions, however, the same behavior is seen.

Figure 15 displays exact calculations of normalized H+1 dose rate f_d, as a function of downwind distance from a 10-MT weapon with 20-mph wind with the crosswind dose factor F_c set equal to 1 (to eliminate spreading effects), along with this ratio multiplied by the ratio of dose to H+1 dose rate. The logarithms of these values are shown in Figure 16. As is evident from Figure 16, an exponential approximation to the decay of H+1 dose rate fits very well for distances over 20 miles and approximates the dose variation reasonably well over appreciable distances. In this figure a straight line is shown as a fit to the calculated doses, which are indicated by the points. The error is within 20 percent from 20- to 400-mile distances.

For future use, the integrals of normalized dose rates and normalized dose, as well as the ratio of the integrals, are shown in Figure 17. The differences in the curves are due to the drop-off in the ratio of dose to H+1 dose rate. (No particular significance should be placed in the final asymptotic values of these curves; in fact, it is accidental that the numerical values are so close.)

Now for an infinitely wide strip with constant weapon density, we can write

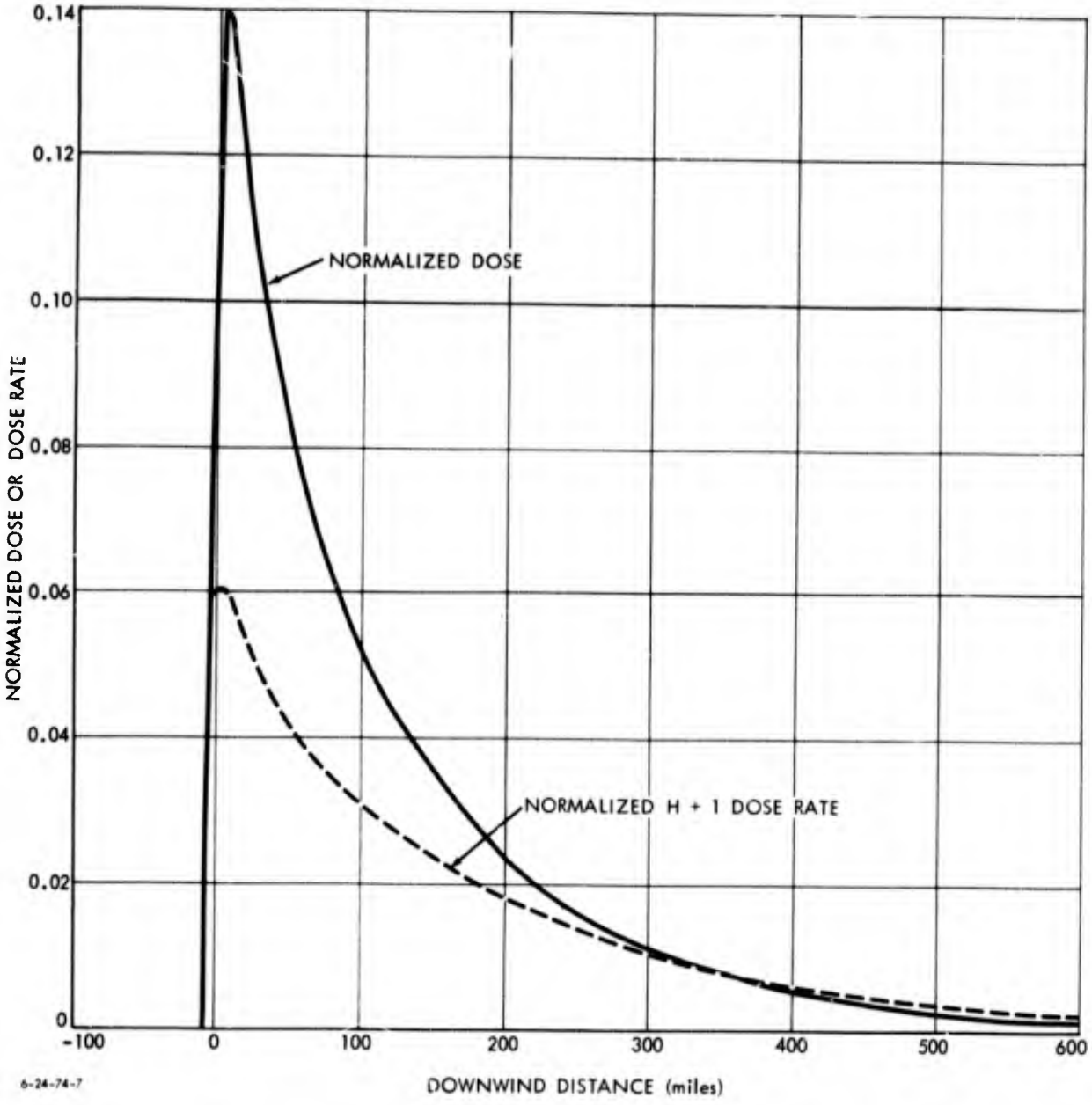

Figure 15. NORMALIZED H+1 DOSE RATE AND DOSE AS FUNCTIONS OF DOWNWIND DISTANCE

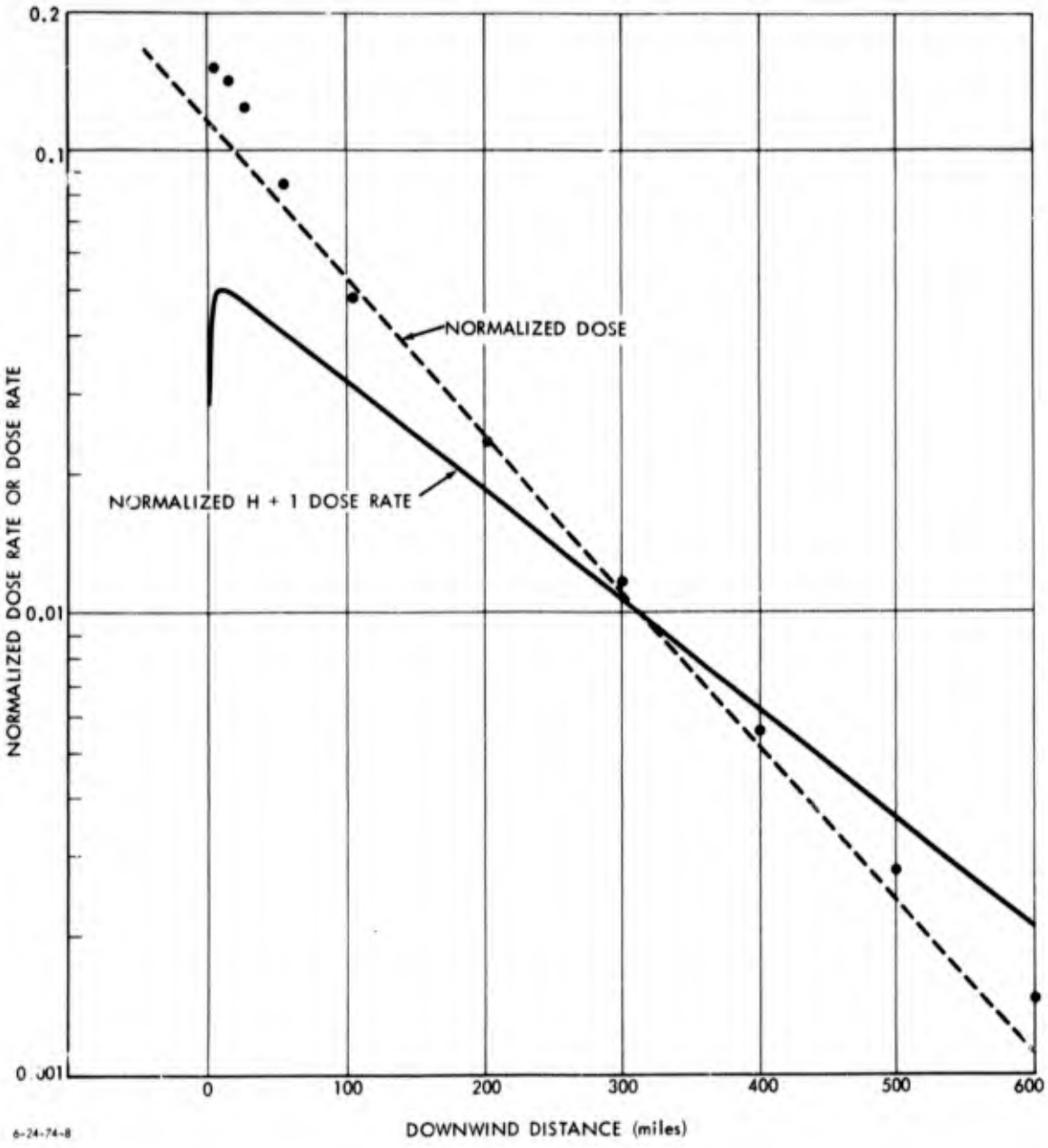

Figure 16. LOGARITHM OF H+1 DOSE RATE AND DOSE AS FUNCTIONS OF DOWNWIND DISTANCE

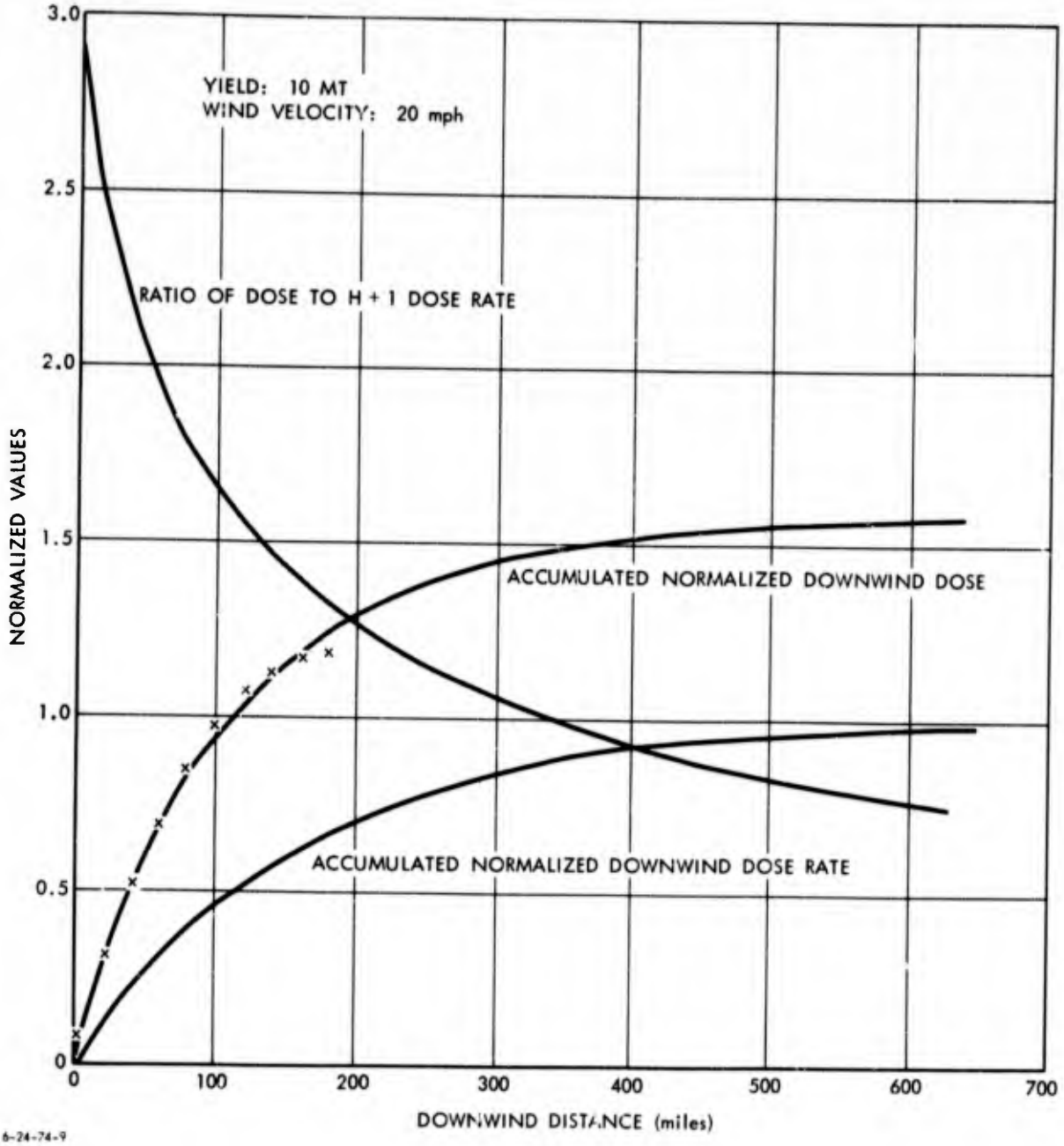

Figure 17. ACCUMULATED NORMALIZED H+1 DOWNWIND DOSE RATE (ACCUMULATED DOWNWIND OF DOSE) AND RATIO OF DOSE TO H+1 DOSE RATE, AS FUNCTIONS OF DOWNWIND DISTANCE

$$F_d(x) = \begin{cases} 0, & \text{if } A < x ; \\ \dfrac{F}{B - A}\displaystyle\int_A^x R(x-\tau) f_d(x-\tau)\, d\tau, & \text{if } A \leq x < B ; \\ \dfrac{F}{B - A}\displaystyle\int_A^B R(x-\tau) f_d(x-\tau)\, d\tau = F\bar{R}\bar{f}_d(x-\theta), & \text{if } x \leq B , \end{cases}$$

where $f_d(x-\theta)$ is defined by this equation and represents the dose rate at a distance equal to the distance from x to some point θ in the strip. To a good approximation, θ may be taken as the midpoint of the strip--as is shown in Figure 18, where the integral of $f(\xi) = \exp(-\xi)/\xi^{0.382}$ over a strip of width 2α is compared to the function value at the midpoint.

The character of a linear build-up in dose followed by an exponential decay is again obtained. If a linear build-up in the strip is to be assumed, the degree of approximation in the build-up is represented in the departure of the accumulated dose curve from a straight line in Figure 17. That this approximation is applicable is readily apparent if we translate x coordinates to x′ coordinates, where the origin is at the beginning of the strip. Then in the strip (i.e., for $0 < x' \leq B - A$), we have

$$F_d(x') = \int_0^{x'} R(\tau) f_d(\tau)\, d\tau .$$

As can be seen for strips up to 100 miles wide, the linear approximation is within 10 percent of the exact value.

For the decay portion of $F_d(x)$ where $(x) > B$, the value θ can be well approximated by the midpoint of the strip if the curvature of the intensity curve is small. In this case, once points are beyond the strip, the drop-off in dose can be approximated by a single weapon--or more precisely, by a single line of weapons in the center of a strip. For a group of weapons located in a finite target area, the use of a single weapon located at the center of gravity of the group of weapons is suggested.

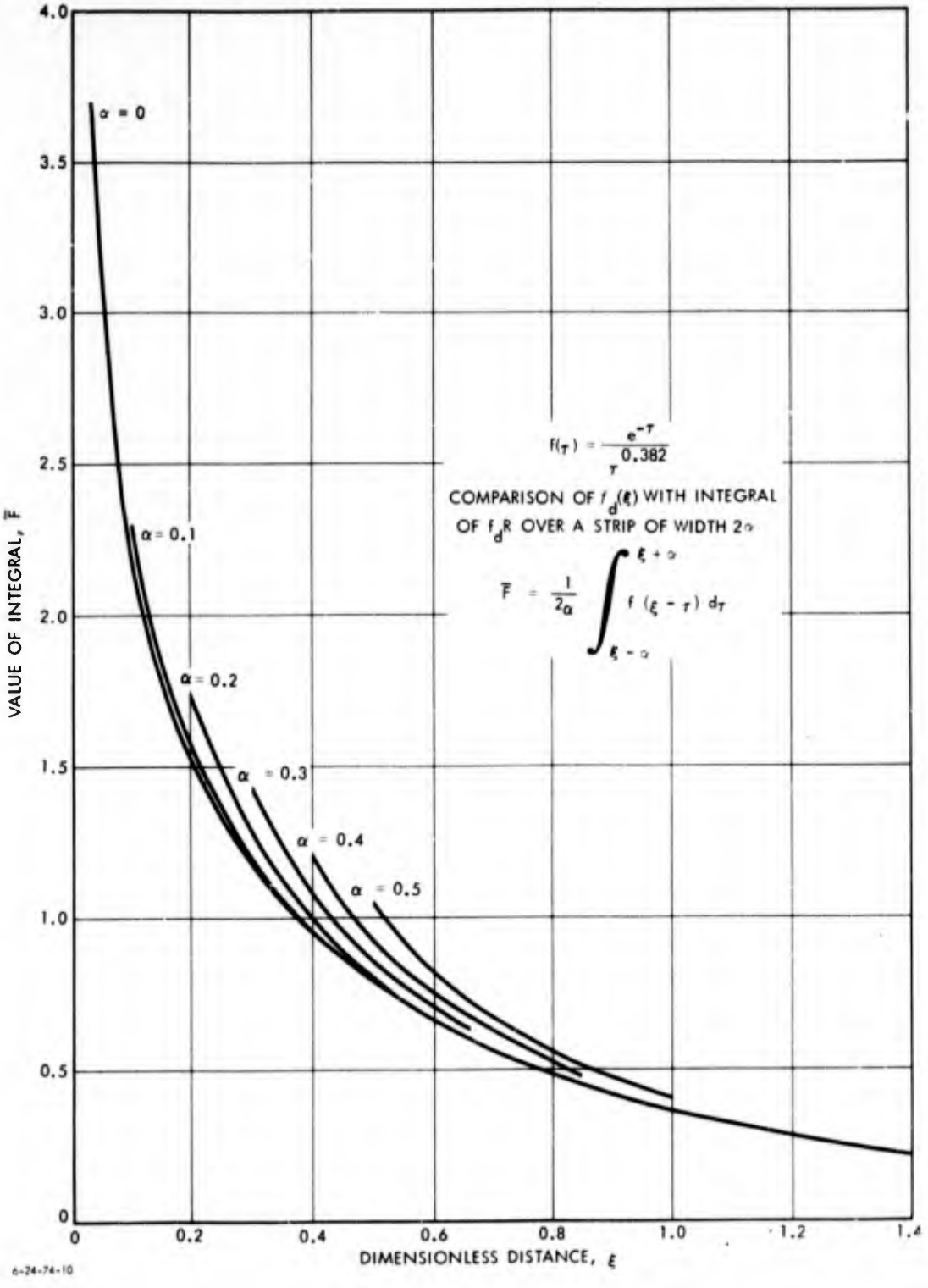

Figure 18. COMPARISON OF $f_d(\xi)$ AND INTEGRAL OF $f_d R$ OVER A STRIP OF WIDTH 2α.

For $x > B$, $F_d(x)$ is of the form

$$F_d(x) = \frac{\exp(-x)}{x^{0.382}} .$$

A polynomial approximation for $F_d(x)$ is

$$F_d(x) = 1/\left(0.69654 + 1.2355x - 1.3259x^2 + 0.68552x^3\right)^4 .$$

The fit is accurate to about 15 percent at $x = 0.02$ and to within about 8 percent over the range $0.04 < x \leq 1$. For larger values of x, we have

$$F_d(x) = 1/\left(0.85419 + 0.42100x - 0.0019286x^2 + 0.00929x^3\right)^4 .$$

In the range $0.6 \leq x \leq 6$, the error is less than 1 percent.

In order to generalize the numerical results for a particular condition to different weapons and wind patterns, the simplified representations of f_d and R of the previous chapter can be used. We have

$$f_d R = \begin{cases} 0, & \text{if } x < 0 ; \\ \dfrac{1}{WT^{1.382}} \exp\left(-\left(\dfrac{x}{WT}\right)\right) \dfrac{2.71}{\left(\dfrac{x}{WT}\right)^{0.382}}, & \text{if } x \geq 0 . \end{cases}$$

Then

$$F_d(x) = \frac{1}{B - A} \int_0^{x'} \frac{1}{WT} \exp\left(-\left(\frac{\tau}{WT}\right)\right) \frac{2.71}{\left(\dfrac{x}{W}\right)^{0.382}} \, d\tau .$$

Let $\xi = \frac{\tau}{WT}$. Then

$$F_d(x) = \frac{1}{B - A} \frac{2.71}{T^{0.382}} \int_0^{\frac{x'}{WT}} \frac{\exp(-\xi)}{\xi^{0.382}} \, d\xi .$$

The integral that was evaluated numerically is shown in Figure 19. In the more complete model, a minimum value of

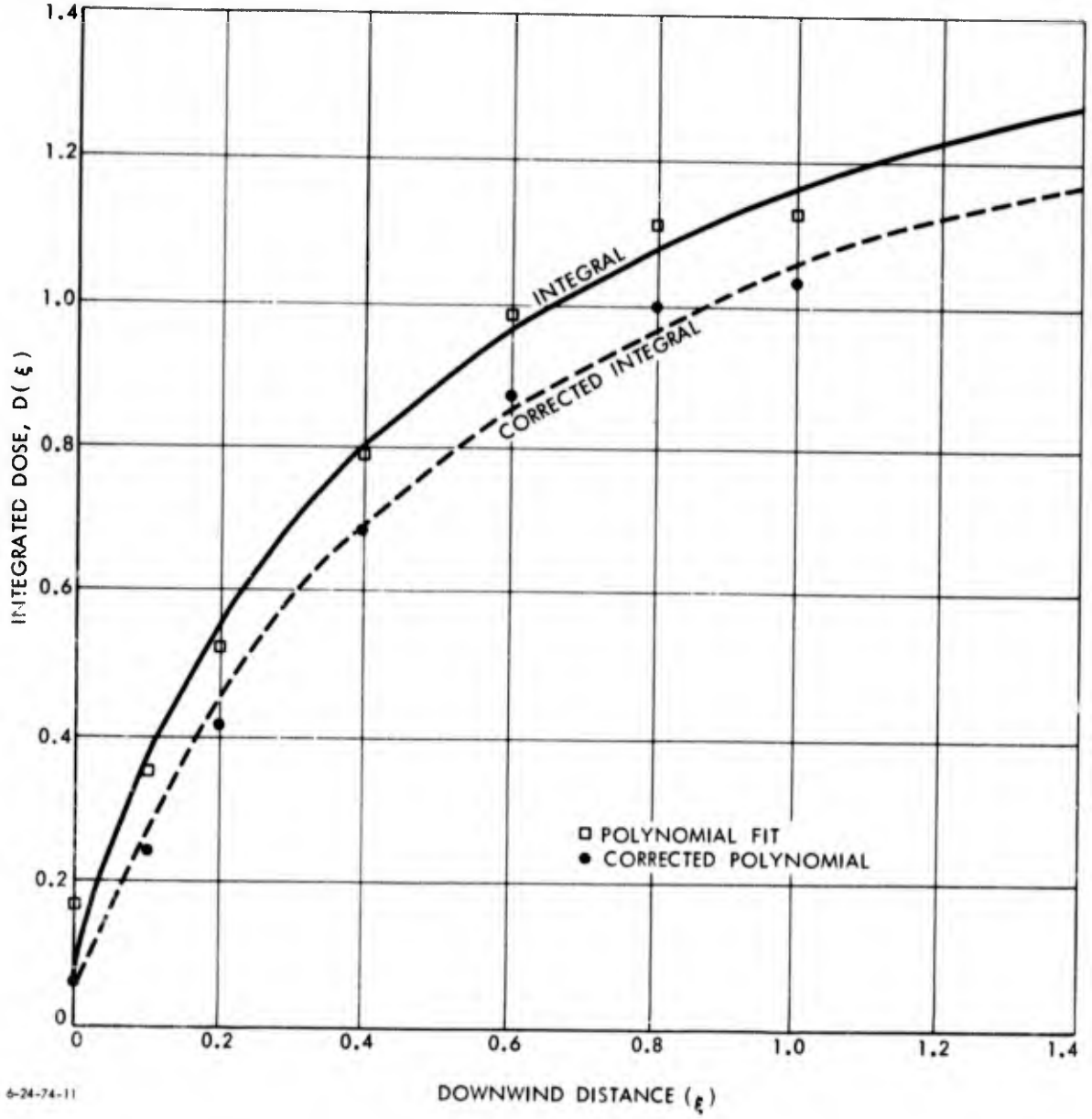

Figure 19. INTEGRAL OF POLYNOMIAL AND POLYNOMIAL FIT TO INTEGRATED DOSE

$x/W = 0.5$ is allowed in computing the ratio of dose to H+1 dose rate. The physical reason is that a finite time occurs before the first fallout is deposited. For a 10-MT weapon, this time corresponds to a value of $\xi = 0.005$. The difference between the actual integral and the values by forcing a minimum value of $\xi = 0.05$ is 0.11. This value was subtracted from the integral, and a second-order polynomial fit was made. The resulting expression for $F_d(x)$ in the strip is

$$F_d(x) = \frac{1}{B - A} \frac{2.71}{T^{0.382}}(0.6373 + 1.9549\xi - 0.9963\xi^2) .$$

Values of this expression are also shown in Figure 19. Moreover, in Figure 17 the fit is compared to the numerically integrated dose. The approximation is quite close for distances in the strip up to 160 miles. Moreover, a straight line with slope 0.012 drawn through the origin in Figure 17 fits quite well to distances of 60 to 70 miles. Again, an x' coordinate system has its origin at A. Then, within the uniform density strip, $F_d(x')$ becomes

$$F_d(x') = \frac{1}{B - A} \frac{4.72\left(x' + \frac{B - A}{2}\right)}{WT^{1.382}} .$$

Finally, using the simplified expression for T gives

$$F_d(x') = \frac{4.72\left(x' + \frac{B - A}{2}\right)}{W(7.5 + 1.66 \log_{10} Y)^{1.382}(B - A)} .$$

Suppose it is now assumed that over a strip of width C the weapon density is constant, that F_s is the total yield released in that strip, and that this strip is surrounded by identical strips, so that no side effects occur. Then the dose within the strip can be calculated by assuming that $F_c = 1/C$. We have for dose

$$D_B = KF_s F_d(x') F_c$$

$$= \frac{KF_s}{c} F_d(x') \ .$$

For the linear form of $F_d(x')$,

$$D_B = \frac{4.72KF_s x'}{CW(7.5 + 1.66 \log_{10} Y)^{1.382}(B - A)} \ .$$

B. WEAPONS DETONATED IN REGULAR PATTERNS

In this section, fallout from groups of weapons detonating in several different hexagonal patterns will be compared. In the calculations all weapons will be 10 MT, with a 10-mph wind and 0.2-mph/kilofoot shear assumed. For each pattern the total fission yield will be 70 MT. If a scaled comparison is desired, each of these values would be divided by 70 to give dosage/MT of fission in the pattern. The pattern here could be typified by a sizable attack in a large urban area.[1]

Figure 20 shows contours of constant dose for a single 10-MT weapon with a fission fraction of 7. This pattern has a peak dose of 142,500 ERDs. This high value is obtained since a fission fraction of 7 is used--which is done to compare this pattern with other patterns where the weapons are spread out. Figure 21 shows contours of constant dose for seven weapons in a hexagonal pattern with a 10-mile half-width. Since the fission fraction of each weapon is 1, the total fission yield deposited is the same as in Figure 20, but the deposition is spread over the hexagon pattern. The peak dose is 64,000 ERDs; and, as is clear by inspection of the two figures, the entire pattern is more spread.

---

[1]These high values of doses, of course, do not reflect many factors that tend to reduce the actual values. Rather than suggest values of these factors here, the limiting values are presented in the expectation that each reader will multiply them by his own degradation factor.

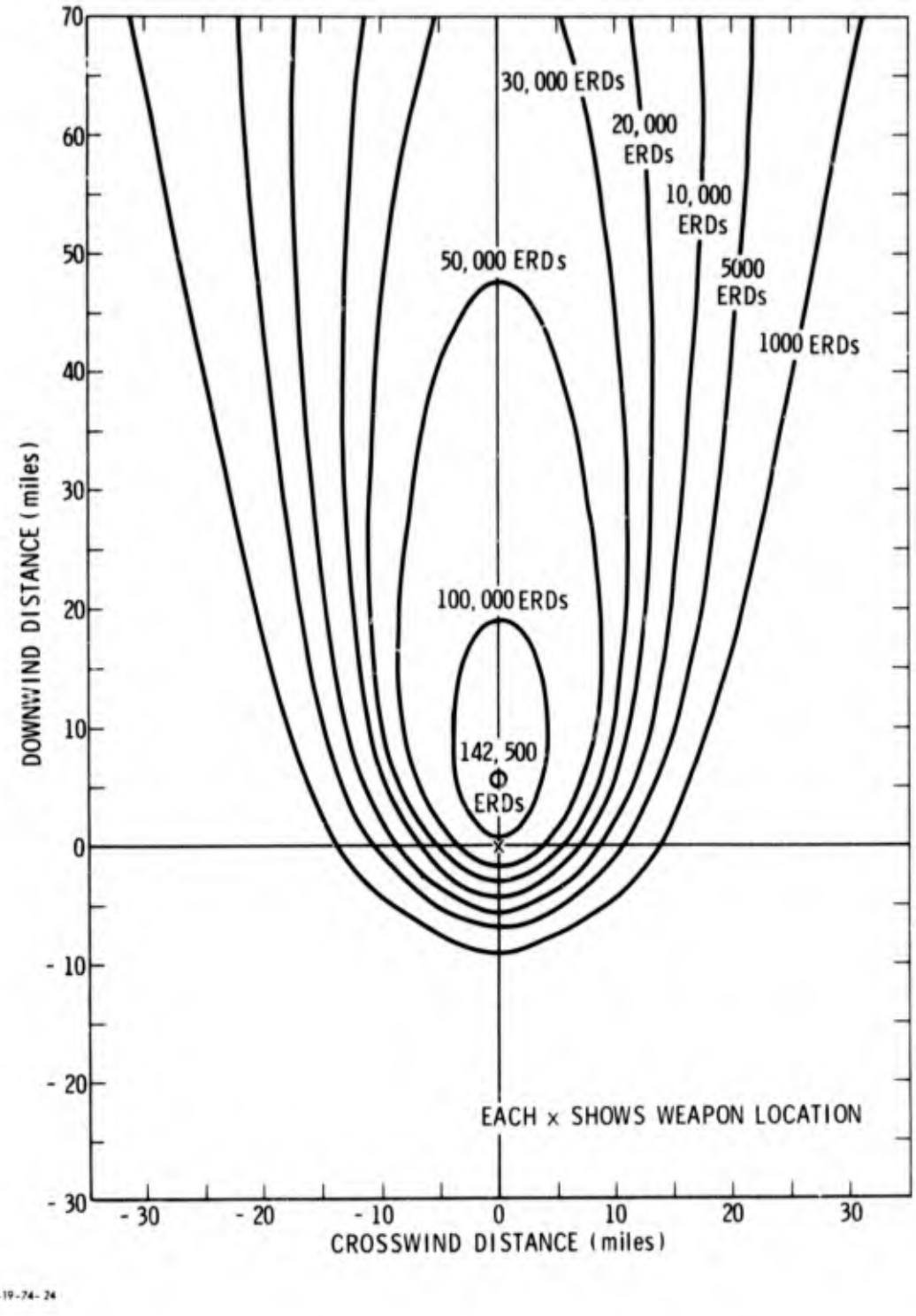

Figure 20. CONTOURS OF CONSTANT DOSE FOR ONE WEAPON WITH SAME FISSION YIELD AS HEXAGON WEAPONS

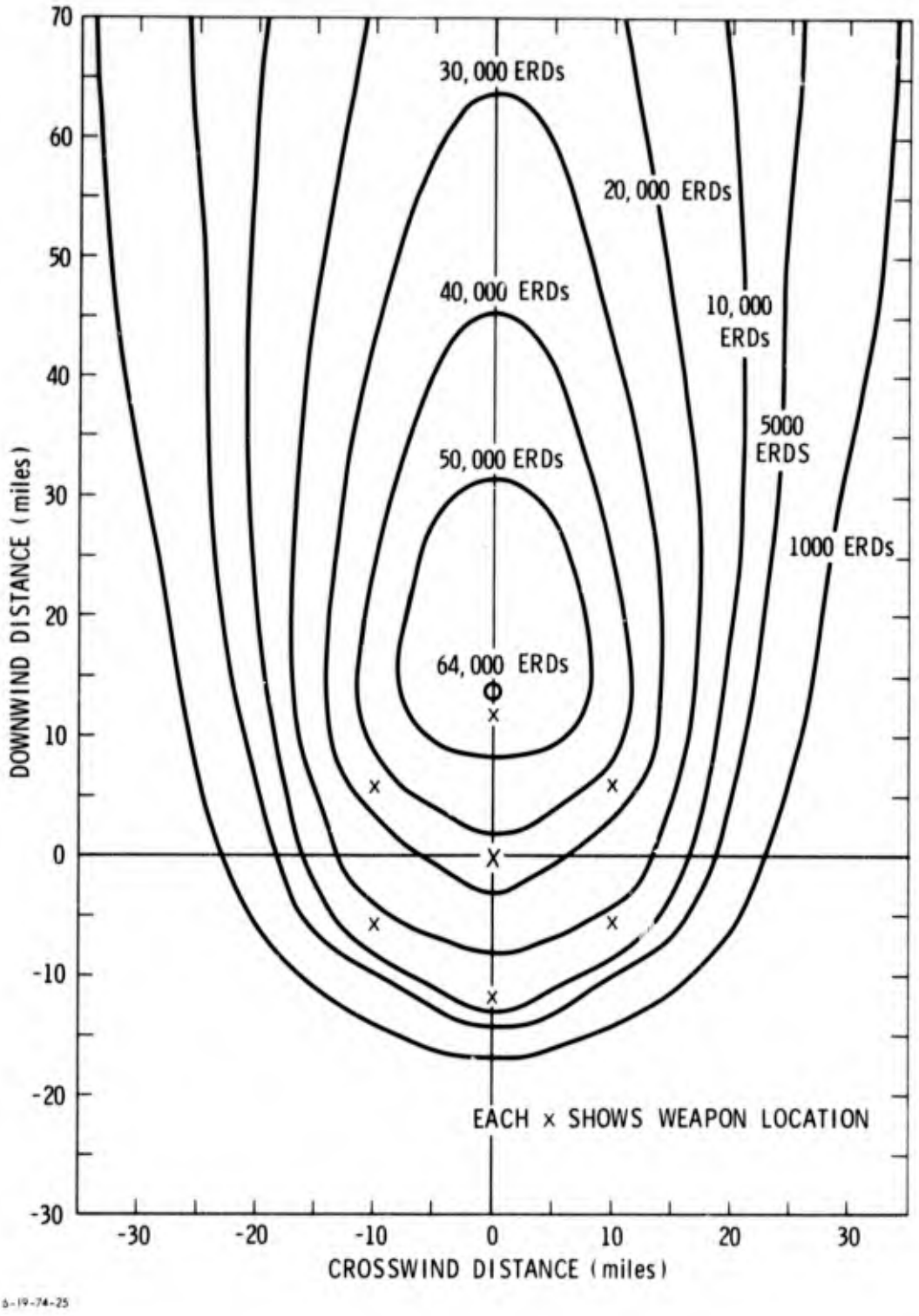

Figure 21. CONTOURS OF CONSTANT DOSE FOR SEVEN WEAPONS IN A ONE-RING HEXAGON WITH 10-MILE HALF-WIDTH

Figure 22 shows contours of constant dose spread over a 20-mile half-width pattern with seven weapons in a single ring, and Figure 23 shows 19 weapons spread over the same half-width pattern in two rings. In Figure 24, seven weapons are spread over a 40-mile half-width pattern in one ring; in Figure 25, 19 weapons are spread in two rings; and in Figure 26, 61 weapons are spread in four rings. The following table indicates both the maximum distance of any point in the pattern from a weapon and the minimum overpressure from surface bursts corresponding to these distances.

Figure Number	Maximum Distance From a Weapon	Minimum Pressure (psi)
21, 23, 26	6-2/3 miles	4.0
22, 25	13-1/3 miles	1.5
24	26-2/3 miles	0.5

As can be seen from inspection of Figures 21, 23, and 26, at the 10-mile distance between rings, the patterns coalesce into a single pattern. The 20-mile separation between rings in Figures 22 and 25 gives marginal coalescence, in the sense that at doses less than 5,000 ERDs a relatively smooth envelope is obtained, while at doses of 10,000 ERDs or above some sensitivity to specific weapon locations is seen. For the 40-mile separation between rings of Figure 24, the weapon patterns are almost independent in the crosswind direction until doses of about 1,000 R are reached. If an attack on a city is designed to cover the city with at least 4 psi (which is the case against many urban targets for various optimized targeting schemes and corresponds to the separations in the top line of the above table), then coalescence of the effects from individual weapons into a single overall pattern is to be expected. Even with attacks against more widely separated targets, at the lower dose levels coalescence into a single pattern is obtained at appreciable distances from a target.

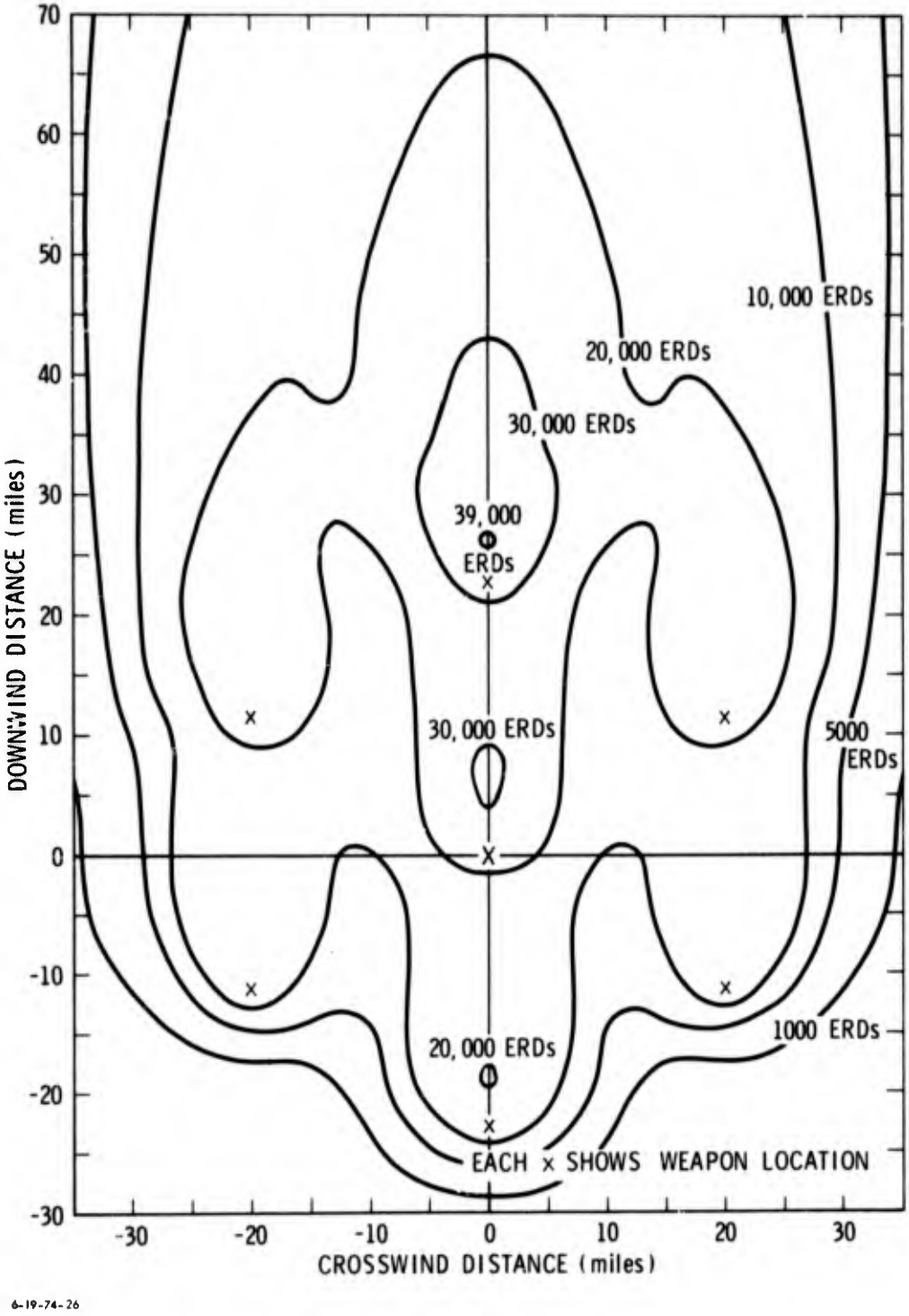

Figure 22. CONTOURS OF CONSTANT DOSE FOR SEVEN WEAPONS IN A ONE-RING HEXAGON WITH 20-MILE HALF-WIDTH

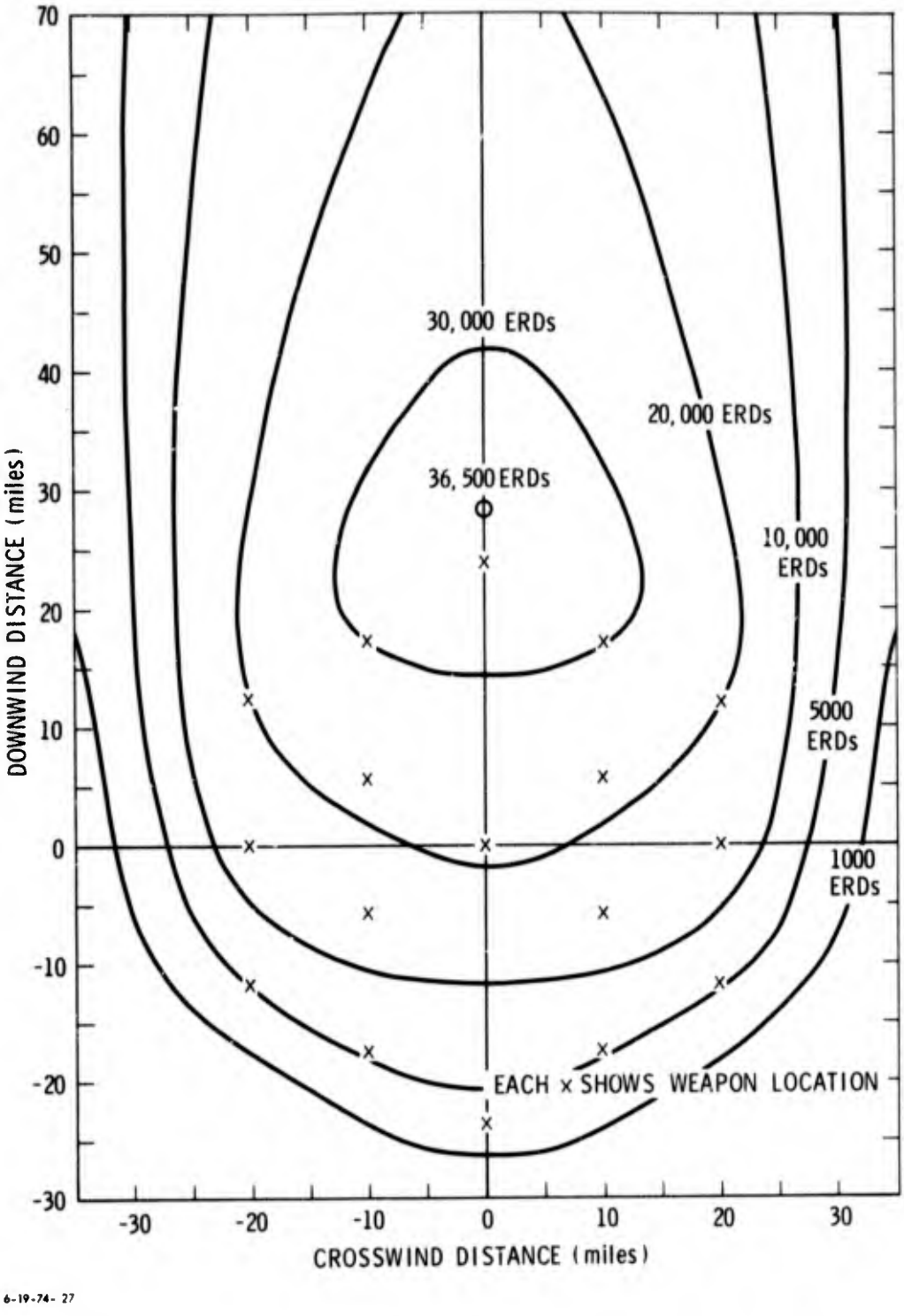

Figure 23. CONTOURS OF CONSTANT DOSE FOR 19 WEAPONS IN A TWO-RING HEXAGON WITH A 20-MILE HALF-WIDTH

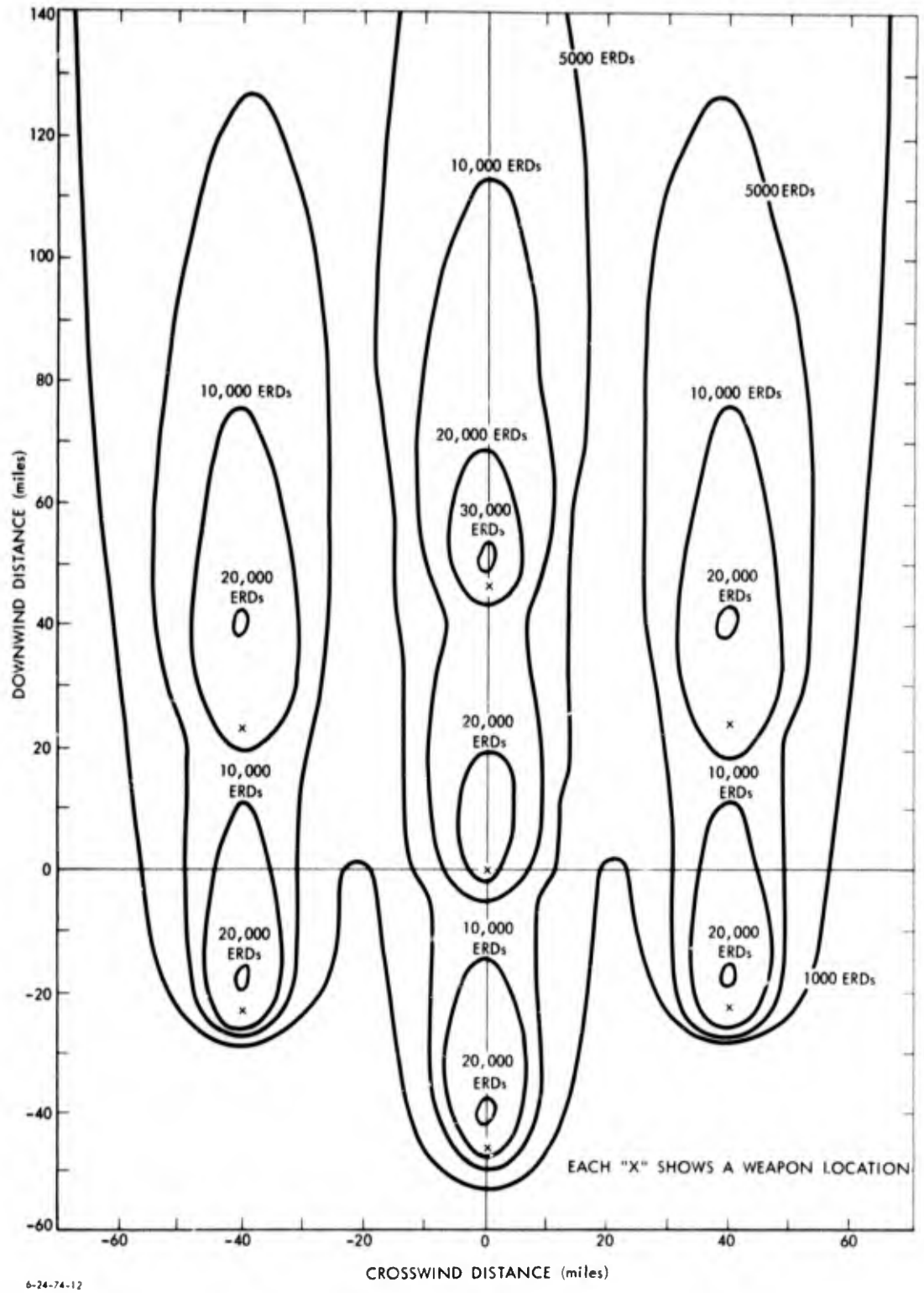

Figure 24. CONTOURS OF CONSTANT DOSE FOR SEVEN WEAPONS IN A ONE-RING HEXAGON WITH 40 MILE HALF-WIDTH

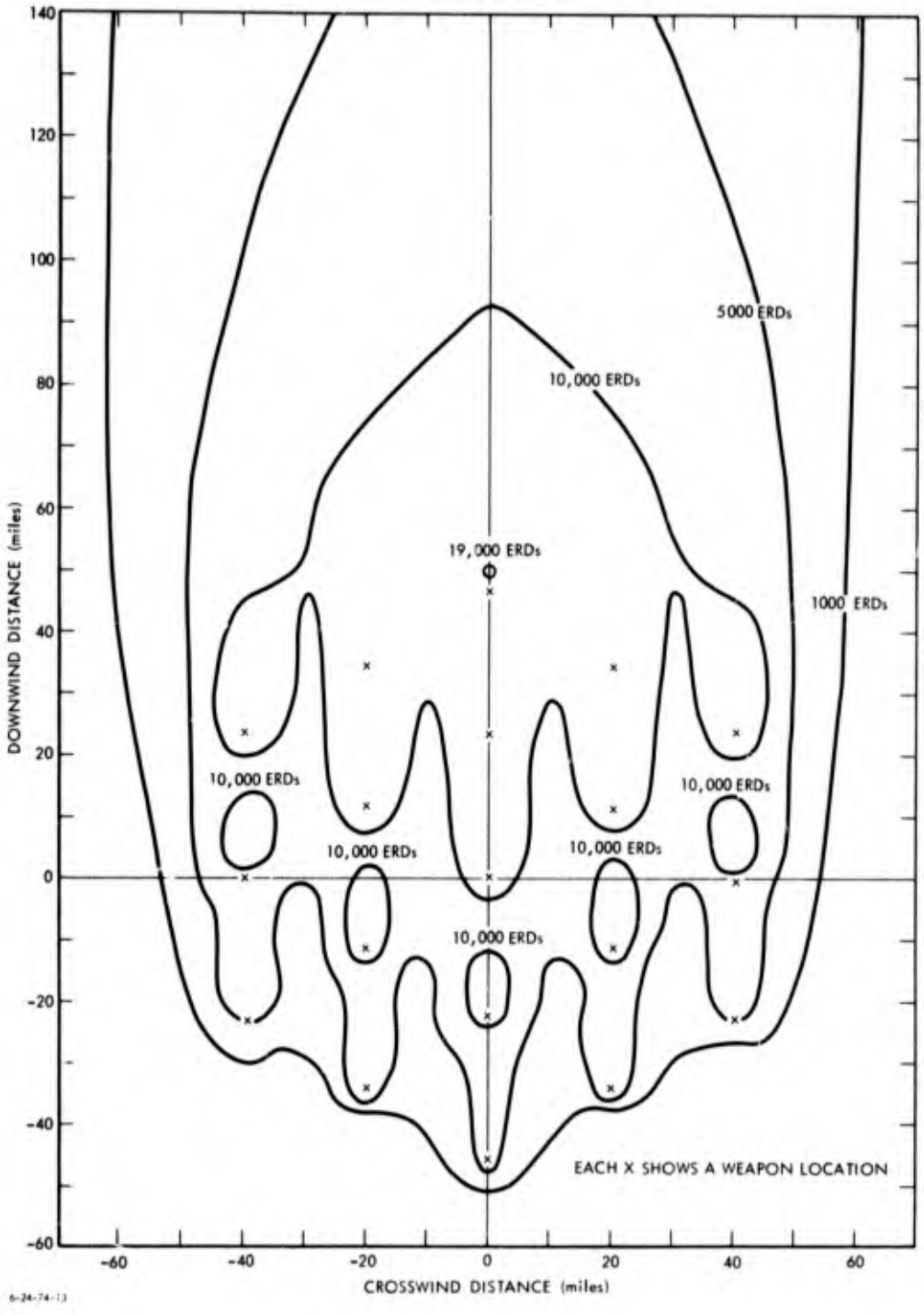

Figure 25. CONTOURS OF CONSTANT DOSE FOR 19 WEAPONS IN A TWO-RING HEXAGON WITH 40-MILE HALF-WIDTH

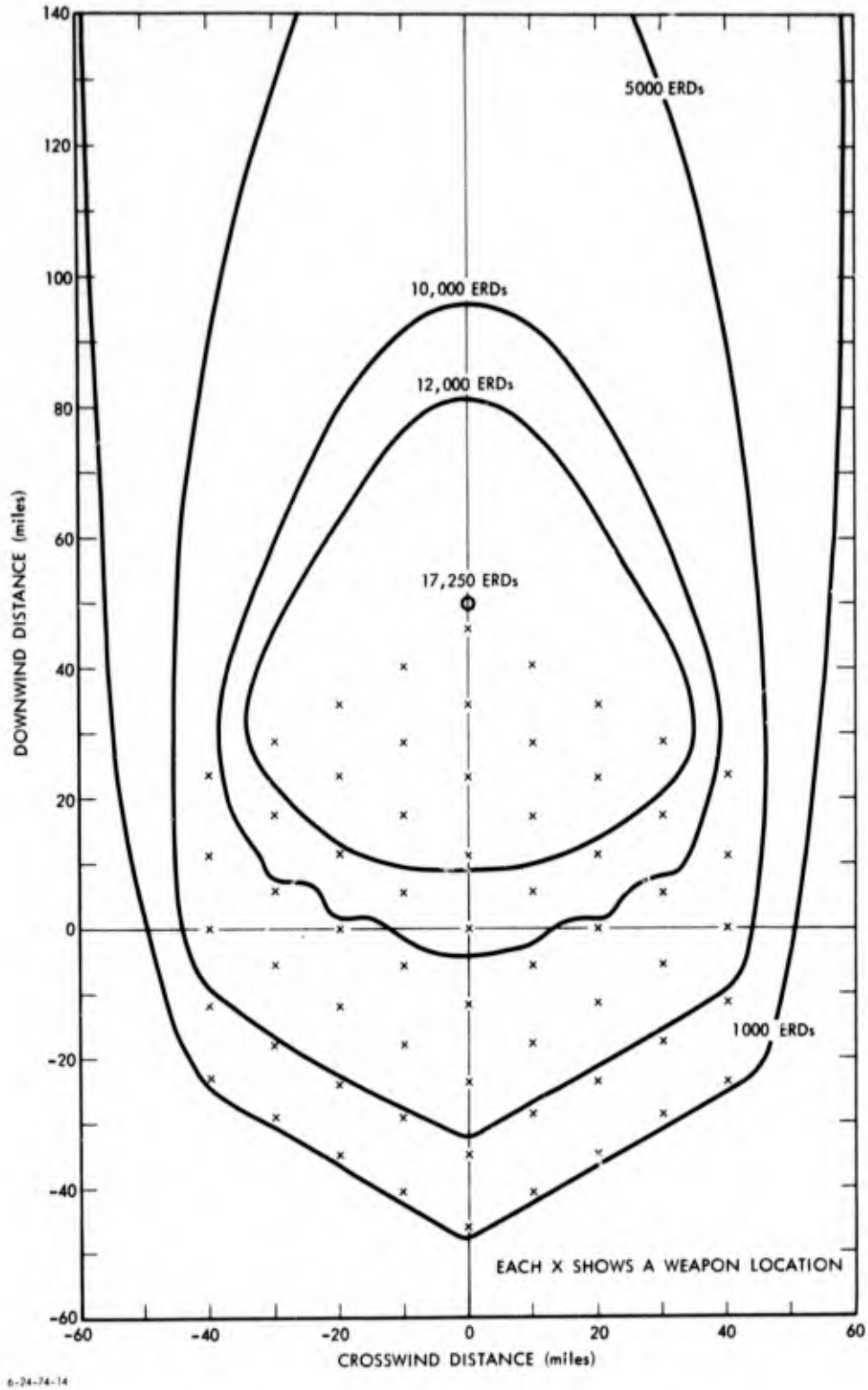

Figure 26. CONTOURS OF CONSTANT DOSE FOR 61 WEAPONS IN A FOUR-RING HEXAGON WITH 40-MILE HALF-WIDTH

The scaling of this pattern with yield is difficult to follow directly, since the scaling of the fallout patterns does not follow the same simple rules as for blast. This difference occurs because near ground zero the initial cloud dimension governs the pattern spread, whereas farther downwind the cloud spread due to wind shear governs; and as was seen earlier, these effects have different yield dependence. In Figures 27 and 28, the patterns of Figures 23 and 26 are repeated for 1-MT weapons, with the weapon spacing decreased by the cube root of the yield to maintain the same minimum overpressure. The fission fraction is decreased by yield to the 2/3 power to maintain the same density of fission released in the center of the patterns. As can be seen, a coalescence of patterns is again achieved.

The extent to which the patterns from individual weapons merge into a uniform pattern is further illustrated in Figures 29-33, where dose as a function of crosswind distance is plotted for the various weapon patterns at downwind distances of 0, 20, 50, 100, and 200 miles. In each figure, the dose is plotted for single-ring hexagon patterns with half-width distances of 0, 10, 20, and 40 miles. In addition, for 0- and 50-mile downwind distances, the dose is plotted for two-ring patterns with 20- and 40-mile half-widths and four-ring patterns with 40-mile half-widths. As is clear from these figures, the smallest spacings of the 10-mile half-width patterns and the 20-mile two-ring half-width pattern have everywhere a smooth decay in dose.

For intermediate spacing, illustrated by the 20-mile single-ring and 40-mile double-ring patterns, oscillations of about half the mean values are seen at distances of 0 and 20 miles, where the particular pattern influence is strong. However, at 50 miles downwind (which is 2-1/2 times the ring spacing), these particular oscillations have almost dropped out; and at 100 miles, the crosswind pattern is essentially smooth.

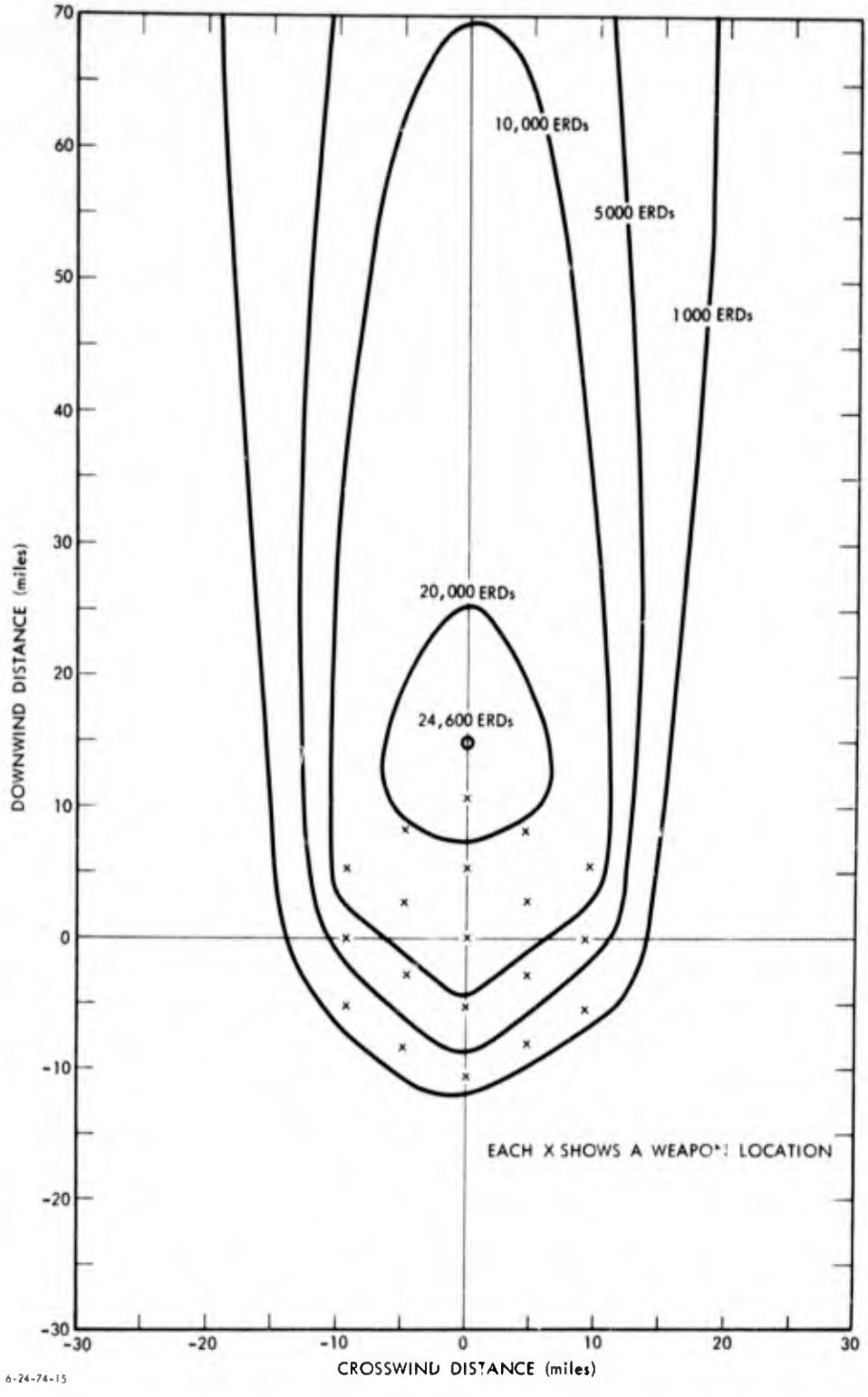

Figure 27. CONTOURS OF CONSTANT DOSE FOR 19 ONE-MEGATON WEAPONS IN A TWO-RING HEXAGON WITH 9.28-MILE HALF-WIDTH

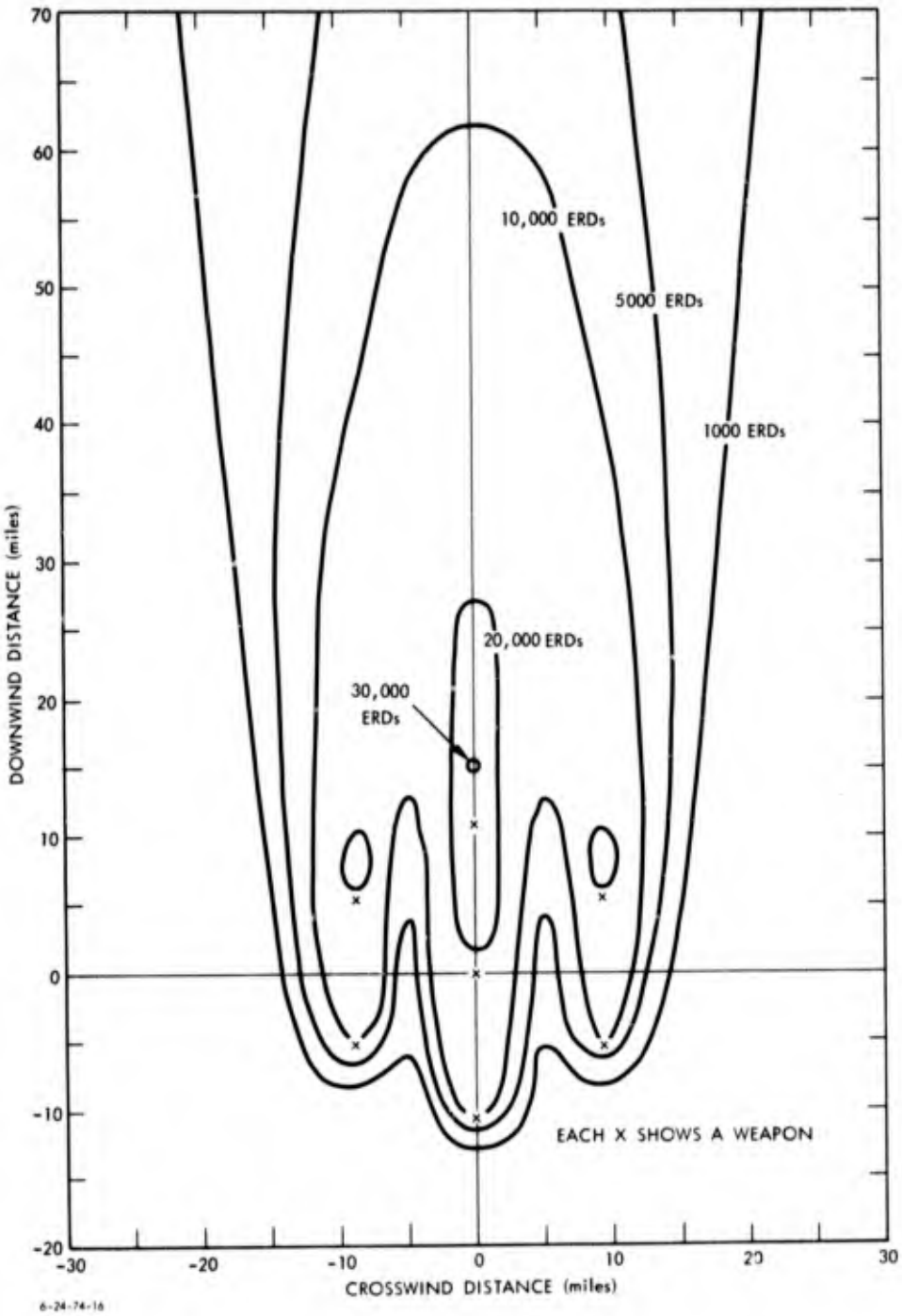

Figure 28. CONTOURS OF CONSTANT DOSE FOR SEVEN ONE-MEGATON WEAPONS IN A ONE-RING HEXAGON WITH 9.28 MILE HALF-WIDTH

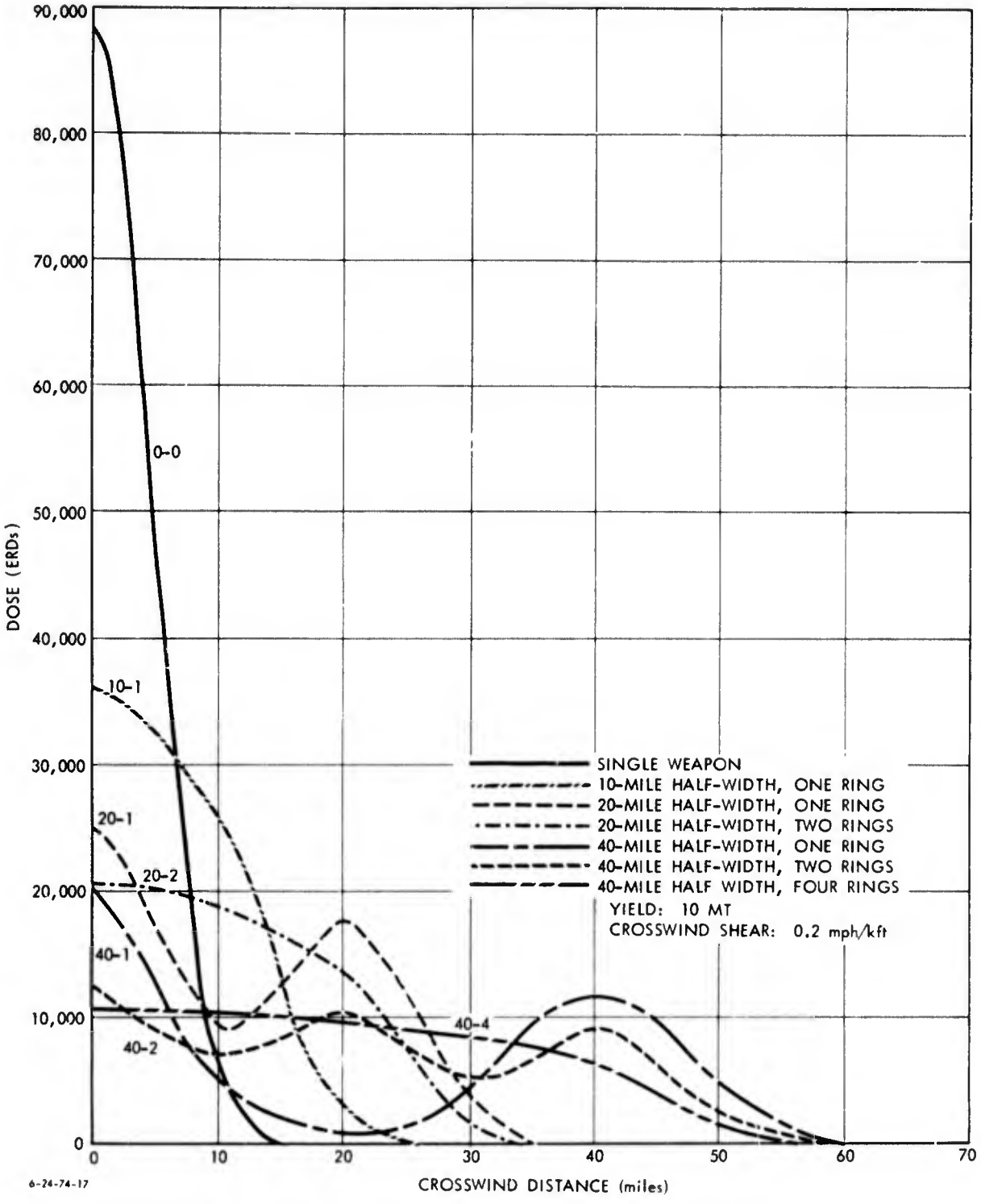

Figure 29. DOSE AS A FUNCTION OF CROSSWIND DISTANCE AT 0 MILES DOWNWIND, FOR HEXAGON PATTERNS

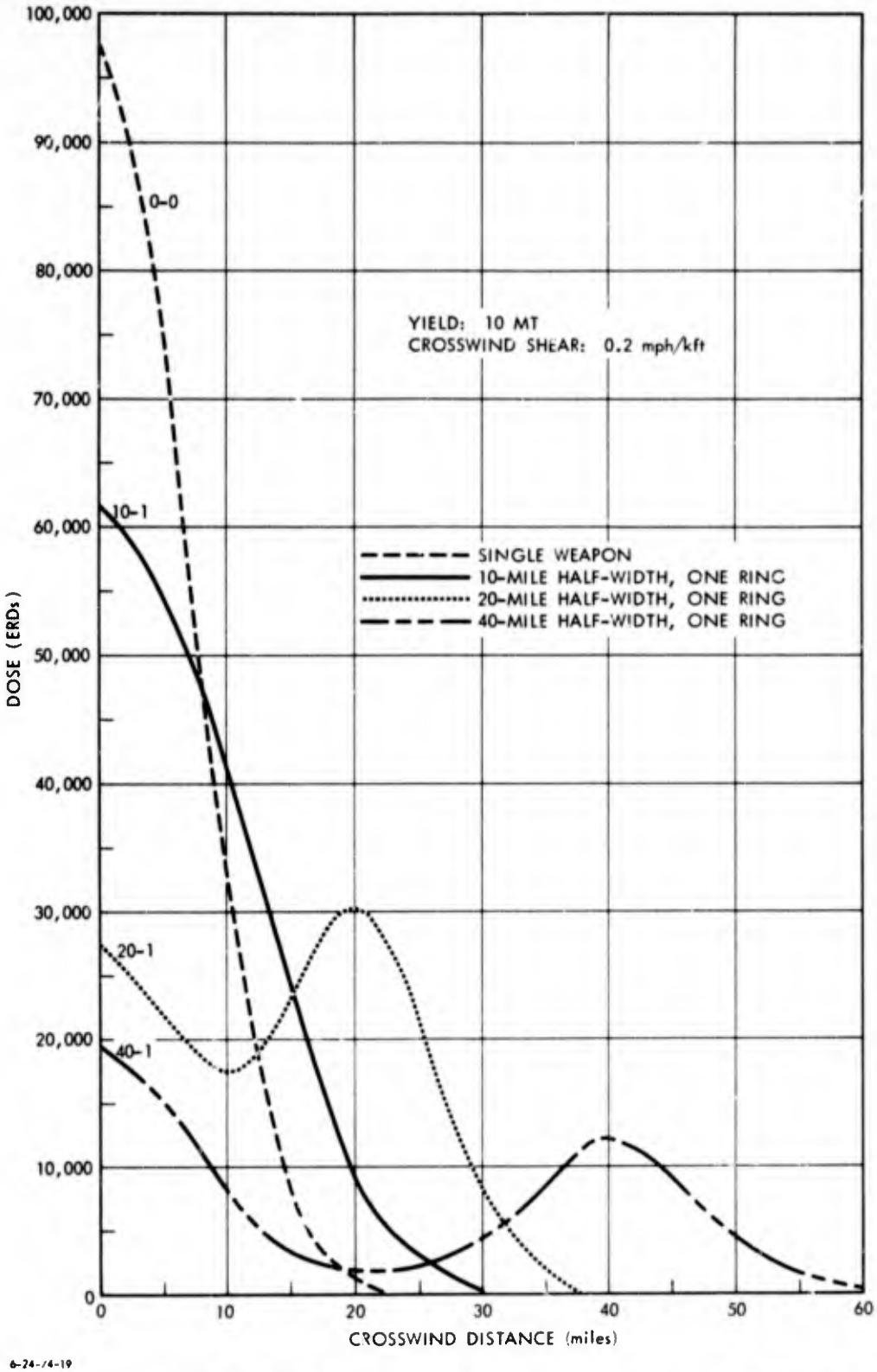

Figure 30. DOSE AS A FUNCTION OF CROSSWIND DISTANCE AT 20 MILES DOWNWIND, FOR HEXAGON PATTERNS

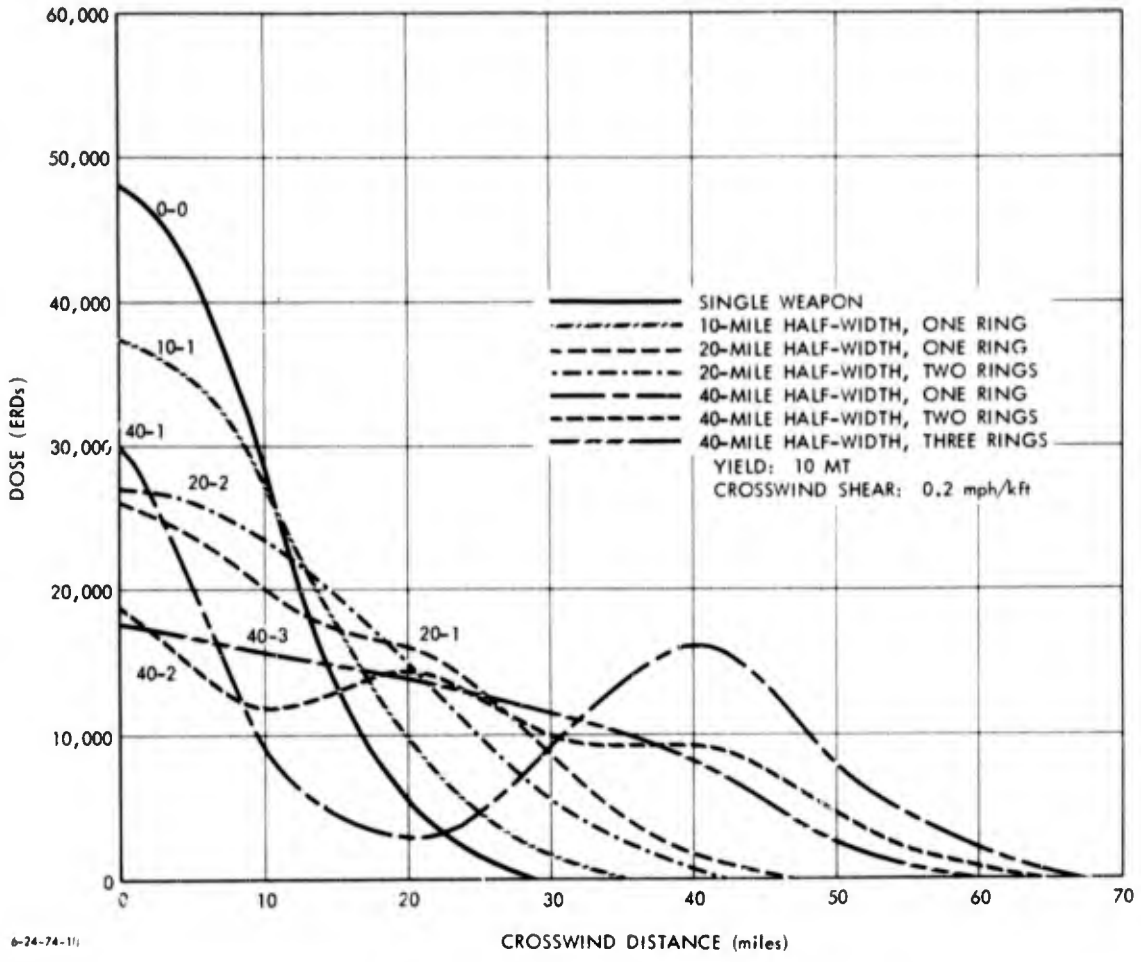

Figure 31. DOSE AS A FUNCTION OF CROSSWIND DISTANCE AT 50 MILES DOWNWIND, FOR HEXAGON PATTERNS

For the 40-mile single-ring pattern at small downwind distances, the weapons are essentially independent. At 100 miles downwind (again 2-1/2 times the ring spacing), the oscillation is about the same as--possibly a little more than--the oscillation at the same relative distance downwind with the 20-mile spacing. At 200 miles downwind, where the peak dose is down to 3,500 ERDs for the 40-mile spacing, a smooth drop-off is observed. In this case, a scaled downwind distance of about 4 is needed for the oscillation to be substantially smoothed out.

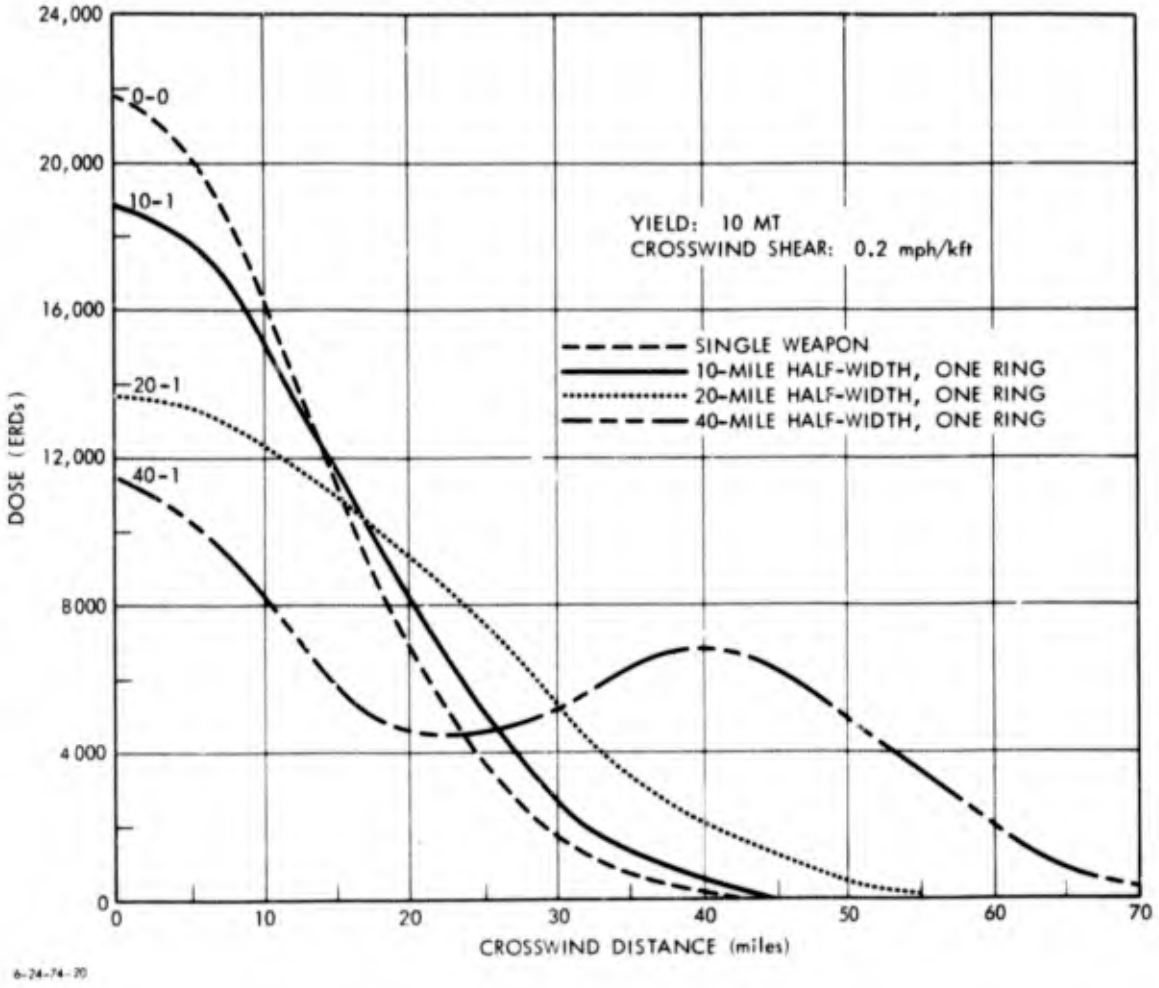

Figure 32. DOSE AS A FUNCTION OF CROSSWIND DISTANCE AT 100 MILES DOWNWIND, FOR HEXAGON PATTERNS

In Figures 34-37, the dose is presented as a function of downwind distances for several crosswind distances. The first three figures have the small weapon spacing, in which a coalescence of patterns occurred for one-, two-, and four-ring hexagon patterns; here a near linear rise followed by an exponential-like decay is evident. In Figure 37, however, the intermediate weapon spacing is used--which gives peaks in the rising portion; but a linear rise might well be superimposed on this pattern. Figure 36 shows the dose that would be computed (by using the

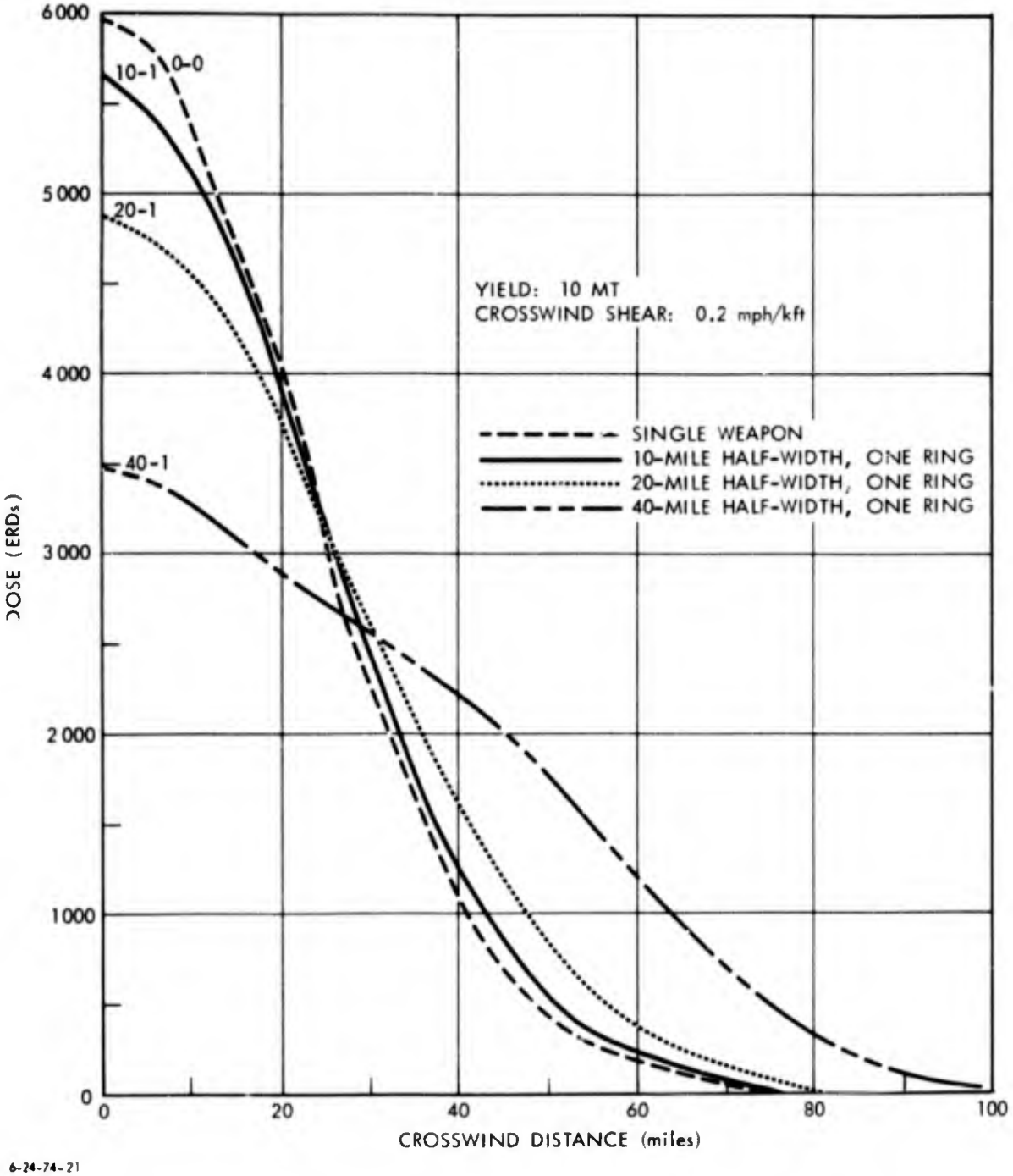

Figure 33. DOSE AS A FUNCTION OF CROSSWIND DISTANCE AT 200 MILES DOWNWIND, FOR HEXAGON PATTERNS

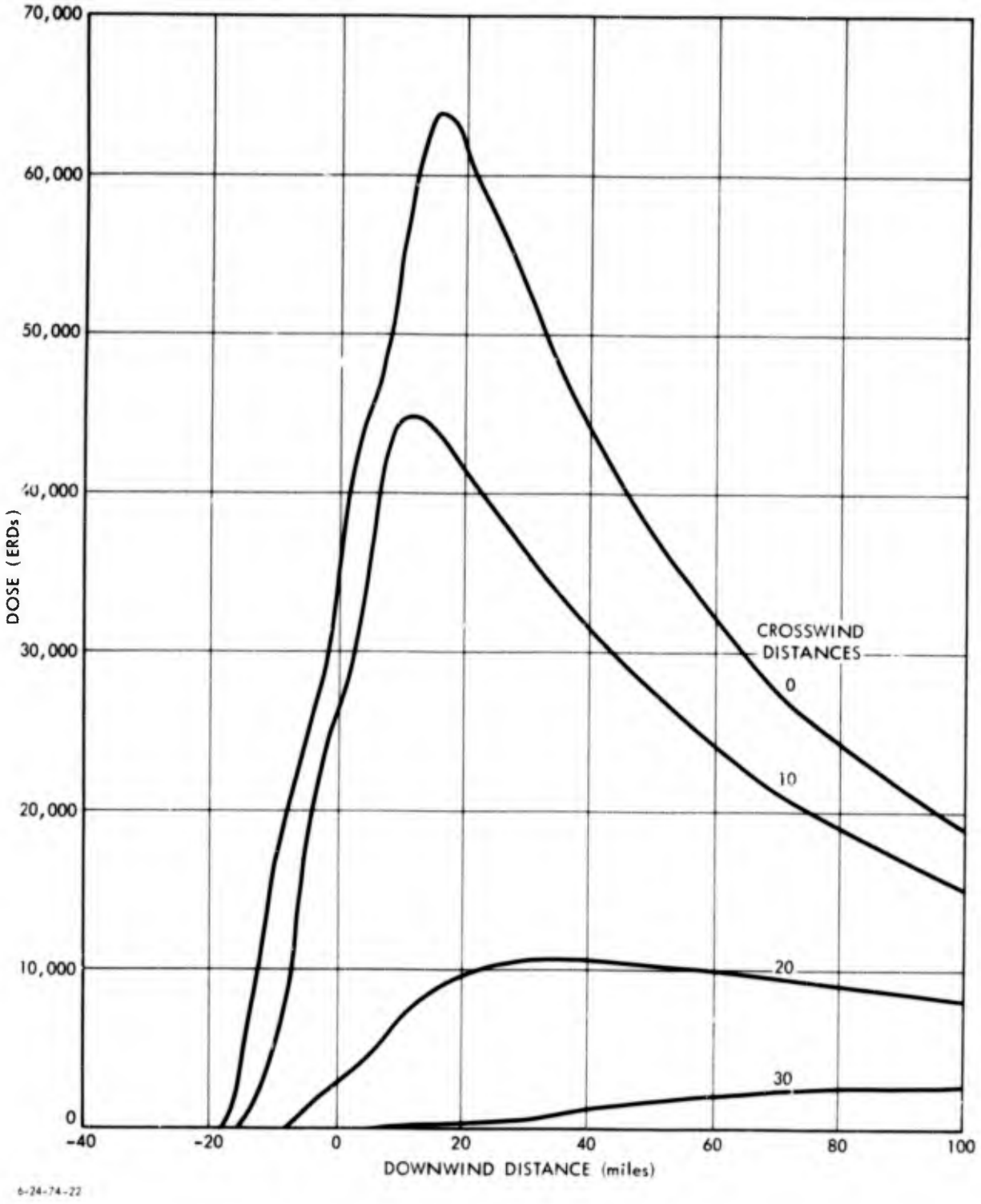

Figure 34. DOSE AS A FUNCTION OF DOWNWIND DISTANCE AT SEVERAL CROSSWIND DISTANCES FOR A SEVEN-WEAPON ONE-RING HEXAGON WITH 10-MILE HALF-WIDTH

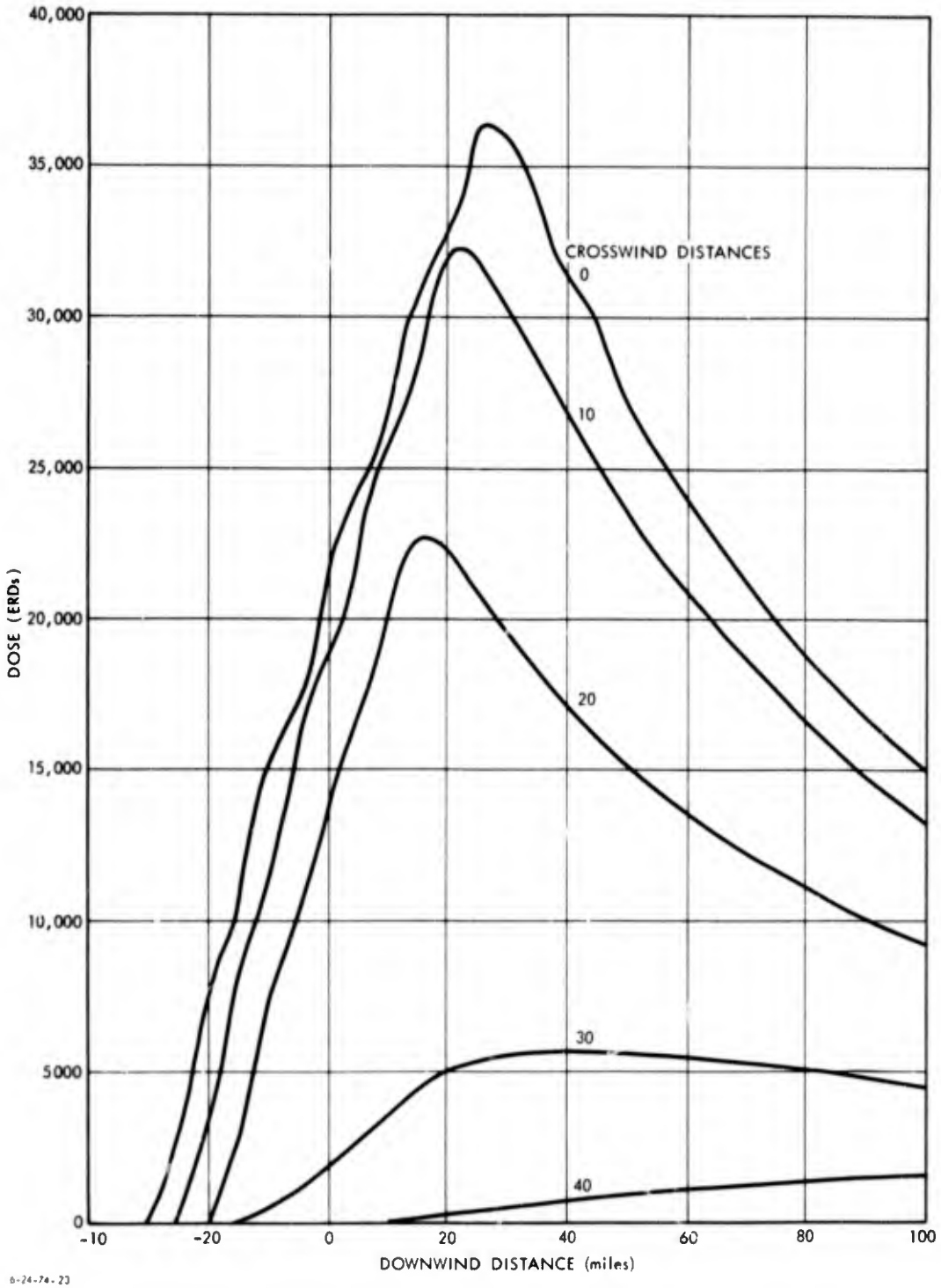

Figure 35. DOSE AS A FUNCTION OF DOWNWIND DISTANCE AT SEVERAL CROSSWIND DISTANCES FOR A 19-WEAPON TWO-RING HEXAGON WITH 20-MILE HALF-WIDTH

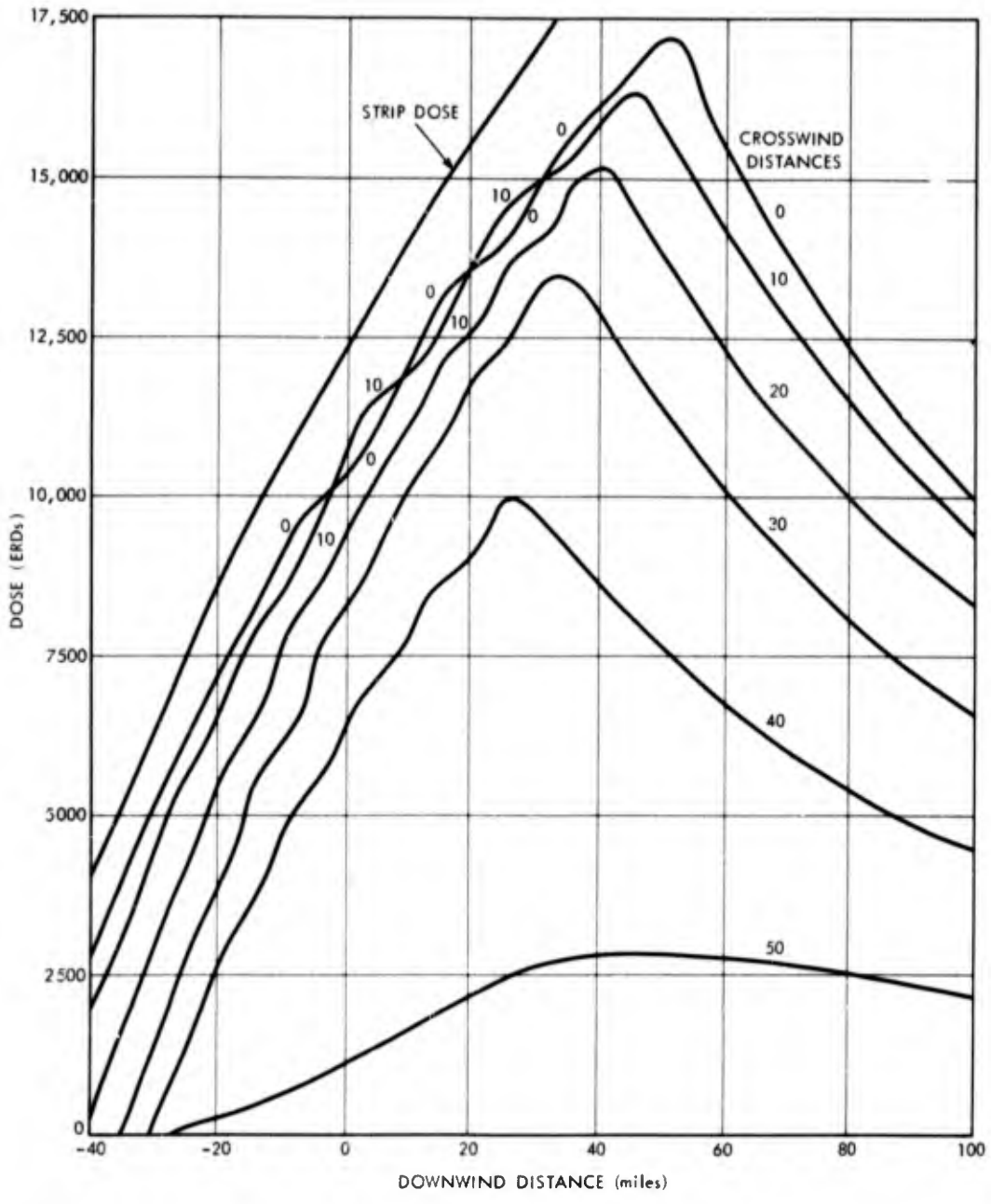

Figure 36. DOSE AS A FUNCTION OF DOWNWIND DISTANCE AT SEVERAL CROSSWIND DISTANCES FOR A 61-WEAPON THREE-RING HEXAGON WITH 40-MILE HALF-WIDTH

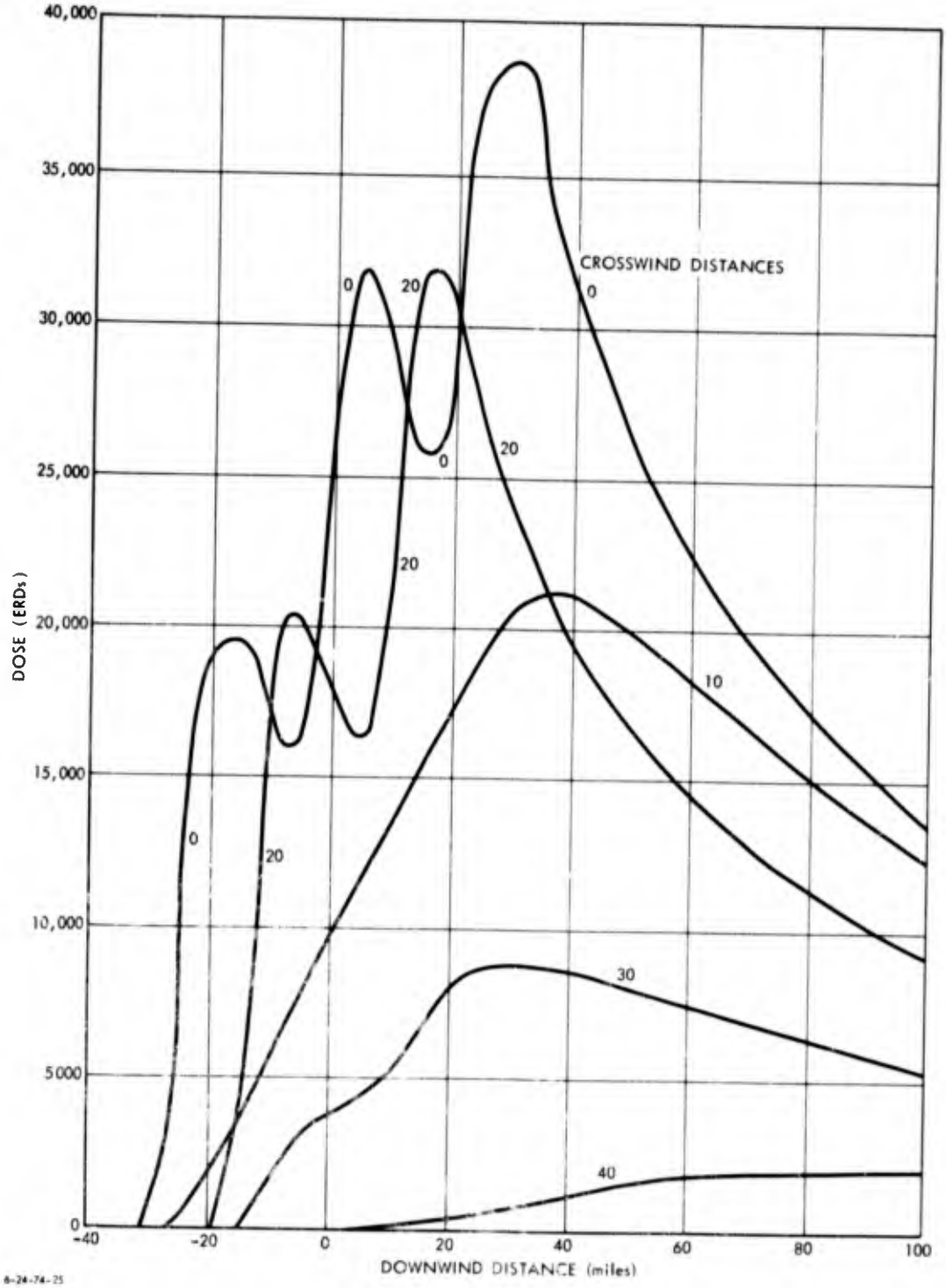

Figure 37. DOSE AS A FUNCTION OF DOWNWIND DISTANCE AT SEVERAL CROSSWIND DISTANCES FOR A SEVEN-WEAPON ONE-RING HEXAGON WITH 20-MILE HALF-WIDTH

methods of Section A.3, above) for the center strip of the weapon pattern by using a constant weapon density--assuming a strip length of 104 miles (to give the proper downwind weapon spacing) and a strip width of 10 miles. As can be seen, the dose calculated for the strip is about 15 percent higher than the centerline dose of the pattern. This difference could be due to several effects (e.g., improper placement of the strip; leakage from th center strip to adjacent, less heavily exposed strips; and the continuous density assumption). An experimental correction of about 15 percent seems to be appropriate.

C. WEAPONS IN A SAMPLE ATTACK PATTERN

Figure 38 shows the ground zeros and the overpressure patterns for a blast-optimized attack on Detroit, Michigan--using 15 five-MT weapons. In this attack, the median lethal overpressure was assumed to be 6.5 psi; and the weapon reliability, 0.75. There were 25-percent expected survivors from blast effects. In Figure 39, contours of constant dose are shown for this attack--assuming that each weapon arrived, the weapon fission fraction was 0.5, a 20-mph wind was blowing due east, and the shear was 0.2 mph/kft. It will be noticed that the fallout contours do coalesce into a single pattern. Moreover (with the exception of a bump in the lower right-hand corner of Figure 39, which represents the weapon targeted on Pontiac, Michigan), a rather regular pattern is obtained. The peak dose of 50,000 ERDs is obtained at the downwind edge of the weapon pattern, and the rise up to this value is approximately linear. Thus many of the features seen in the hexagon patterns are duplicated in this sample attack pattern.

D. AN APPROXIMATE CALCULATION METHOD

In this section, a scheme that may be used to calculate dose from patterns of weapons is presented. To do this, the

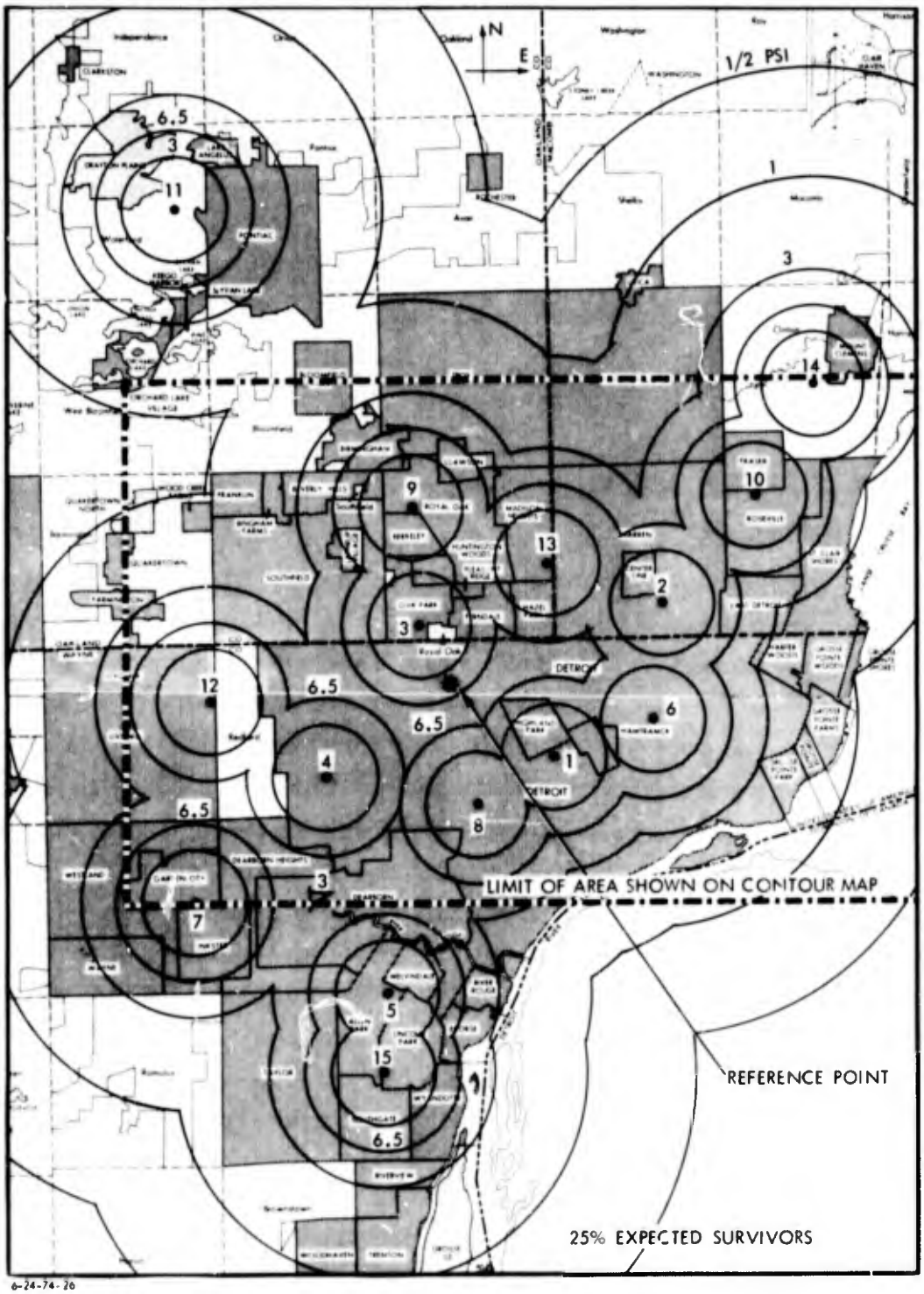

Figure 38. OVERPRESSURE CONTOURS FOR OPTIMIZED 15-WEAPON ATTACK ON DETROIT

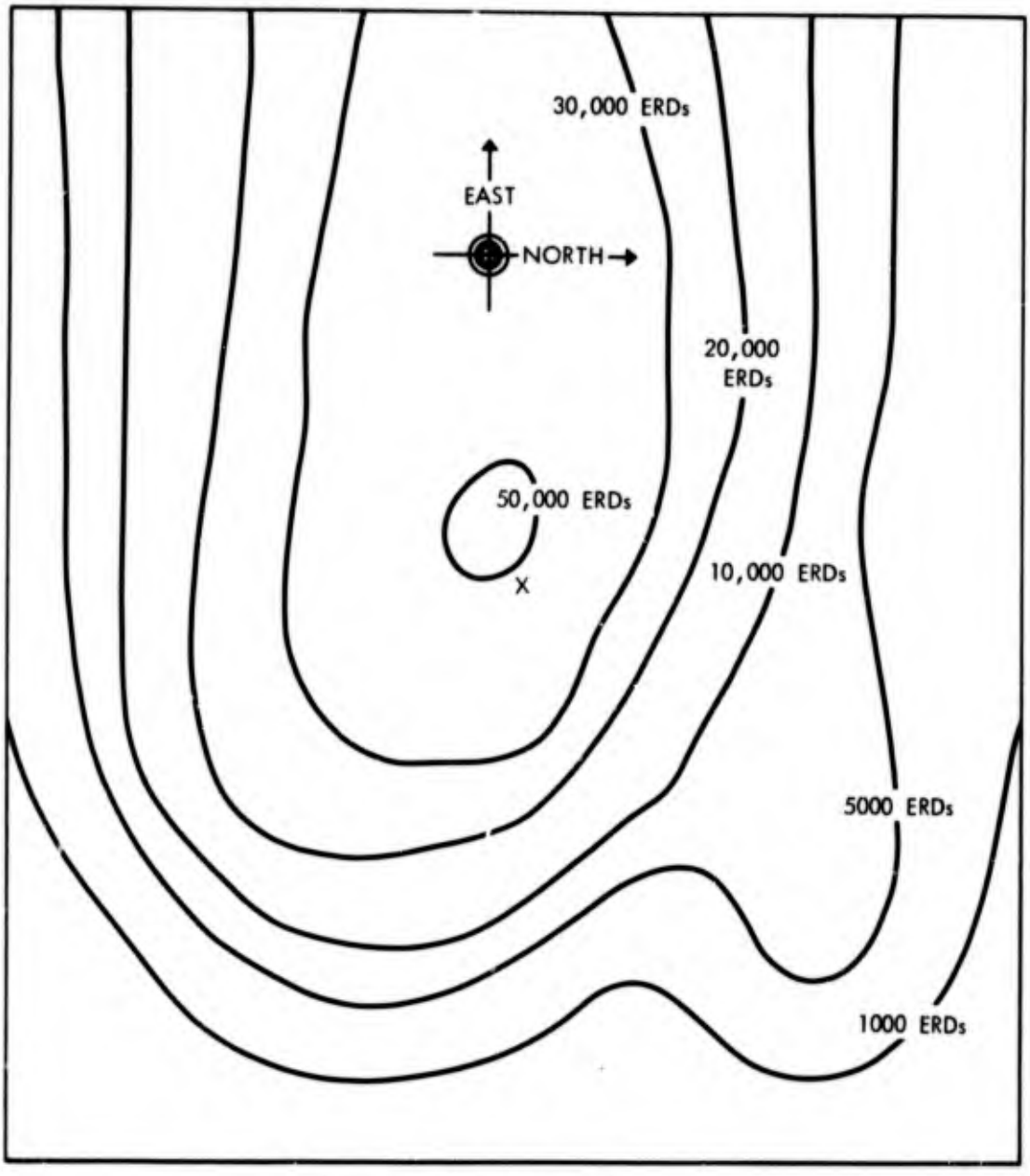

FISSION FRACTION: 0.5
WIND: 20 MPH DUE EAST
CROSSWIND SHEAR: 0.2 mph/kft
SCALE: |←10 MILES→|

6-24-74-27

Figure 39. CONTOURS OF CONSTANT DOSE FOR 15 FIVE-MEGATON WEAPONS BLAST OPTIMIZED ATTACK ON DETROIT

simplest possible representation that will resonably reproduce the hexagon patterns is chosen. In addition, the same basic formulation is desired to hold over all ranges.

The dose D will again be written as a product of downwind and crosswind terms. Thus,

$$D = KFYF_d(x)F_c(y) \ .$$

We assume that weapons are regularly dropped over a pattern represented by a half-width R and half-length L, centered at the origin of the coordinate system. F_d is simply represented by a linear rise over the pattern, followed by a decay--as if all the weapon yield were delivered at the origin. Thus,

$$F_d(x) = \begin{cases} 0, & \text{if } x < -L \ ; \\ \dfrac{2.71}{WT^{1.382}} \dfrac{x + L}{2L} \dfrac{\exp\left(-\left(\frac{L}{WT}\right)\right)}{\left(\frac{L}{WT}\right)^{0.382}}, & \text{if } -L \leq x < L \ ; \\ \dfrac{2.71}{WT^{1.382}} \dfrac{\exp\left(-\left(\frac{x}{WT}\right)\right)}{\left(\frac{x}{WT}\right)^{0.382}}, & \text{if } L \leq x \ . \end{cases}$$

where $T = 7.5 + 1.66 \log_{10} Y$.

If desired, the rational polynomial expression for the exponential divided by the power given earlier may be used for computational speed. Clearly, the alternative for $F_d(x)$ presented earlier (based on integrating over the strip) might also be used to yield some increase in accuracy.

$F_c(y)$ can be taken from the formula based on a uniform density of crosswind deposition. Then

$$F_c = \frac{1}{2R}\left\{\text{cumnor}\left(\frac{y}{\sigma_c} + \frac{R}{\sigma_c}\right) - \text{cumnor}\left(\frac{y}{\sigma_c} - \frac{R}{\sigma_c}\right)\right\} \ .$$

σ_c may be calculated by

$$\sigma_c = A + B \frac{(x + L)S_c}{W},$$

with $A = 2 + 3 \log_{10} Y$ and $B = 7.5 + 1.5 \log_{10} Y$.

In Figure 40, contours of constant dose are shown for this model for a 10-MT weapon with fission fraction of 7,[1] W = 20 mph, S_c = 0.2, R = 20, and L = 25. These values were chosen to approximate the 19-weapon, 20-mile half-width hexago shown in Figure 23. The general features of that pattern are reproduced in Figure 40.

One measure of the goodness of fit, the peak doses, is compared between the hexagon pattern and the simple model in the following table:

Pattern Half-Width	Hexagon Pattern Peak Dose (ERDs)	Model Peak Dose (ERDs)
0	142,500	172,787
10	64,000	85,790
20	36,500	40,000
40	17,250	13,823

It can be seen that the simple model tends to overestimate peak dose for small patterns and underestimate the peak dose for larger patterns.

The calculation for σ_c measures distances from the upwind edge of the pattern. This choice is somewhat arbitrary; a case could be made for measuring σ_c from the center of the pattern. The present method was chosen simply to match peak doses better for smaller pattern sizes. In the other method of computing peak doses, σ_c values of 94,000 and 41,000 ERDs are obtained for 10- and 20-mile half-width patterns.

[1]The weapon yield is selected as the average weapon yield in the cluster (here, 10 MT), and the "fission fraction" is then determined as the value that gives the same total fission yield as for the cluster being approximated.

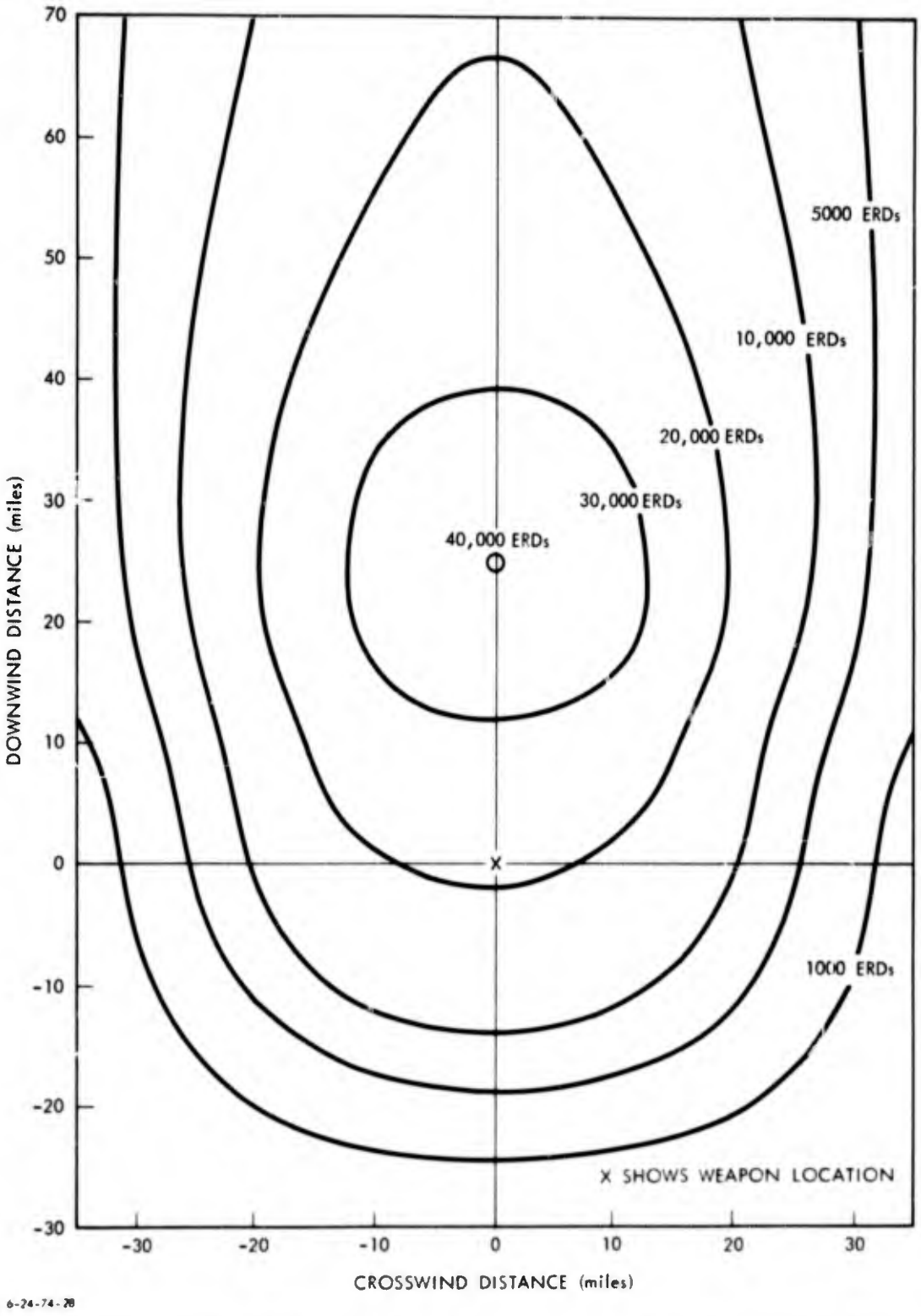

Figure 40. CONTOURS OF CONSTANT DOSE FROM SIMPLIFIED MODEL, WITH 20-MILE HALF-WIDTH

An alternative method of computing $F_c(y)$, which probably would be more appropriate for large downwind distances, would be to compute $F_c(y)$ by

$$F_c(y) = \frac{1}{\sqrt{2\pi}\sigma_u} \exp\left(y^2/2\sigma_u^2\right) ,$$

with $\sigma_u = \sqrt{\sigma_c^2 + \sigma_w^2}$, where σ_w is the second moment of the weapon density in the crosswind direction. If the total fission yield deposited at some crosswind distance y is g(y), then

$$\sigma_w^2 = \int_{-\infty}^{\infty} y^2 g(y)\, dy \Big/ \int_{-\infty}^{\infty} g(y)\, dy .$$

For the sake of simplicity in this application, the distance used to compute σ_c should be taken as the centroid of the fission deposition.

When R/σ_c becomes small (say, less than 0.25), the first form for F_c approaches the second, since when the difference in the cumulative normal functions becomes small the difference approaches the value of the derivative, which by definition is simply the exponential. For downwind distances of over 100 miles the second form is probably preferable, even when the crosswind fission deposition over the target area tends toward uniform density. When the targeting is more concentrated at the center of the target area, this second form is definitely to be preferred.

In Figures 41-43 (at downwind distances of 50, 100, and 200 miles, respectively), the logarithm of dose is presented as a function of crosswind distance squared for a single 10-MT weapon with a fission fraction of 7 and for hexagons with seven weapons and 10-mile half-width, 19 weapons and 20-mile half-width, and 61 weapons and 40-mile half-width. In this form of presentation, the second form of F_c should give a straight line. The dose that would be theoretically calculated with the second form of

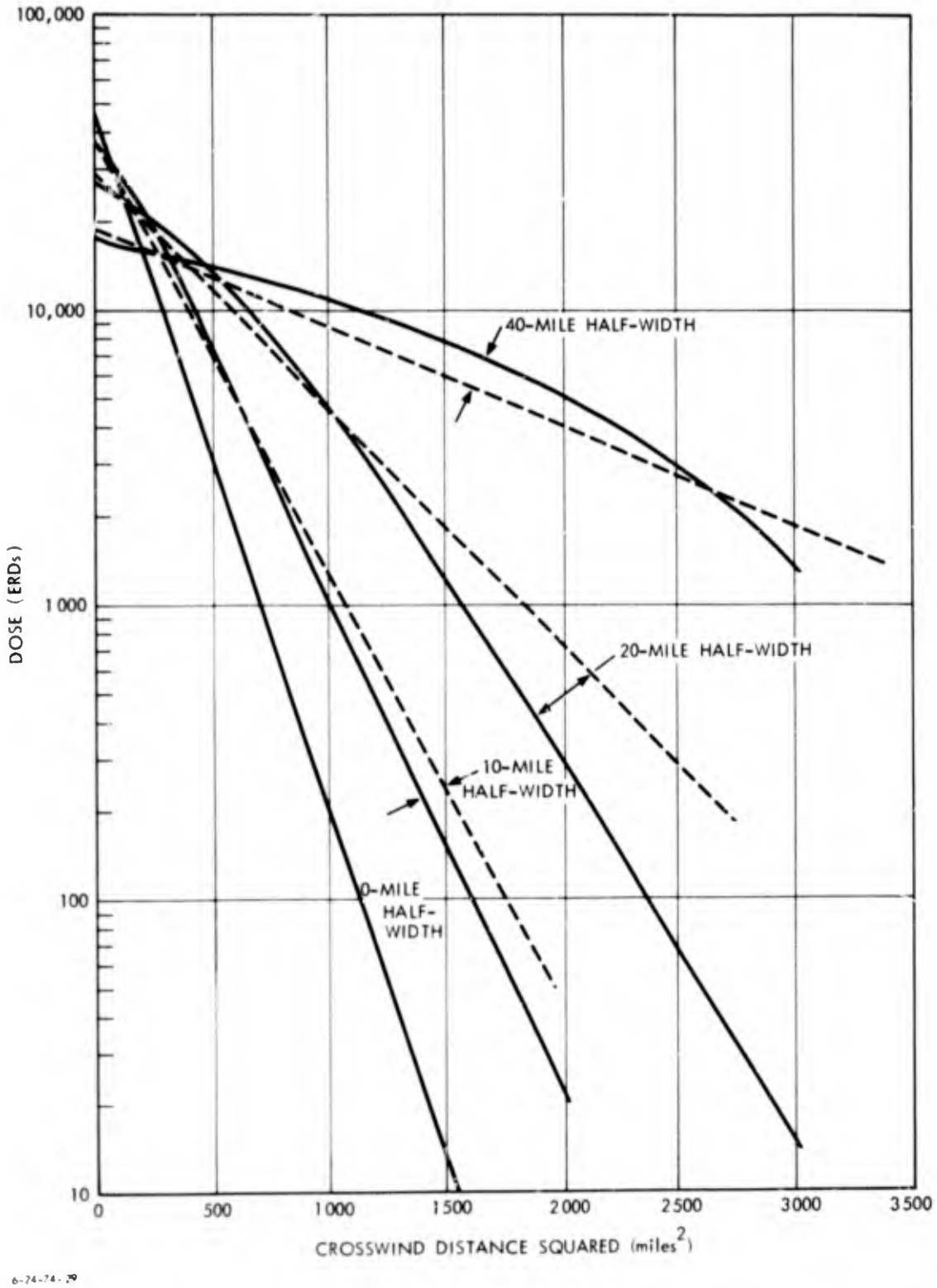

6-24-74-29

Figure 41. LOGARITHM OF DOSE AS A FUNCTION OF CROSSWIND DISTANCE SQUARED, AT 50 MILES DOWNWIND, FOR SEVERAL CLOSELY SPACED HEXAGON PATTERNS

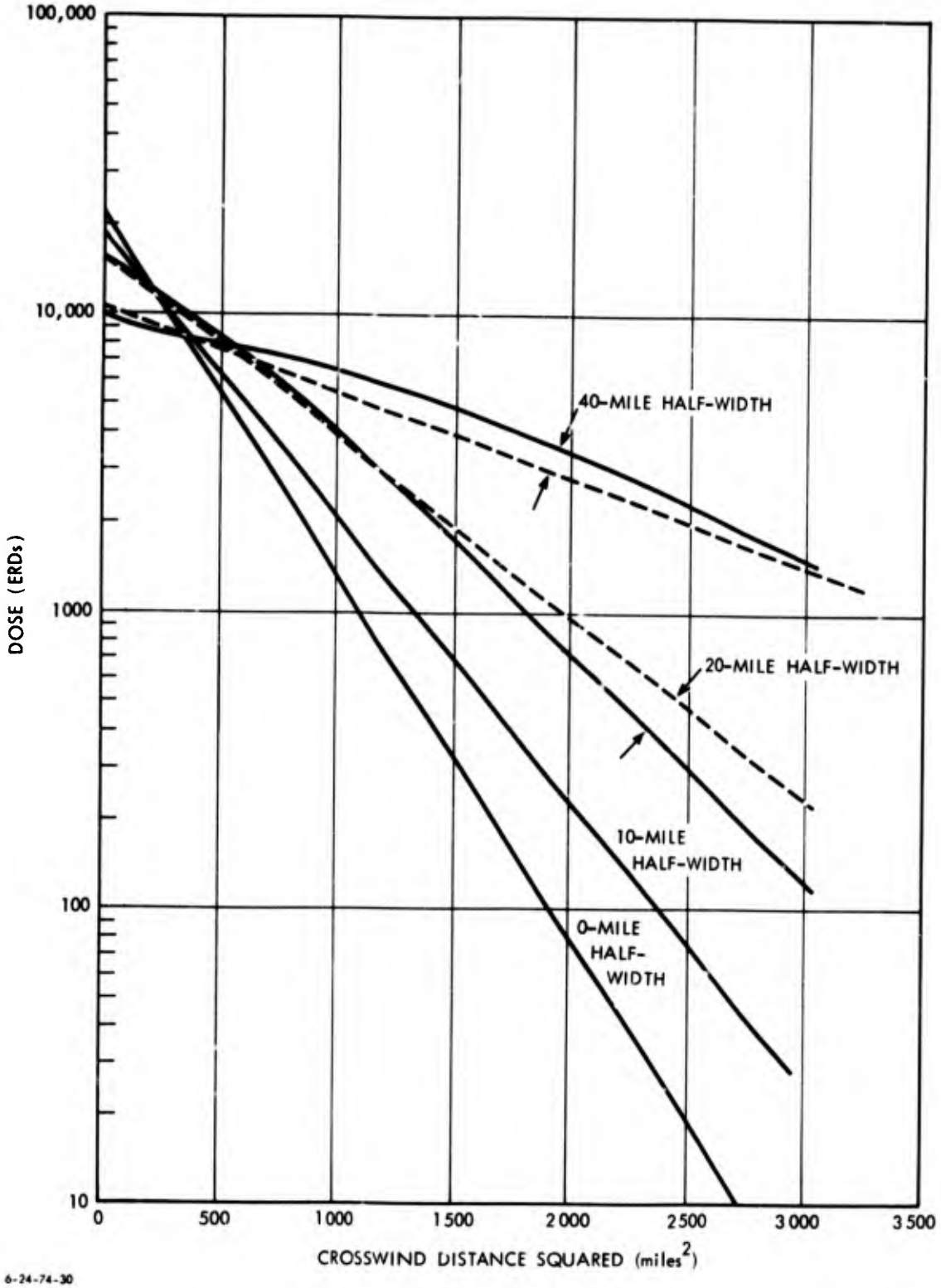

Figure 42. LOGARITHM OF DOSE AS A FUNCTION OF CROSSWIND DISTANCE SQUARED, AT 100 MILES DOWNWIND, FOR SEVERAL CLOSELY SPACED HEXAGON PATTERNS

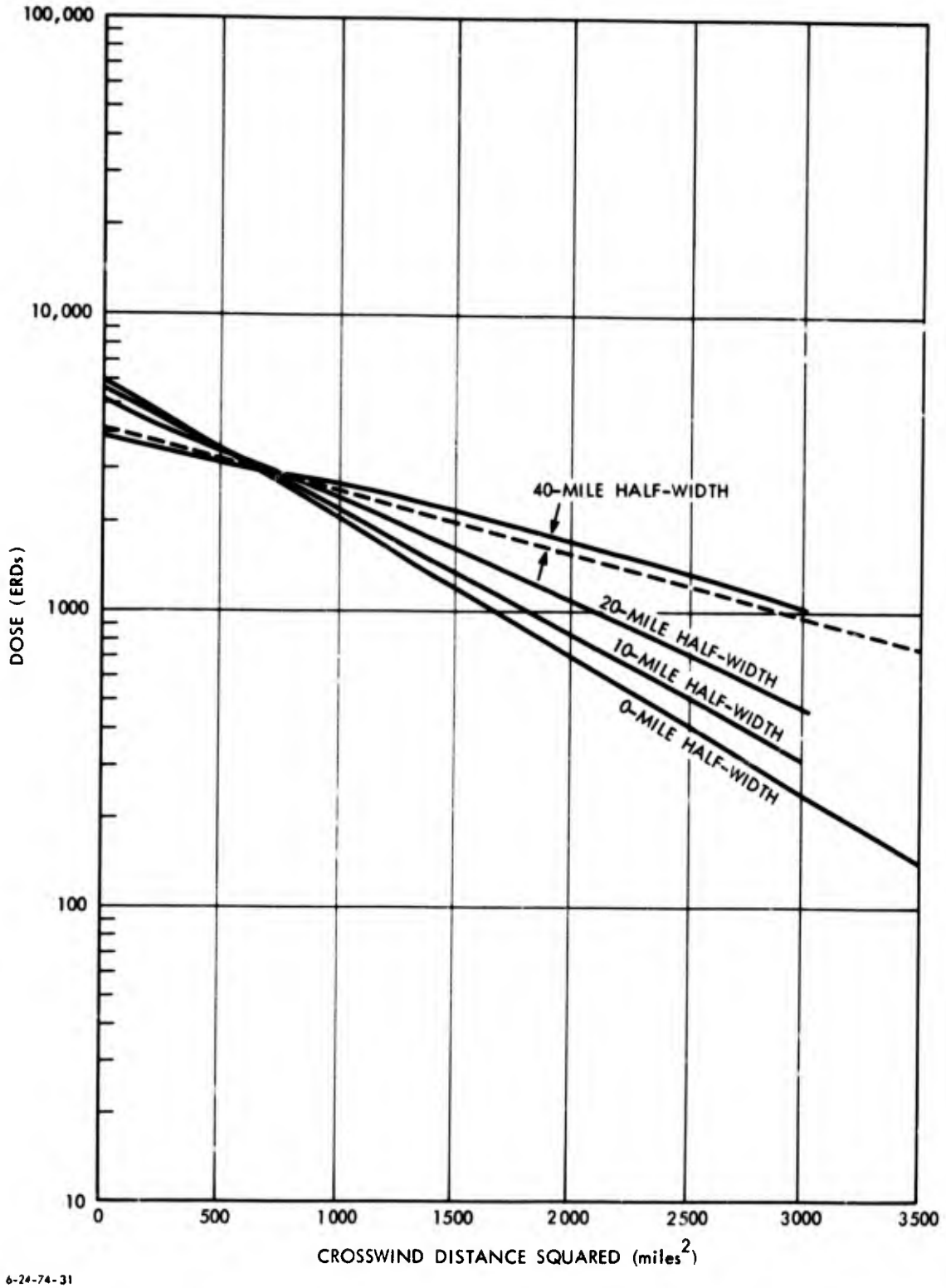

Figure 43. LOGARITHM OF DOSE AS A FUNCTION OF CROSSWIND DISTANCE SQUARED, AT 200 MILES DOWNWIND, FOR SEVERAL CLOSELY SPACED HEXAGON PATTERNS

F_c using the actual second moments of fission deposition is shown on these figures by dashed lines, except when the theoretical line is too close to the plotted hexagon values to be distinguished. Since the purpose is to compare methods of calculating F_c, the theoretical curves are all normalized to the value of F_d as it is obtained with a single weapon. The method shows considerable robustness. Even the 40-mile pattern at 50 miles downwind is approximated in general shape by this simple calculational scheme.

In the simulation used in Chapter V (below), the exponential expression for $F_d(x)$ just given is used when $x/WT < 0.6$; the polynomial fit to F_d is used when $0.6 \leq x/WT \leq 8$; and 0 is used for larger values of x/WT. When x is less than the cluster-length L, the exponential form is used to compute the peak dose at $x = L$, which is used to find the slope of the linear increase in dose. When $x \leq 5\sigma_w$, the cumulative normal form is used for F_c; otherwise, the exponential of crosswind distances squared just described is used.

Since the item fitted by the cluster model is the dose and not the H+1 dose rate, normalization of F_d is not preserved. However, it still is possible to determine the integral (over distance) of the H+1 dose rate. When F_d is represented by the exponential form, this integral is given by $\exp(-L/WT)\ (1 + L/WT)$. For $L/WT = 0$, this value is 1; for L/WT under 0.15, within one percent of 1; and for L/WT under 0.5, within 10 percent of 1. Thus this form slightly underestimates the total H+1 dose rate from a cluster of weapons. For the form used in the simulation, the integral is 1.16 for L/WT less than 0.1, and it decreases approximately linearly to 0.92 for L/WT = 1. Since values of L/WT are usually less than 0.1 and almost always less than 1, the values of H+1 dose rate for the cluster model are almost always within 15 percent of the normalized values. This normalization correction to the H+1 dose rate could be included if

desired, but in the interest of conceptual simplicity it has not been here.

Chapter III

DISTRIBUTION OF WIND VARIABLES

A. WIND STATISTICS

The statistical description of wind speed and direction will be based partly upon data suggested by DCPA for use in fallout planning.[1] These data are based upon observation of mean-wind speed and direction from altitudes of 0 to 80,000 feet, taken from 1 March 1951 through 29 February 1956. For each of the four seasons, the mean vector wind speed and direction were computed; and a vector standard deviation was determined. These basic data, plus some observations in Alaska and Hawaii, are reproduced in Table 1. Moreover, maps from the DCPA report drawn from the tabular data are included as Figures 44-47.

In accordance with frequent meteorological practice, the vector standard deviation will be assumed to represent a circular normal distribution.[2] By selecting a sample from such a circular normal distribution, constructing a vector from the center of the distribution to the point selected, and adding this vector to the mean vector wind a sample wind would be

---

[1] *User's Manual - Meteorological Data for Radiological Defense*, Department of Defense, Office of Civil Defense, FG-E-5.6/1, July 1970; Government Printing Office 0-454-240, 1972.

[2] For more complete sets of wind statistics (including zonal and meridional components, see *Upper Wind Statistics of the Northern Hemisphere*, Harold L. Crutcher, NAVAER50-1C-535, U.S. Navy, Chief of Naval Operations; and Harold L. Crutcher, *Meridional Cross-Sections - Upper Winds Over the Northern Hemisphere*, Technical Paper 41, Weather Bureau, U.S. Dept. of Commerce, June 1961.

Table 1. CLIMATOLOGICAL MEAN-WIND DIRECTION (D) AND SPEED (S) IN KNOTS (IN THE LAYER FROM 80,000 FEET TO EARTH'S SURFACE AND VECTOR STANDARD DEVIATION (V)

Location	Spring			Summer			Fall			Winter			Annual	
	D	*S*	*V*	*D*	*S*	*V*	*D*	*S*	*V*	*D*	*S*	*V*	*D*	*S*
Albrook	276	02.5	08.3	277	14.7	07.3	275	08.8	07.6	044	02.2	09.3	279	6
Albuquerque	082	24.9	19.4	035	03.6	13.2	095	17.1	19.5	092	28.9	22.3	087	18
Anchorage	056	05.8	19.4	049	03.7	17.0	053	14.3	20.4	080	17.7	28.0	064	10
Annette	077	12.9	22.4	098	05.0	18.9	076	22.0	21.7	090	24.0	23.5	084	16
Big Spring	078	30.7	18.7	284	05.3	13.8	093	15.5	20.0	084	35.6	21.2	084	19
Bismark	097	17.1	20.0	085	16.8	15.1	087	23.9	20.5	109	27.8	20.5	095	21
Boise	096	16.6	20.0	062	15.7	14.8	097	19.4	20.7	102	25.9	22.9	092	19
Brownsville	078	24.4	15.4	275	12.8	10.7	088	08.2	17.7	077	29.5	16.5	075	13
Buffalo	096	26.3	23.1	107	16.6	16.5	083	28.8	22.6	089	37.4	23.7	092	27
Burrwood	087	28.1	18.7	261	09.5	11.8	088	14.0	19.4	083	37.0	17.8	086	18
Caribou	089	19.0	22.7	093	16.4	18.7	080	29.9	23.3	081	29.7	24.1	084	23
Charleston	092	29.8	22.3	229	03.6	13.6	079	19.0	21.6	088	42.4	19.4	089	22
Columbia	087	28.2	22.6	099	08.4	13.4	096	23.8	21.3	091	38.5	25.3	092	24
Dayton	092	28.7	23.5	115	11.5	14.9	089	24.9	20.9	090	41.5	26.0	092	26
Denver	090	20.7	20.2	073	10.0	13.5	103	18.6	19.7	104	26.0	22.0	097	18
Dodge City	083	25.7	20.4	072	06.7	13.1	096	20.8	20.7	093	32.2	23.2	090	20
Edmonton	099	12.8	17.8	076	09.5	15.3	102	23.0	18.5	109	27.1	18.2	100	17
Ely	095	17.7	20.0	052	12.9	13.0	092	16.9	19.0	102	24.0	23.0	089	17
Fairbanks	067	06.8	18.2	060	04.6	14.8	061	15.3	18.4	085	18.7	25.5	072	11
Fort Worth	082	31.5	20.4	282	03.7	13.2	095	16.5	20.7	085	37.8	22.3	087	20
Great Falls	095	18.8	19.4	069	16.8	15.3	102	24.1	20.3	106	30.0	21.8	098	22
Green Bay	096	21.7	21.5	105	17.3	16.1	097	26.2	22.1	098	32.4	23.0	099	24
Greensboro	092	30.2	22.8	137	05.0	14.5	081	22.3	21.5	087	43.4	21.2	090	25
Hempstead	094	29.0	24.4	104	13.6	16.7	081	29.0	24.2	089	42.7	25.3	090	29
Internat'l Falls	099	16.3	20.2	098	17.8	16.5	106	24.0	21.4	107	27.9	21.2	104	21
Jacksonville	094	27.7	20.8	253	06.5	12.0	083	16.5	20.7	088	39.0	18.2	090	20
Lake Charles	083	29.6	19.0	263	08.2	12.1	094	15.3	19.8	082	38.8	19.3	085	19
Lihue	093	15.8	15.0	289	04.5	09.8	123	01.0	12.0	100	15.1	16.8	100	07
Little Rock	085	31.1	21.8	212	01.9	13.2	096	19.7	20.8	085	40.5	23.2	089	22
Long Beach	093	20.7	20.4	029	07.6	13.2	082	12.7	17.1	101	22.2	23.3	098	14
Maniwaki	097	20.5	22.7	108	16.2	17.0	085	27.3	23.0	089	30.8	22.2	092	23
Medford	100	18.8	21.2	064	12.0	16.0	092	17.0	22.2	099	26.3	24.3	092	18
Miami	097	21.8	17.2	267	12.4	10.7	080	06.5	18.4	088	29.5	17.2	092	11
Montgomery	092	30.7	22.5	246	05.4	13.4	087	18.5	21.5	086	42.2	21.4	091	21
Mt. Clemens	089	26.2	24.0	109	16.2	16.4	088	26.9	22.3	090	37.0	24.7	093	26
Nantucket	090	29.3	24.3	091	14.6	17.7	077	30.3	23.6	085	42.6	26.2	085	29
Nashville	088	31.2	22.7	146	03.7	13.3	089	22.0	21.2	086	42.7	22.8	089	24
Nome	042	05.7	18.8	040	03.2	17.0	066	11.1	19.5	081	17.4	25.7	066	09
Norfolk	095	31.0	23.0	124	06.8	15.7	079	23.9	22.9	089	44.9	22.3	089	26
Oakland	104	19.5	21.5	060	11.2	15.1	093	14.0	20.7	105	25.1	25.6	096	17
Omaha	089	24.2	22.0	089	11.8	13.9	100	24.2	21.2	098	32.3	22.9	097	23
Pittsburgh	093	29.5	23.7	110	13.1	15.8	083	27.3	22.2	089	43.0	23.6	092	29
Rantoul	092	28.2	23.5	110	11.9	14.8	095	25.3	21.4	091	39.0	24.9	096	27
Rome	094	26.8	24.2	104	17.0	18.1	081	29.2	23.7	088	37.6	28.4	090	27
San Juan	105	10.5	12.7	276	13.4	09.0	250	05.7	13.1	114	11.8	13.6	172	02
Seattle	003	16.8	21.8	076	11.0	18.0	091	21.4	21.8	097	25.7	24.0	092	18
Sault Ste. Marie	098	19.9	22.0	110	17.7	17.0	095	25.3	22.9	098	30.4	23.5	100	21
St. Cloud	095	18.9	21.0	095	17.7	16.8	103	25.2	21.3	103	29.1	22.0	101	23
Tucson	081	26.7	20.3	349	05.1	14.4	085	14.4	18.6	083	27.4	22.7	078	16
Washington	094	30.5	24.1	112	10.5	16.5	080	26.7	22.9	089	44.7	24.2	089	27
Whitehorse	060	08.3	19.7	071	02.9	15.1	066	17.8	19.5	087	21.3	23.9	073	12
Mean Value		24.27	21.38		10.88	14.70		21.10	21.08		34.40	22.52		

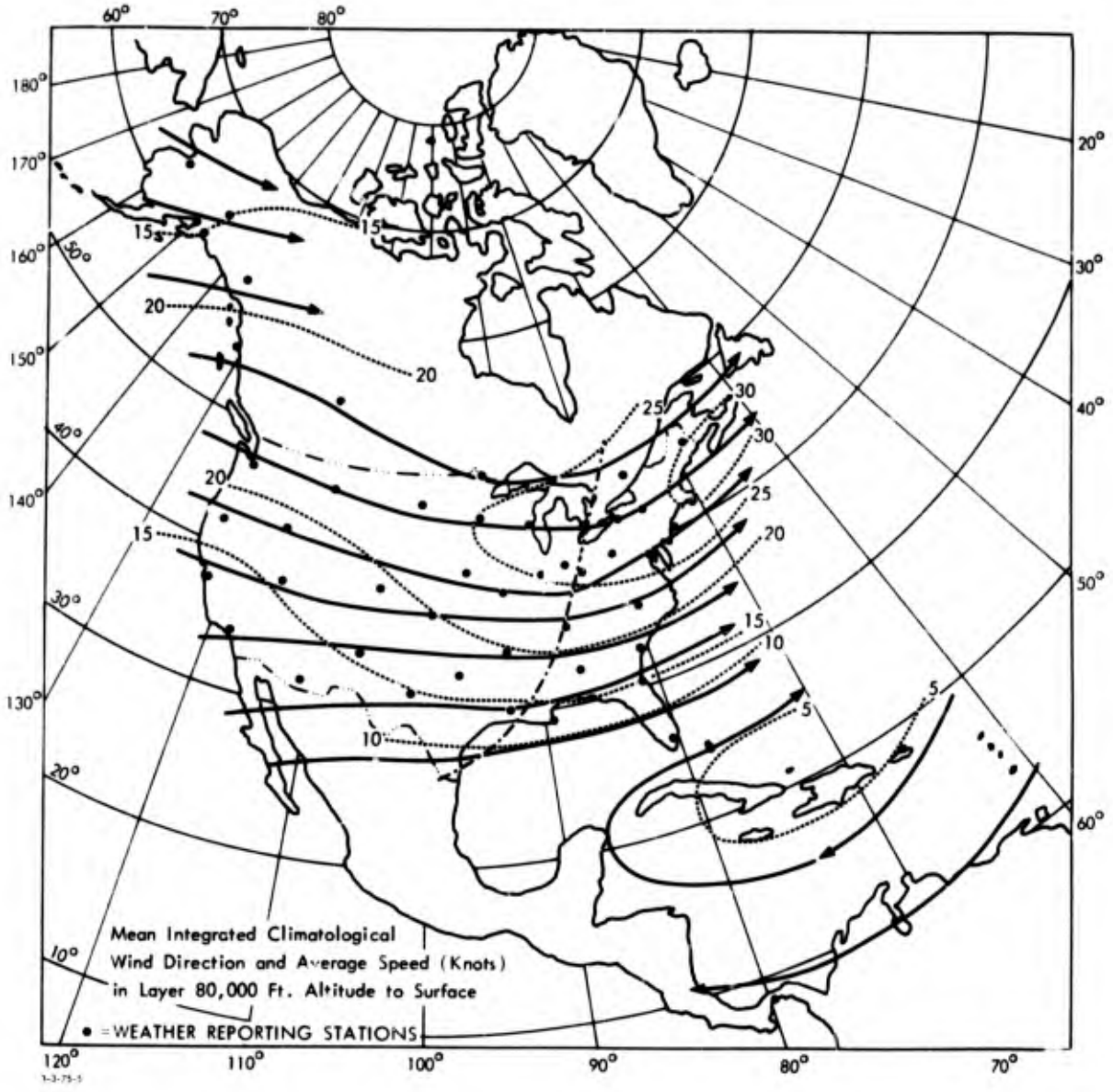

Figure 44. FALL CLIMATOLOGICAL MEAN-WIND DIRECTION AND SPEED

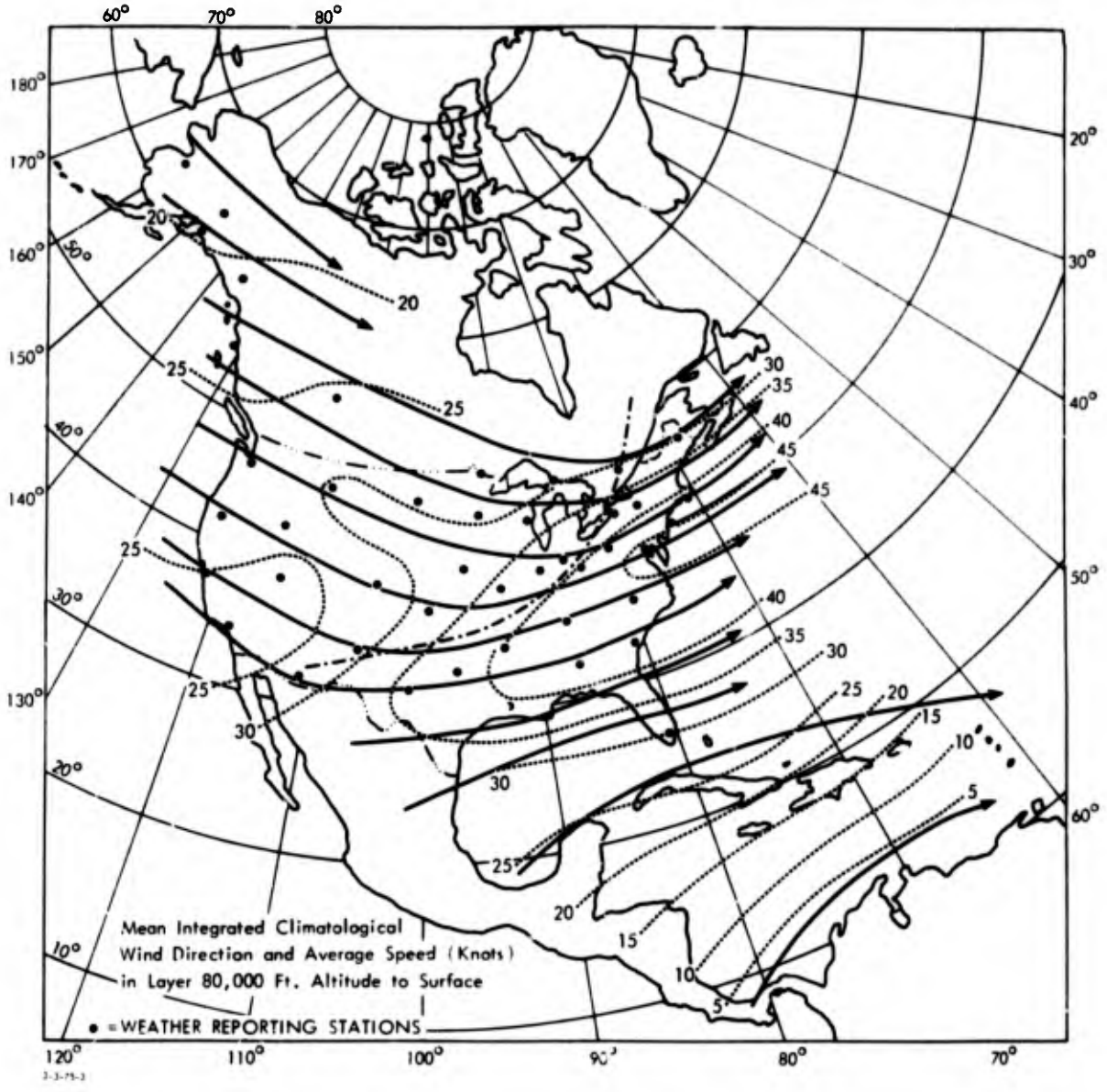

Figure 45. WINTER CLIMATOLOGICAL MEAN-WIND DIRECTION AND SPEED

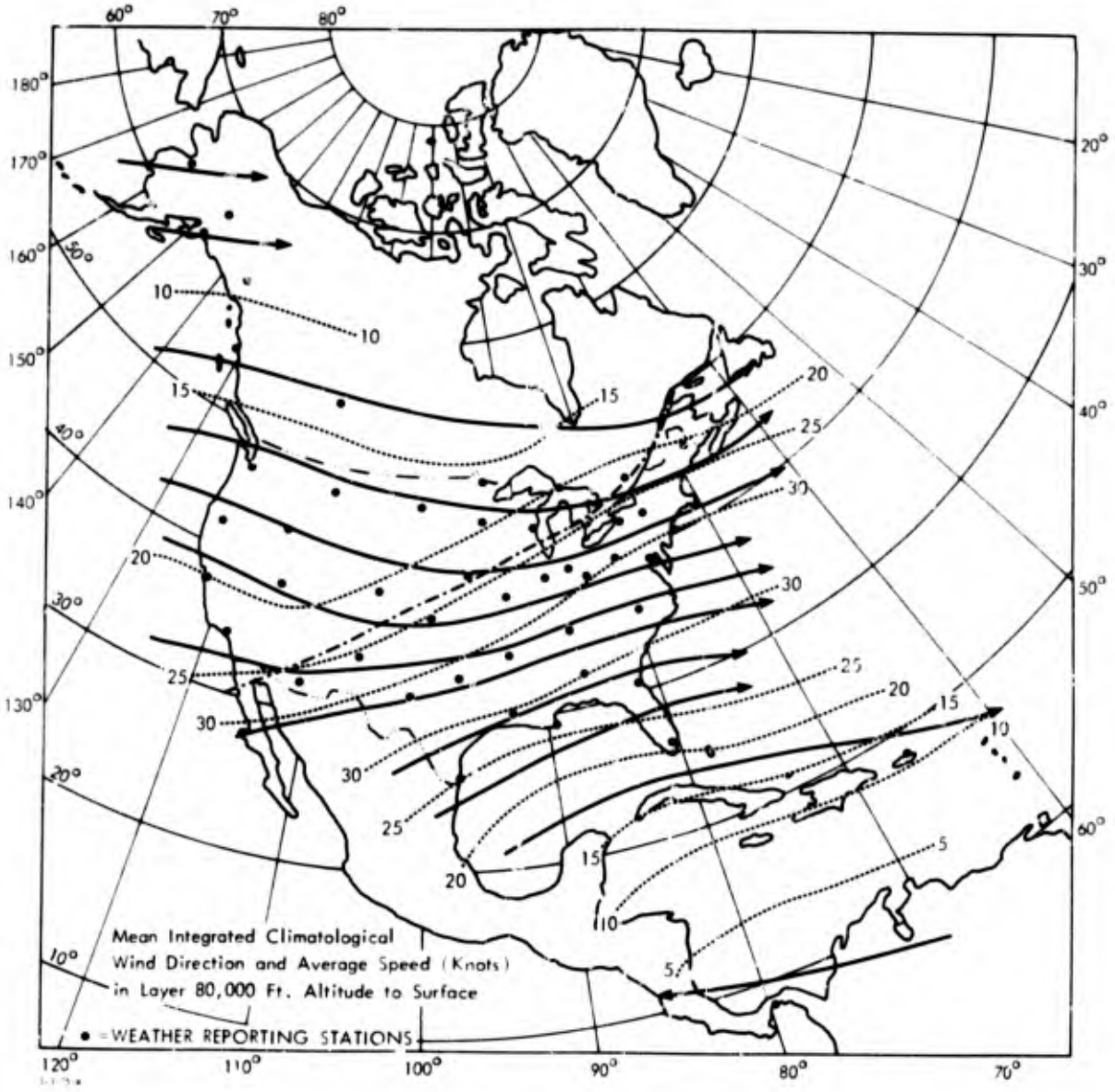

Figure 46. SPRING CLIMATOLOGICAL MEAN-WIND DIRECTION AND SPEED

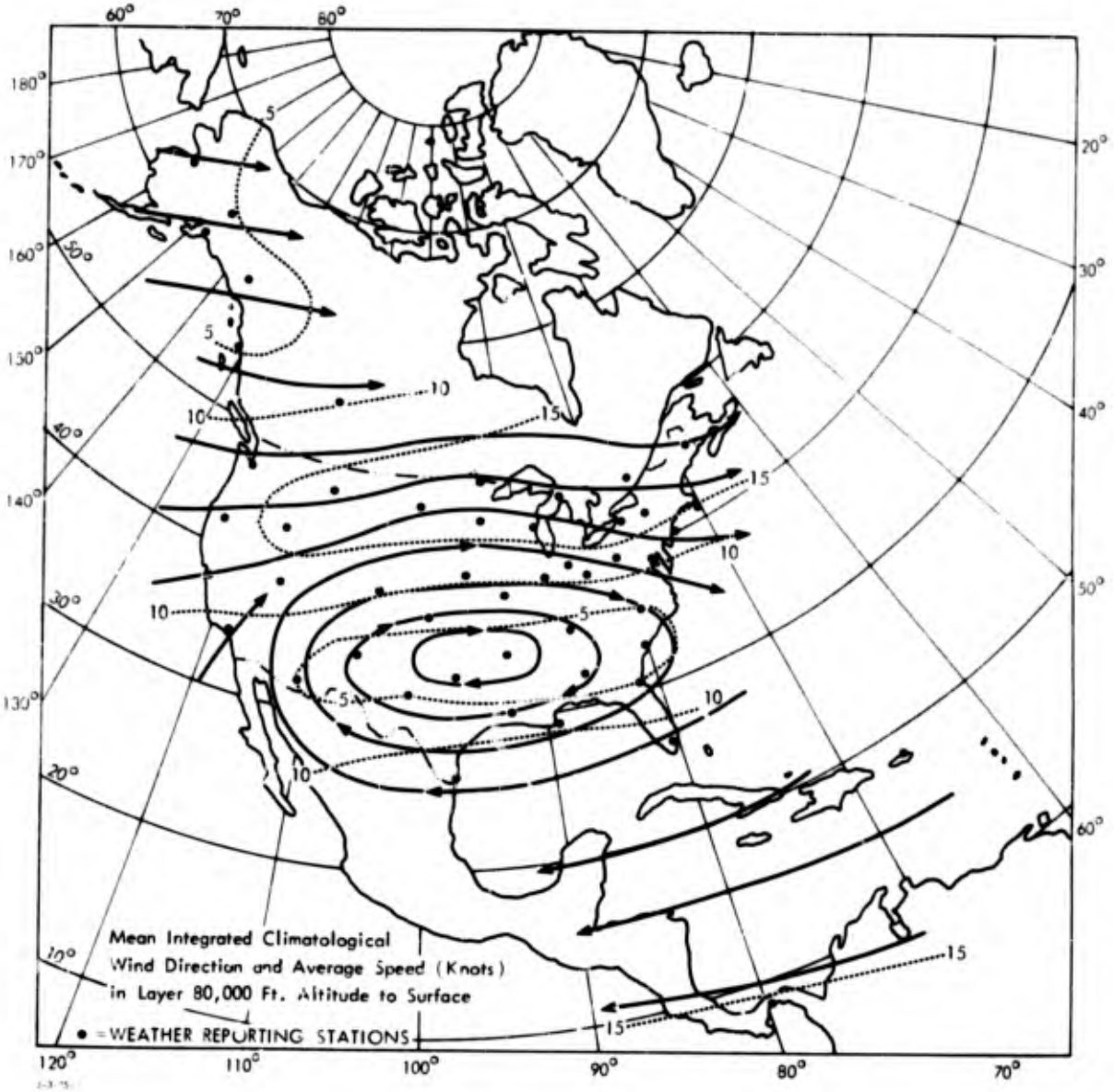

Figure 47. SUMMER CLIMATOLOGICAL MEAN-WIND DIRECTION AND SPEED

obtained. A measure of the variability of wind speed is the value of the vector standard deviation; and, of wind direction is the ratio of mean wind speed (S) to standard deviation (V). Figures 48 and 49 show such ratios for summer and winter. Since the contours presented were drawn relatively smooth, some of the data points are inconsistent with the contours. Statistical fluctuation or local conditions could cause these inconsistencies to occur. The winter mean-wind speeds are a factor of 3 higher than summer--with the average value for winter being 35 knots (or 40 mph); for summer, 11 knots (or 12.5 mph). The mean-wind direction for winter is generally west to east, whereas the wind for summer in the southern part of the country shows a reversal in direction. The speeds in winter are less variable than in summer, particularly in the southern part of the country. Average values of V/S are 1.79 in summer and 0.68 in winter. The average values of V/S for summer indicate a high variability; the wind is quite likely to come from any direction.

B. WIND SHEAR

The above data yield no hints concerning wind shear. In fact, analysis of wind data in sufficient detail to determine shear values are not available on the same basis as wind velocity data. An analysis (by R. B. Mason[1]) of northern hemisphere winds on 12 typical days (one for each month) provide shear data for use in the WSEG model. The data used here from his report apply to weapon yields of 1 MT or greater and for latitudes from 30° to 50°. The number of joint occurrences of wind in each of three wind groups (0-10 knots, 10-30 knots, and over 30 knots) and each of four shear groups (0-15 knots/1,000 ft, 25-35 knots/1,000 ft, and over 35 knots/1,000 ft) was recorded. A total

[1]R. B. Mason, *Wind Shear and the WSEG Fallout Model*, Technical Memorandum TM 66-71, National Military Command System Support Center, Defense Communications Agency, 10 June 1971.

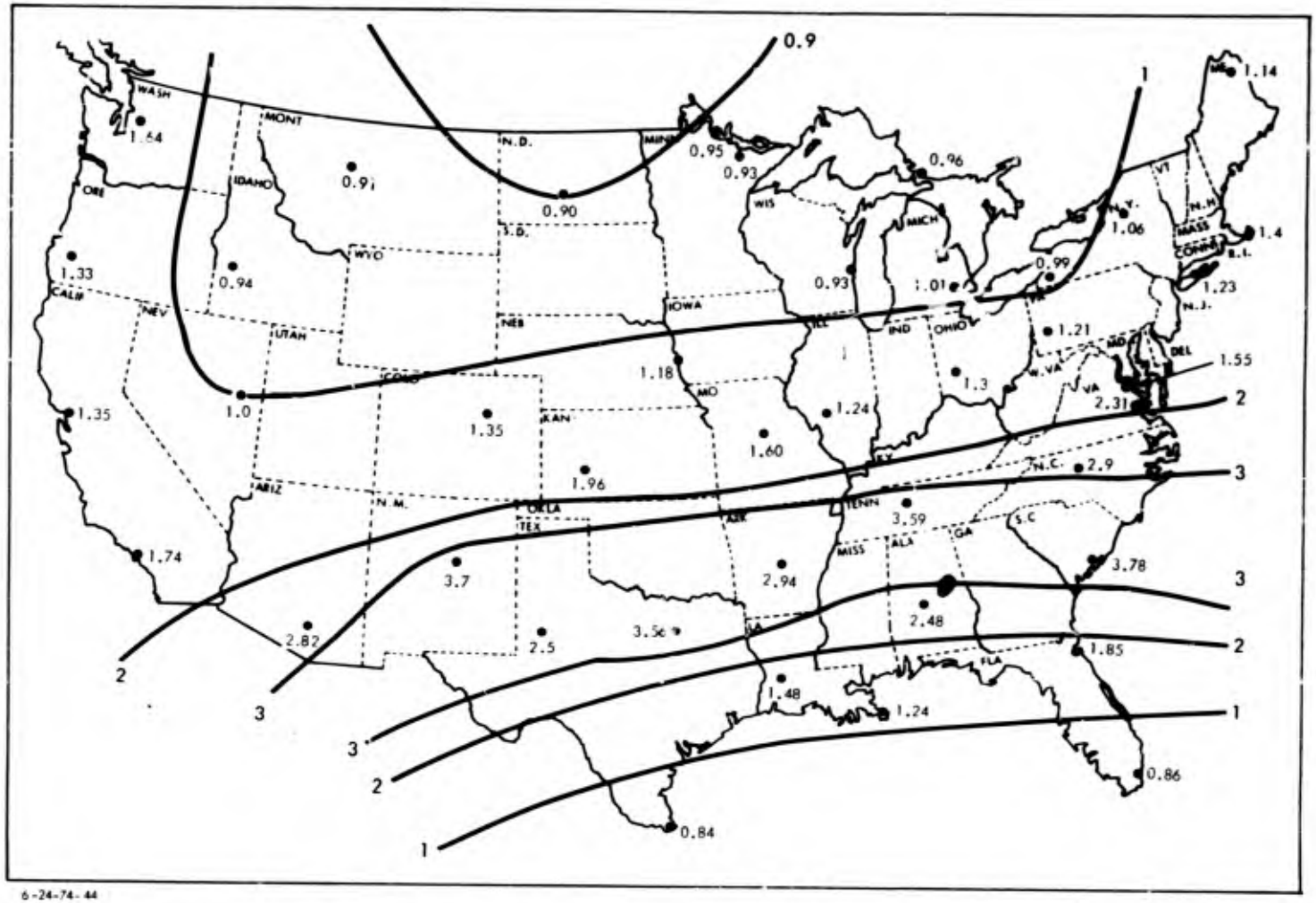

Figure 48. CONTOURS OF CONSTANT RATIO OF VECTOR MEAN-WIND SPEED TO STANDARD DEVIATION, FOR SUMMER WINDS

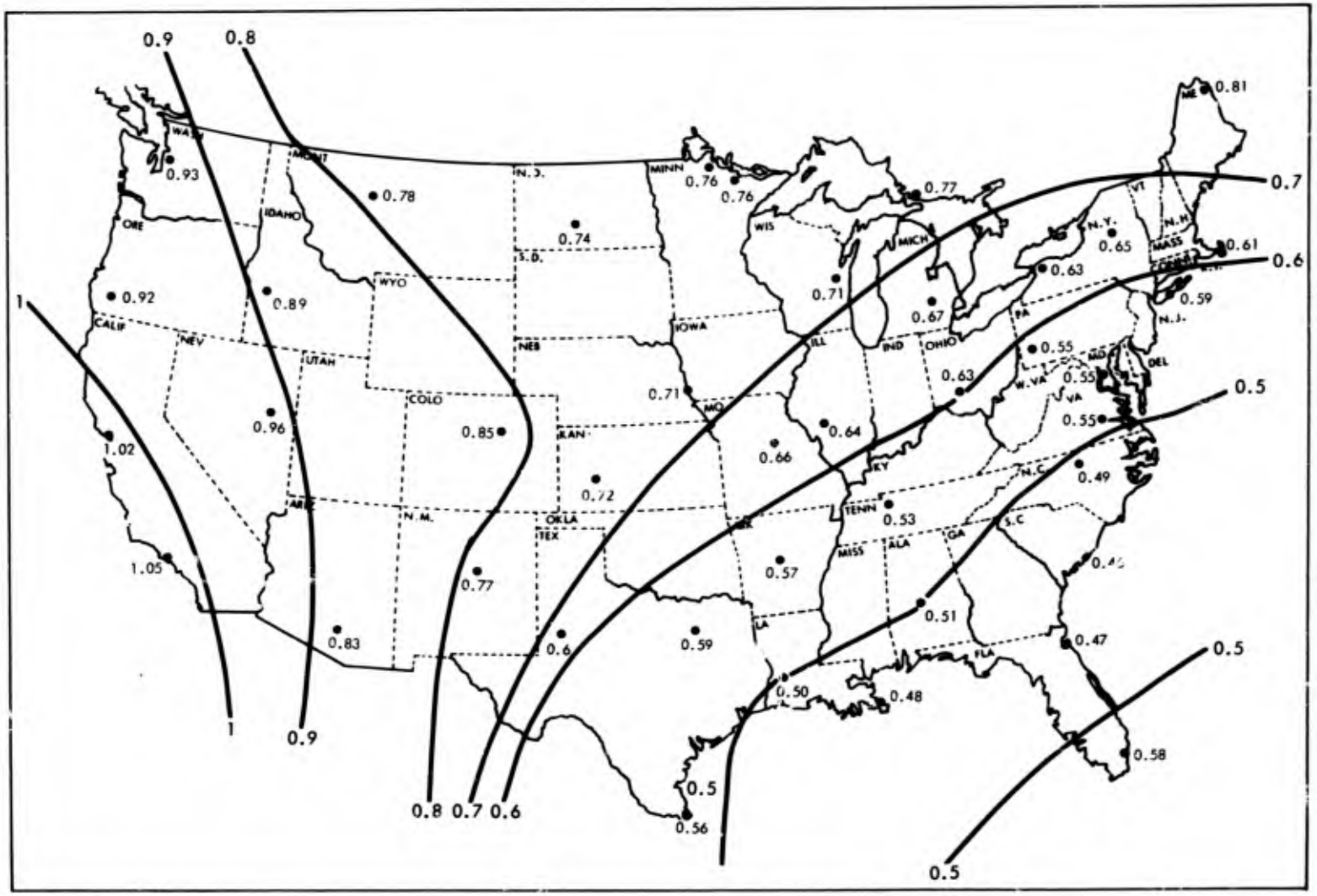

6-24-74-45

Figure 49. CONTOURS OF CONSTANT RATIO OF VECTOR MEAN-WIND SPEED TO STANDARD DEVIATION, FOR WINTER WINDS

of 692 occurrences for each of 12 months was analyzed. An analysis-of-variance calculation from these data showed a significant interaction in the number of occurrences between wind speed and wind shear. The probability that the shear will be in the lowest group decreases as the wind speed increases. However, this change is not large; the probability is 67 percent for the lowest, 65 percent for the intermediate, and 61 percent for the highest wind group. For the shear groups other than the lowest, no tendency to vary with wind speed is evident. Because of this small change, it appears justified (on the basis of these data and for the purposes of fallout calculations) to take the wind shear as independent of the wind speed. While some correlation effects are neglected, only a small error would be present in most applications.[1]

The following table presents the probability of shear values being in each group for each season:

Season	Shear Group Range (mph/1,000 ft)				Mean Shear	Max. Shear
	1	2	3	4		
	0-.173	.173-288	.288-.403	.403-∞		
Fall	69	11	16	4	0.143	8.25
Winter	54	13	22	11	0.210	1.97
Spring	57	13	23	7	0.184	1.86
Summer	71	12	14	3	0.124	0.85
Overall	63	12	19	6	0.165	1.97

[1] An excellent set of maps (prepared by the NMCSSC) of these wind data gives wind-velocity vectors and wind shear in a combined presentation. From these maps a correlation of wind shear with synoptic wind conditions can be readily ascertained. While these data indicate a strong correlation of wind shear with meteorological conditions, no analyses or methods are available to make such predictions.

The most pronounced seasonal tendency is a shift from low values of shear in summer to higher values in winter. However, by taking a single yearly average, a maximum of 9-percent error is made.

The wind statistics from the Mason data are presented in the following table:

	Wind Group Range (mph)		
	1	2	3
Season	0-11.5	11.5-34.5	34.5-∞
Fall	19	54	27
Winter	3	20	77
Spring	5	28	67
Summer	19	54	27
Overall	9	34	57

It should be remembered that these data are averaged over the entire Northern Hemisphere between latitudes of 30° and 50°. The wind values are higher than those for the United States only (presented above). Thus, one might expect the wind-shear values over the United States only might also have somewhat different values. However, in the absence of other data (and recalling the low correlation between wind speed and wind shear), this data is used as representative of the United States.

In Figure 50, a histogram of average wind shear is shown for the four wind-shear groups. In this histogram the maximum shear has arbitrarily been set at 1. The low value of probability density in the 0.7-0.24 range occurs for each season, as well as for the averaged data. While this bimodal character appears to be a real phenomenon, the complexities of a bimodal-distribution function do not seem justified. Instead, a modified Gaussian function of the form

$$f(x) = \begin{cases} 0, & \text{if } x < 0 ; \\ \dfrac{2}{\sqrt{2\pi}\sigma} \exp\left(-\tfrac{1}{2}\left(\dfrac{x}{\sigma}\right)^2\right), & \text{if } x \geq 0 \end{cases}$$

was chosen. The mean of this distribution is $(2/\sqrt{2\pi})\sigma$. If the distribution mean is set equal to the wind-shear mean, a value of 0.2 is obtained for σ. This distribution function is shown in Figure 50. It tends to preserve the high likelihood of very low shear values--which probably is the most important practical effect to preserve. It should be noticed that while the mean-shear value is the usual value of 0.2, the most probable shear value is 0--which in turn implies a fallout pattern that is long and thin.

C. DISTRIBUTION FUNCTION FOR WIND VELOCITY

The most significant fluctuation due to wind variability is the changing wind direction. The resultant wind for a particular wind sample is the vector sum of a mean wind S and a random wind component V, which is assumed to have a circular normal distribution with standard deviation σ. The relation between the resultant wind (W) and the random wind (V) is shown in Figure 51. The angle from the mean downwind direction for the random wind is α; for the resultant wind, θ. Of interest is the distribution of θ, given the ratio of V/S.

In order to determine the distribution of θ, it is sufficient to determine the distribution of tan θ.[1] In other words, for a given value θ, we wish to find

$$F(\theta) = \text{prob } (\tan \theta \leq \tan \bar{\theta}) .$$

[1]Since $-180° \leq \theta \leq 180°$ is the range of interest for the distribution, and tan 90° is ∞, care must be taken to insure that θ is in the proper quadrant for a given value of tan θ. For simplicity, these problems will be bypassed in this discussion.

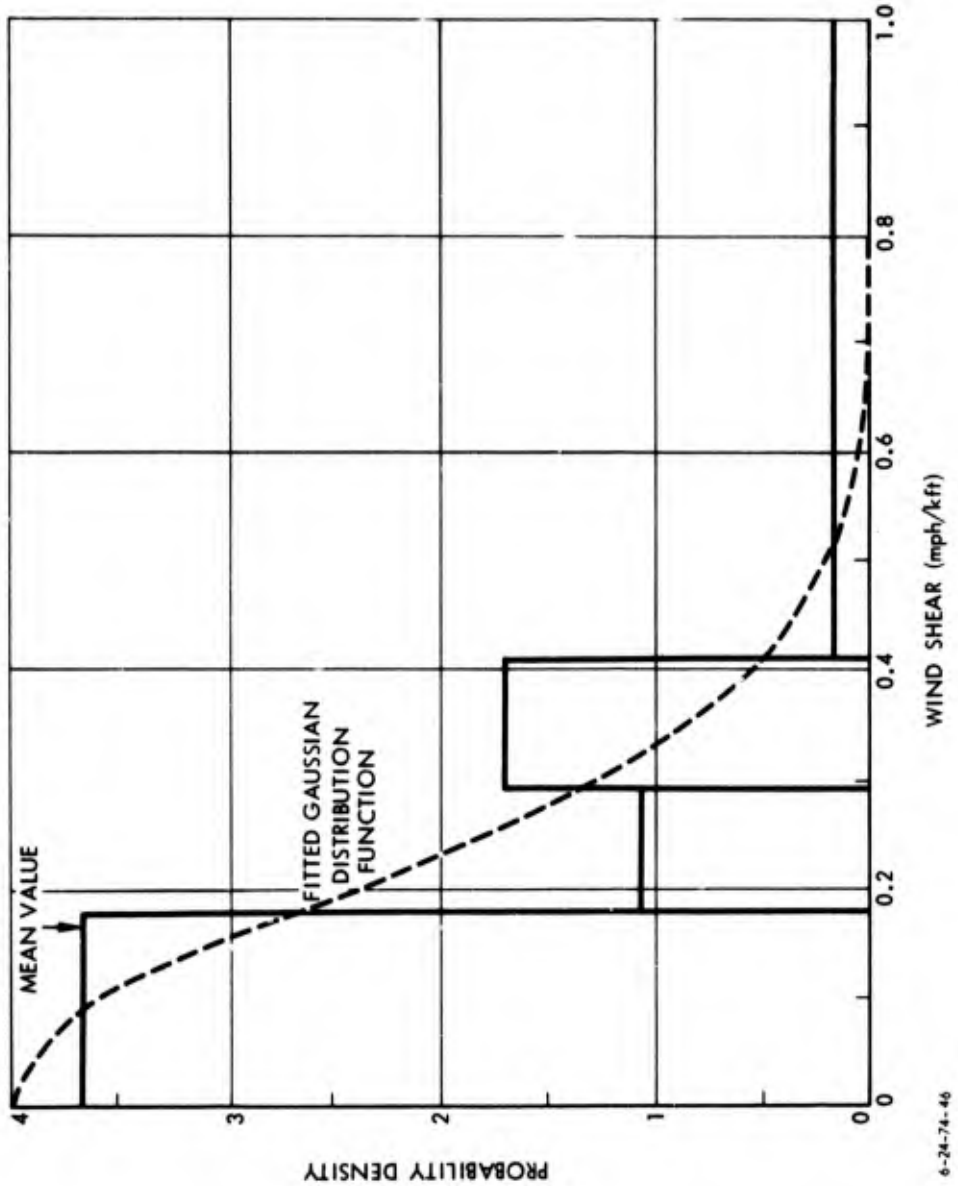

Figure 50. HISTOGRAM OF WIND SHEAR AND FITTED DISTRIBUTION FUNCTION

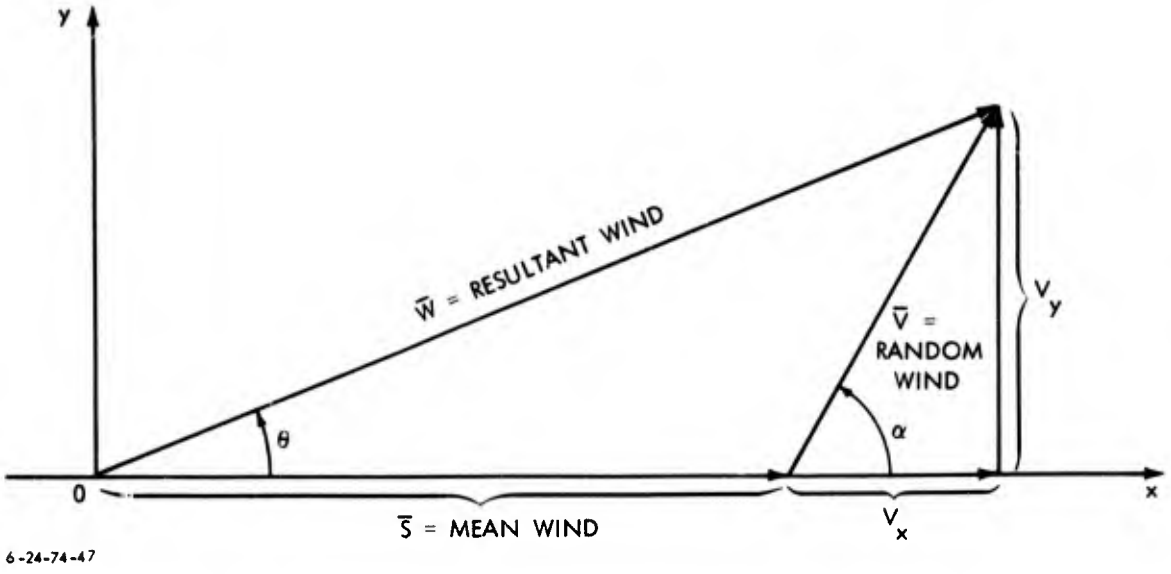

Figure 51. RELATIONSHIP BETWEEN RANDOM WIND VECTOR AND RESULTANT WIND VECTOR

The expression gives the probability that $-180° < \theta < \bar{\theta}$. Since the distribution is symmetric, it is sufficient to determine $F(\theta)$ for $-180° \leq \theta \leq 0°$, with $F(0) = 0.5$. Since, from Figure 51,

$$\tan \theta = \frac{V_y}{V_m + V_x}$$

we have

$$F(\theta) = \text{prob}\left(V_y \leq \tan \theta \, (V_m + V_x)\right) .$$

Now V_y and V_x are both normally distributed, since V is assumed circular normal. Thus,

$$F(\theta) = \text{prob}\left(V_y \leq \tan \theta \, (V_m + V_x) \mid V_x\right) \cdot \text{Prob}\,(V_x)$$

or

$$F(\theta) = \int_{-\infty}^{\infty} \left\{ \int_{-\infty}^{\tan \bar{\theta}\,(V_m + V_x)} \frac{1}{2\pi\sigma} \exp\left(-V_y^2/2\sigma^2\right) dV_y \, \frac{1}{2\pi\sigma} \exp\left(-V_x^2/2\sigma^2\right) \right\} dV_x .$$

The inner integral is the cumulative normal function, so that $F(\theta)$ is of the form of the integral of the cumulative normal function weighted by the normal probability function. This function, evaluated numerically, is shown in Figure 52; the probability density function is shown in Figure 53.

The values in Figure 52 have the appearance of a power-law function. The cumulative probabilities are presented as a logarithmic plot in Figure 54. If the power law holds exactly, a series of straight lines should be obtained. For cumulative probabilities over 0.1, a reasonable approximation is obtained. The reciprocal values of the power-law form are quite close to hyperbolic in shape. Thus, $F(\theta)$ is approximated by

$$F(\theta) = 0.5\left(1 - \frac{\theta}{180}\right)\left(1 + \frac{2}{\sigma/s}\right), \text{ for } -180 \leq \theta \leq 0 .$$

The probability density is given by

$$\frac{dF(\theta)}{d\theta} = -\frac{0.5}{180}\left(1 - \frac{\theta}{180}\right)^{2/(\sigma/S)}, \text{ for } -180 \leq \theta \leq 0 .$$

These sample forms appear to give an adequate expression for the distribution of wind angle.

In order to obtain a complete description of wind statistics, the distribution of wind velocity should be calculated under the assumption that θ has a fixed value. If θ is given, we have

$$V_y = \tan\theta\ (S + V_x) .$$

The value of wind velocity squared is for a given value of V_x:

$$V^2 = (S + V_x)^2 + V_y^2$$

$$= \frac{(S + V_x)^2}{\cos^2\theta} .$$

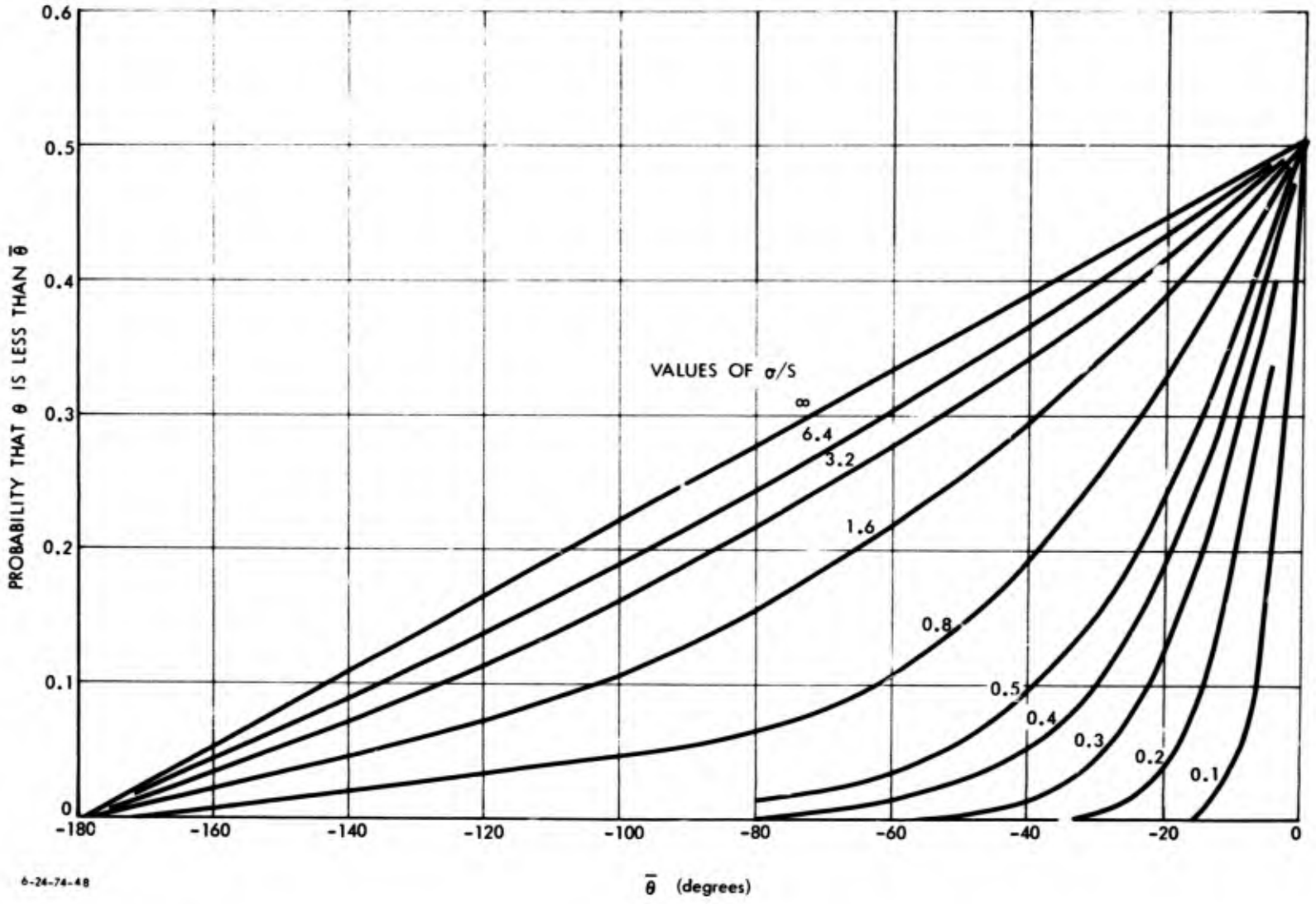

Figure 52. CUMULATIVE PROBABILITY THAT θ IS LESS THAN θ, AS A FUNCTION OF $\bar{\theta}$, FOR SEVERAL VALUES OF WIND STANDARD DEVIATION/MEAN WIND

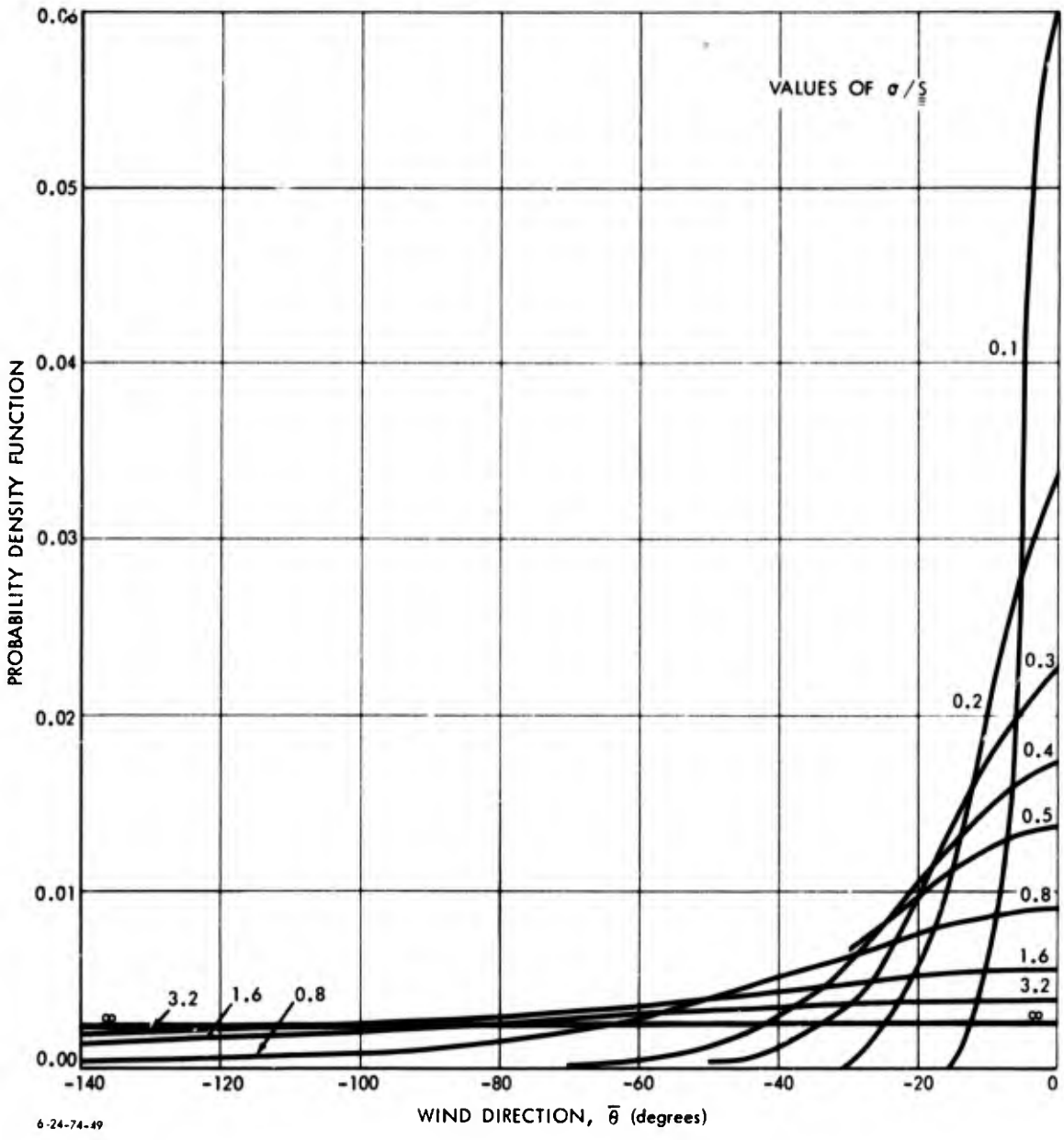

Figure 53. PROBABILITY DENSITY FUNCTION FOR WIND DIRECTION AS A FUNCTION OF $\bar{\theta}$

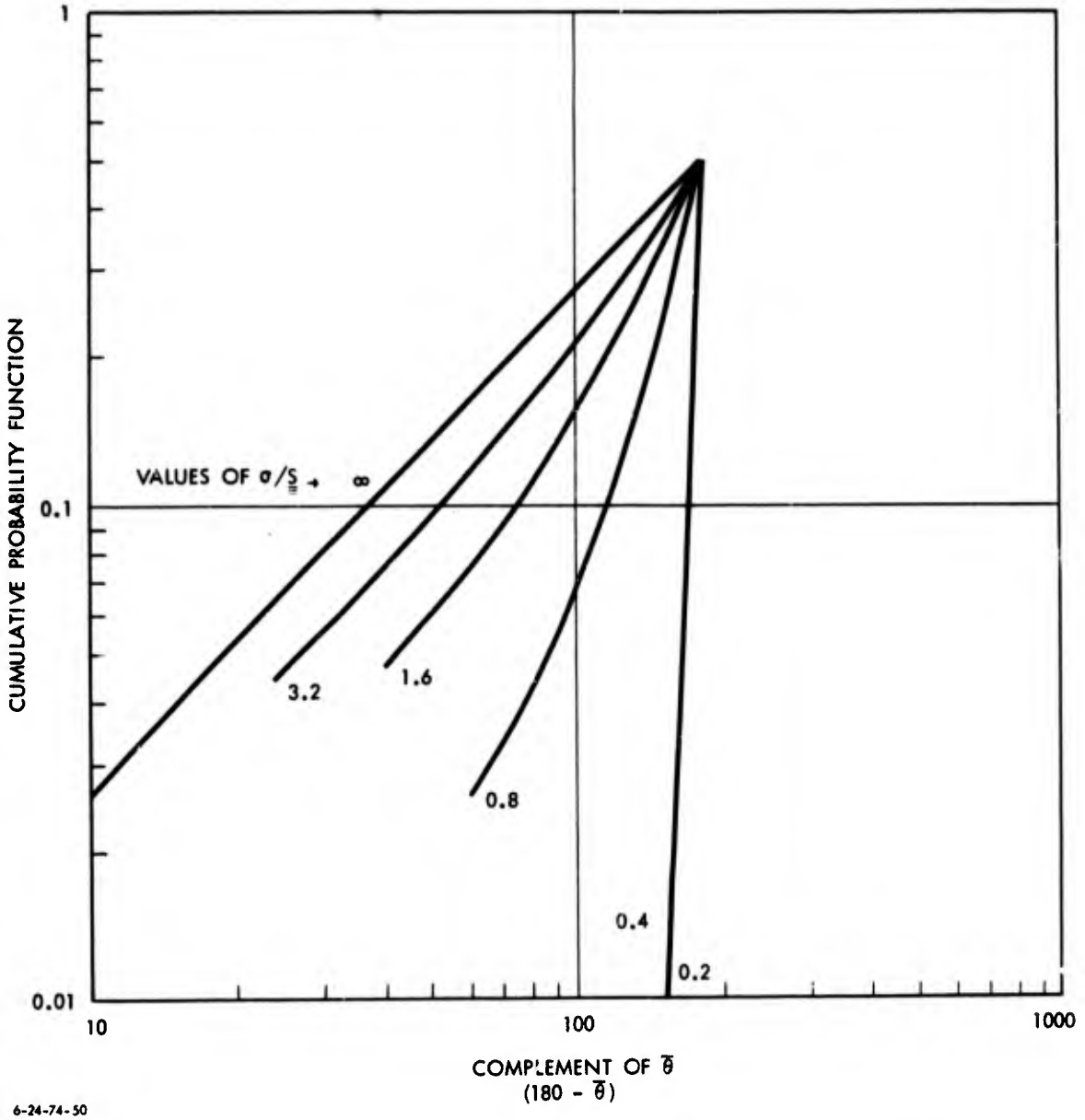

Figure 54. LOGARITHM OF CUMULATIVE PROBABILITY THAT θ IS LESS THAN $\bar{\theta}$, AS A FUNCTION OF THE LOGARITHM OF (180 - $\bar{\theta}$)

From this we have, for any V_x,

$$\frac{V}{S} \cos \theta = 1 + \frac{V_x}{S} .$$

Now V_x/S is normally distributed with mean zero and standard deviation σ. Thus, $V/S \cos \theta$ is normally distributed with mean 1 and standard deviation σ. Finally, V is normally distributed with mean $S/\cos \theta$ and standard deviation $S\sigma/\cos \theta$. We see, therefore, that the most probable value of V is $S/\cos \theta$ and that the standard deviation of V is directly proportional to the measure of wind variability σ.

Chapter IV

FALLOUT-RISK STATISTICS IN IDEALIZED SITUATIONS

This chapter discusses the fallout risks obtained when the model is combined with wind statistics in probabilistic calculations. The calculations here will be based on a Monte Carlo simulation, since the analytic structure becomes too unwieldy to give useful closed-form results. Three simple situations will be considered here: a uniform pattern of weapons, a single-weapon pattern, and weapons in a hexagon pattern. (In the next chapter, more typical targeting situations are discussed.)

A. DOSES FROM A UNIFORM PATTERN OF WEAPONS

A limiting calculation that can be readily done is the case in which a constant weapon density on an infinite plane is assumed. As an example, consider a 6,000-MT attack with weapons having a fission fraction of ½ on the United States--assumed to have an area of 3×10^6 miles. Then a weapon density of 1KT/mile^2 is obtained. If the fallout is assumed to be uniformly deposited, then the H+1 dose rate is the k-factor (2,000 ERDs/hr/KT/mile^2) times the density, times the fission fraction--or 2,000 ERDs/hr. The dose cannot be as directly calculated, since the fallout from different points arrives at different times. The simplifications described in Chapter II (above) give downwind dose fraction F_d times ratio of dose R to H+1 dose rate as

$$f_d R = \begin{cases} 0, & \text{if } x < 0 ; \\ \dfrac{1}{WT^{1.382}} \exp\left(-\dfrac{x}{WT}\right) \dfrac{2.71}{\left(\dfrac{x}{WT}\right)^{0.382}}, & \text{if } x \geq 0 , \end{cases}$$

which may be integrated with respect to x. Then, using the simplified expression for T, we get the ratio of dose to H+1 dose rate as

$$R = \frac{1}{7.5 + 1.66 \log_{10} Y} ,$$

where Y is the yield in MT. With Y = 1, for example, we have R = 0.43; and with Y = 10, we have R = 0.53. For the hypothetical attack, if the weapons are all 10 MT in yield, the dose is 1,060 ERDs.

B. DOSE STATISTICS FROM A SINGLE WEAPON

The calculation of dose statistics from a single weapon uses the model described in Chapter II, along with the wind statistics described in Chapter III. One repetition of the calculation selects a wind at random from a circular normal distribution, adds vectorially a mean wind, and determines the dose received by a monitor point. The input parameters are those needed to define the location of the monitor point relative to the weapon, the weapon characteristics needed to calculate the fallout patterns, and the parameters needed to calculate the wind statistics. The wind shear can be either taken as constant or selected randomly from a distribution. A computer program (LASH) repeats the calculation a specified number of times and displays the appropriate statistics. An input option allows either random sampling from the circular normal wind distribution or stratified sampling. With stratified sampling, the circular normal distribution is divided into 100 equal probability cells by defining 10 equal probability angular rings and 10 equal angle sectors. For each 100 times that the calculation is repeated, one sample is randomly drawn from each cell. With this option, the total number of trials must therefore be an even multiple of 100.

The initial calculation described assumes a 20-mph vector mean wind (with a standard deviation of the random wind 0.3 times the mean wind)[1] and a constant shear of 0.2 mph/kft with a sample size of 10,000. A 1-MT ground-burst weapon with a fission fraction of 1 was used. A monitor point 100 miles downwind along the mean-wind vector and zero miles crosswind would receive a dose of 518 ERDs from a wind with a velocity of 20 mph. In the simulation, the mean dose was 140 ERDs with a standard deviation of 185 ERDs. The maximum dose was 728 ERDs. The following table indicates the number of times doses were in the indicated range:

Dose Range (ERDs)	Number of Times in Range
0-100	6,144
100-200	935
200-300	795
300-400	732
400-500	704
500-600	485
600-700	197
700-800	8

Of the values in the range 0-100, 4,191 are under 10 ERDs and 3,137 are under 1 ERD. Thus, in this case, for a considerable fraction of the time only a low dose is obtained.

For this monitor point, for a 20 mph wind the value of σ_c is 8.78 miles. Dose as a function of wind speed is shown in Figure 55. There is a probability of about 0.9 that the wind speed is between 10 and 30 mph. If the dose as a function of wind speed were linear and the probability density constant in this range, then the increase in dose due to larger wind speed would be compensated for by decreases in dose at lower speeds and the average dose would be unaffected. The dose at 30 mph is only 660 ERDs, rather than the 800 ERDs that would be

[1]Compared to the wind statistics in the previous chapter, low values of wind variability are used. These values were selected as those that appeared best to exhibit the qualitative nature of the probabilistic results.

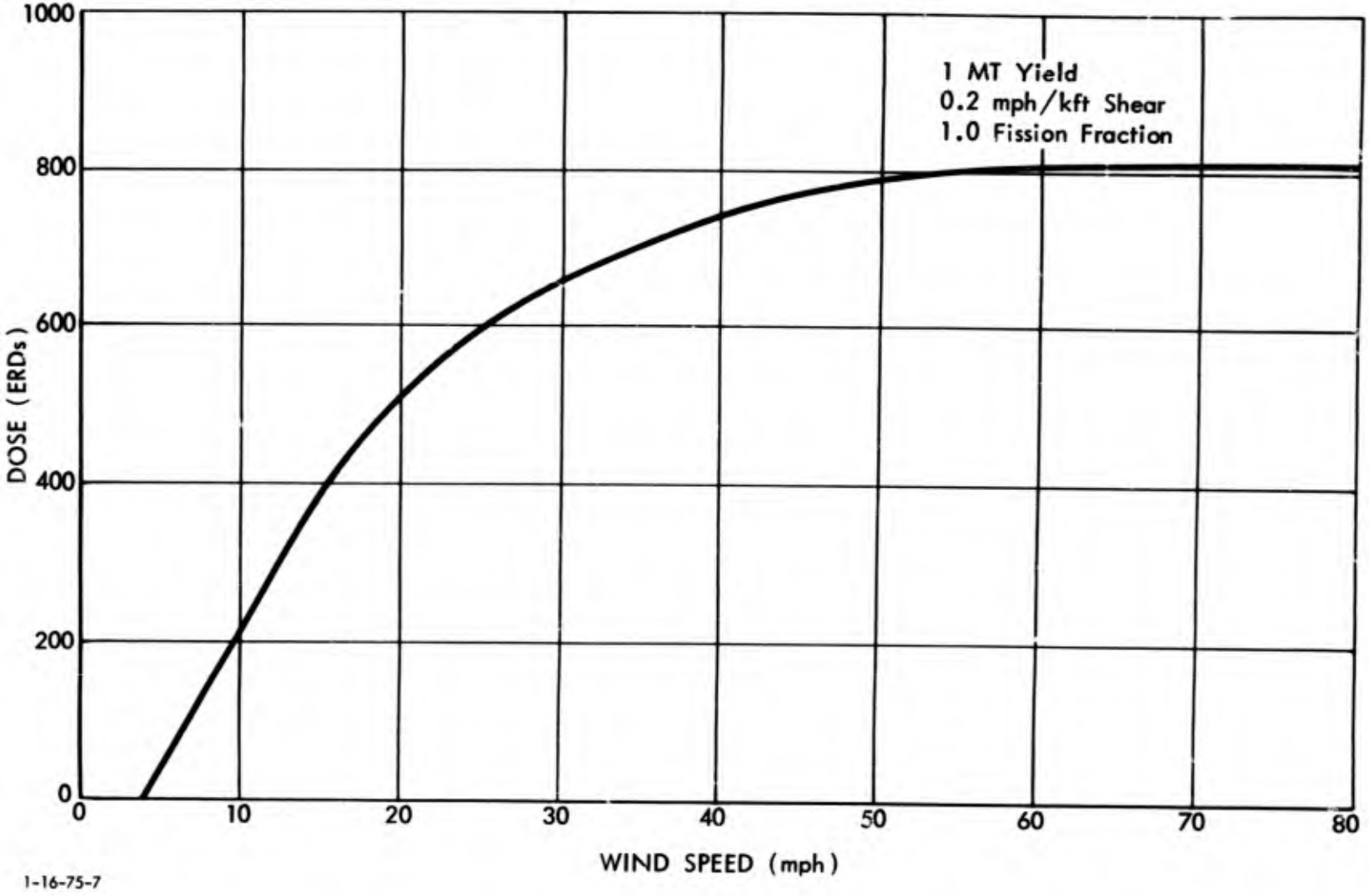

Figure 55. DOSE AS A FUNCTION OF WIND SPEED FOR A 100-MILE DOWNWIND MONITOR POINT

obtained from a linear extrapolation of the dose at a distance of from 10 to 20 mph--which would indicate that wind-speed fluctuations would decrease the average dose somewhat. On the other hand, the scalar wind speed (the mean is about 22 mph) has a higher value than the vector mean wind, which compensates in the opposite direction.

One might expect that an appreciable portion of the variation in dose is due to changes in wind direction rather than in wind speed. To determine the significance of wind-direction fluctuation, a calculation assuming that all fluctuations are due to wind-direction effects will be made; and trial results will be compared to this calculation. Suppose that (1) crosswind distances from a monitor point are measured by a coordinate y and (2) y_o is the crosswind distance of a line along the mean-average-wind vector drawn through the weapon location. If an actual wind through the weapon has a distance y from the monitor point, the dose is given by

$$I = I_o \exp(-y^2/2\sigma_c^2) ,$$

when I_o is the centerline dose.

Now, since over appreciable ranges the cumulative probability is approximately a linear function of the tangent of the wind angle from the mean wind (and hence of y), the use of the logarithm of the dose is suggested. Hence,

$$\log I = \log I_o - \frac{y^2}{2\sigma_c^2} .$$

Now, since log I as a function of y is an inverted parabola in shape, a given dose I can be obtained from two values of y: y_U (farther from the monitor point than the mean wind) and y_L (closer to the monitor point). Let $P(y,y_o)$ be the probability density function for a particular value of y with a wind offset y_o. Then the probability density function P(log I) for a

particular value of log I is given by

$$P(\log I) = \left[P(y_U) + P(y_L)\right] \frac{dy}{\log I} .$$

So

$$P(\log I) = \frac{\sigma^2}{y} \left[P(y_U) + P(y_L)\right] .$$

In Figures 56 and 57, the sum of the two probabilities in the bracket is given for values of ratio of wind standard deviation to mean wind speed of 0.3 and 0.5. In these figures, the value of y is normalized by dividing by the downwind distance to the monitor point to obtain tan θ, with θ being the offset angle. As is clear from these figures, for large enough offsets of the monitor point from the mean-wind line, the largest dose is not the most probable.

Figures 58 and 59 present these probability density values divided by y--which gives the shape of the probability density curve for log I as a function of distance from the monitor point. As can be seen from Figure 58, for $\sigma/S = 0.3$, offsets of at least 0.6 are needed for any decrease in probability with increasing dose level.

In Figure 60, a histogram of the number of times a dose was received in a constant interval of log I is presented for the calculation discussed (i.e., with the monitor point) on the mean-wind line 100 miles downwind, with 20-mph mean wind and $\sigma/S = 0.3$. The interval in $\log_{10} I$ is 1.58. Also presented as a function of dose in this figure are (1) the crosswind distances to give such a dose (assuming that the hot-line dose of 5×10^8 ERDs--which would be obtained if σ/S were 0--is used for I_o), (2) the cumulative probability the wind is outside the angle needed to give the indicated dose, and (3) the computed number of events in an interval. The cumulative probability is determined by finding the probability that the wind is greater than

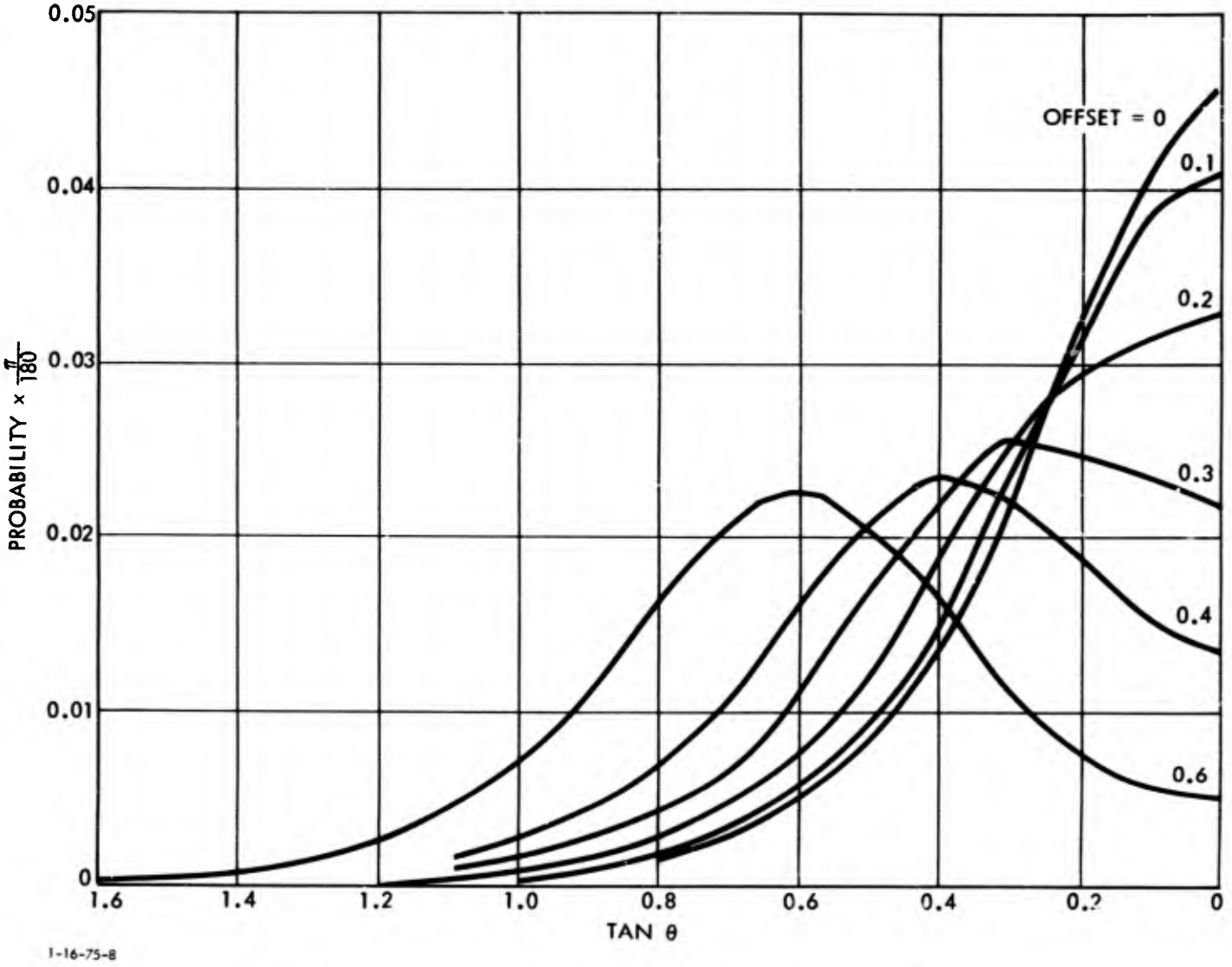

Figure 56. PROBABILITY DENSITY AS A FUNCTION OF TAN θ FOR VARIOUS OFFSETS, WITH σ/S = 0.3

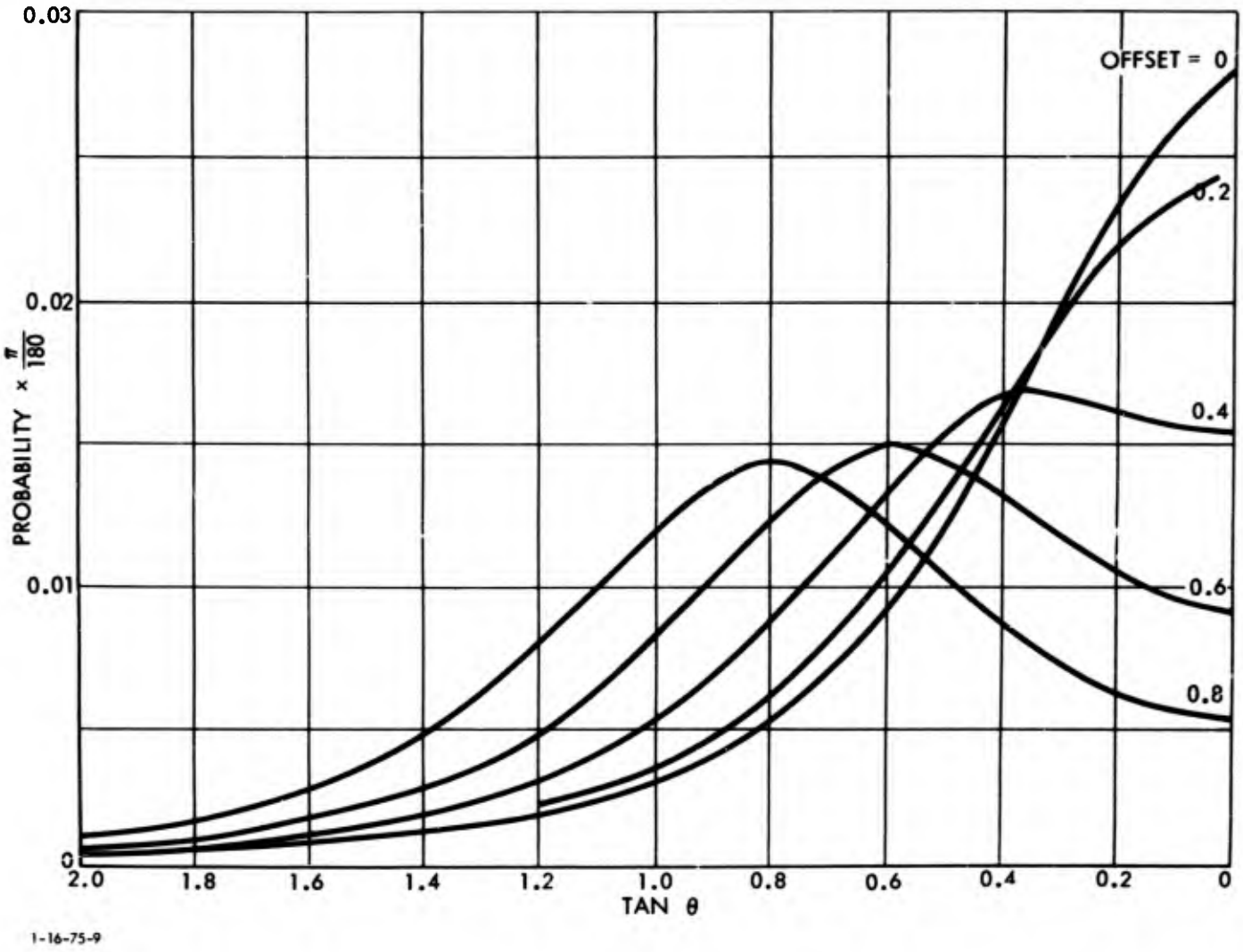

Figure 57. PROBABILITY DENSITY AS A FUNCTION OF TAN θ FOR VARIOUS OFFSETS, WITH σ/S = 0.5

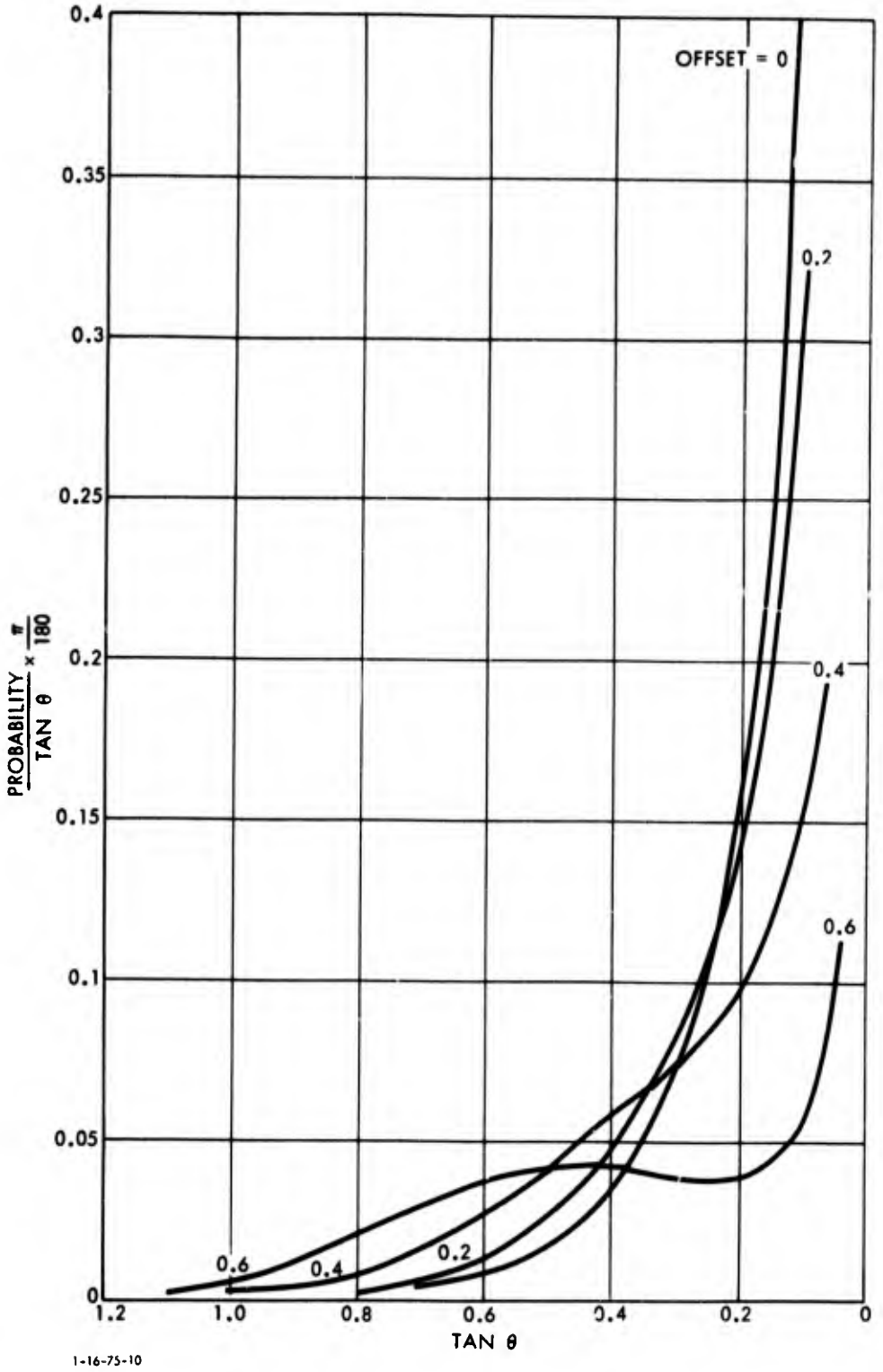

Figure 58. PROBABILITY DENSITY/TAN θ AS A FUNCTION OF TAN θ FOR VARIOUS OFFSETS, WITH σ/S = 0.3

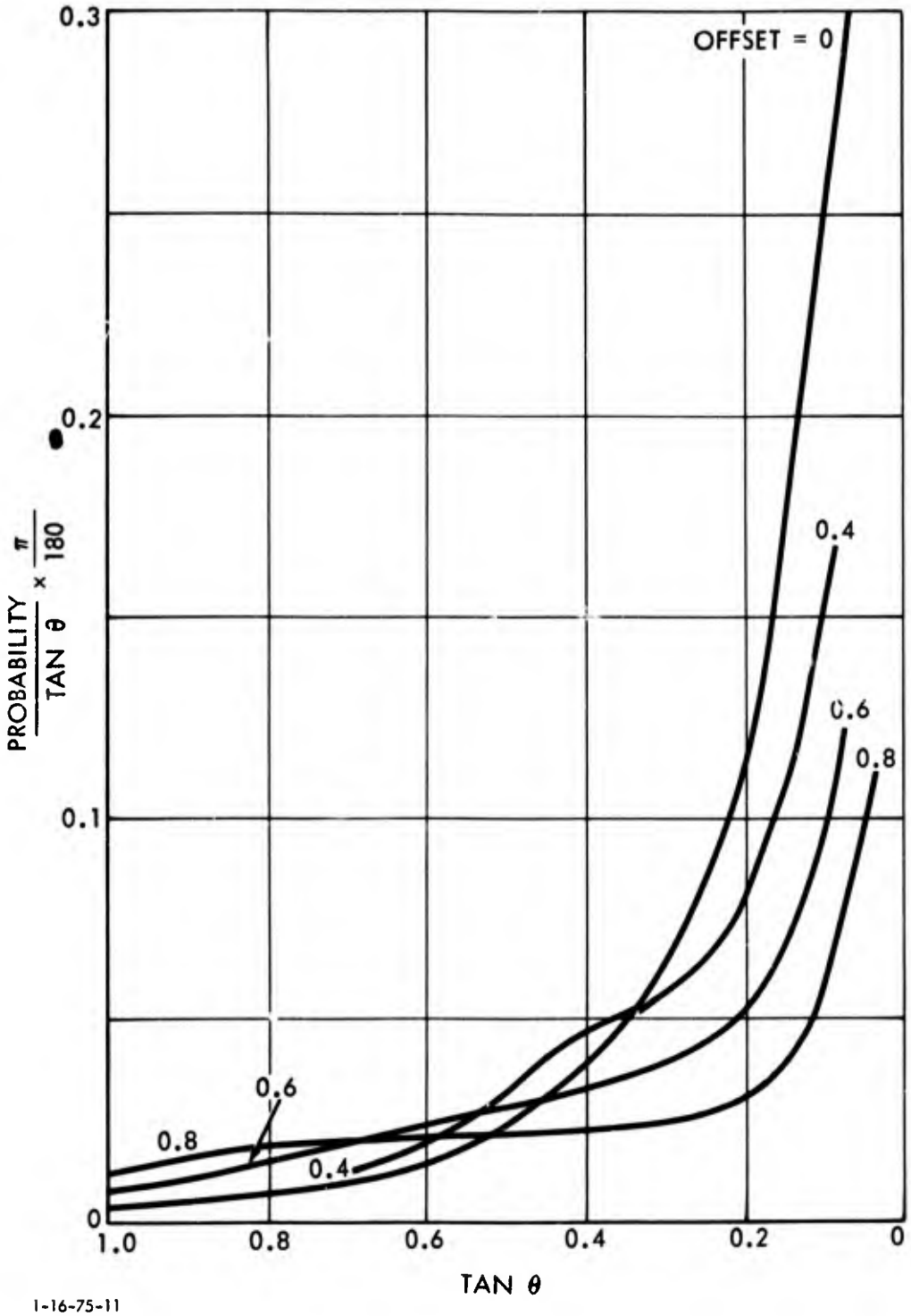

Figure 59. PROBABILITY DENSITY/TAN θ AS A FUNCTION OF TAN θ FOR VARIOUS OFFSETS, WITH σ/S = 0.5

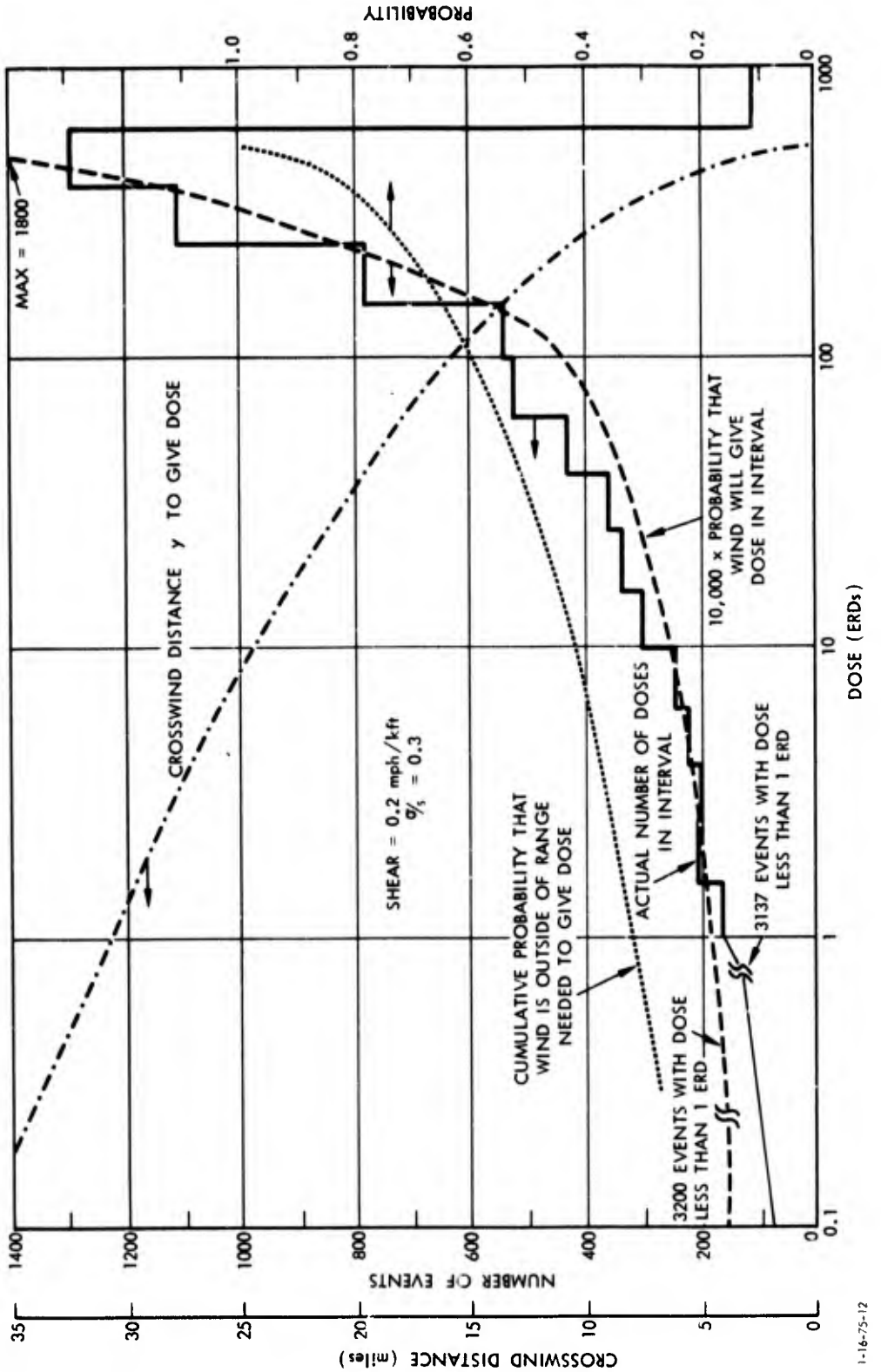

Figure 60. DOSE STATISTICS FOR A 100-MILE DOWNWIND, 0-MILE CROSSWIND MONITOR POINT

the two angles determined by the crosswind distance associated with the indicated dose. The probability that this dose is in the interval is the difference in cumulative probabilities for these two ends of the interval.

As can be seen from the figure, reasonably good agreement is obtained between the actual number of times that the doses lie in an interval and the number obtained from the calculated probability density--assuming that the variation is due to cross-wind fluctuations only.

The same presentation is given in Figure 61 for a monitor point 40 miles downwind but 20 miles offset from the mean-wind line. Here the likelihood of a dose (up to doses of about 300 ERDs) being in a logarithmic interval is almost constant--which corresponds roughly to the range in tan θ (from 0.2 to 0.4) in Figure 58, where the probability density is about constant. Again, the wind-angle fluctuations alone are adequate to describe most of the values observed.

With equal dose intervals (rather than equal ratios) the presentation of results appears different. Figure 62 shows the number of occurrences in equal intervals for several monitor points of the same basic case of 20-mph mean wind and $\sigma/S = 0.3$. The arrow near 0 points to the number of doses below the 10-ERD level. The values plotted for the first interval (0-200) are actually the number of occurrences in the 10-200 ERD level. The conditions are identical to those of the previous case; but, since a different set of random numbers was used, the actual values are slightly different. The simple analytical explanation for histograms with equal logarithmic intervals does not apply to equal arithmetic intervals. Moreover, doses at which various categories of biological effects occur (onset of symptoms, mild sickness, severe sickness, etc.) seem to be more in a constant ratio to each other rather than constant difference; thus an argument can be given to use the logarithm of the dose as the basic variable to describe radiation effects.

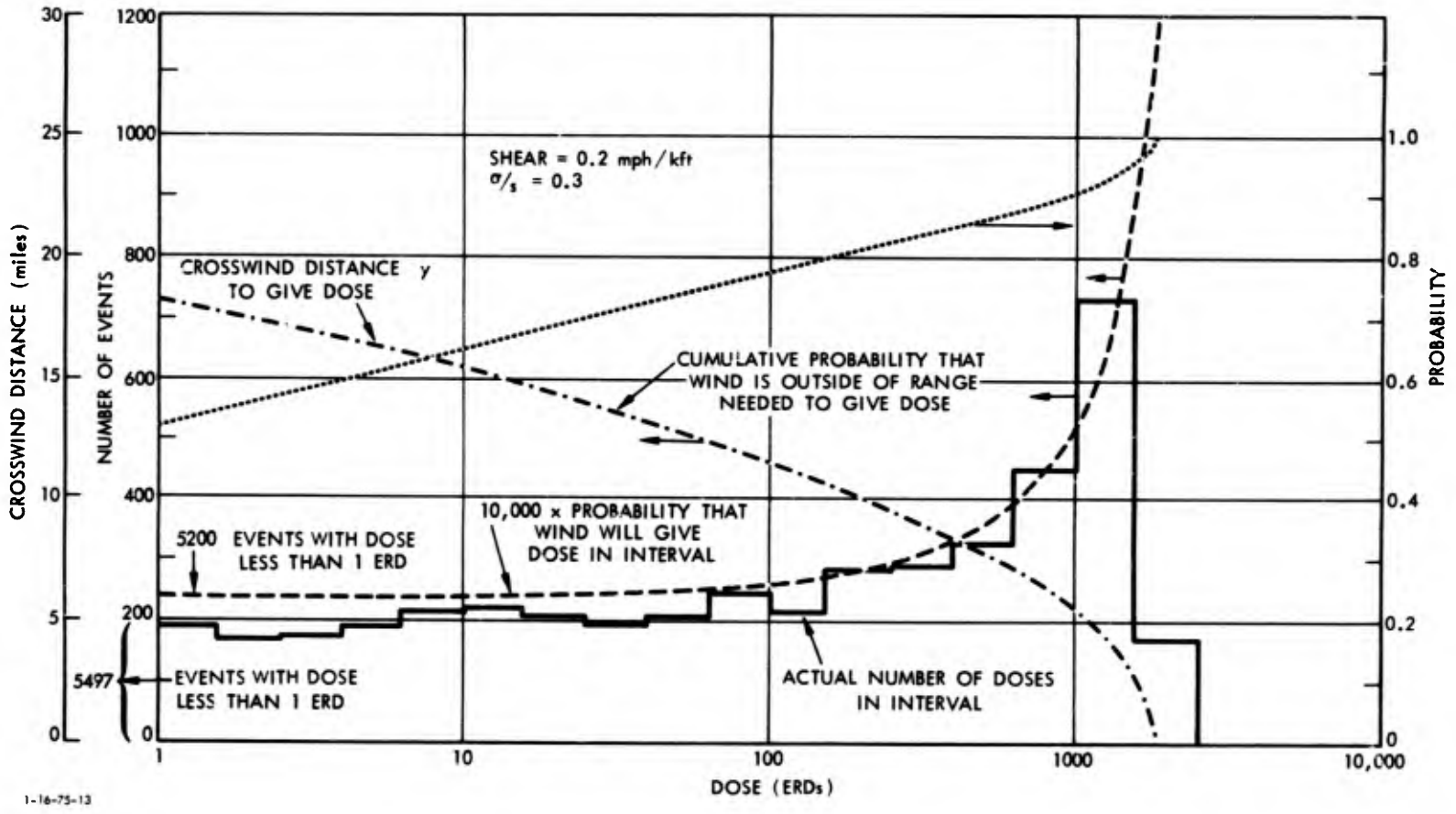

Figure 61. DOSE STATISTICS FOR A 40-MILE DOWNWIND, 20-MILE CROSSWIND MONITOR POINT

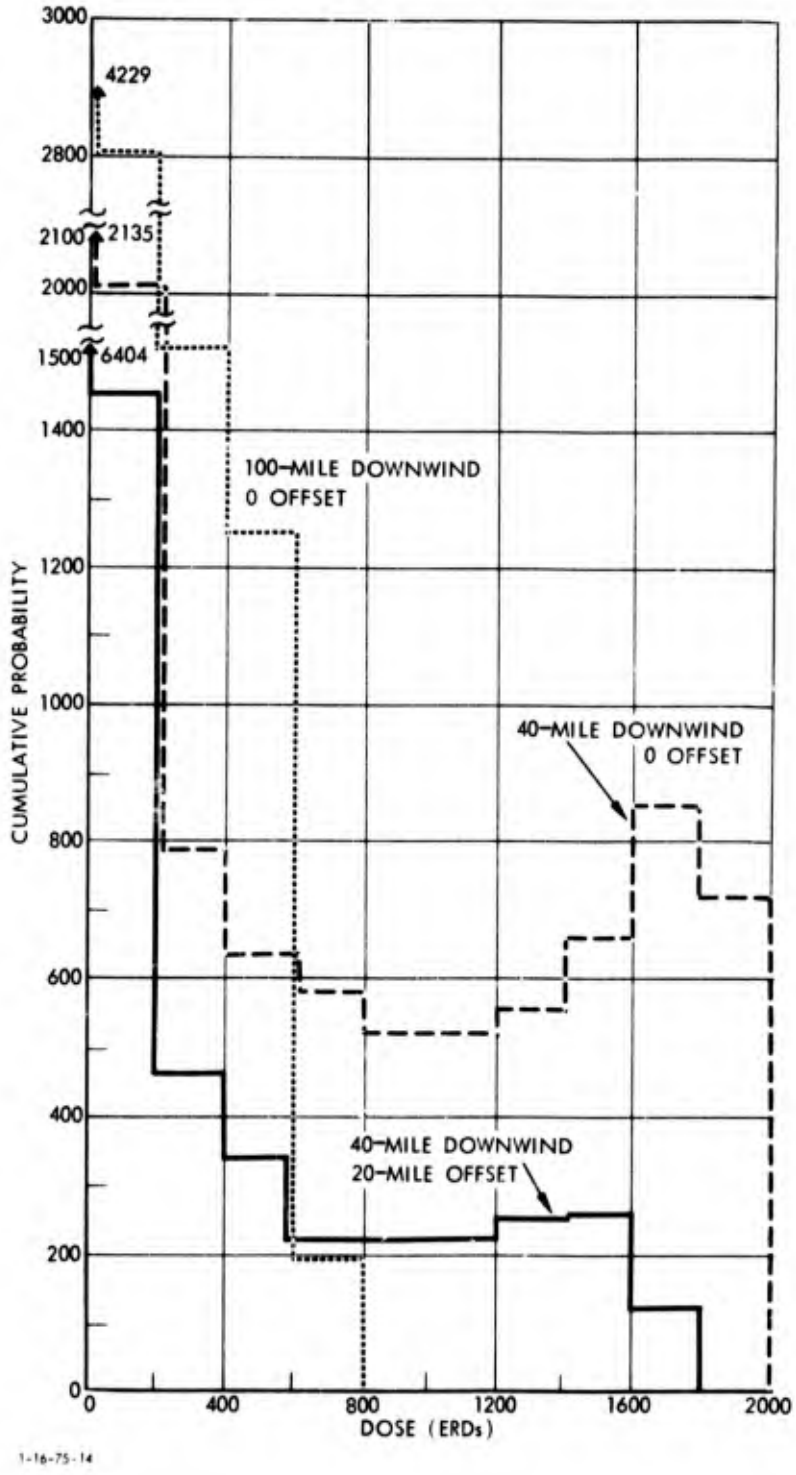

Figure 62. NUMBER OF OCCURRENCES OF DOSES IN EQUALLY SPACED INTERVALS FOR $\sigma/A = 0.3$

As already mentioned, the values of σ/S used for illustration here are abnormally low; the minimum value of σ/S indicated for the Unites States is in winter, with a value of 0.47. In Figure 63, numbers of occurrences are presented for the same situations as for Figure 62 except that σ/S has a more typical value (of 1.0). As expected, the number of cases when the dose is low, is greater. Allowing for this difference, the shapes of the distribution curves for higher doses are quite similar--with, typically, a decrease from initially high values, followed by an increase to higher values near the maximum dose. The rate of this increase depends upon the offset; at large offsets from the hot line, fewer (but more uniformly distributed) doses are greater than 10 ERDs. This cup-shaped distribution occurs with uniform distribution and is even more accentuated with logarithmic distribution at increasing dose level.

In a fashion analogous to the previous formulas for a logarithmic distribution, we can write for a uniform distribution

$$P(I) = \left(P(y_U) + P(y_L)\right)\frac{dy}{dI} ,$$

so that

$$P(I) = \left(P(y_U) + P(y_L)\right)\frac{\sigma}{\sqrt{\sigma 2}}\,\frac{1}{I\sqrt{\log\,(I_o/I)}} ,$$

where I_o is the centerline dose.

This formula can be simplified if it is assumed that the probability density for P(y) is constant over the region of interest. We can then write

$$P(I) = \frac{\sigma_c A}{2\pi D}\,\frac{1}{I\sqrt{\log\,(I_o/I)}} ,$$

where d is the downwind distance along the centerline; σ_c is the constant in the crosswind-dose decay; and A is a ratio of

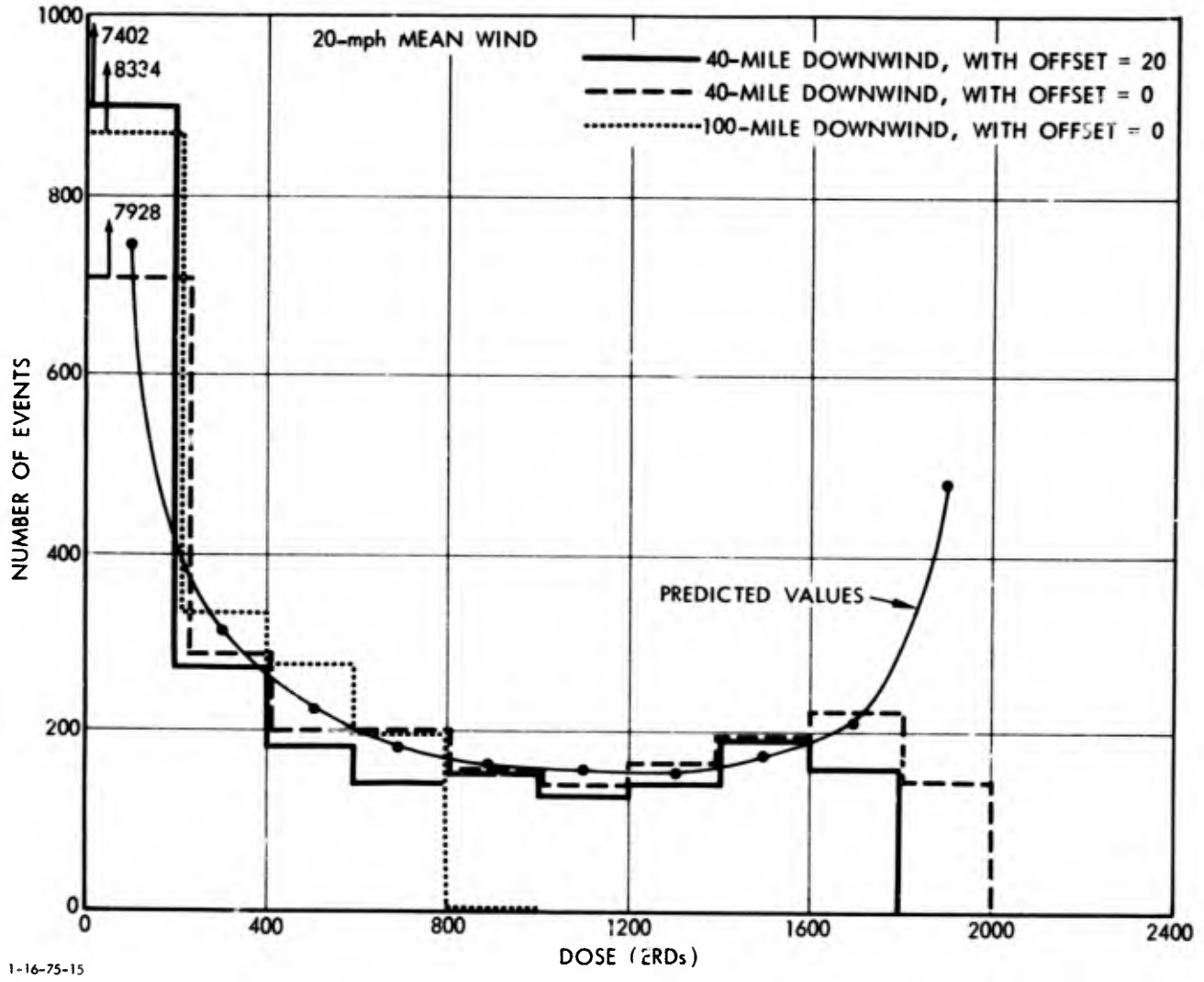

Figure 63. NUMBER OF OCCURRENCES OF DOSES IN EQUALLY SPACED INTERVALS FOR $\sigma/S = 1.0$

the probability density of the wind, considered in the region of interest to that of a completely random wind (V/S = ∞).

In Figure 63, this probability density is multiplied by 200 (the dose interval) times 10,000 (the number of samples), to give a predicted curve for 40 miles downwind with no offset. From Figure 53, A was taken as 2.4. As can be seen, this sample formula predicts the observed frequencies fairly well. For cases where the probability density cannot be assumed constant, letting A be a function of I may give desired results.

In Table 2, some dose statistics are presented for seven monitor points under four wind conditions (the first three are values of V/S = 0.3, 1.0, and 1.5 for a constant shear of 0.2 mph/kft, and the fourth wind is V/S = 1.0, with the shear a normally distributed random variable having both mean and standard deviation = 0.2 mph/kft--negative values of shear are set equal to zero). The mean wind is 20 mph, and 10,000 points are in the sample. For each case, the left-hand entries are the mean value of dose, the standard deviation of dose, and the maximum dose. The right-hand numbers are the mean and standard deviation when all doses under 10 ERDs are deleted. The number of doses under 10 ERDs is the bottom right-hand entry. As can be seen from the table, the standard deviation is generally an appreciable value compared to the mean--even considering only the doses over 10 ERDs--due to the bimodal tendency of these probability distributions. For points with zero offset, an increase in wind variability from 1.0 to 1.5 is not nearly as significant as an increase from 0.3 to 1.0. The values at 1.5 are close to what would be obtained with completely random wind directions (V/S = ∞). For example, the monitor point 40 miles downwind would have about 8,800 doses below 10 ERDs for random winds--compared to the 8,325 doses observed.

The values of mean dose for all the samples fluctuate grossly with wind variability. Since the distribution with V/S = 1 or more has at least half the doses very low and the

Table 2. DOSE STATISTICS FOR SEVERAL WIND VARIABILITIES

Monitor Point Distance			V/S = 0.3; σ_s = 0		V/S = 1.0; σ_s = 0		V/S = 1.5; σ_s = 0		V/S = 1.0; σ_s = 0.2	
Down-wind	Cross-wind	Statistic	All Doses	Over 10 ERDs	All Doses	Over 10 ERDs	All Doses	Over 10 ERDs	All Doses	Over 10 ERDs
20	0	M	1,640	1,771	438	1,216	258	1,075	429	1,179
		σ	1,260	1,271	887	1,114	680	1,023	868	1,090
		D_{max}/N_e	3,624	743	3,623	6,400	3,619	7,600	3,759	6,362
40	0	M	667	848	184	707	113	667	176	678
		σ	676	654	449	638	356	612	435	622
		D_{max}/N_e	1,938	2,135	1,936	7,402	1,937	3,325	2,001	7,399
40	0	M	199	553	132	638	89	621	132	610
		σ	419	541	367	571	304	559	366	572
		D_{max}/N_e	1,743	6,404	1,746	7,928	1,746	8,567	1,907	7,834
40	40	M	24	313	69	478	55	485	69	463
		σ	127	347	239	448	213	441	233	428
		D_{max}/N_e	1,331	9,234	1,398	8,551	1,398	8,869	1,477	8,515
60	0	M	355	514	102	477	65	470	96	450
		σ	408	400	276	423	226	423	266	415
		D_{max}/N_e	1,314	3,099	1,322	7,865	1,321	8,609	1,373	7,861
100	0	M	141	244	44	261	30	269	41	244
		σ	187	188	135	229	116	240	129	227
		D_{max}/N_e	720	4,229	805	8,334	805	--	856	8,338
150	0	M	60	119	20	150	14	166	49	141
		σ	36	89	70	129	63	143	67	129
		D_{max}/N_e	409	5,038	519	8,662	538	9,138	563	8,685

rest more or less uniformly distributed, the mean value is a questionable descriptor of the sample, especially when it might be used to determine expected fatalities. A better description is given by the number of doses below some preassigned low value and by the mean of those doses above this value. As can be seen from the table, the mean of the higher doses is less affected by wind variability. For zero offset, this mean of high values decreases as wind variability increases near the burst but increases with wind variability far from the burst. The changes reflect changes in the shape of the distribution function. As can be seen from Figures 62 and 63, there is a large number of values that significantly affect the mean value between 10 and 200 ERDs. There this mean value is sensitive to the cutoff value chosen.

Figure 64 presents plots of cumulative probability of exceeding a certain fraction of the maximum dose. The curves in such a presentation can be taken as straight lines for some types of risk calculations. Here a simple predictive scheme might be utilized. The maximum dose is found (along the centerline) from the maximum of dose as a function of wind speed. On the basis of wind-direction statistics, the likelihood of the dose's being under some value such as 0.1 times the maximum dose is determined. A straight line connecting these points can estimate the cumulative probability.

In the table, the dose statistics for a randomly chosen value of crosswind shear are close to those for constant shear. The variations due to changes in shear are apparently dominated by those due to the fluctuations in wind direction.

C. DOSE STATISTICS FROM HEXAGON PATTERN

In this section, calculations for one set of fallout wind statistics will be exhibited by use of three of the hexagon patterns considered in Chapter II. There are seven weapons in

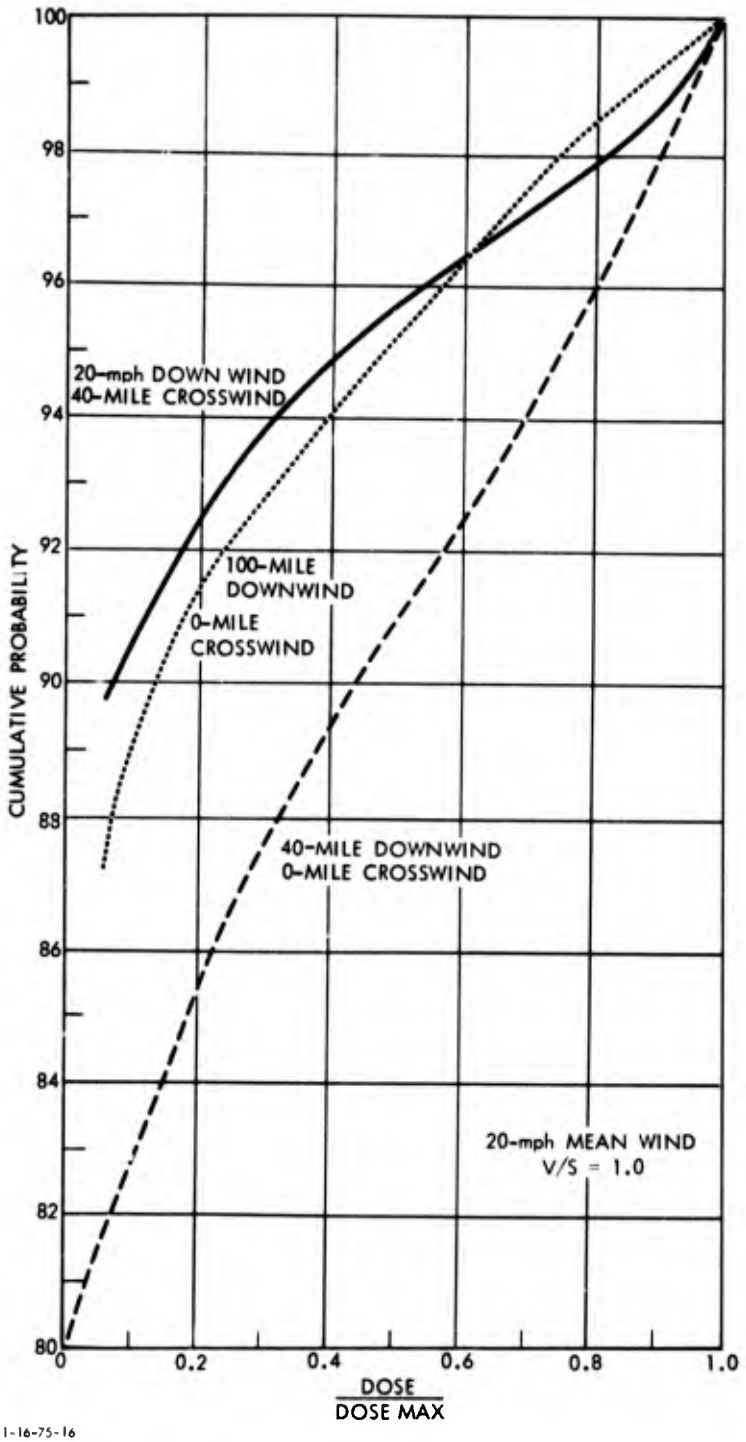

Figure 64. CUMULATIVE PROBABILITY THAT DOSE IS LESS THAN A GIVEN FRACTION OF THE MAXIMUM DOSE

a hexagon pattern with hexagon diameters of 0, 40, and 80 miles. In these calculations each weapon yield is 10 MT with a fission fraction of 1 (for the 0-mile hexagon, only a single 10-MT weapon with fission fraction of 7 is used); the mean wind is 20 mph, with the wind shear = 0.2 mph/kft; and the random wind has a standard deviation of 0.5 from the mean-wind value.

The calculations use stratified sampling, with a sample size of 100. The distribution of doses was determined at the set of 91 monitor points shown in Figure 65 for each of the weapon patterns. From these monitor points, contours of dose level at various probability values were drawn. The lack of a finer grid and the statistical fluctuations from the Monte Carlo process introduce some error in the location of the contours. These errors in location may be estimated as generally less than 10 percent of the distance of the contour from the origin. Figures 66, 67, and 68 present contours of the dose that occur 90-or-less percent of the time. The downwind and crosswind directions refer to the mean wind. In other words, in Figure 66, a point 200 miles downwind and 75 miles crosswind had a dose of 4,000 ERDs or less 9/10 of the time and a dose of more than 4,000 ERDs 1/10 of the time. Contour values are shown for 200, 1,000, 2,000, 4,000, 10,000, and 40,000 ERDs. In these figures, the hexagon weapon locations are indicated by x's. Figures 69, 70, and 71 show the same data at the 50-percent-probability level (i.e., at the median value). Figures 72, 73, and 74 present the data at the 10-percent-probability level (viz, in these figures the dose presented was exceeded 90 percent of the time and was less than the stated value 10 percent of the time). Figures 75, 76, and 77 present contours of mean dose for the same conditions.

The 90-percent contours at appreciable distances are quite close for all hexagon diameters. Close to the hexagons the patterns are more spread for the larger hexagons, with the

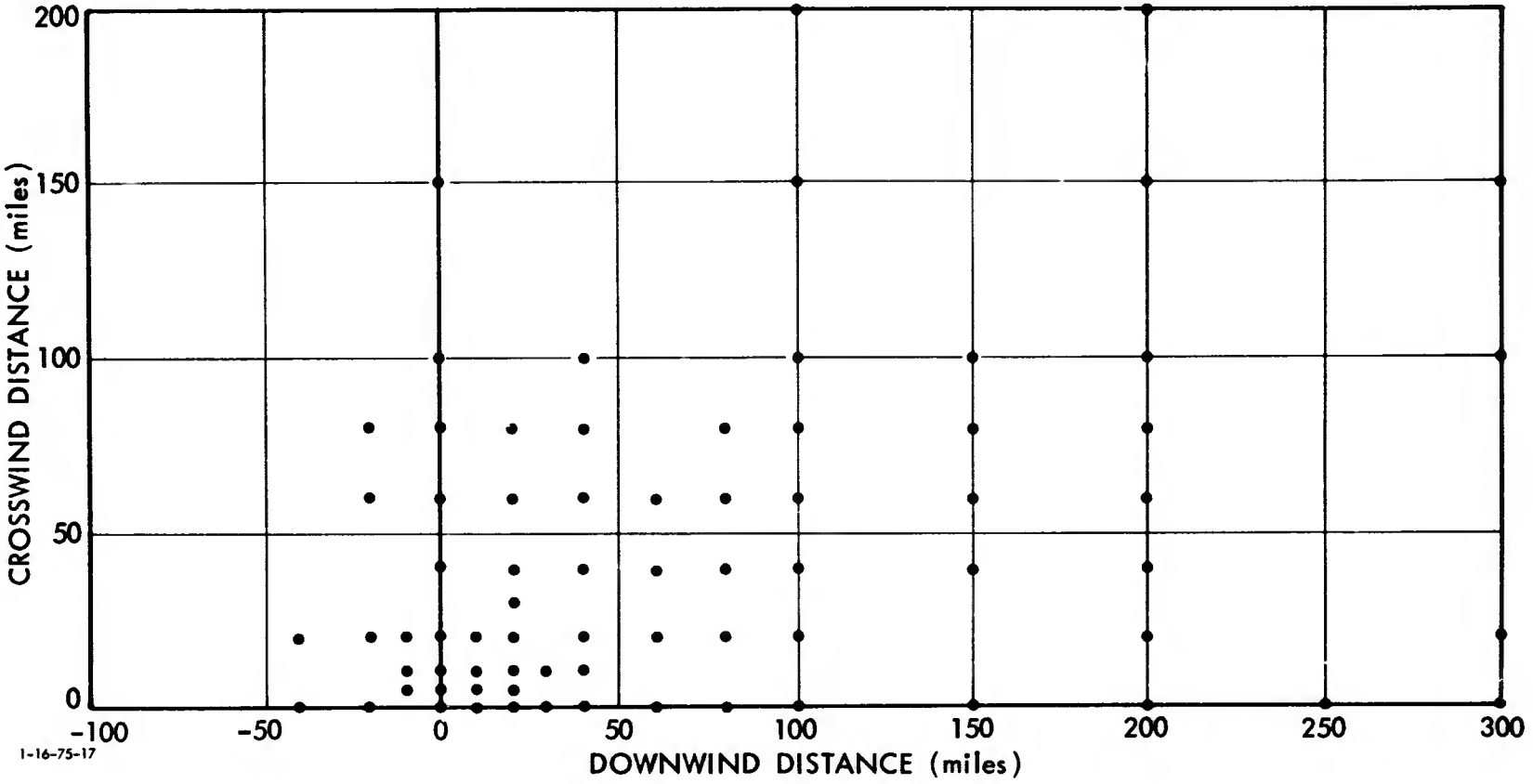

Figure 65. MONITOR POINTS FOR DETERMINING DOSE STATISTICS

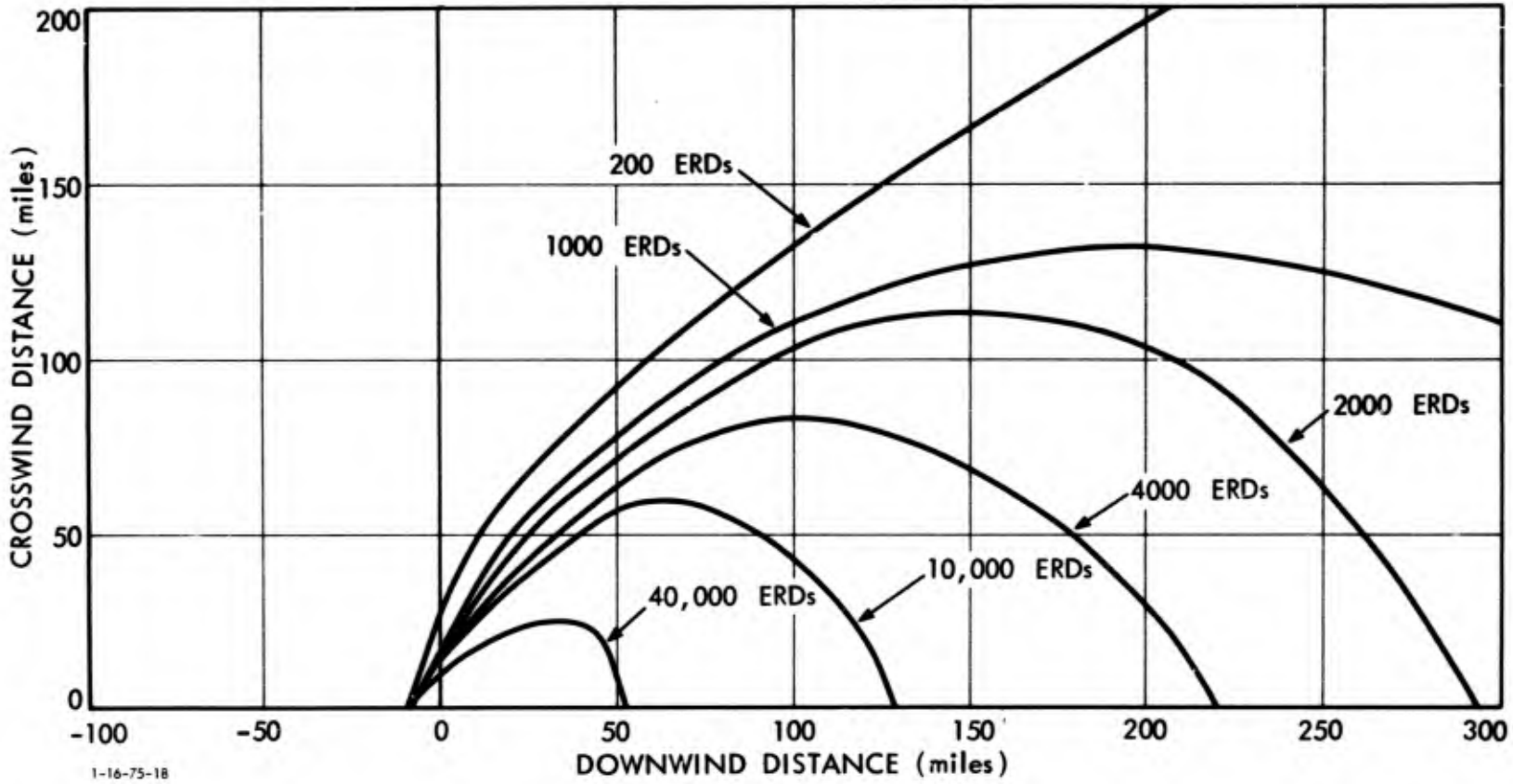

Figure 66. CONTOURS OF DOSE NOT EXCEEDED AT 90-PERCENT PROBABILITY FOR 0-MILE HALF-WIDTH HEXAGON PATTERN

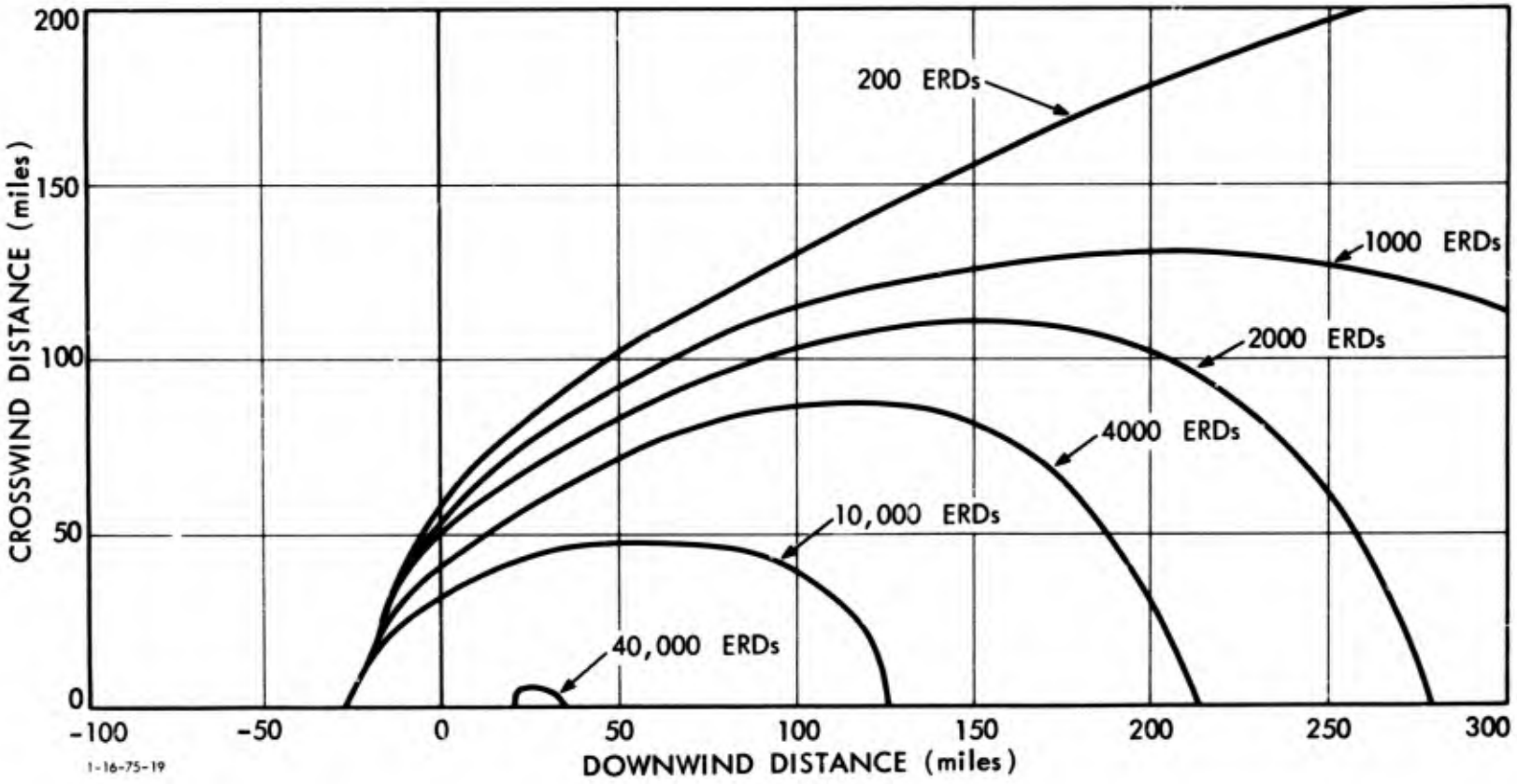

Figure 67. CONTOURS OF DOSE NOT EXCEEDED AT 90-PERCENT PROBABILITY FOR 20-MILE HALF-WIDTH HEXAGON PATTERN

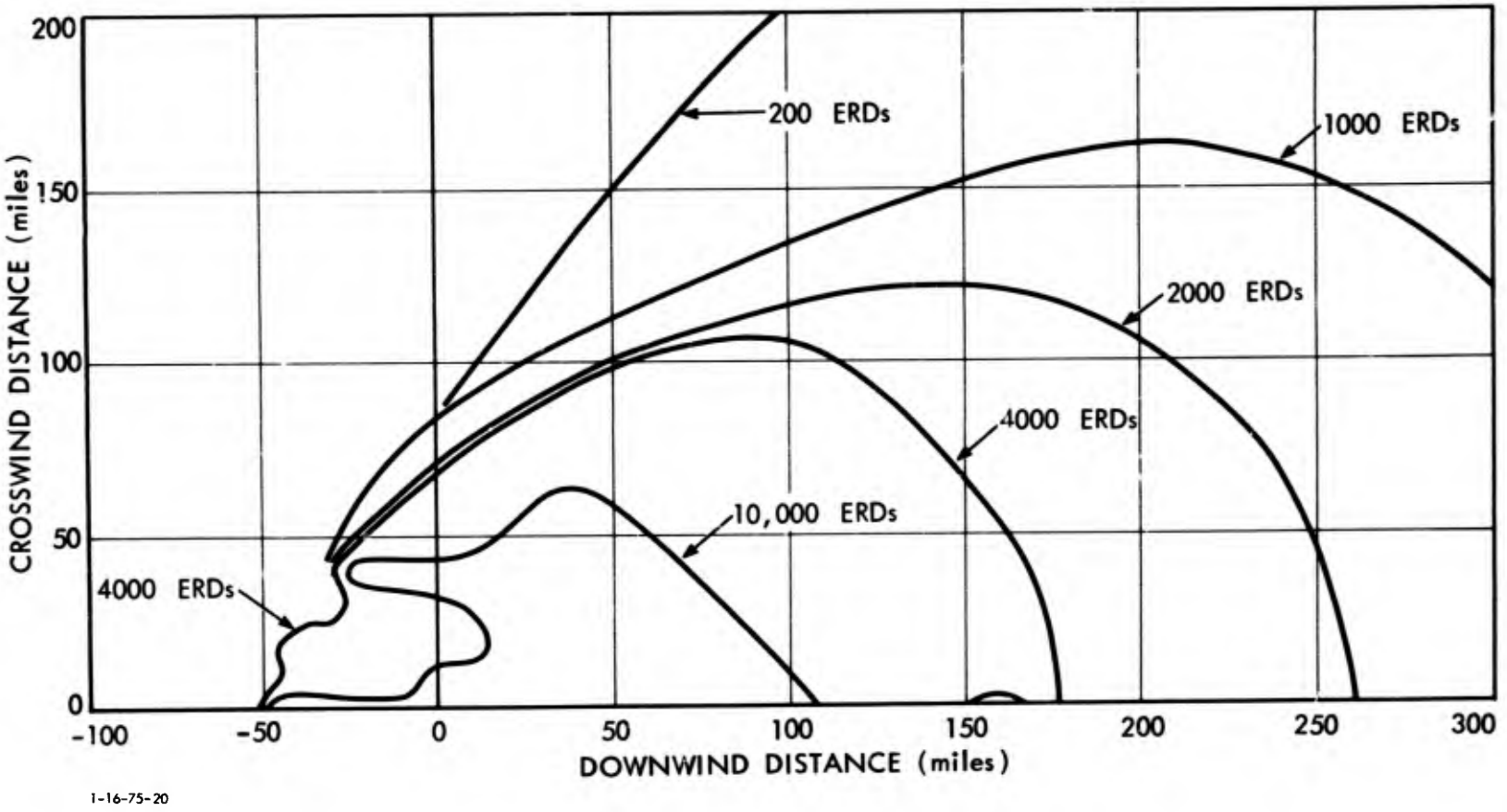

Figure 68. CONTOURS OF DOSE NOT EXCEEDED AT 90-PERCENT PROBABILITY FOR 40-MILE HALF-WIDTH HEXAGON PATTERN

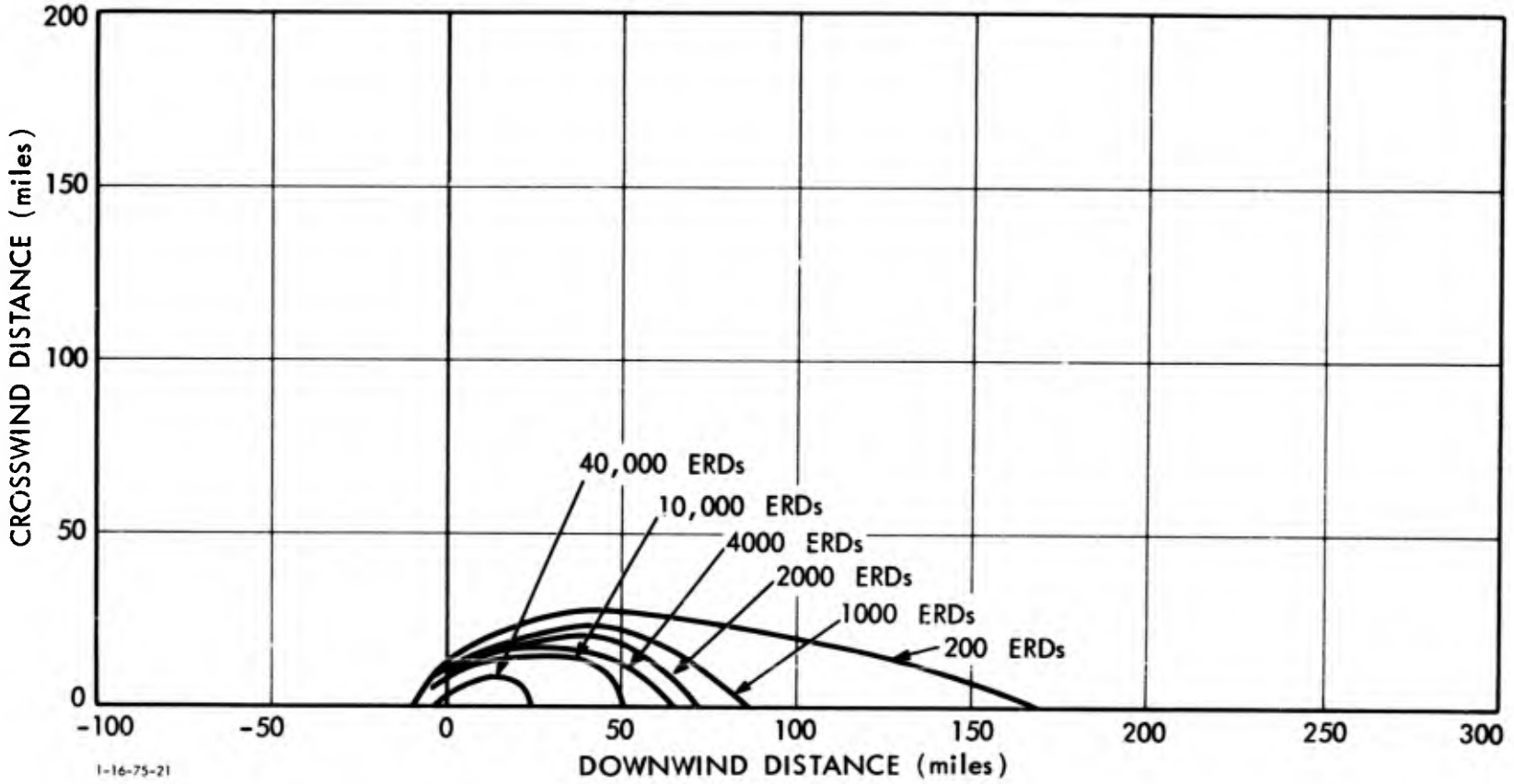

Figure 69. CONTOURS OF DOSE NOT EXCEEDED AT 50-PERCENT PROBABILITY FOR 0-MILE HALF-WIDTH HEXAGON PATTERN (POINT DETONATION)

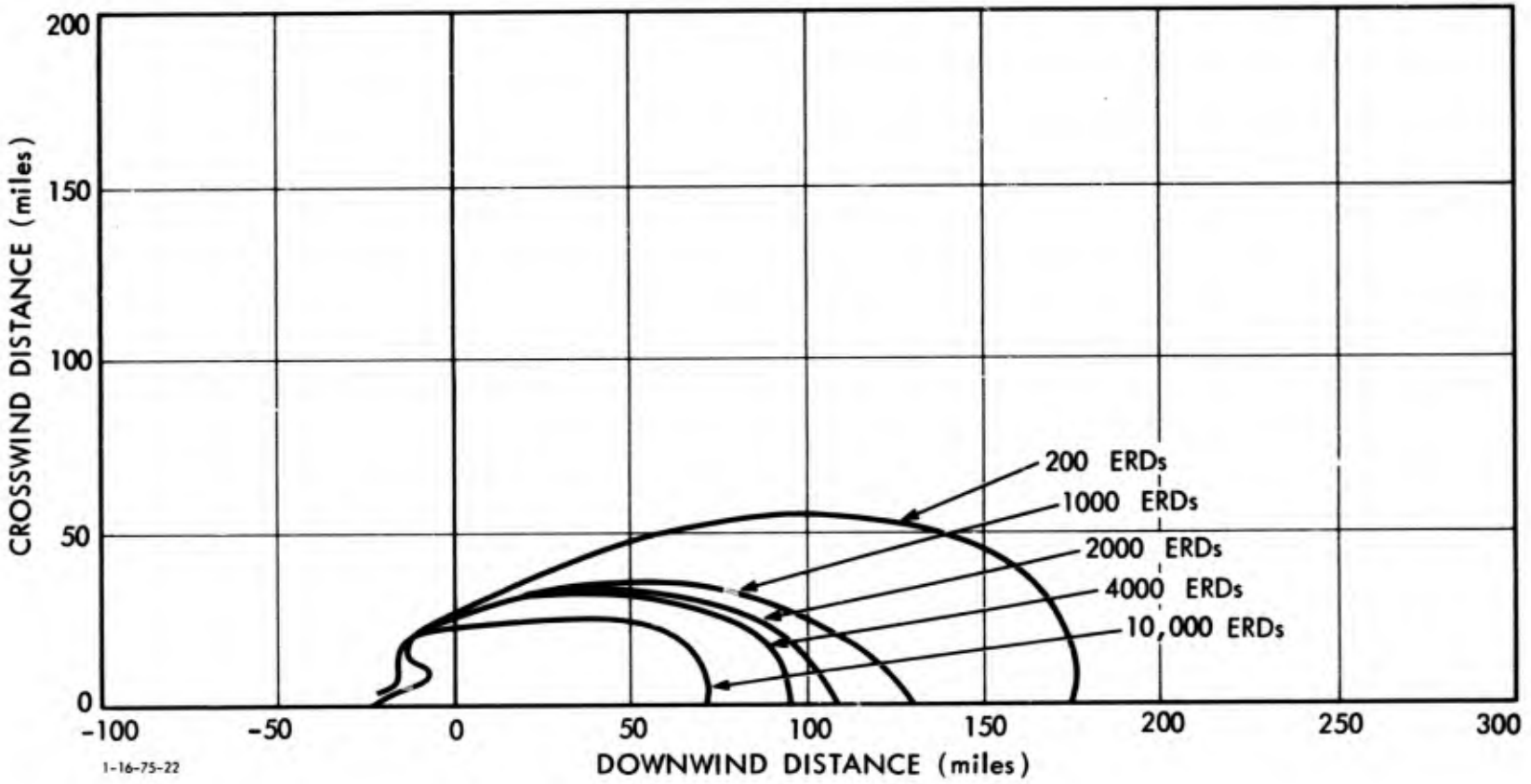

Figure 70. CONTOURS OF DOSE NOT EXCEEDED AT 50-PERCENT PROBABILITY FOR 20-MILE HALF-WIDTH HEXAGON PATTERN

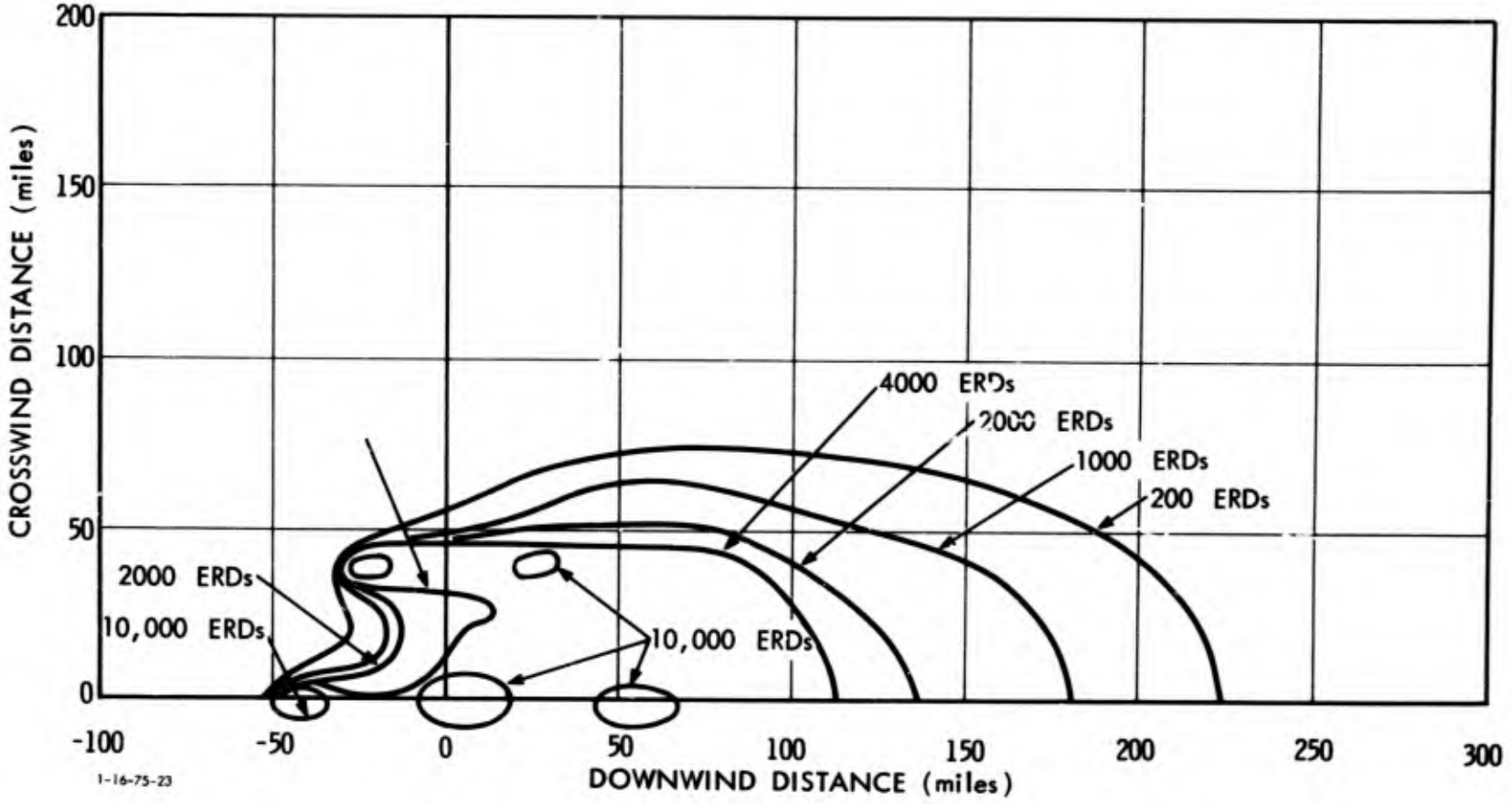

Figure 71. CONTOURS OF DOSE NOT EXCEEDED AT 50-PERCENT PROBABILITY FOR 40-MILE HALF-WIDTH HEXAGON PATTERN

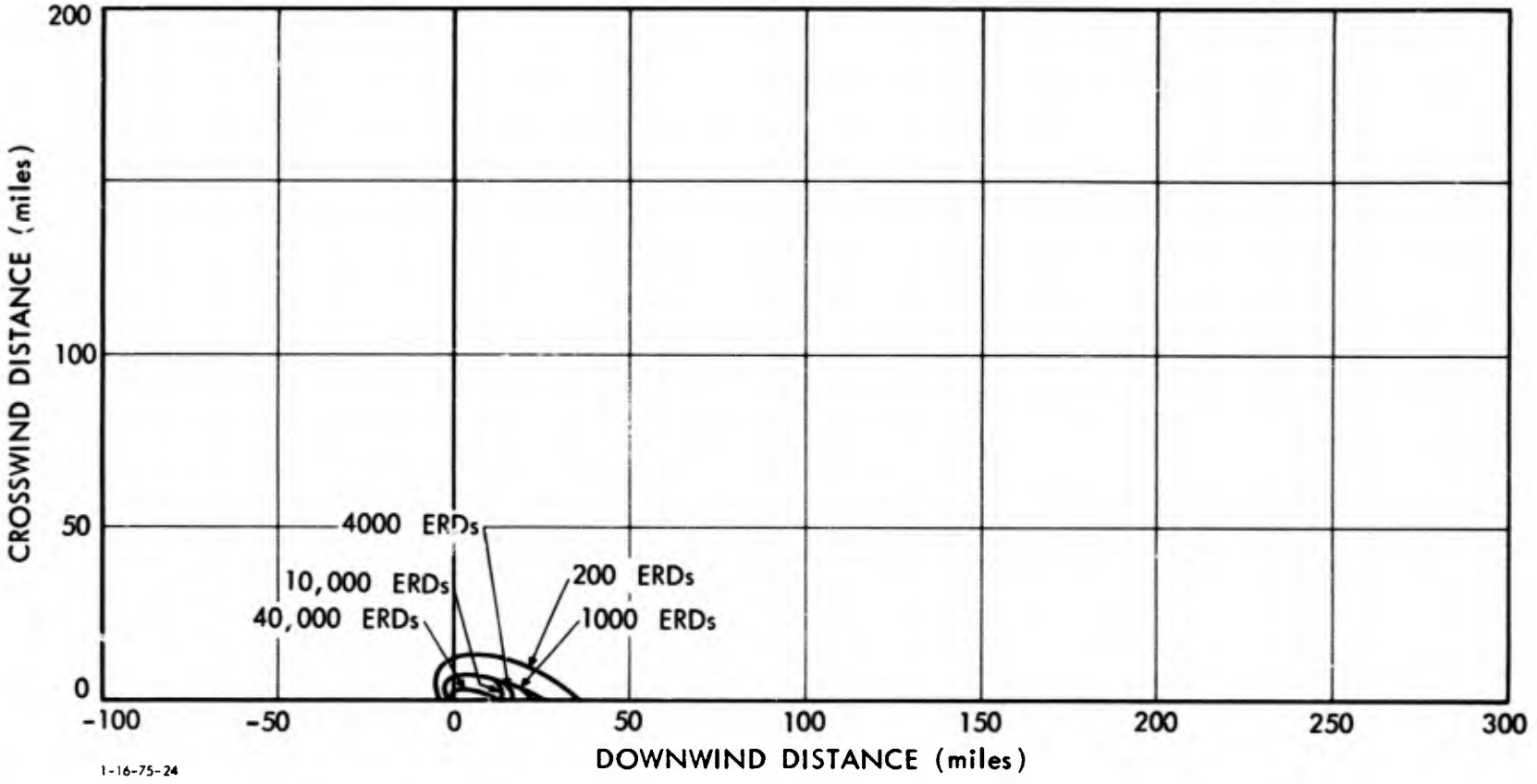

Figure 72. CONTOURS OF DOSE NOT EXCEEDED AT 10-PERCENT PROBABILITY FOR 0-MILE HALF-WIDTH HEXAGON PATTERN (POINT DETONATION)

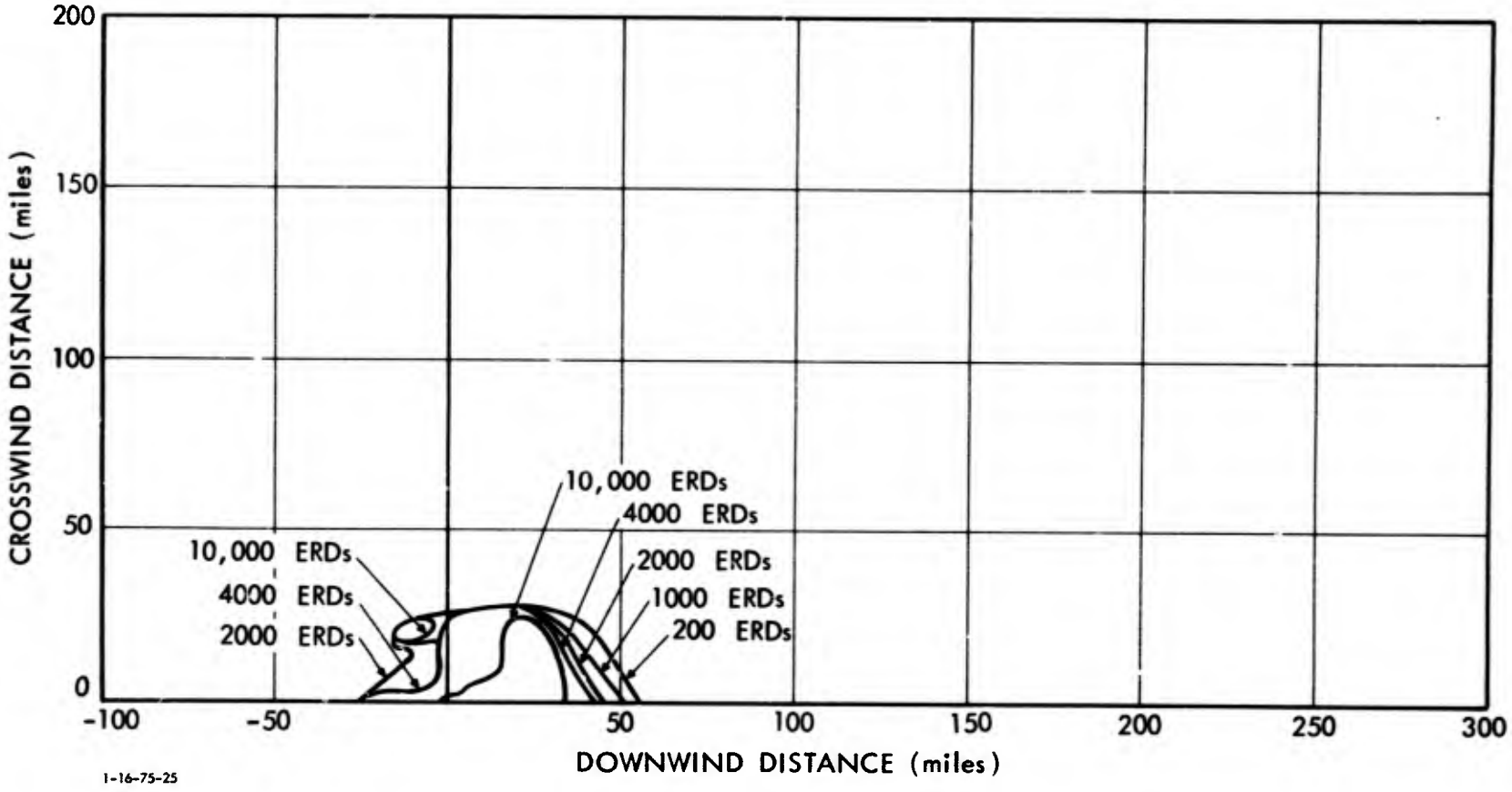

Figure 73. CONTOURS OF DOSE NOT EXCEEDED AT 10-PERCENT PROBABILITY FOR 20-MILE HALF-WIDTH HEXAGON PATTERN

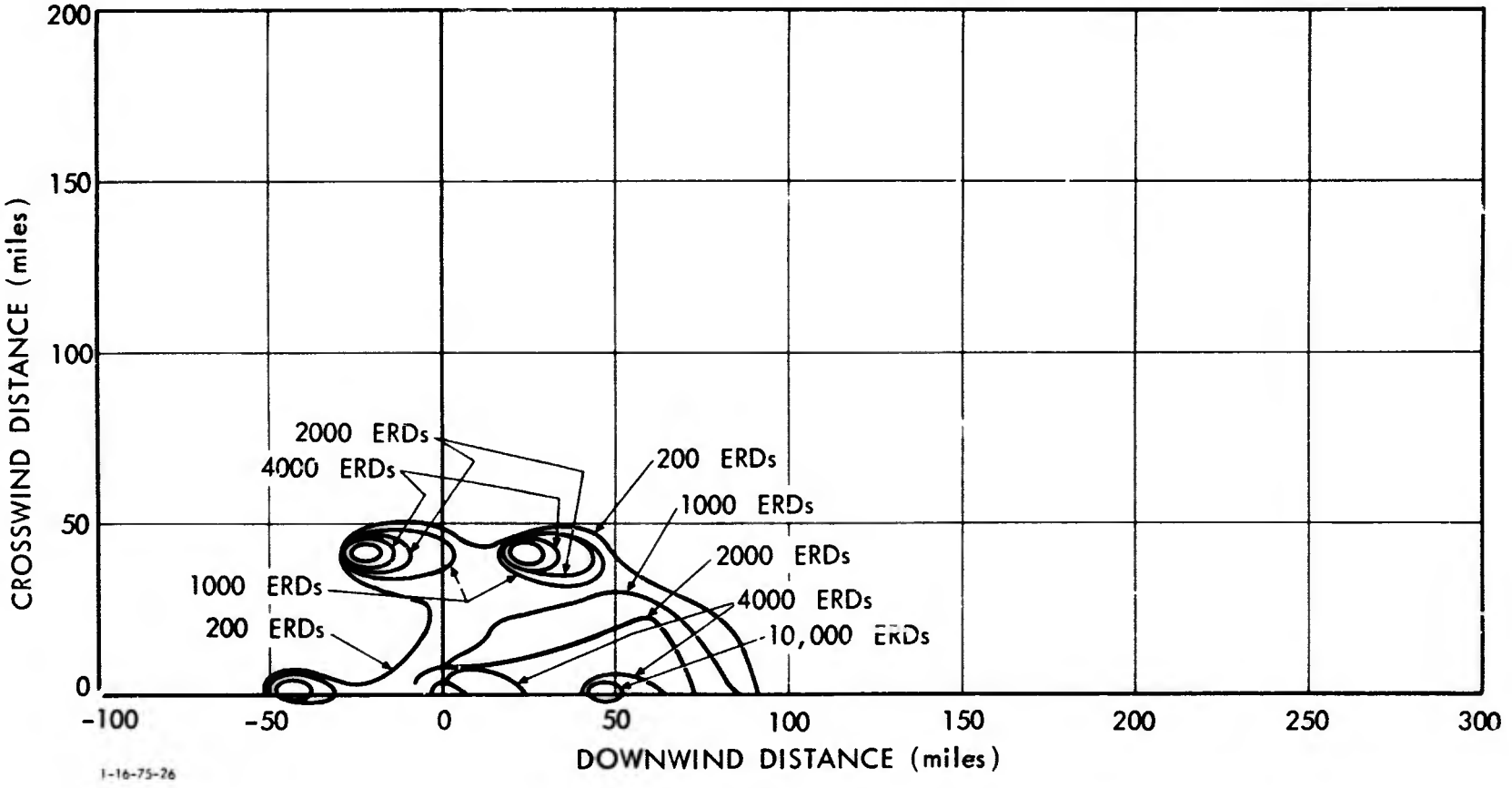

Figure 74. CONTOURS OF DOSE NOT EXCEEDED AT 10-PERCENT PROBABILITY FOR 40-MILE HALF-WIDTH HEXAGON PATTERN

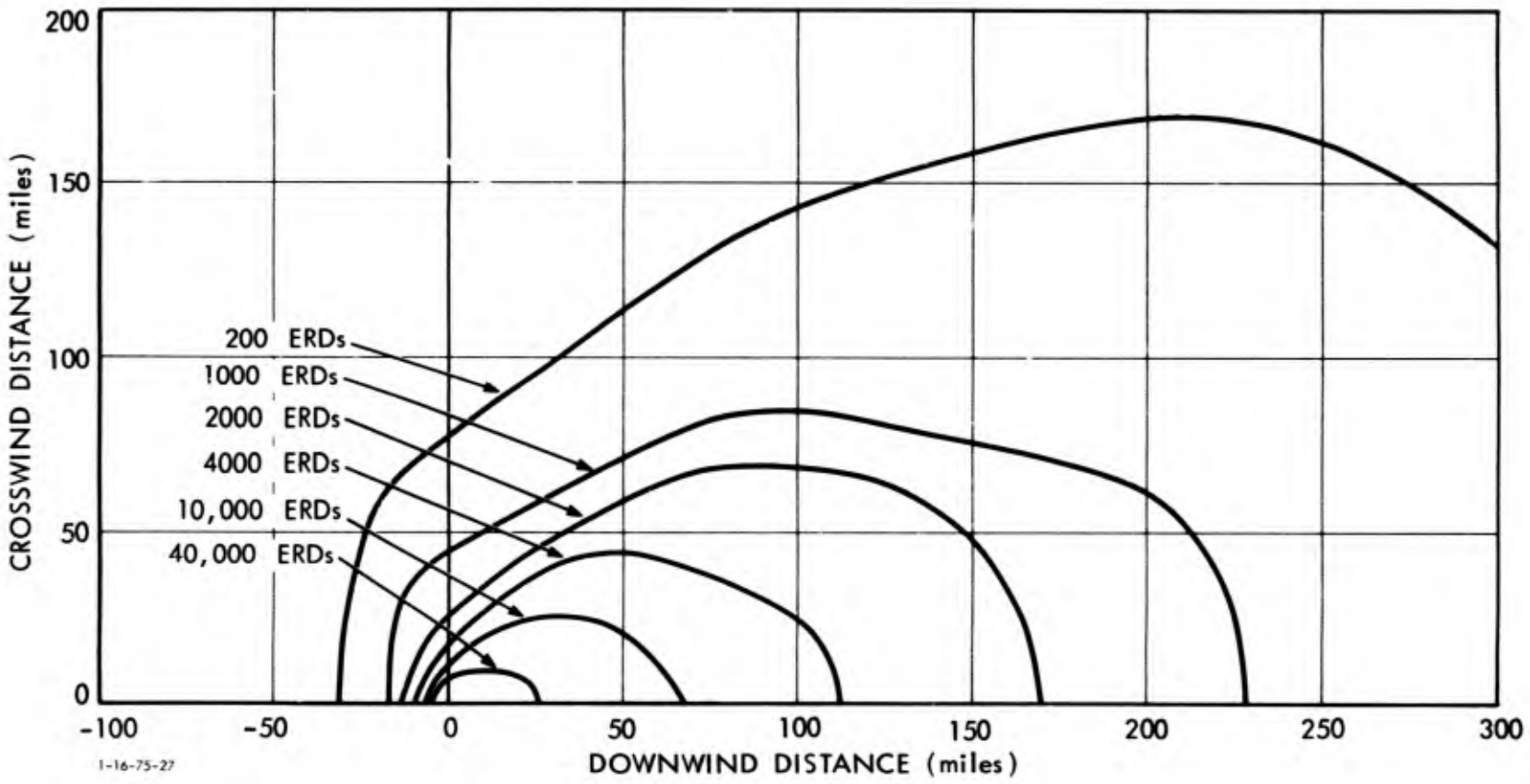

Figure 75. CONTOURS OF MEAN DOSE FOR 0-MILE HALF-WIDTH HEXAGON PATTERN (POINT DETONATION)

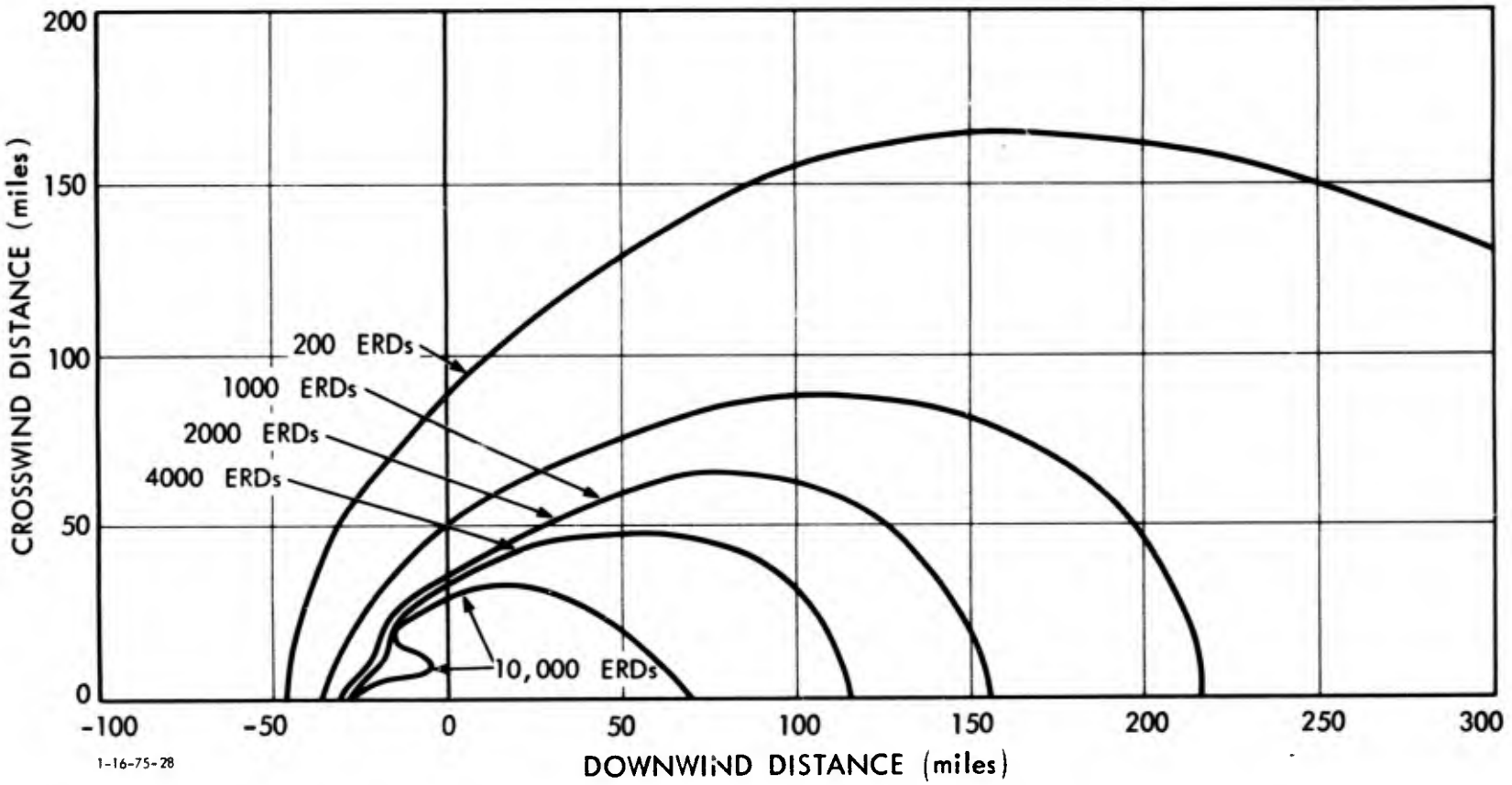

Figure 76. CONTOURS OF MEAN DOSE FOR 20-MILE HALF-WIDTH HEXAGON PATTERN

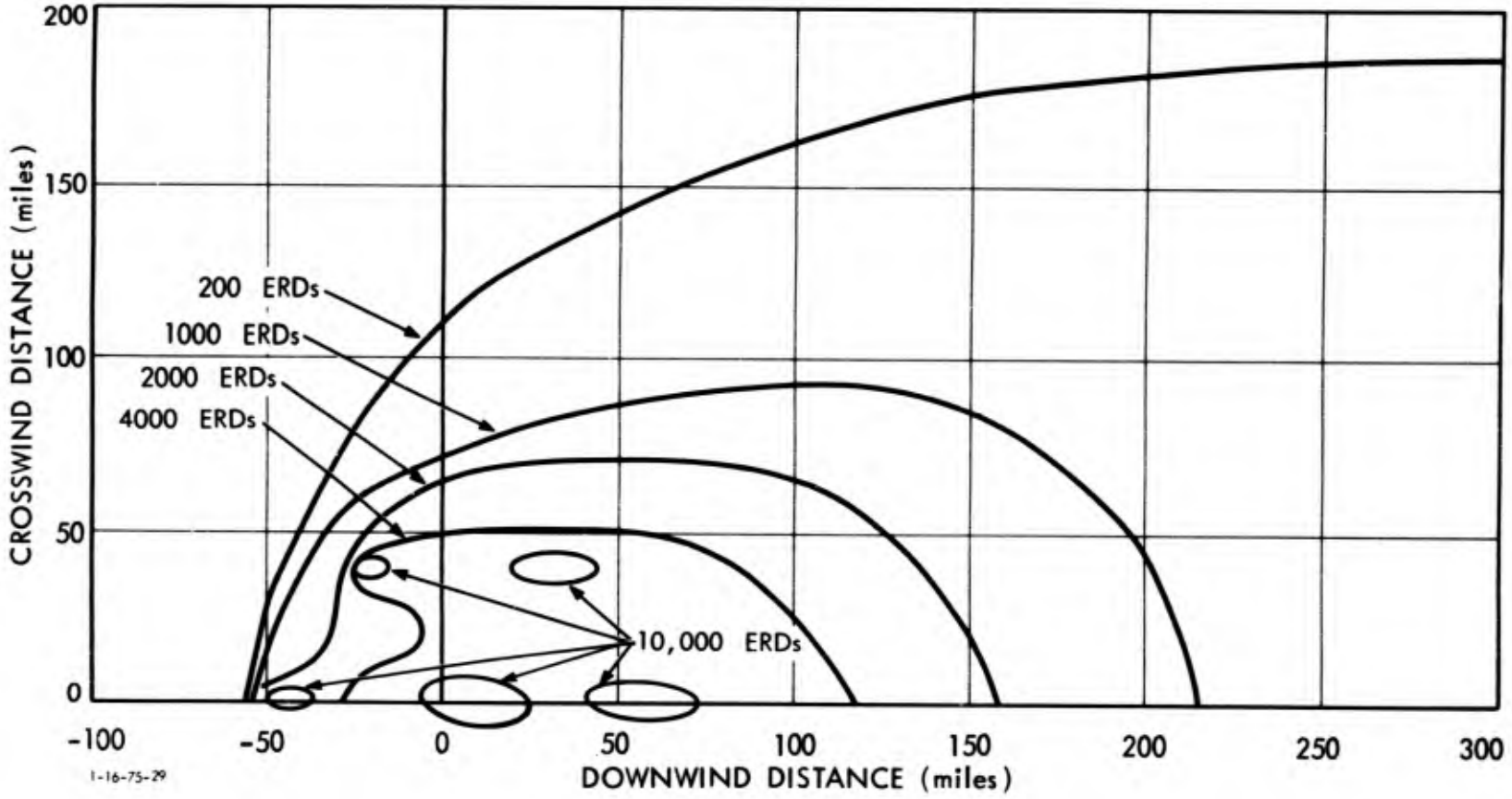

Figure 77. CONTOURS OF MEAN DOSE FOR 40-MILE HALF-WIDTH HEXAGON PATTERN

effects from each weapon showing for appreciable distances in the downwind direction. Since the standard deviation of the random wind is 0.5 of the mean wind, the actual wind would be blowing in a direction more than 90 degrees from the mean-wind vector in less than 5 percent of the cases. Since the figures are at the 90-percent-probability level, occurrences happening less than 5 percent of the time would not show on the figures. Thus, upwind of the mean wind, the contours rapidly fade; and downwind, the contours show the regions of larger dose.

A simple calculation helps illustrate the general nature of the curves generated. In Figure 66, the 40,000-ERD contour intersects the downwind axis at 50 miles for the 0-mile hexagon. At this distance downwind from a 10-MT burst with a weapon having fission fraction 7, the value of the dose is 47,770 ERDs, for a wind speed of the vector mean-wind value. The value of σ_c here is 9.50 miles. Thus, any wind that places the hot line within 5.5 miles of the downwind axis at 50 miles downwind will give a dose of 40,000 ERDs or greater. This distance requires an angle of the wind within 6.3° from the mean-wind direction--which in Figure 52 (above) is seen to occur only 10 percent of the time. Thus, the location of this particular contour near the mean-wind axis is well explained by variations of wind direction alone--as might be expected. For the larger hexagon patterns, similar sensitivity to wind direction could be expected; but the patterns are spread more to complicate the situation. Thus, doses between 10,000 and 40,000 ERDs in the region just downwind of the hexagon pattern might be expected 10 percent of the time. As can be seen from the figures, a coalescing into a single pattern is fairly evident for the 40-mile pattern and even somewhat evident for the 80-mile pattern in the region far downwind. In the latter case, this pattern occurs (even though such coalescing does not occur for the single-wind patterns of Chapter III), since the weapons are

still close enough that at least 10 percent of the time the wind is in a direction that yields a dose at least in the indicated range.

For the 50-percent-probability level, the patterns are much smaller and less coalescing occurs. The patterns are rather irregular within the hexagon patterns but, even so, in the downwind direction the irregularities smooth out.

The 10-percent-level probability patterns are where the indicated dose is found at least 90 percent of the time--which for the 0-diameter hexagon occurs over quite small areas. For the 40-mile-diameter hexagon, at least 10,000 ERDs occur most of the time in the rear of the hexagon and just downwind. For the 80-mile hexagon, only lower levels of doses are seen to be this likely.

Chapter V

FALLOUT-RISK STATISTICS FOR HYPOTHETICAL ATTACKS

This chapter presents fallout-risk statistics for several hypothetical attack situations. A descriptive (rather than analytic) treatment of this subject is used--due partly to the inherent complexity of the statistics (which more naturally leads to a case-by-case treatment) and partly because at this point it appears appropriate to combine dose statistics with fallout-shelter-distribution statistics to develop methods of making fatality calculations. The latter subject is better treated in a separate paper.

This chapter first presents dose statistics on a "typical" target from an attack on the region surrounding the target, but avoiding the target itself. These calculations use the same simulation as in Chapter IV (above), with the many-weapon, single-target situation here representing a counterbalance to the single-weapon, many-target cases there. This case is used to study some of the statistical properties of the calculation. A simulation that uses clusters of weapons to produce doses is then described. The results from this simplified but more rapid simulation will be compared with a direct use of the WSEG model. Finally, several sets of statistics for a nationwide attack will be illustrated.

A. FALLOUT RISK FROM AN ATTACK SURROUNDING DETROIT, MICHIGAN

A special attack was constructed to consider in a reasonably simple fashion a hypothetical attack for the region around Detroit, Michigan. The weapon laydown is illustrated in

Figure 78. Where more than one weapon is used on a single city, the weapons are assumed to be colocated. A fission fraction of 1 was assumed for these calculations, so the quoted doses should be multiplied by the weapon fission fraction ½ (e.g., ½ if a fission fraction of ½ is assumed). The mean wind is assumed to be from due west to east in all calculations.

The distribution of doses on the population centroid of the Detroit urbanized area from 1,000 trials with wind statistics for autumn is shown in Figure 79 for logarithmic intervals and in Figure 80 for constant 200-ERD intervals. In Figure 80, a constant value is used over 10,000 ERDs, since the dose statistics were computed only for broader intervals. This value will represent the average value that would be obtained for 200-ERD intervals. Beyond the range of the figure, values of 2.3 were obtained for 15,000 to 20,000 ERDs; 2.4, for 20,000 to 23,000 ERDs; and 0, for larger doses. The distribution for doses over 200 ERDs is seen to be slowly decreasing in likelihood with increasing dose level. The logarithmic distribution shows a peak at about 3,000 ERDs. Up to this level, the shape is not too dissimilar from some single-weapon examples. However, this distribution at higher dose levels shows a significant tail that is absent in the single-weapon cases. This tail appears to derive from those cases when the wind is blowing to bring fallout from a few other particularly serious target areas over Detroit.

The maximum dose on Detroit from the 1-MT weapon on Ann Arbor for the worst wind conditions is about 2,000 ERDs, the highest dose from the 20-MT weapon on Toledo is about 9,700 ERDs, and the highest dose from the eight 20-MT weapons on Chicago is about 19,000 ERDs. The peak dose was 23,091 ERDs, which appears to have occurred where a high wind was blowing from Chicago; and contributions from other targets along the route were also received.

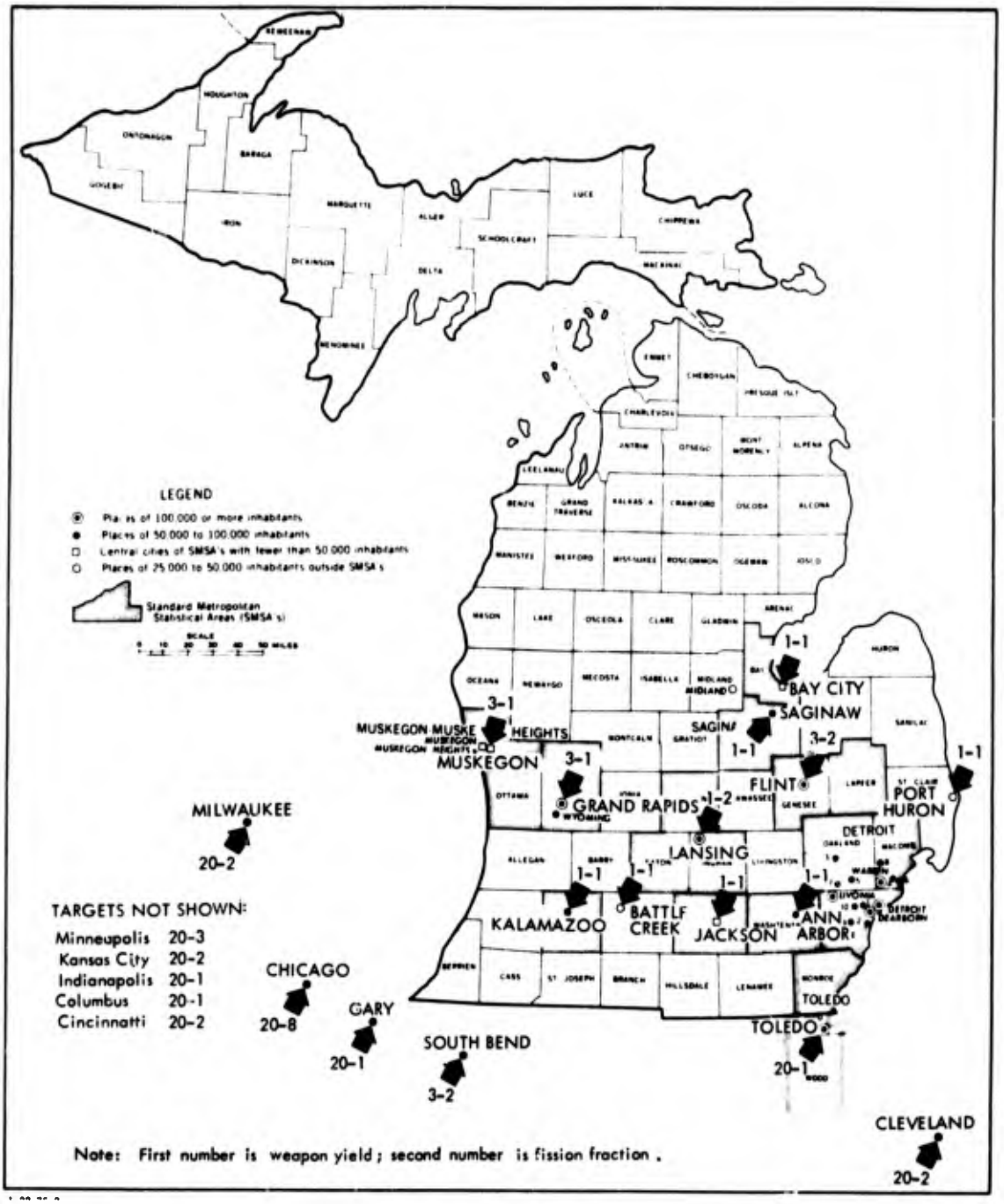

Figure 78. MAP OF ATTACK ON REGION NEAR DETROIT

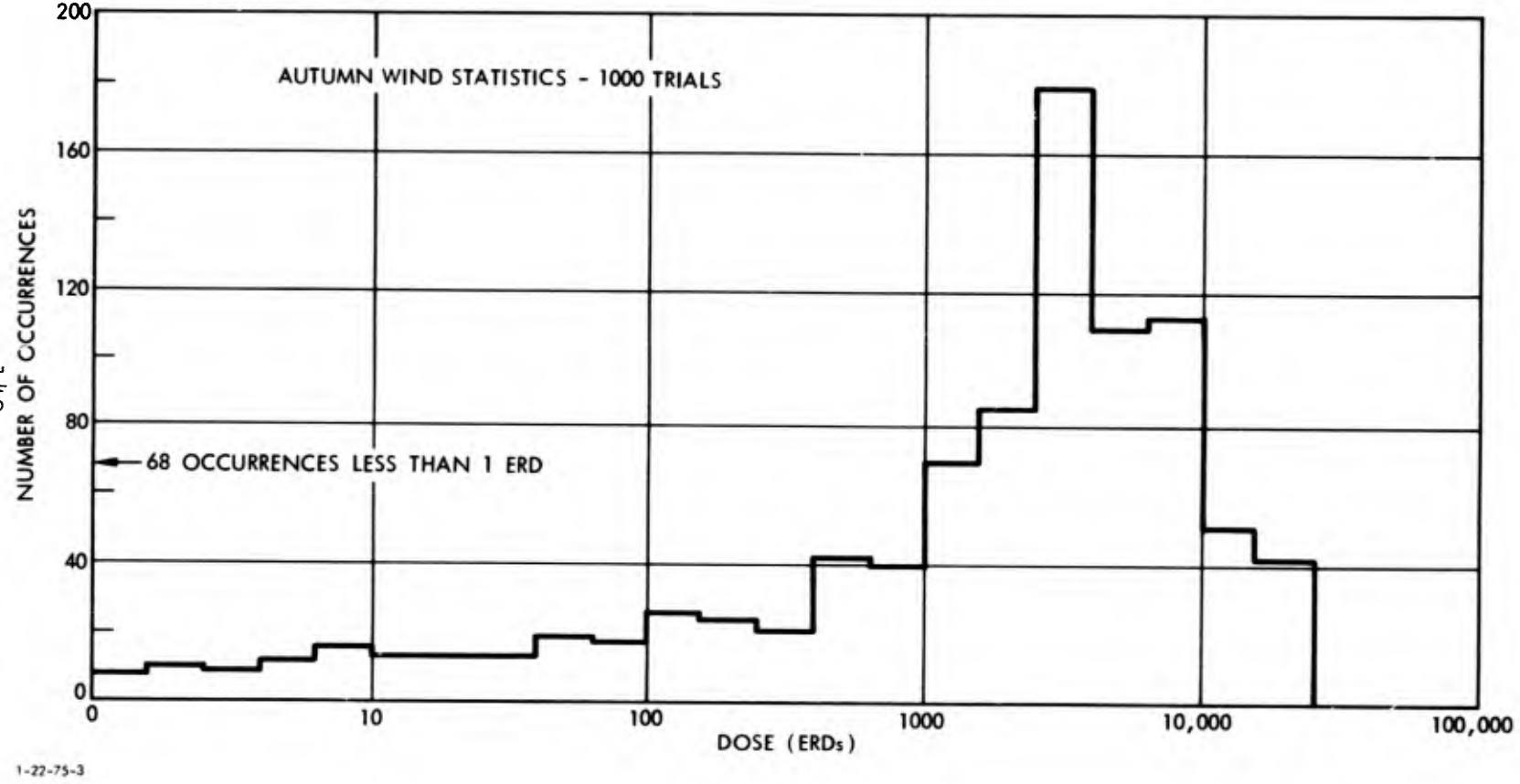

Figure 79. HISTOGRAM OF DOSE DISTRIBUTION FOR DETROIT, WITH LOGARITHMIC INTERVALS

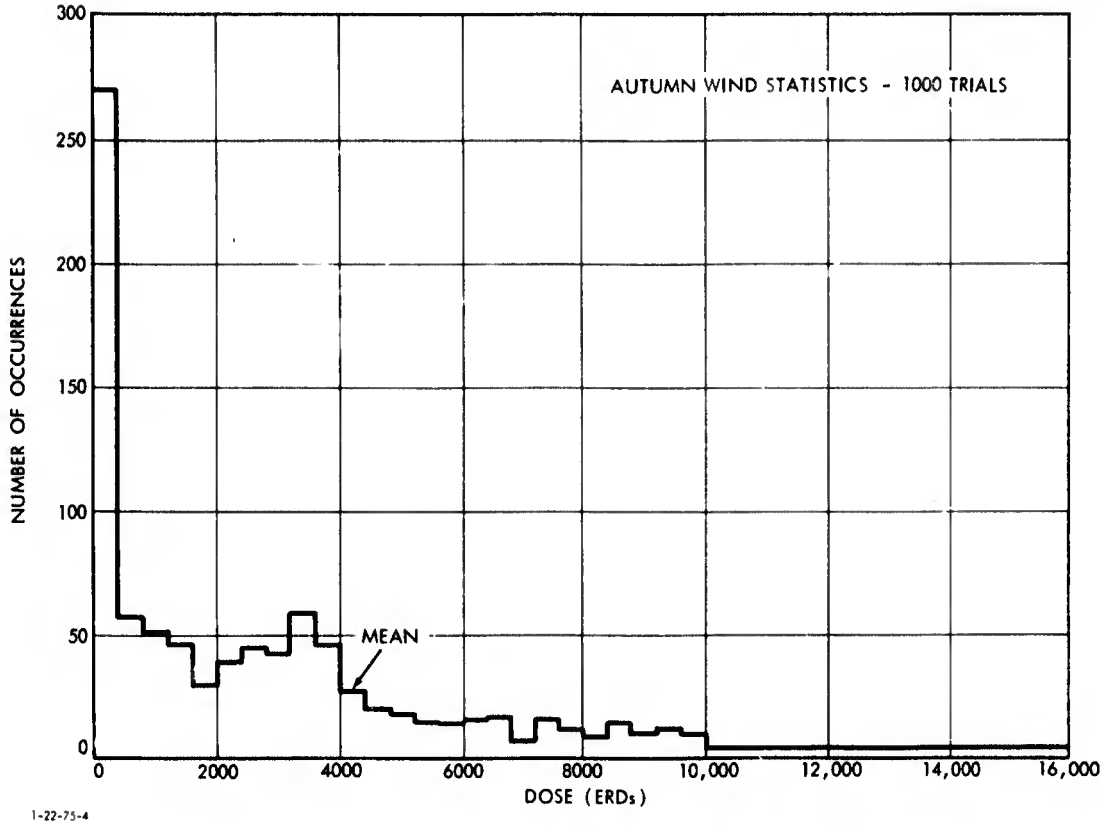

Figure 80. HISTOGRAM OF DOSE DISTRIBUTION FOR DETROIT, WITH EQUAL INTERVALS

Dose statistics for various seasons are shown in Table 3. For each season the table shows the magnitude of the mean-velocity vector and the standard deviation of the random vector divided by mean velocity. Wind shear is either constant at 0.2 or randomly selected from a normal distribution with mean value 0.2 and standard deviation 1.5 (negative values are set to zero).

Using random shear rather than constant shear does not greatly affect the statistics, but apparently does so more than for a single weapon. The worst difference is in winter, when an 8-percent decrease in the mean dose occurs with random shear. The season does not yield major differences in mean dose level;

Table 3. SEASONAL DOSE STATISTICS FOR DETROIT

Season	Shear Value	Mean Dose	Standard Deviation	Maximum Dose	Number of Times	
					< 10 ERDs	< 200 ERDs
Spring						
(V = 29.94 mph; Vσ = 0.89)	Constant	4,001	4,732	22,908	116	218
	Random	3,979	4,899	23,119	123	234
Summer						
(V = 17.25 mph; Vσ = 1.07)	Constant	3,931	4,233	22,790	180	159
	Random	3,872	4,051	21,155	70	154
Autumn						
(V = 32.2 mph; Vσ = 0.82)	Constant	3,827	4,704	23,091	123	240
	Random	3,935	4,825	23,137	131	225
Winter						
(V = 47.2 mph; Vσ = 0.66)	Constant	4,050	5,018	23,067	120	221
	Random	3,726	4,674	23,334	146	243
Autumn						
(V = 32.2 mph; Vσ = 0.1)	Constant	8,815	5,380	23,878	0	0

however, it must be recalled that in this location the ratio of standard deviation to mean wind does not vary too greatly. The summer gives the greatest variation in low numbers of doses--which is probably due more to the change in mean wind-speed than in the increase in the ratio of random to mean wind-speed. To illustrate a case with considerably different statistics, the bottom entry is for a case where the wind variability is very low. Here significant effects are seen. There are no doses under 200 ERDs; in fact, the minimum dose was between 2,200 and 2,400 ERDs. As shown in Figure 78, a significant number of target areas to the west of Detroit necessitate an appreciable change in wind direction to yield low dose levels. The 0.1 variability simply makes such changes quite improbable. The effects of wind variability will change with different target

areas--due to the nature of the attack surrounding these target areas. Thus, the nature of the results for this target area and this attack will not be the same for all others (as is illustrated later in this chapter).

This attack was used as a test for the statistical variability of the Monte Carlo calculations. Twelve runs with sample size 100 and stratified samples were made, along with 11 runs with the same sample size but with nonstratified sampling. The attack was the same with autumn winds and constant shear. A summary of the sample statistics is given in Table 4. Using all doses gives a mean value of 3,820 ERDs for the stratified sample and 3,961 ERDs for the nonstratified sample. The standard deviation of the distribution of mean values for the set of sample runs are 273 ERDs for the stratified sample and 414 ERDs for the nonstratified sample. The ratio of 1.5 is a measure of the improvement in estimating the mean to be expected from the stratified sampling. The difference between the two averages of mean values is 141 ERDs, which is well within the differences that might be expected from chance occurrence. In fact, Table 3 shows a mean of 3,827 ERDs for a nonstratified run of 1,000 trials. Thus, no evidence of bias in the mean value due to the stratified sampling is seen from these few calculations.

If the basic distribution is normal, the distribution of sample means has a Student-t distribution. For the number of samples used here, this distribution is approximately normal, with standard deviation $s/\sqrt{n}$ (where s is the sample standard deviation and n is the sample size). For the nonstratified sample, this value is 4,847 ERDs/$\sqrt{100}$ (or 485 ERDs). Though the underlying distribution is far from normal, this predicted standard deviation is close to the observed value (or 414 ERDs). Excluding doses under 10 ERDs gives similar statistics, although the improvement from stratified sampling is not as dramatic. The variability of the number of samples under 10 ERDs is reduced--but by about the same ratios as before.

Table 4. STATISTICAL VARIABILITY TEST FOR DETROIT

All Doses	Stratified Sample	Nonstratified Sample
Mean dose	3,820	3,961
Standard deviation of mean dose	273	414
Average standard deviation of distribution	4,570	4,847
Range of mean	3,428 - 4,344	3,808 - 5,234
Doses Over 10 ERDs		
Mean number under 10 ERDs	12.25	11.27
Standard deviation of mean number	2.5	3.2
Mean dose	4,359	4,470
Standard deviation of mean dose	375	463
Average standard deviation of distribution	4,639	4,925
Range of mean	3,505 - 4,778	3,978 - 5,308

Two distributions with high and low values of mean (4,778 ERDs and 3,674 ERDs) were arbitrarily selected and are shown in Figure 81, which gives the number of occurrences in 1,000-ERD intervals. These runs are identical except for the random fluctuations due to the Monte Carlo process. The difference in the means can be explained by the doses over 15,000 ERDs. The high mean sample had 10 occurrences over this level, while the low mean sample had 2 occurrences; and this difference alone is sufficient to explain the differences in means (i.e., in the high case there occurred a larger number of relatively improbable situations where the wind was such as to carry high amounts of radiation from some important target area to the monitor point than occurred in the low case--which suggests the desirability of comparing all doses in the high range for the two cases). For stratified samples from a value of 15,848 ERDs to the maximum dose, the mean number of occurrences is 4.33, with standard deviations of number of occurrences = 1.55; for

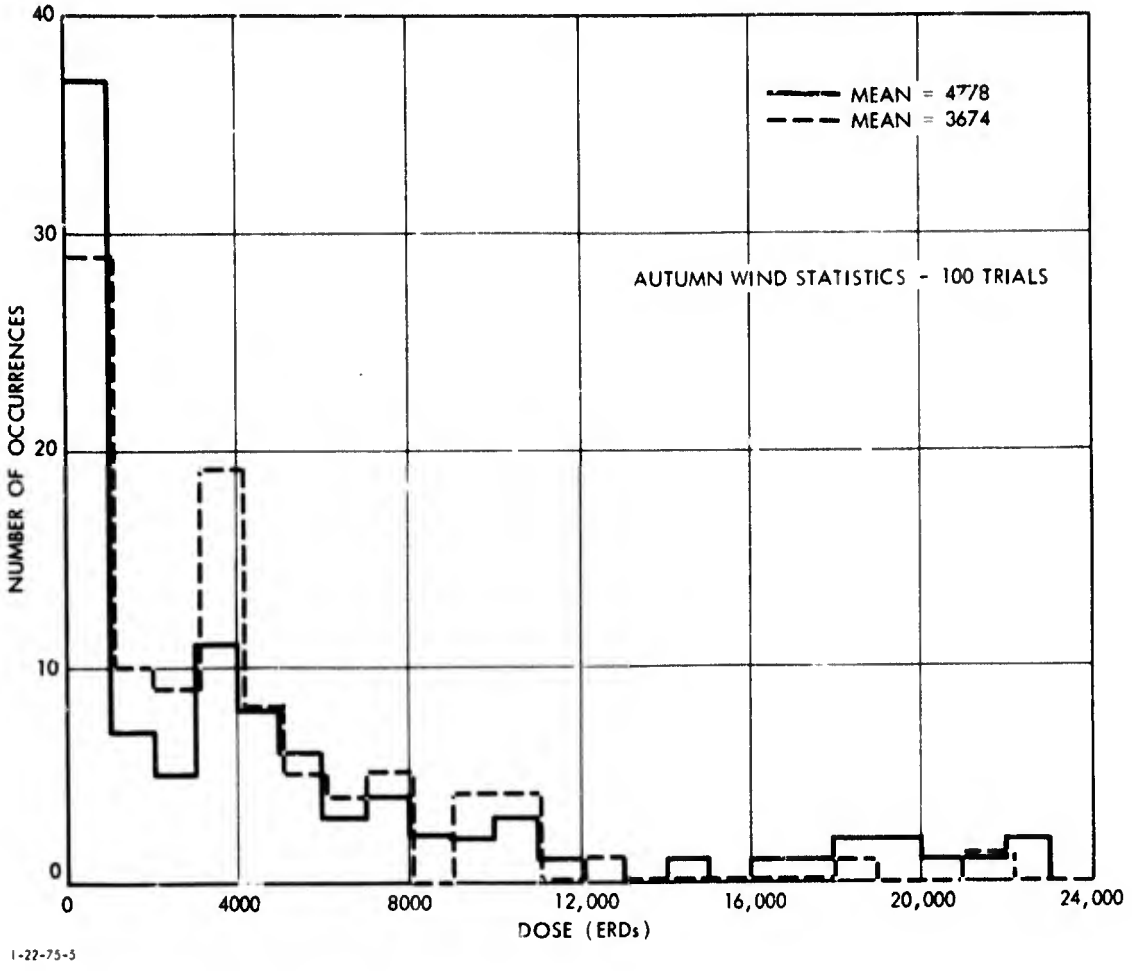

Figure 81. HISTOGRAM OF TWO DISTRIBUTIONS OF NONSTRATIFIED SAMPLES (FOR DETROIT)

nonstratified samples the mean is 5, with standard deviation 2.49. The ratio of standard deviations is 1.6--suggesting higher variability in this range of doses than at lower dose levels.

B. DESCRIPTION OF SIMULATION FOR FALLOUT-RISK CALCULATIONS FROM WEAPON CLUSTERS

If large attacks are to be evaluated against many monitor points in nationwide evaluations, a direct application of the previous type of simulation (i.e., using each weapon individually) could lead to excessive computer running times for the

calculations. This time can be lessened by use of the weapon-cluster-prediction scheme described in Chapter II--for two reasons: (1) fewer evaluations of radiation dose due to the clustering need be considered, and (2) each evaluation is more rapid, because of the simpler form of the calculation scheme.

A computer program called "RUBATO" is based on use of weapon clusters. Data defining the weapon clusters are input. The east-west half-length of the weapon cluster is taken as two times the east-west standard deviation of the weapon yields in the cluster plus 5 miles. The north-south half-length of the cluster is taken as $\sqrt{2}$ times the north-south standard deviation of the weapon yields plus 5 miles. A set of monitor points is sequentially read and processed; in the current implementation, the monitor points are the centers of gravity of the rural population in each of the 3,134 counties in the United States. Summary statistics for each state and for the entire nation are collected, and a fallout-fatality calculation ignoring blast and using the same protection factor for each monitor point is currently implemented.

The simulation of wind statistics is the same as described earlier, except that the values of mean wind-direction, vector wind-speed, and vector standard deviation are taken to be those of the nearest to a set of monitoring wind stations--which allows representation to nationwide variations of wind statistics. Either stratified or nonstratified sampling of the winds can be selected. The results presented here will be for stratified sampling with a sample size of 100.

In order to save computational time, a rapid method of screening out weapon clusters contributing only negligible amounts of radiation is needed. In the present implementation, as each monitor point is processed, north-south and east-west distances from each weapon are computed. Then a sample wind is selected. A crosswind screening distance is calculated (which

is 250 miles for winds under 10 mph or for shear over 0.3 mph/kft; otherwise, it is 175 miles). For a cluster fission yield of 10 MT, this screening limit turns out to be about 2 ERDs. For the attack to be described later, the average cluster fission yield is about 2 MT, and the maximum fission yield is 200 MT.[1] Direction cosines for the wind sample are calculated to allow ready transformation to crosswind-downwind directions. As each weapon cluster is searched, the crosswind-distance check can be made by two multiplications and two additions in such a way that, with a minimum of computational effort, many clusters can be ignored. If the crosswind screening check is passed, an upwind screening is performed. A cluster is accepted if it is less than a minimum of 80 or of 2 times the east-west standard deviation of cluster plus 5 miles upwind. No downwind screening is used. If these tests are passed, the cluster fallout model is used except for wind of less than 5 mph where the approximation to the WSEG Model (see Chapter I, above) is used. Calculations have been made on the Control Data 3600 for 3,134 monitor points, with a nationwide attack combined into 450 clusters and a sample size of 100. Computing time was 8.5 hours.

Because of the nature of the screening processes used, the winds at the weapons were assumed to be the same as those at the targets. At the expense of some increase in computing time due to a somewhat more complex screening process, curved wind patterns could be introduced. A related question is the correlation in wind patterns to be used between adjacent monitor points. The present implementation allows for either no correlation in winds between monitor points (except for that inherent in the stratified sampling procedure) or correlation by using the same

[1]With this attack, these screening limits seem to be larger than necessary; probably about one-half the screening distances could be used. Care must be used in selecting such screening distances, since too small a distance would result in a downward bias in dose statistics and too large a distance unnecessarily increases computing time.

string of random numbers at each monitor point to select the sample winds. The latter option has been used for the calculations exhibited here. Although, in fact, the winds at nearby monitor points are usually rather highly correlated on individual days, it seems that such correlations are not important for the types of results presented here (i.e., mean values and percentile values, which by their natures do not present these correlations).[1] Moreover, outside of presenting fallout patterns for each of a number of specific winds (which might be the best procedure), no good method of presenting a massive amount of properly correlated results is immediately apparent.

C. COMPARISON OF RESULTS, CLUSTERED AND UNCLUSTERED MODELS

Calculations were performed to see how well statistical results from the weapon-cluster simulations compared with the direct WSEG-10 Model. St. Louis was used as a monitor point, with spring wind statistics giving a mean wind-speed of 31 mph, a mean wind-direction of 271° clockwise from the North, and a vector standard deviation of 0.181 of the mean wind-speed. A shear of 0.2 mph/kft is used. The attack is assumed to be 75 MT of fission yield on the 150 Minuteman silos at Whiteman AFB in western Missouri, which could come from a 1-MT weapon upon each launching silo. The attack is assumed to be either concentrated at one point or spread into 15 points--each of the points corresponding roughly to the population centers of the counties over which the Minuteman silos are spread. The locations of these points are shown in Figure 82. The results of the calculations are given in Table 5. The LASH program does the calculations with the regular WSEG model; the RUBATO program, with the weapon-cluster model. The attacks with a single aim point consist of one weapon at the center of gravity of the cluster,

[1]In some types of fallout-protection measures, the activities carried out at one monitor point would depend upon the doses received at all monitoring points in the neighborhood.

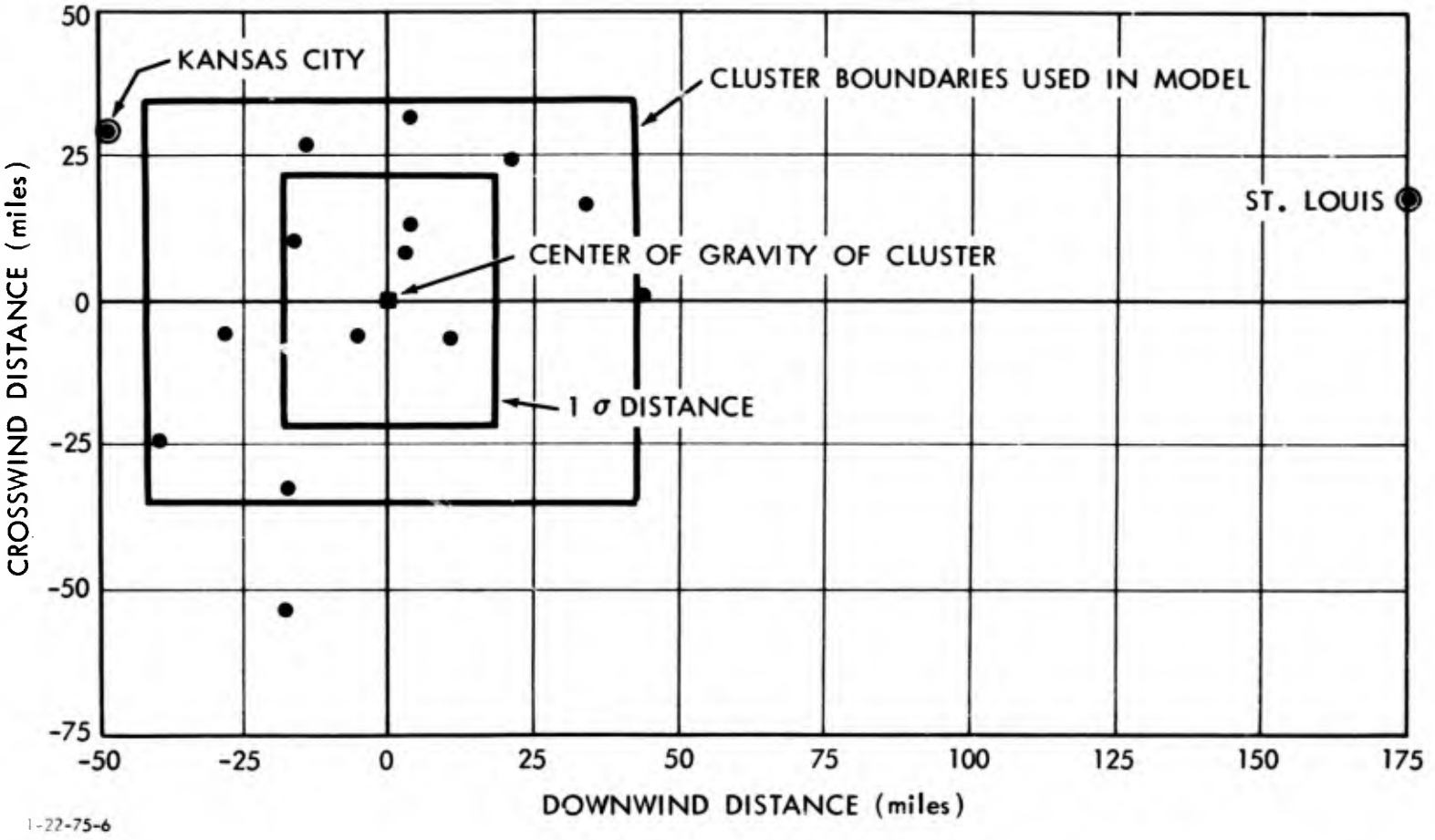

Figure 82. MAP OF ASSUMED WEAPON LOCATIONS FOR ATTACK ON WHITEMAN AFB

Table 5. COMPARISON OF TWO SIMULATION MODELS ON ST. LOUIS

Line Number	Model	Attack	Number of Aim Points	Weapon Yield (MT)	Cluster Standard Deviation (miles)	Mean Dose (ERDs)	Standard Deviation (ERDs)	Maximum Dose (ERDs)	Fraction of Time		Median Dose (ERDs)	90th-Percentile Dose (ERDs)
									< 10 ERDs	< 1,000 ERDs		
1	LASH	Whiteman	1	2	--	2,573	8,512	52,918	0.79	0.85	<1	5,700
2			15	2	--	2,561	5,043	18,959	0.62	0.71	<1	12,300
3			15	20	--	2,320	4,200	14,757	0.56	0.69	<1	10,500
4	RUBATO		1	2	20	2,301	3,241	8,306	0.54	0.64	<1	7,780
5			1	2	0	2,092	6,265	32,679	0.77	0.83	<1	4,080
6			1	20	20	2,088	2,821	7,649	0.52	0.60	2	6,790
7			15	2	0	2,084	4,103	15,021	0.56	0.69	<1	9,820
8			15	2	11	1,806	4,678	27,773	0.16	0.58	190	8,100
9		Nationwide	--	--	--	9,830	8,189	83,097	0.00	0.00	9,030	13,370
10		Nationwide w/o St. Louis	--	--	--	2,975	3,056	9,151	0.00	0.48	1,350	7,390
11		Nationwide w/o St. Louis or Whiteman	--	--	--	1,081	898	5,809	0.00	0.57	860	2,180

with 15 of the attack aim points having a weapon at each of the points shown. The fission fractions are determined so that the total fission yield is always 75 MT. The other parameters are the same except that a constant shear of 0.2 mph/kft is used with the LASH model, and a normally distributed shear with mean 0.2 mph/kft and standard deviation 0.04 mph/kft is used in the RUBATO model. For the LASH model, the best representation of the actual situation appears in line 2, where 2-MT weapons (each with a fission fraction of 10) are spread over 15 aim points. Each weapon is intended to represent a group of 20 2-MT weapons, each with a fission fraction of 0.5, exploded in promixity to each other. The standard use of the RUBATO model would have a single cluster with a standard deviation of 20 miles (as shown in line 4). (The actual standard deviation of the cluster and the area on the ground assumed occupied by the cluster are shown in Figure 82.) A comparison of lines 2 and 4 gives the agreement of the two models. As can be seen, the RUBATO model gives a smaller mean dose and a smaller 90-percentile dose. On the other hand, the LASH model has a higher number of doses under 10 ERDs.

The other lines indicate variations from the basic case. Line 1 shows all weapons clustered at a point. Here the mean dose is not significantly affected, but the shape of the distribution is; for example, the 90th-percentile dose is halved. Lines 3 and 6 compare the models for 20-MT weapon yields. Line 5 shows the results of setting the standard deviation of the cluster to zero, and lines 7 and 8 show the results with the assumption of a cluster centered on each of the counties.

Finally, for comparison, line 9 shows results from the nationwide attack; line 10, results for this attack minus the St. Louis weapon cluster; and line 11, this attack minus the St. Louis and Whiteman weapon clusters. As is evident from the table, the St. Louis weapon cluster itself is a major contributor to the dose. On line 10, it is seen that just removing the

St. Louis cluster yields only about 25-percent higher mean value than from the Whiteman-only attack. Removing the Whiteman cluster as well indicates the general background from other attack sources (i.e., a more uniform distribution).

D. SELECTED RESULTS FROM A NATIONWIDE ATTACK

The hypothesized attack used in the sample calculations in this study is an unclassified attack developed by the Defense Civil Preparedness Agency for a study of evacuation requirements. The attack consisted of some 1,660 weapons with yields ranging from 1 to 20 MT. The total attack yield was 6,600 MT. This attack included a mixture of counterforce and countervalue objectives. It was developed so that each of the urbanized areas of the United States was attacked with at least one weapon. The attack upon missile sites was simplified by assuming that one 20-MT weapon was used against a group of about 15 missile silos, instead of a weapon targeted against each silo. All the Minuteman and Titan II missile silos were targeted. For the purposes of these calculations, a weapon reliability of 1, a fission fraction of ½, and a zero height of burst were assumed for all weapons. Spring wind statistics are used for this calculation, with the wind shear taken as a normal distribution, mean shear = 0.2 mph/kft, and standard deviation = 0.04 mph/kft.

The areas covered by 2 psi or more from each weapon were determined (assuming for the blast-wave calculation that the weapons were air-burst at a height to maximize the ground covered by overpressures of at least 10 psi). Weapons close enough so that the 2-psi contours touched were grouped into clusters. Where a cluster covered more than one urbanized area or both military and urbanized-area targets, the clusters were divided into subclusters. A total of about 450 clusters was obtained, of which 247 were over urbanized areas. A map showing the areas covered by 2 psi or more is shown in Figure 83. This

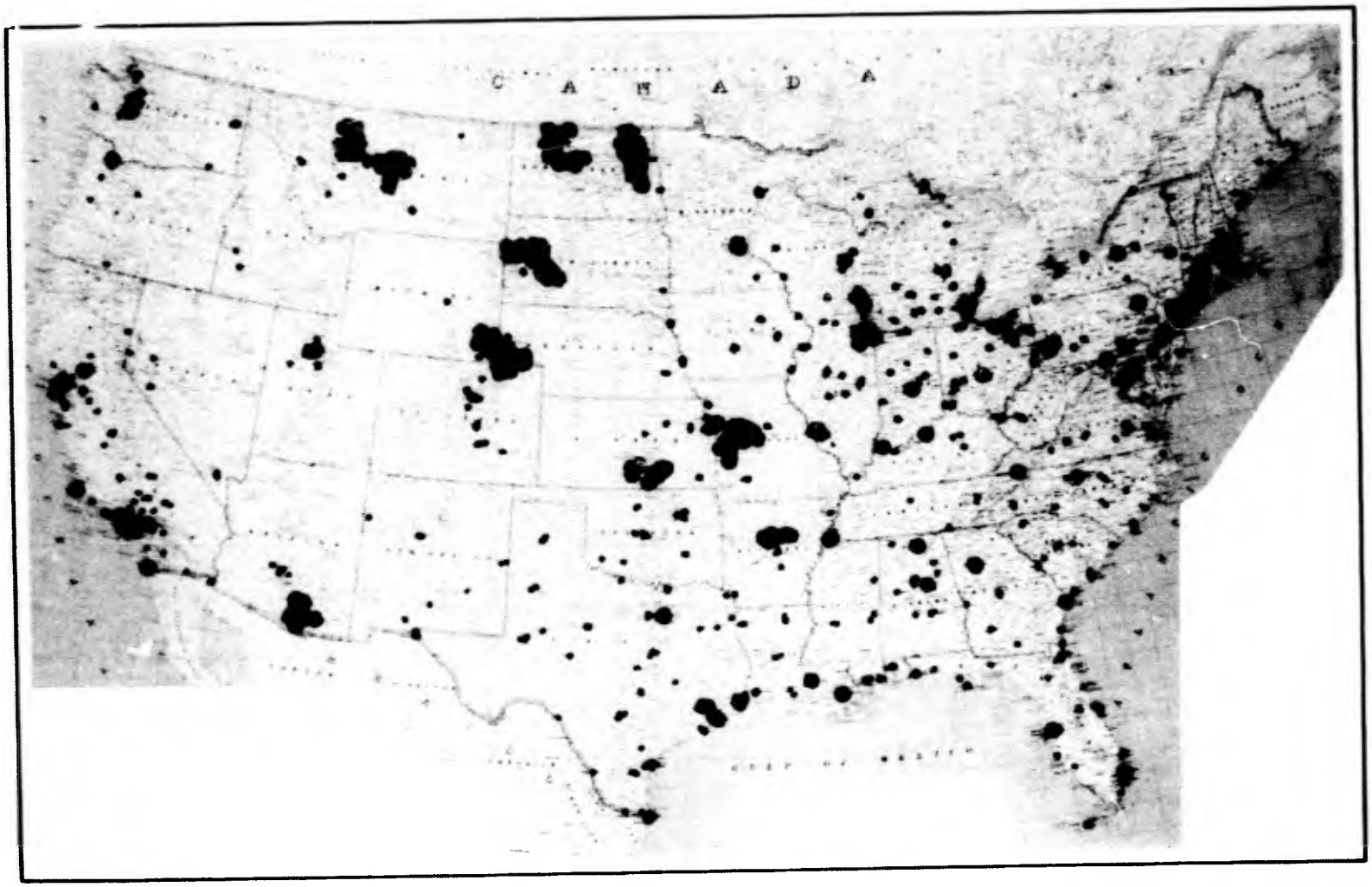

Figure 83. MAP OF AREAS COVERED BY MORE THAN 2-PSI OVERPRESSURE AS A RESULT OF NATIONWIDE ATTACK

map represents a slightly different attack, where the locations of some 10 to 20 weapons are changed.

In Figure 84, the weapon clusters in and near the State of Michigan are shown. As can be seen, this attack is similar to the hypothetical attack near Detroit (discussed earlier in this chapter). Two calculations of 1,000 trials were performed both with and without the Detroit weapon cluster in the attack. The Detroit weapon cluster is located 2.8 miles south and 2.4 miles west of the center of population for Wayne County, Michigan, which was used as the Detroit monitor point. The following table presents a summary of the dose statistics:

Attack Type	Mean Dose (ERDs)	Standard Deviation (ERDs)	Maximum Dose (ERDs)	Number of Times < 10 ERDs	Number of Times < 200 ERDs
With Detroit Cluster	11,933	17,776	243,351	0	0
Without Detroit Cluster	2,754	1,903	13,749	1	20

Though this calculation without the Detroit cluster gives somewhat lower mean values than the previous calculation, it has fewer occurrences with small doses. With the Detroit cluster, the dose from the cluster dominates the new dose values. The distribution of doses is shown on a logarithmic scale in Figure 85 and on a linear scale in Figure 86. Compared to the earlier distribution, the nonclustered distribution shows a smaller number of low doses and a double peak. Repeating the nonclustered calculation with 100 and 10,000 trials enabled estimation of the fluctuation (in the histogram) due to random effects. The mean deviation of a sample from the true mean was estimated as $0.12(\text{number of trials})^{\frac{1}{2}}$. For the 1,000 trials used here, this value is 3.8. Thus, the structure in the histogram between 4,000 and 7,000 ERDs, for example, could be explained by random fluctuations; in the 10,000-trial histogram this section is, in fact, almost flat (at a value of about 26). The addition of the Detroit weapon cluster separates the distributions almost

Figure 84. MAP OF WEAPON CLUSTERS IN MICHIGAN

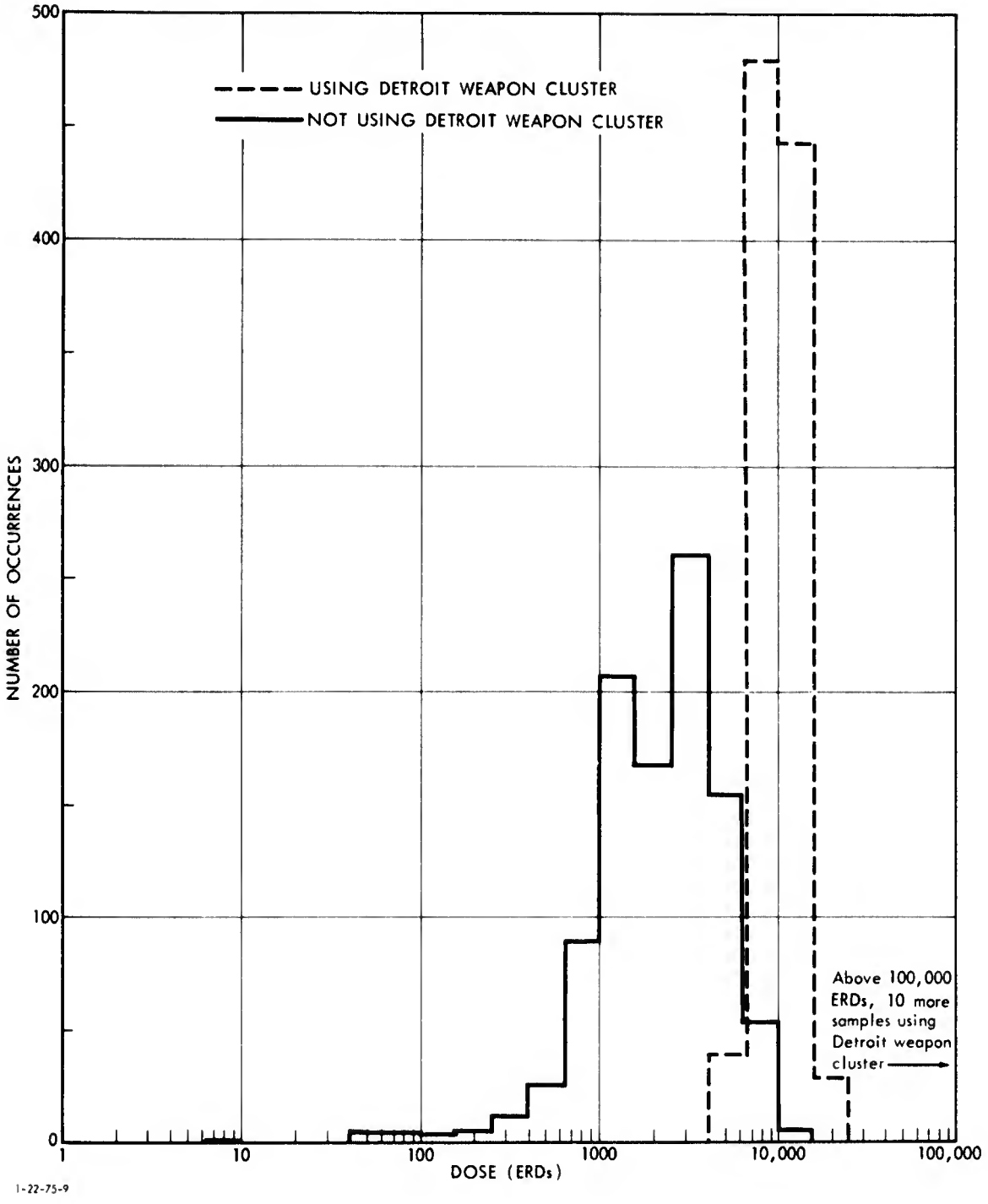

Figure 85. HISTOGRAM OF DOSES ON DETROIT AS A RESULT OF NATIONWIDE ATTACK, WITH LOGARITHMIC INTERVALS

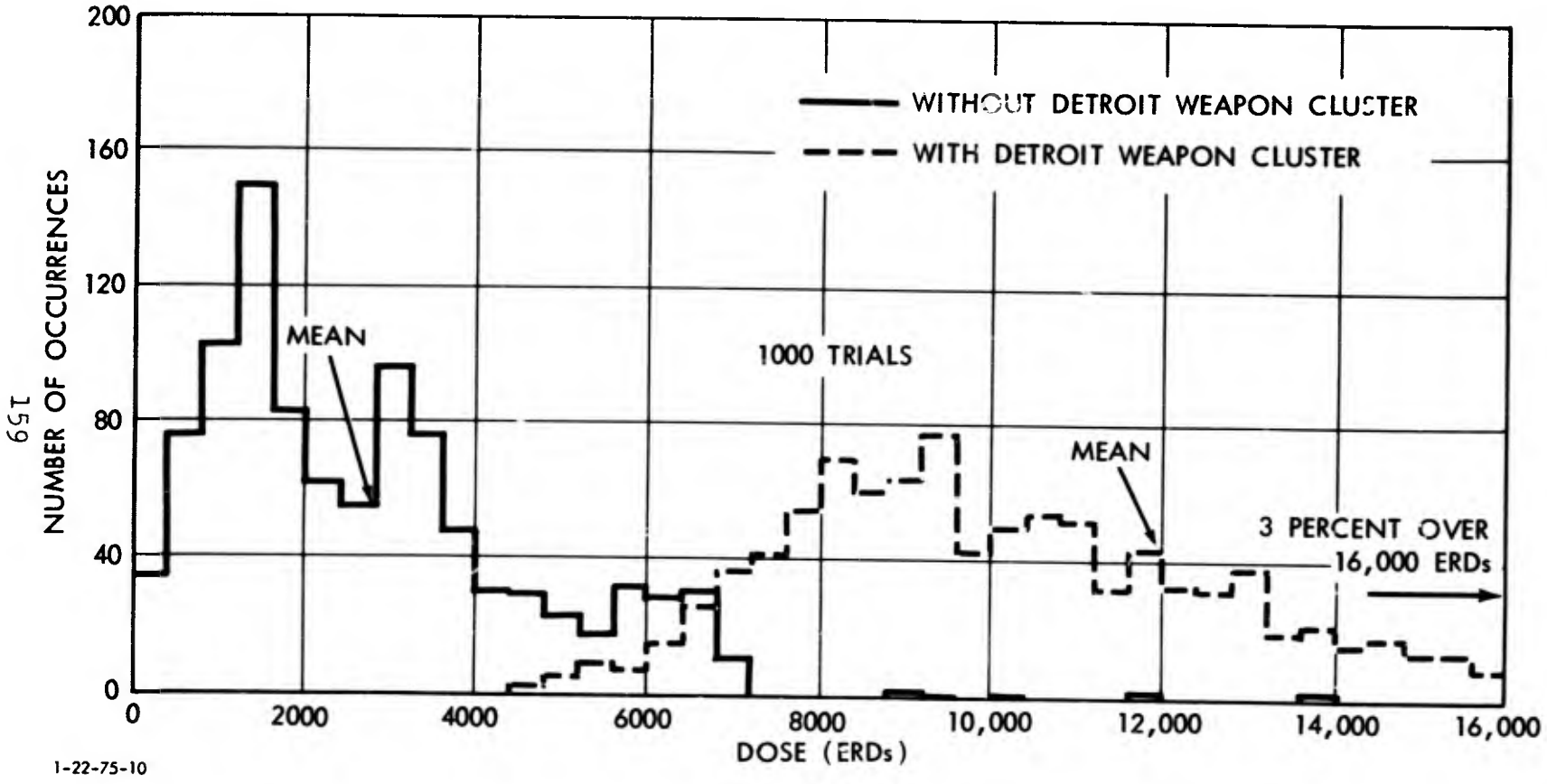

Figure 86. HISTOGRAM OF DOSES ON DETROIT AS A RESULT OF NATIONWIDE ATTACK, WITH EQUAL INTERVALS

completely. The spread in distribution with the cluster is due more to changes in wind speed (since the monitor point is near the cluster center) than in wind direction, as has been usually encountered. It should be clear that the values obtained are strongly dependent upon the location of the monitor point within the cluster, since the dose from the cluster weapons rises more or less linearly from zero at the upwind edge to a maximum at the downwind edge of the cluster. A more detailed representation than a single monitor point is thus needed for each area that contains a weapon cluster as a prerequisite for a reasonably accurate application of fallout- and blast-fatality calculation models.[1]

In order to depict the distribution of dose over an area, the doses were separated into a set of classes as follows:

Class Name	Dose Range (ERDs)	Adjusted Dose Range (ERDs)
A	0 - 1,000	0 - 250
B	1,000 - 2,000	250 - 500
C	2,000 - 4,000	500 - 1,000
D	4,000 - 10,000	1,000 - 2,500
E	10,000 - 30,000	2,500 - 7,500
F	30,000 - ∞	7,500 - ∞

Various factors that have not been considered in this study would tend to degrade the actual doses received, even if an enemy attempted to surface-burst weapons.[2] Such factors would include terrain shielding, weathering of fallout particles, influence of trees and buildings to give small (but not zero) heights of burst, and various factors to make moderate shelter better than nominal values. The influence of all such factors

---

[1]Such calculations on an urbanized area should be combined with blast-fatality calculations. To the author's knowledge, a combined model that is both reasonably fast and reasonably accurate remains to be developed.

[2]It should be clear that an enemy might choose to detonate weapons at an altitude high enough to give no significant fallout; in fact, such an altitude would maximize the area covered by moderate blast-wave pressure. When fallout effects are estimated, all weapons so used should be eliminated from the assumed attack.

is extremely difficult to assess; but, if an estimate is necessary, a factor of 4 might be used to adjust doses to account for such effects. Moreover, a rough categorization of biological effects might be as follows: less than 50 ERDs causes no clinical effects; 200 ERDs gives a 50-percent sickness level; 450 ERDs gives a 50-percent fatality level. The same six classes with adjusted dose ranges might be interpreted as follows:

A - sublethal doses (but without shelter), extended periods of sickness possible at upper end;

B - home fallout-shelter protection necessary to avoid sickness;

C - home fallout shelter necessary to avoid fatalities, basement shelter to avoid sickness;

D - basement shelter or National Fallout Shelter Survey PF-40 (or better) shelter desirable;

E - PF-40 (or better) spaces necessary to prevent sickness;

F - PF-40 (or better) spaces required.

The reader may, of course, wish to place his own qualitative interpretation on these ranges.

Figure 87 shows the distribution of fallout risk throughout southeastern Michigan. The center of population of each county is used as a monitor point. For each monitor point, a small bar chart showing the fraction of times doses were within each of the specified ranges is given. For example, darkening the B-level dose up 1.5 squares shows that 30 percent of the time the dose was calculated in level B (i.e., between 1,000 and 2,000 ERDs). In the northern portion of the region, for a higher portion of the time, there is little risk; and risk-level C or greater is infrequent. Near Detroit, on the other hand, little or no chance of low fallout levels is found--with a significant chance of relatively high levels.

As can be readily seen in Figure 83, a region of intense weapon usage runs from Washington, D.C., up to Boston. The

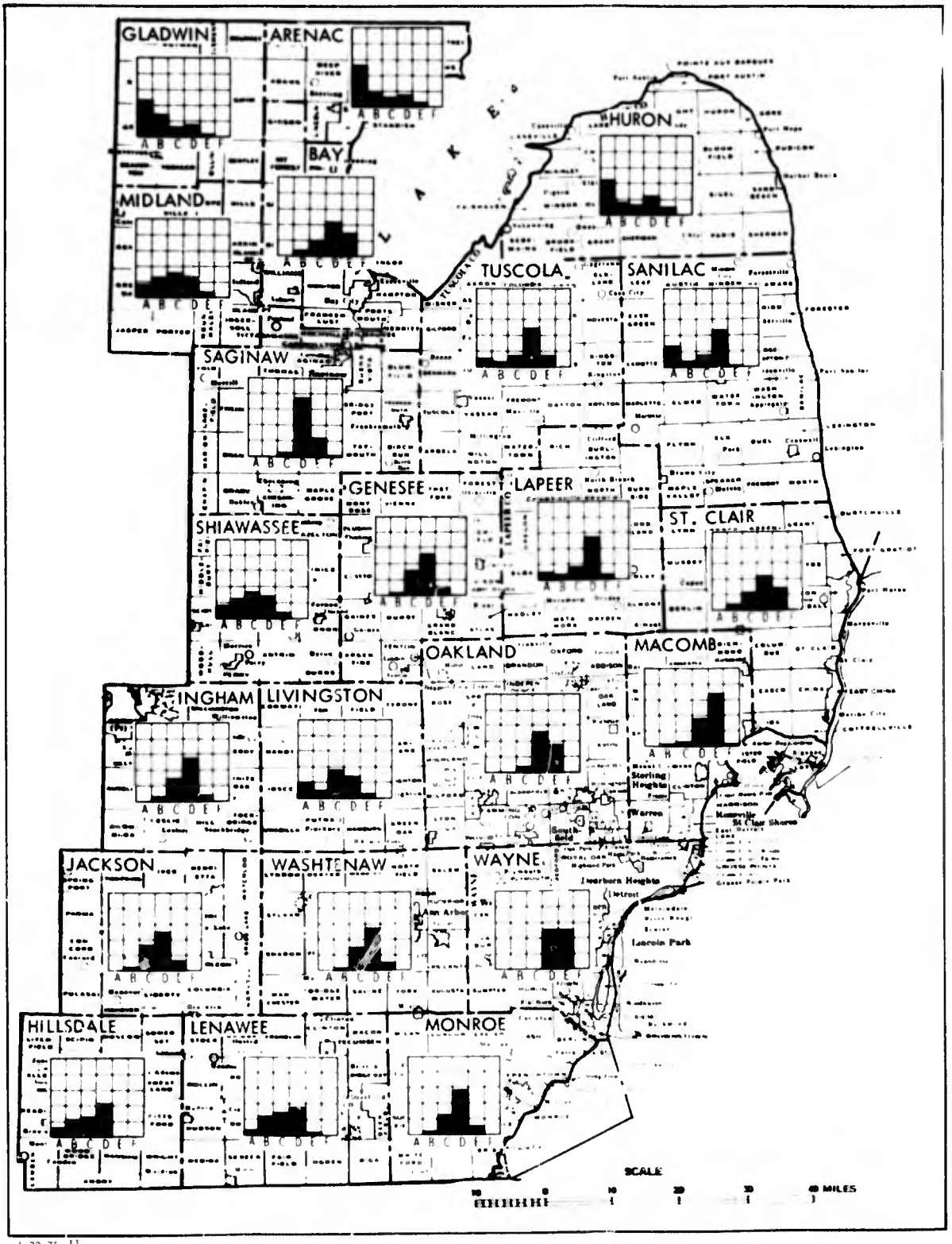

1-22-75-11

Figure 87. FALLOUT RISK IN SOUTHERN MICHIGAN AS A RESULT OF NATIONWIDE ATTACK

dose depositions for three coastal states that have relatively few counties are shown in Figures 88 (Connecticut), 89 (Delaware), and 90 (New Jersey). Many of the monitor points for these states are near (or covered by) a weapon cluster, so that the dose levels are varying considerably in proximity to the monitor point, and the dose statistics shown could change appreciably within a few miles. Nevertheless, the overall high-risk level from the large number of weapons nearby is evident. In southern New Jersey and in Delaware, the chance of level F is small if not nil; but, elsewhere, a significant chance of such dose levels is evident. In contrast to the previous situation, fallout risks for Arizona and Nevada are shown in Figures 91 and 92, where a few monitor points are in or near clusters and where they are frequent at these relatively high dose levels. Elsewhere, most of the time the dose level is low. The concentrations of weapons around Los Angeles and San Francisco can contribute large doses over long distances, yielding some chance of higher dose levels in the states shown when the wind happens to be such that a monitor point is downwind from these large clusters.

The fallout risk on a sample set of counties in the northeastern United States is presented in Figure 93. Each bar chart is centered over a county chosen as a monitor point. In order to illustrate the general risk-level in the area, most of the monitor points were chosen so as to be away from weapon clusters. A comparison of these figures with Figure 83 (above) indicates the general weapon-cluster density in the area. The variability of the shapes of the distributions exhibited in this figure illustrates the need for some quantity other than average dose as a measure of risk. An alternative more commensurate with these varying distribution shapes is either the dose at one of several percentile safety-levels (e.g., there is a 90-percent chance of the dose being less than x ERDs) or the chance of exceeding one of several dose levels (e.g., the chance of the dose being over 2,000 ERDs is y percent).

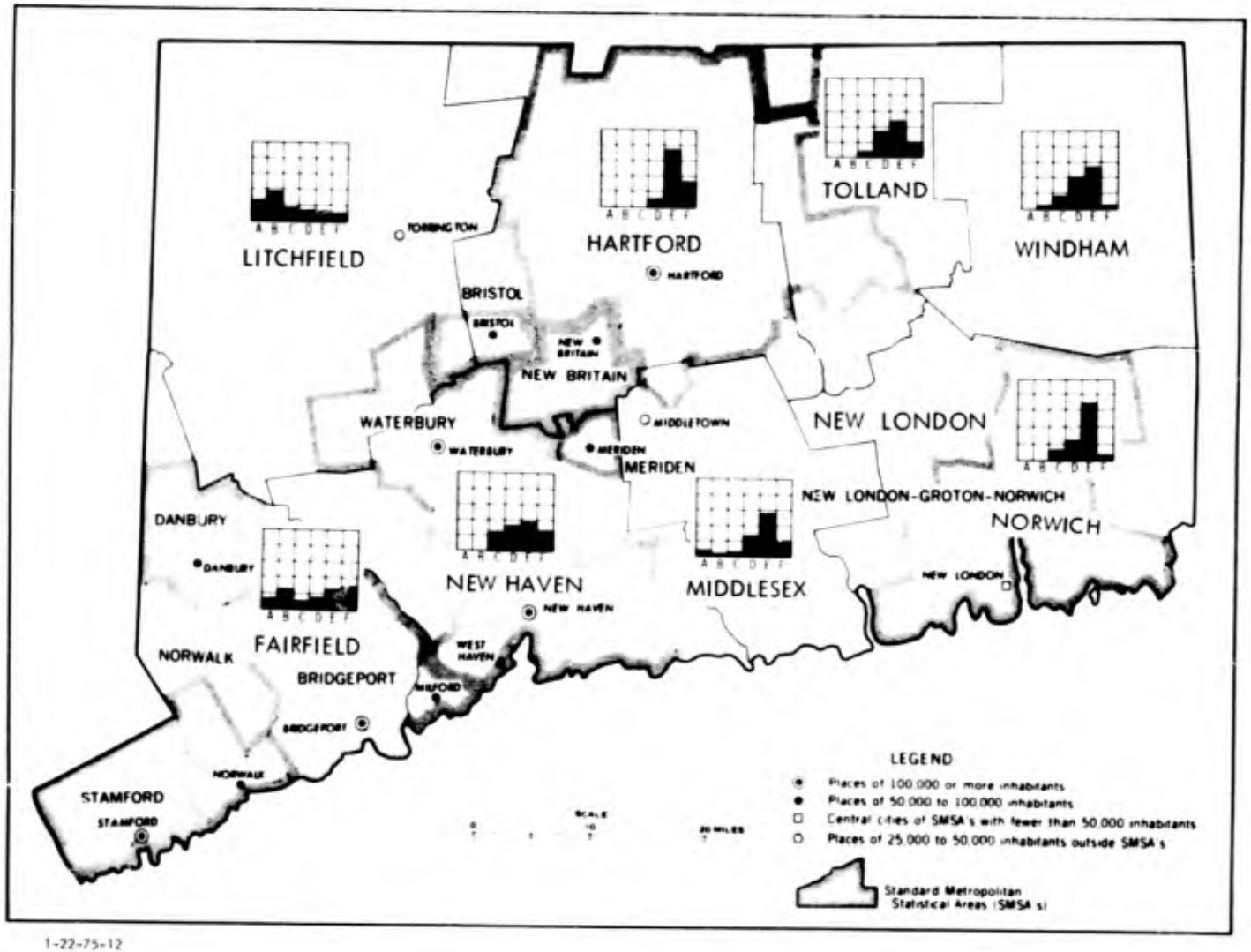

Figure 88. FALLOUT RISK IN CONNECTICUT AS A RESULT OF NATIONWIDE ATTACK

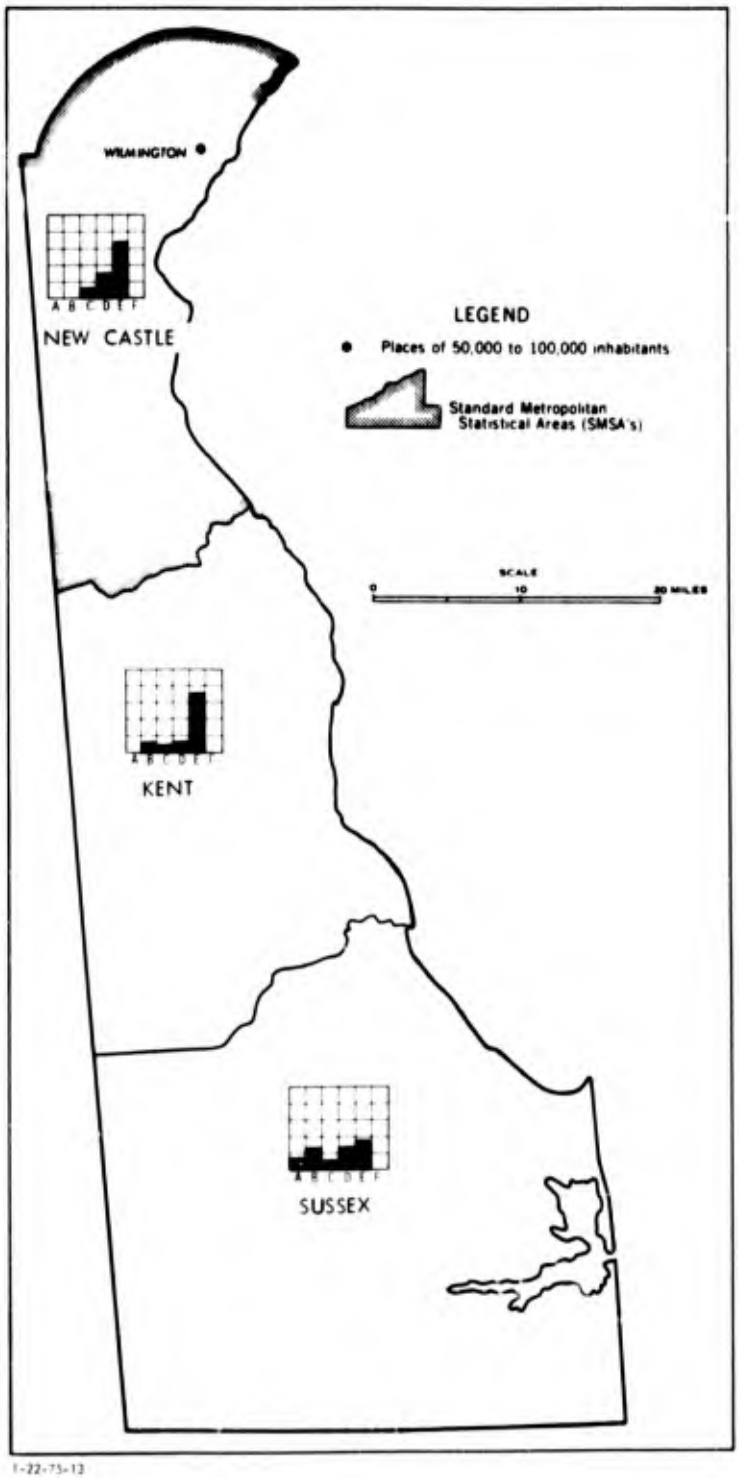

Figure 89. FALLOUT RISK IN DELAWARE AS A RESULT OF NATIONWIDE ATTACK

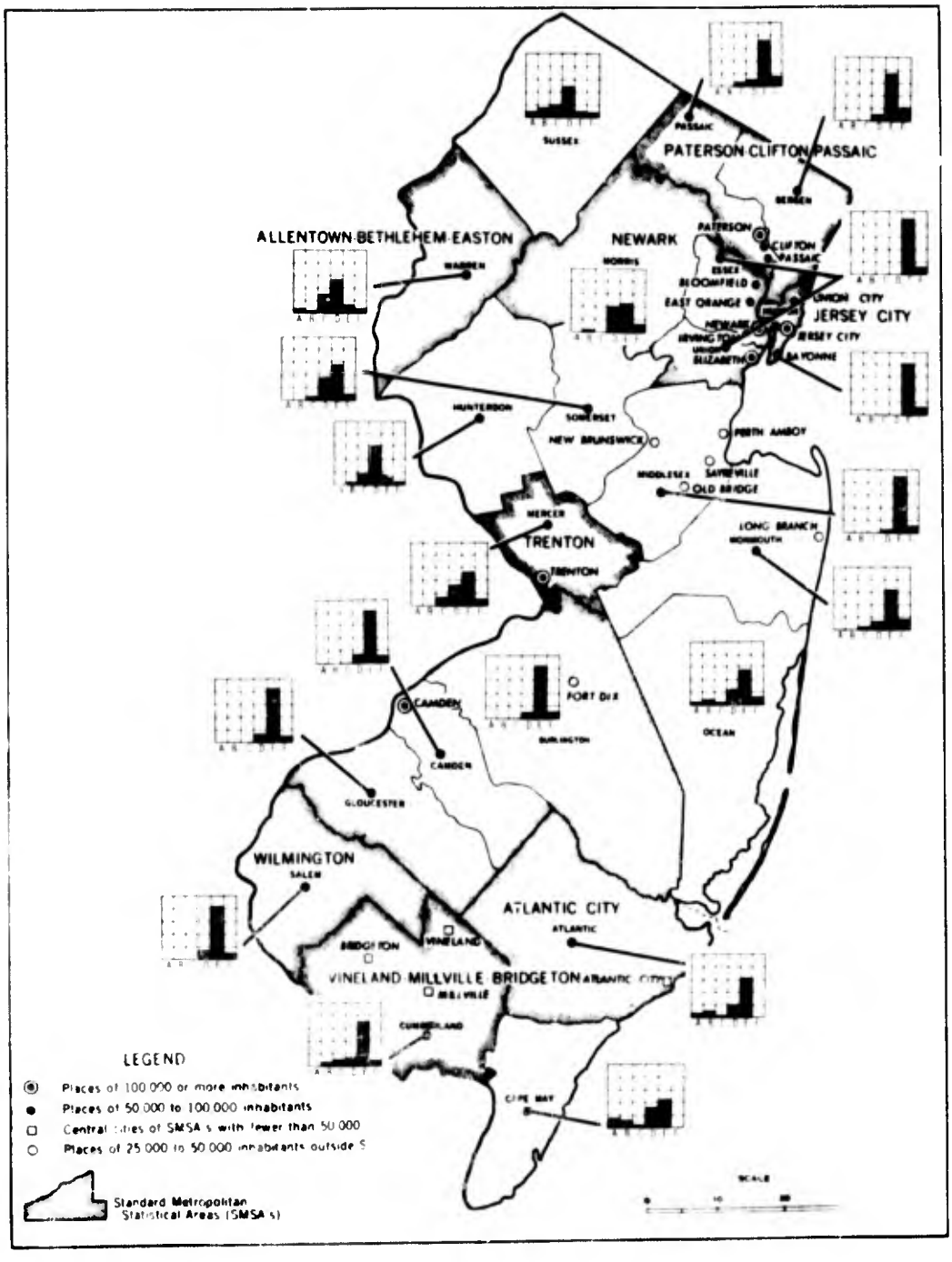

1-22-75-14

Figure 90. FALLOUT RISK IN NEW JERSEY AS A RESULT OF NATIONWIDE ATTACK

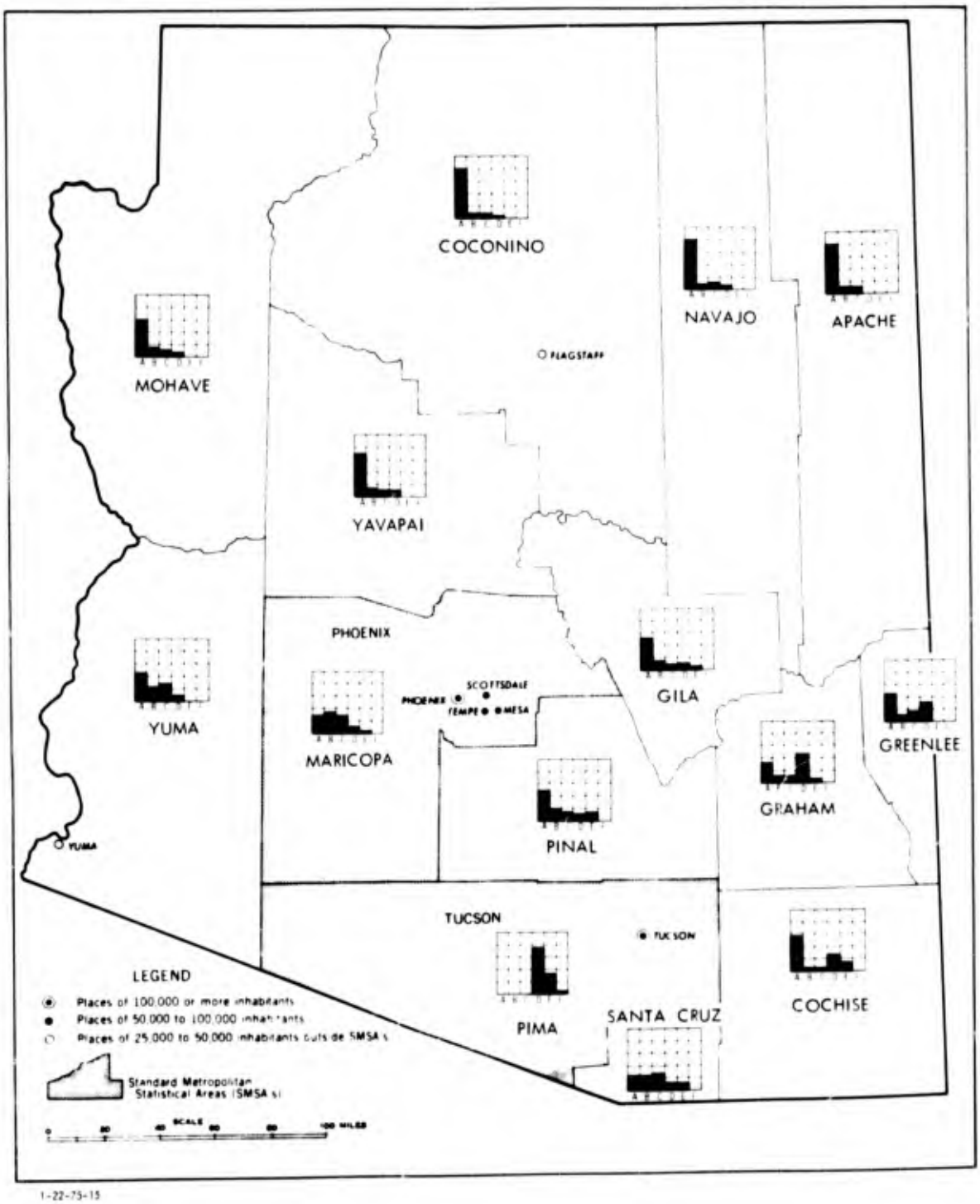

Figure 91. FALLOUT RISK IN ARIZONA AS A RESULT OF NATIONWIDE ATTACK

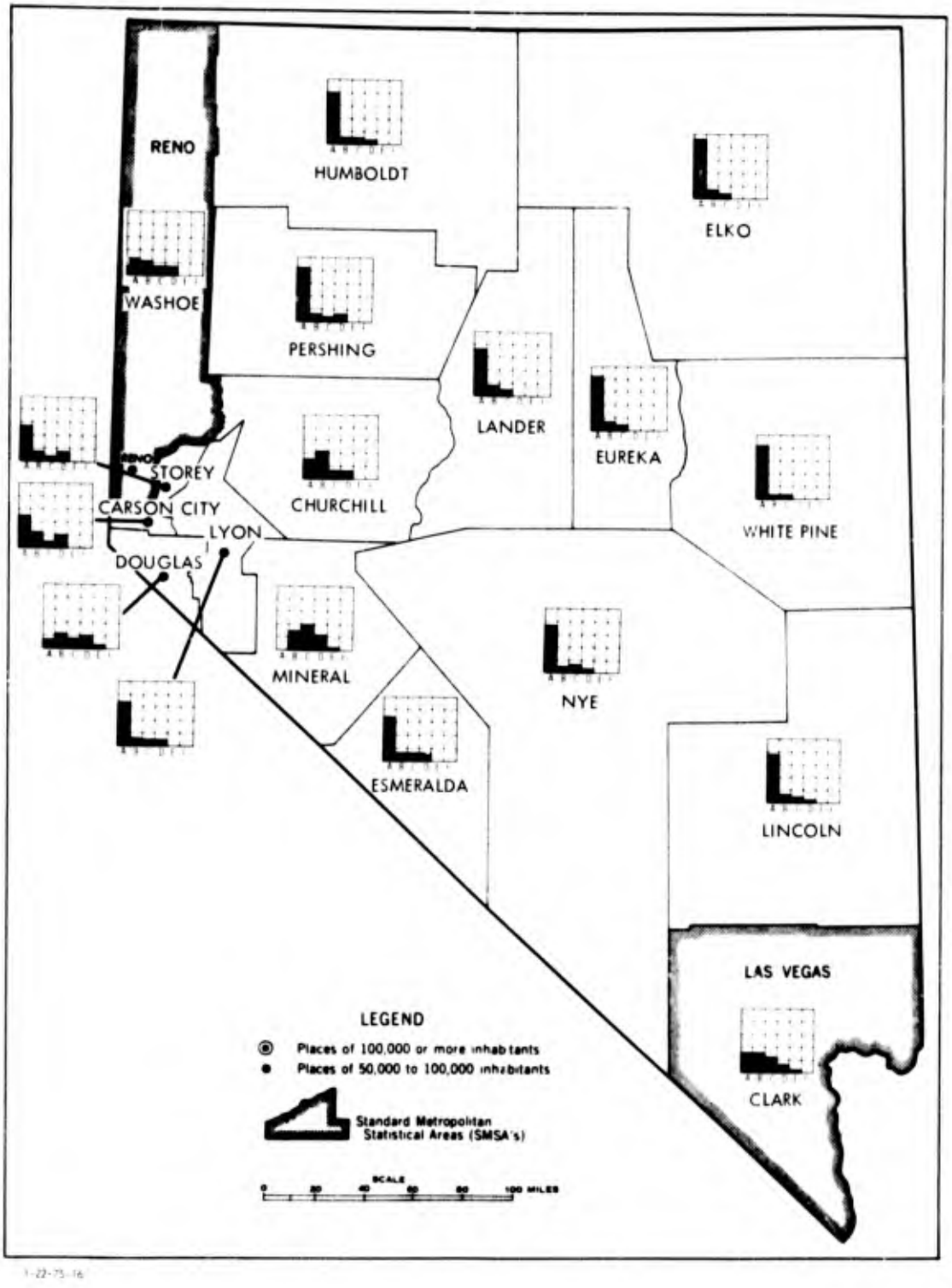

Figure 92. FALLOUT RISK IN NEVADA AS A RESULT OF NATIONWIDE ATTACK

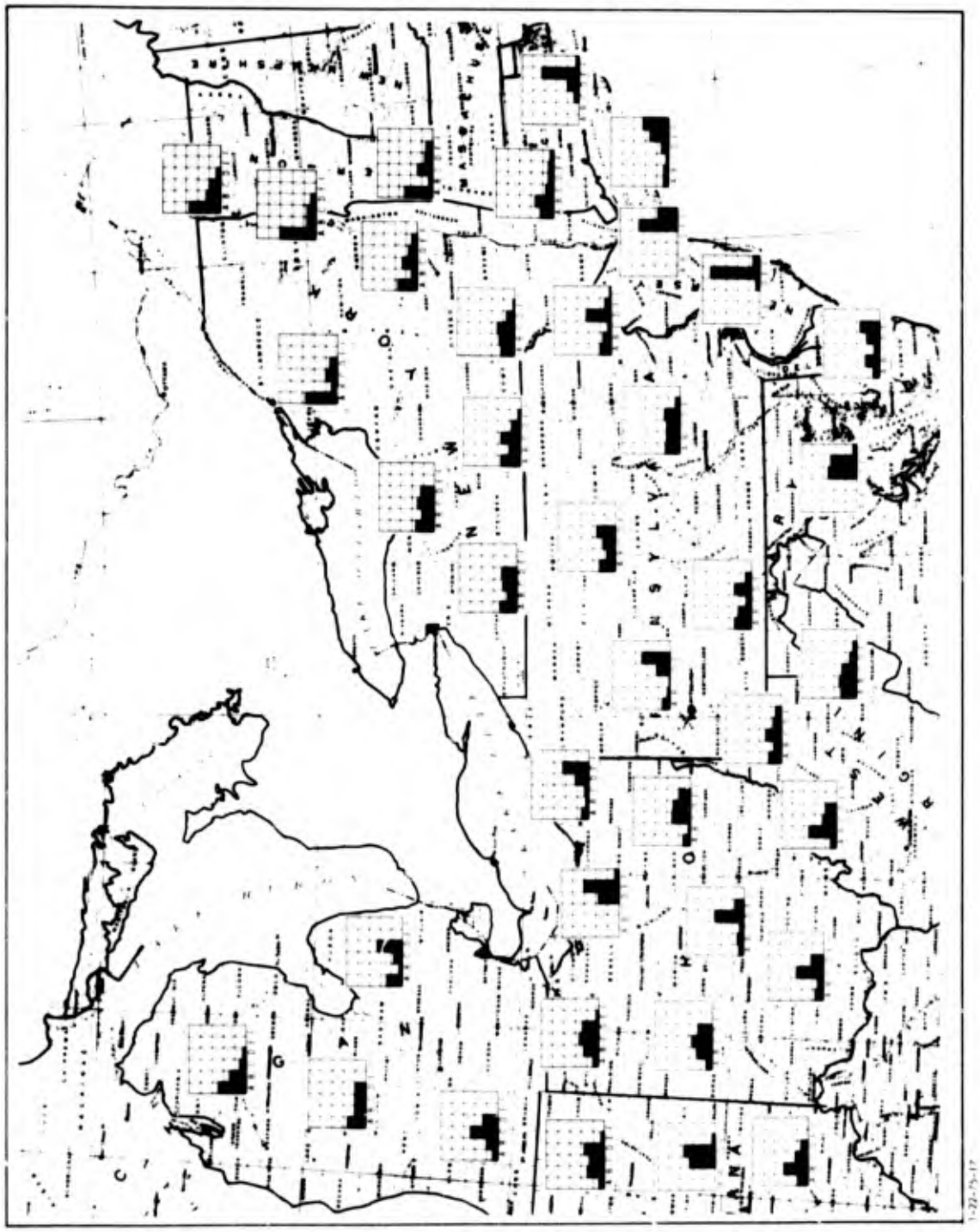

Figure 93. FALLOUT RISK AT SELECTED PLACES IN NORTHEASTERN UNITED STATED AS A RESULT OF NATIONWIDE ATTACK

The State of Colorado was used to illustrate an area with several isolated weapon clusters. The total yield in each of the weapon clusters in Colorado is illustrated in Figure 94. Bar charts for each of the counties in Colorado are presented in Figure 95. For most of the counties in western Colorado, there is a very good chance of their being at level A. The tails on these distributions show some chance of the wind carrying fallout either from small nearby clusters or from larger weapon clusters further upwind. Over the State, the mean wind-direction is almost due west-to-east; and the mean wind-velocity and vector standard deviation are both about 25 mph. Over all of the State, some chance of level-C-or-above fallout is possible; but, as can be seen, there is often less than a 10-percent chance of such fallout levels. The influence of the weapons near the center of the State (and from the missile fields in the north-eastern corner) can be readily seen from the statistics.

In Figure 96, the likelihood of a less-than-200-ERD dose is shown for each county monitor point in Colorado. As is clear from this figure (although there is a very high chance of doses being less than 1,000 ERDs), the 200-ERD level is small enough that the maximum chance of being less than this level is 60 percent. As the areas outlined by dashes indicate, only in the western part of the State is there more than a 40-percent chance of such dose levels. This percentage occurs because at a dose level of 200 ERDs there is a fairly significant chance of the dose being exceeded--due to some fairly remote weapon cluster.

Some insight into the ratio rate for the results can be gained through a more detailed analysis of the source of the doses. The dose statistics for Chaffee County, Colorado, were collected in detail. This county is slightly southwest of the center of the State. The mean dose was 563 ERDs, the median was 338 ERDs, and there were seven times when total doses were over 1,000 ERDs. Table 6 shows the source of the major contributions

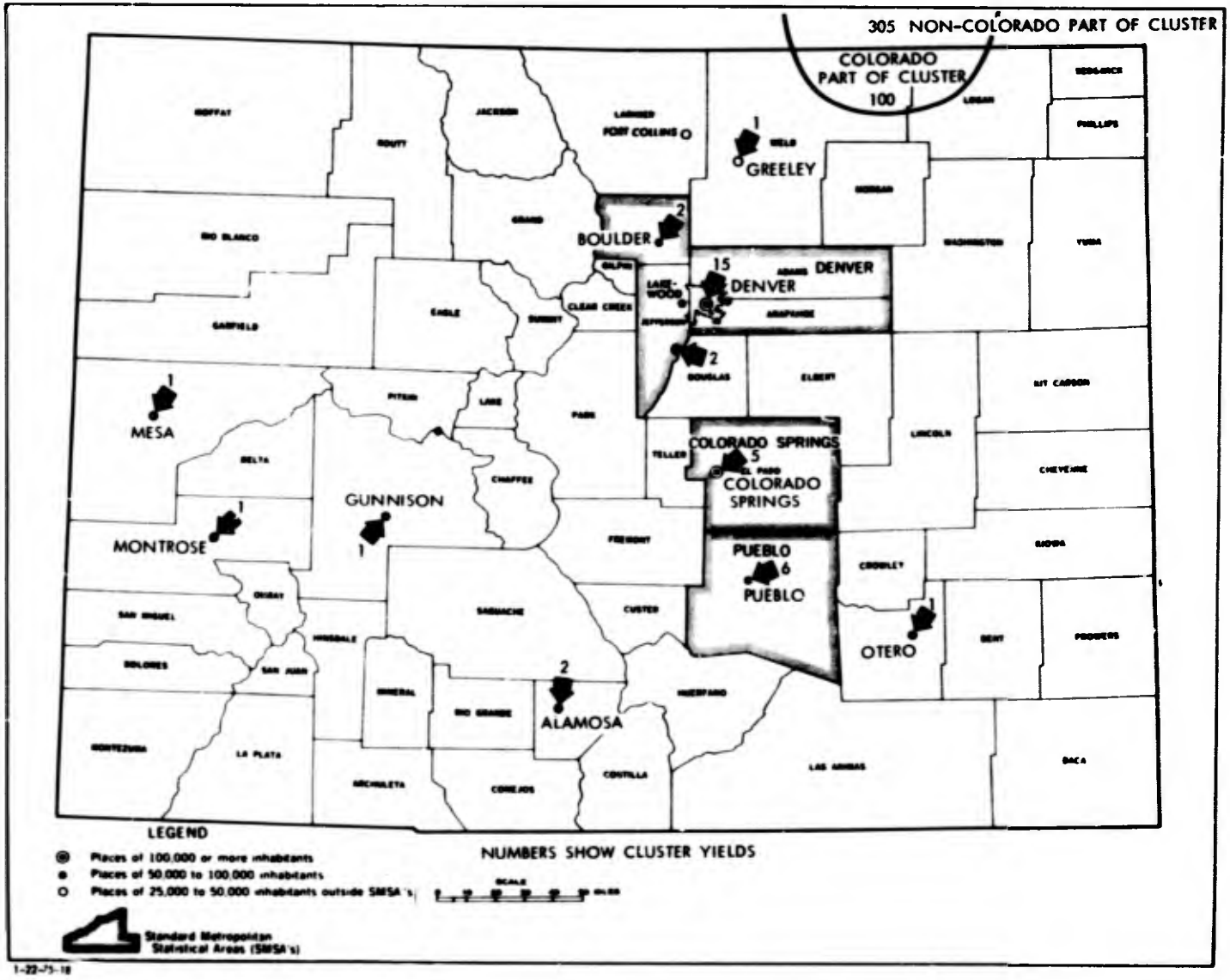

Figure 94. MAP OF WEAPON CLUSTERS IN COLORADO

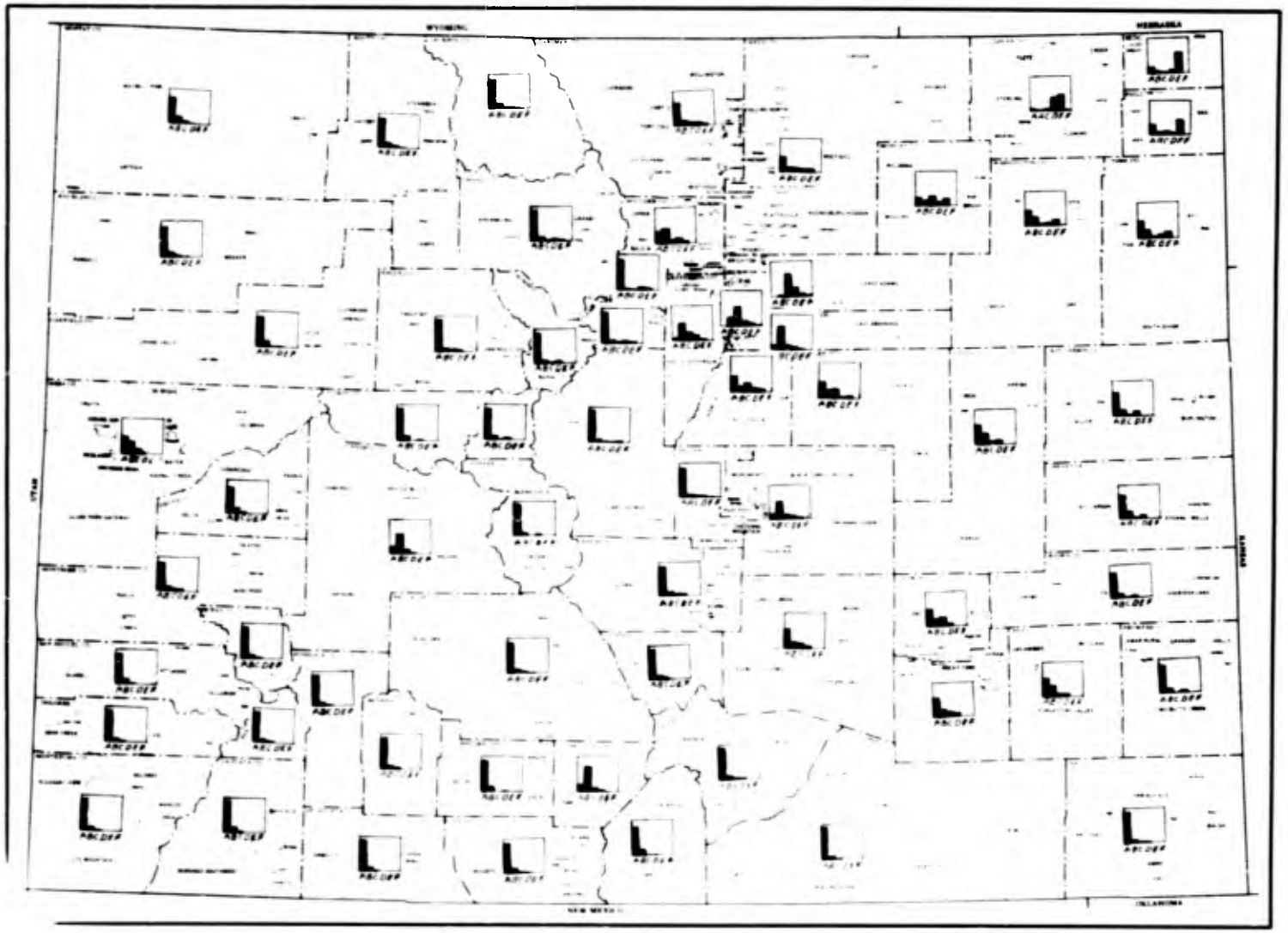

Figure 95. FALLOUT RISK IN COLORADO FROM NATIONWIDE ATTACK

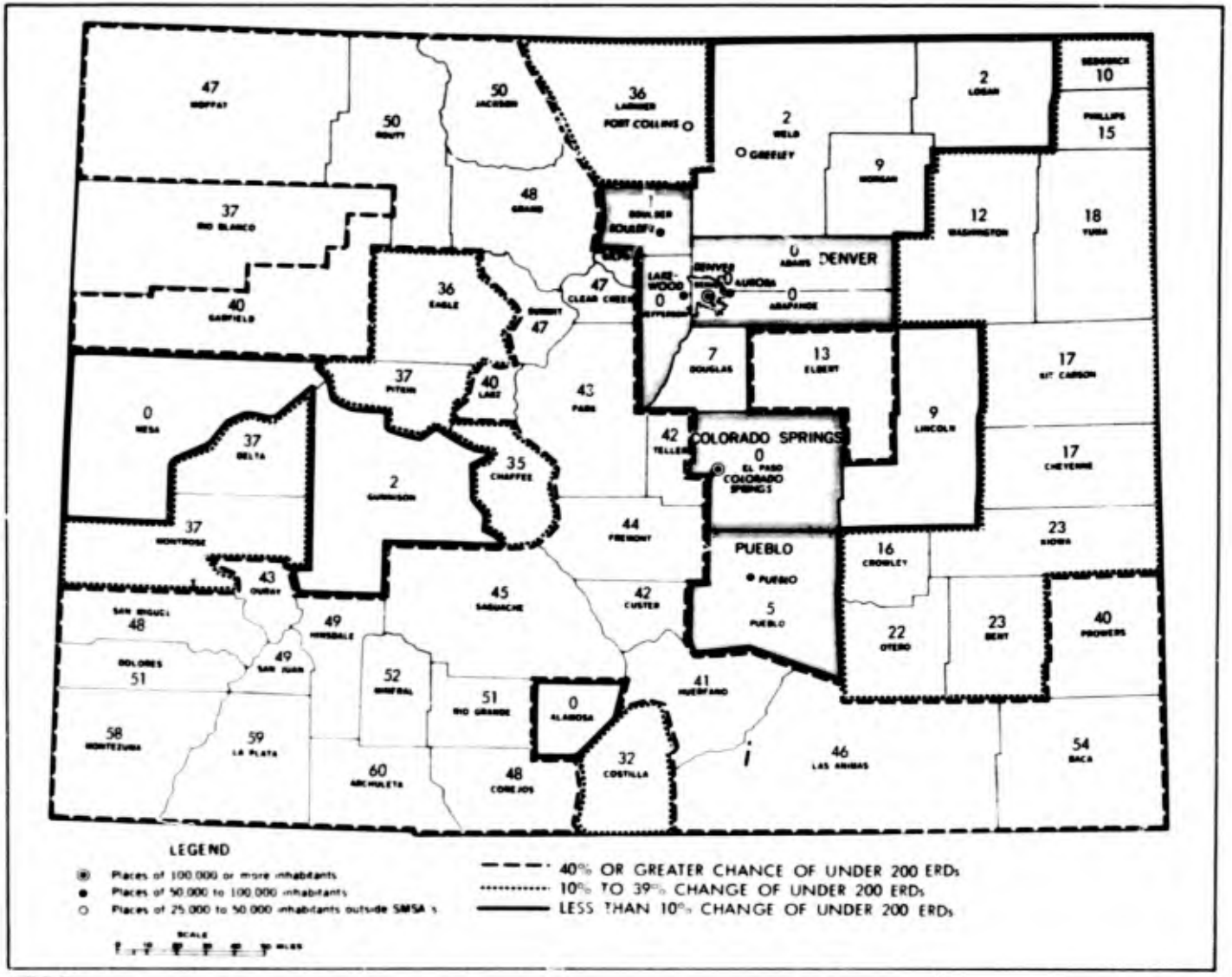

Figure 96. LIKELIHOOD OF LESS THAN 200-ERD DOSE IN COLORADO AS A RESULT OF NATIONWIDE ATTACK

Table 6. DOSE CONTRIBUTIONS TO INDIVIDUAL SAMPLES FOR CHAFFEE CO., COLORADO

Dose (ERDs)	Wind From--	Wind Velocity (mph)	Cluster Dose (ERDs)	Cluster Name	Cluster Yield	Distance	
						Downwind (miles)	Crosswind (miles)
8,731	NE	30	6,220	Warren AFB, Wyo.	405	213	36
			1,373	Ellsworth AFB, S.Dak.	301	440	5
			430	Denver, Colo.	15	96	30
			359	Minot AFB, N.Dak.	301	700	46
			213	Boulder, Colo.	2	99	11
6,755	NE	16	1,600	Warren AFB, Wyo.	405	214	33
			1,456	Denver, Colo.	15	100	3
			460	Jefferson Co., Colo.	2	75	3
			95	Ellsworth AFB, S.Dak.	301	419	135
			90	Boulder, Colo.	2	97	21
4,332	NE	12	3,108	Warren AFB, Wyo.	405	216	20
			728	Denver, Colo.	15	98	22
			176	Boulder, Colo.	2	99	4
			137	Jefferson Co., Colo.	1	72	21
			134	Ellsworth AFB, S.Dak.	301	440	27
1,289	SW	45	1,159	Tucson Missile Base, Ariz.	181	529	4
			36	Gallup, N.Mex.	2	264	10
			44	Tucson, Ariz.	4	525	8
1,215	W	68	1,151	Salt Lake City, Utah	52	347	7
			58	Toole, Utah	3	321	17
1,061	W	48	974	Salt Lake City, Utah	52	347	10
			75	Toole, Utah	3	322	14
1,071	SW	73	512	Los Angeles, Calif.	251	744	52
			201	Gunnison Co., Colo.	1	48	6
			102	Simi Valley, Calif.	20	761	25

to these seven doses. The three largest doses were when the wind blew from the northwest and carried fallout from these missile fields in this direction over the monitor point. The Tuscon missile field contributed significant doses, as did Salt Lake City and Los Angeles. Though San Francisco contributed doses of 600-700 ERDs, other clusters do not add to the fallout when the wind comes from this direction. The number of samples is not sufficient to evaluate directly from the single run the number of times a particular source might contribute to a monitor point (the methods of the previous chapter, given the likelihood that the wind is in a certain range, could be used here). However, a glance at the map in Figure 83 (above) does show that most of those spots appearing qualitatively as potential contributors of large doses are found in the statistics (presented in Table 6). It is also interesting to observe that Denver is not a significant contributor to the distribution observed--which occurs, even though a dose of 1,456 ERDs is obtained from Denver, since the dose from Warren AFB also is present with wind from this direction and overwhelms the Denver values.

For this county, no simple generalizations are apparent for doses near the median value. Some are from large clusters where the wind missed by enough to give smaller doses; some are from nearby clusters with the appropriate wind; some are from one source or (possibly) two large sources; and some are from more (typically up to six or seven) sources or more nearly equal value. The minimum dose experienced was 8 ERDs, from a wind flowing through a corridor between the Tucson and Albuquerque clusters. Whether another set of random numbers could yield a still lower value was not tested.

Table 7 presents dose sources for individual samples for Sussex County, New Jersey. This county had a mean dose of 7,078 ERDs, a median dose of 4,647 ERDs, and a maximum dose of 53,772 ERDs. Forty-nine doses were in the interval from 4,000 to 10,000 ERDs.

Table 7. DOSE CONTRIBUTIONS TO INDIVIDUAL SAMPLES FOR SUSSEX CO., NEW JERSEY

Dose (ERDs)	Wind From--	Wind Velocity (mph)	Cluster Dose (ERDs)	Cluster Name	Cluster Yield (MT)	Distance	
						Downwind (miles)	Crosswind (miles)
53,773	SE	4	52,616	New York, N.Y.	331	39	5
			746	Trenton, N.J.	32	41	55
			101	New Haven, Conn.	26	57	72
			101	Atlantic City, N.J.	2	59	22
			Sum = 53,564				
39,446	SE	32	39,276	New York, N.Y.	313	38	10
			164	Atlantic City, N.J.	2	61	15
			Sum = 39,440				
19,774	SW	43	7,090	Philadelphia, Pa.	72	83	4
			6,636	New York, N.Y.	313	9	39
			2,090	Trenton, N.J.	32	65	20
			1,750	Wilmington, Del.	17	107	9
			850	Baltimore, Md.	113	162	13
			325	Allentown, Pa.	5	36	20
			308	Richmond, Va.	8	286	2
			277	Norfolk, Va.	13	248	18
			183	Annapolis, Md.	2	140	9
			Sum = 19,509				
7,780	SW	91	3,264	Baltimore, Md.	113	162	13
			2,174	Washington, D.C.	67	198	9
			737	Allentown, Pa.	5	41	5
			657	New York, N.Y.	313	6	39
			260	Danville, Va.	22	439	26
			100	Harrisburg, Pa.	7	116	35
			Sum = 7,192				

(continued on next page)

Table 7 (continued)

Dose (ERDs)	Wind From--	Wind Velocity (mph)	Cluster Dose (ERDs)	Cluster Name	Cluster Yield (MT)	Distance	
						Downwind (miles)	Crosswind (miles)
6,037	W	59	1,702	Cleveland, Ohio	85	363	4
			1,293	Scranton, Pa.	23	55	16
			829	Chicago, Ill.	160	675	21
			512	Lorain-Elyria, Ohio	24	389	3
			418	Wilkes-Barre, Pa.	3	60	8
			248	Youngstown, Ohio	12	356	29
			227	Akron, Ohio	25	317	18
			210	Detroit, Mich.	93	446	56
			134	Joliet, Ill.	21	697	3
			100	Warren AFB, Wyo.	405	1,512	92
			70	South Bend, Ind.	7	596	13
			69	Toledo, Ohio	4	468	8
			76	Rock Island, Ill.	10	823	9
			25	Pittsburgh, Pa.	63	275	65
			Sum = 5,883				
4,979	W	13	4,117	Scranton, Pa.	23	57	3
			562	Wilkes-Barre, Pa.	3	60	6
			94	Cleveland, Ohio	85	354	79
			64	Detroit, Mich.	93	447	47
			Sum = 4,837				
4,645	SW	36	1,570	Pittsburgh, Pa.	63	283	7
			1,454	New York, N.Y.	313	31	25
			277	Scranton, Pa.	23	50	27
			268	Columbus, Ohio	25	440	13
			163	Wilkes-Barre, Pa.	3	57	20
			163	Whiteman AFB, Mo.	329	1,034	47
			127	St. Louis, Mo.	81	839	13
			Sum = 4,022				

(concluded on next page)

Table 7 (concluded)

Dose (ERDs)	Wind From--	Wind Velocity (mph)	Cluster Dose (ERDs)	Cluster Name	Cluster Yield (MT)	Distance	
						Downwind (miles)	Crosswind (miles)
3,672	NE	32	3,193	New York, N.Y.	313	-2	39
			315	Albany, N.Y.	10	122	24
			155	Pittsfield, Mass.	2	120	12
			7	Springfield, Mass.	21	121	53
			1	Aroostook Co., Me.	1	521	49
			Sum = 3,671				
302	NW	39	234	Utica-Rome, N.Y.	4	149	13
			61	St. Lawrence, N.Y.	6	268	28
			7	Syracuse, N.Y.	26	151	53
			Sum = 302				

In Table 7, the samples are selected to show a variety of cases, including the meximum dose, the minimum dose, and doses from representative wind directions. The New York weapon cluster often has a dominating effect upon the doses received. As represented in the model, this county is at the northeast edge of the New York weapon cluster. The nearest weapon in the New York cluster is 3.7 miles from the monitor point for Sussex County. As can be seen, the maximum dose is achieved when a low wind velocity blows the fallout from the New York cluster back over Sussex County.

Also close to Sussex County is the Scranton weapon cluster, in a direction generally upwind from the mean wind. The sample with a total dose of 4,979 ERDs illustrates a case chosen to maximize the effects of the fallout of this cluster.

The doses listed generally comprise the large majority of the contribution to the total dose received. The cutoff-dose levels for the samples with total doses of 39,446, 3,672, and 302 ERDs include all significant contributions. For the sample with total dose of 6,037 ERDs, the cutoff dose was carried to 20 ERDs, which excludes 2.5 percent of the total dose received. In this case, there remained 22 samples with doses over 1 ERD and 52 samples with doses in the range 0.001 to 1 ERD.

One surprising feature of this table is the large distances from which some contributions come. For example, for the sample with total dose of 6,037 ERDs where the wind passes near Cleveland, a dose of 829 ERDs is contributed from Chicago, even though the distance away is 675 miles. In fact, even Warren AFB contributes 100 ERDs though it is 1,500 miles away. In a nationwide attack for some monitor points, a large yield from relatively distant sources can significantly modify the dose statistics when for a large fraction of the samples the wind direction is such that radioactivity from at least one of these large sources is carried to the monitor point. The actual

significance of such sources is ultimately based upon the basic assumption of this paper, namely, the physical validity of the WSEG-10 Fallout Model. It thus becomes of interest to determine, on a physical basis, whether these fallout-model predictions for long distances and under typical wind conditions appear reasonable.